Microbial Iron Reduction Influenced by Humic Acids and Redox Transformation of Arsenic by Reactive Iron Minerals

Dissertation

zur Erlangung des Grades eines Doktors der Naturwissenschaften

der Geowissenschaftlichen Fakultät
der Eberhard Karls Universität Tübingen

vorgelegt von
Katja Amstätter
aus Kulmbach

2009

Two sorts of truth:

Trivialities, where opposites are obviously absurd, and

profound truths, recognized by the fact that

the opposite is also a profound truth.

Niels Bohr

Erklärung

Hiermit versichere ich wahrheitsgemäß, dass ich die vorliegende Arbeit selbständig verfasst, keine anderen als die angegebenen Quellen und Hilfsmittel benutzt und wörtlich oder inhaltlich übernommene Stellen als solche gekennzeichnet habe.

Kulmbach, den 22.5.2009

Katja Amstätter

Summary

Iron is an important redox active element in soils and sediments. Bacteria change the mineralogy by oxidation or reduction of iron minerals and potentially form reactive minerals which are involved in the transformation of organic and inorganic pollutants in anoxic environments. Objectives of the present study were to determine influencing factors for microbial iron reduction, in particular the role of humic acids and additionally to investigate the potential of mixed-valent biogenic iron minerals for the redox transformation of arsenic.

The work presented in this thesis showed concentration-dependent aggregate formation of 2-line ferrihydrite. Determination of microbial iron reduction rates of *Shewanella oneidensis* MR-1 in these setups showed limited microbial accessibility of the aggregates depending on the mineral concentration. In addition, the accessibility of the mineral aggregates varied in the presence of different concentrations of humic acids. Adsorbed humic acids changed the surface charge of the mineral aggregates and either lead to further interlinking of the aggregates or repulsion of identically charged particles. Dissolved humic acid in turn can be used by bacteria to transfer electrons to hardly soluble Fe(III) minerals at neutral pH. In particular it was shown that only a very restricted range of dissolved humic acid concentrations (~10-130 mg HA/l) lead to stimulation of microbial iron reduction.

Furthermore, the electron transfer properties of humic acids were affected by ionic strength. It was shown that an increase in ionic strength lead to an increase of electrons transferred to Fe(III) by reduced humic acids. Since reduced humic acids formed larger, porous particles they offered a greater number of reactive sites to potential oxidants like Fe(III). In addition to structural changes by electrostatic repulsion between dissolved ions and humic acid we also detected a decrease of particle charge (zeta potential) with increasing ionic strength. This effect may have facilitated interaction between cells and humic acids and enhanced the electron shuttling function of humic acid.

In addition to determination of reduction rates, the influence of humic substances on the formed biogenic iron minerals was followed using sequential extraction, μ-XRD analysis and Moessbauer spectroscopy. The results demonstrated that the identity and crystallinity of the minerals formed strongly depend on the initial concentration of ferrihydrite, the local ratio of Fe(II) to Fe(III) and the presence of phosphate or humic acid, with the latter leading to decreased crystallinity with increasing concentration. Potentially reactive Fe(II)-Fe(III) minerals may be formed, which could have substantial impact on the fate of contaminants in anoxic environments.

In order to determine the potential of such reactive Fe(II)-Fe(III) minerals for the redox transformation of arsenic under anoxic conditions, abiotic batch experiments were set up containing goethite, dissolved Fe(II) and As(III) or As(V), respectively. Separate analysis of the surface bound arsenic by synchrotron-based XANES and analysis of dissolved arsenic by ICP-MS provided quantity and identity of arsenic species in iron mineral systems. Using these techniques oxidation of As(III) to As(V) by Fe(II)-goethite suspensions was observed whereas reduction of As(V) to As(III), the expected reaction, was not observed. It was attempted to identify the reactive iron phase by μ-XRD, SEM, HR-TEM and Moessbauer spectroscopy, but it was not possible to identify the oxidizing redox reactive iron species. Instead, we confirmed previous findings showing electron transfer from the adsorbed Fe(II) to the underlying goethite, with subsequent formation of goethite by oxidation of the adsorbed Fe(II). During this process a short-living intermediate state of iron could probably cause the redox transformation of arsenic bound in a surface complex.

Such reactive phases could not be found in iron-reducing batch cultures containing a mixture of 2-line ferrihydrite and goethite. Obviously goethite could not serve as adsorption template for formed biogenic Fe(II) in a similar way as in the abiotic experiments. This could be a consequence of surface blockage by formed secondary iron minerals which may prevent sorption of Fe(II). However, the reduction of As(V) at an intermediate stage of Fe(III) reduction in cultures containing ferrihydrite as the only Fe(III) source showed the potential of

biogenic reactive Fe(II)-Fe(III) mineral systems for redox transformation of arsenic.

Conclusively, the present studies show the limitations (concentration, ionic strength) and implications (reduction rates, mineral formation) of humic substances for the stimulation of electron shuttling in microbial Fe(III) reduction. In particular the variations in mineral crystallinity caused by humic acids potentially influence the reactivity of the formed iron precipitates towards pollutant transformation. Since the fate of arsenic in anoxic environments depends on many different factors further elucidation of redox reactions with Fe(II)-Fe(III) minerals may contribute to knowledge about the natural speciation of this metalloid. Finally it follows that humic substances take a key role in microbial iron reduction if they are present in sufficient amounts to support electron shuttling. Then they determine consumption rates for poorly crystalline Fe(III) sources like ferrihydrite and may even affect the potential for natural attenuation in contaminated anoxic aquifers due to their effect on biogenic mineral formation.

Zusammenfassung

Eisen ist in Böden und Sedimenten ein bedeutendes, redoxaktives Element. Durch Oxidation oder Reduktion von Eisenmineralen verändern Bakterien die Mineralogie und können reaktive Minerale bilden. Diese Minerale sind an der Umwandlung von organischen und anorganischen Schadstoffen unter anoxischen Bedingungen beteiligt. Ziele dieser Arbeit waren die Bestimmung von Faktoren, die die mikrobielle Eisenreduktion beeinflussen ins Besondere der Einfluss von Huminsäuren. Weiterhin wurde untersucht, ob biogene Eisenminerale gemischter Oxidationszustände Redoxumwandlungen von Arsen verursachen können.

Im Rahmen dieser Arbeit wurde eine konzentrationsabhängige Aggregatbildung von 2-line Ferrihydrit gezeigt. Die mikrobiellen Eisenreduktionsraten von *Shewanella oneidensis* MR-1 in diesen Ansätzen deuteten auf eine eingeschränkte Zugänglichkeit der Aggregatoberfläche für Bakterien abhängig von der Mineralkonzentration hin. Zusätzlich variierte die Zugänglichkeit der Aggregate mit verschiedenen Huminsäurekonzentrationen. Adsorbierte Huminsäure veränderte die Oberflächenladung der Mineralaggregate und führte entweder zu einer weiteren Vernetzung der Aggregate oder zu einer Abstoßung gleichartig geladener Partikeln. Bei neutralem pH können gelöste Huminsäuren desweiteren von Bakterien zum Elektronentransfer auf schwerlösliche Fe(III)-Minerale genutzt werden. Dabei wurde ins Besondere ein sehr eng begrenzter Bereich von gelösten Huminsäurekonzentrationen (~10-130 mg HA/l) ermittelt, in dem die Stimulation der mikrobiellen Eisenreduktion zunahm.

Weiterhin wurden die Elektronentransfereigenschaften von Huminsäuren durch die Ionenstärke beeinflusst. Mit steigender Ionenstärke erhöhte sich die Menge der Elektronen, die von reduzierten Huminsäuren übertragen wurde. Da reduzierte Huminsäuren größere, poröse Partikel bildeten waren mehr reaktive Gruppen für Oxidantien wie Fe(III) zugänglich. Neben der strukturellen Veränderung durch elektrostatische Abstoßung zwischen gelösten Ionen und Huminsäure

sank auch die Partikelladung (Zeta-Potential) mit steigender Ionenstärke. Dies erleichterte Wechselwirkungen zwischen Bakterien und Huminsäuren und führte zu schnellerem Elektronenübertrag über Huminsäuren.

Neben der Bestimmung der Reduktionsraten wurde auch der Einfluss von Huminstoffen auf die biogene Mineralbildung mit Hilfe von sequenzieller Extraktion, µ-XRD-Analyse und Mössbauerspektroskopie verfolgt. Es wurde gezeigt, dass sowohl die Identität als auch die Kristallinität der gebildeten Minerale stark von der Ferrihydritmenge zu Beginn des Versuches, dem lokalen Fe(II)-Fe(III)-Verhältnis und der Anwesenheit von Phosphat bzw. Huminsäure abhingen, wobei letztere mit steigender Konzentration zu geringerer Kristallinität führte. Dabei könnten möglicherweise reaktive Minerale gebildet werden, die den Verbleib von Schadstoffen unter anoxischen Bedingungen beeinflussen können.

Um das Potenzial solcher reaktiven Fe(II)-Fe(III)-Minerale für die Redoxumwandlung von Arsen unter anoxischen Bedingungen abschätzen zu können wurden abiotische Batchversuche durchgeführt, die Goethit, gelöstes Fe(II) und As(III) bzw. As(V) enthielten. Die separate Analyse von oberflächengebundenem Arsen und gelöstem Arsen lieferte Menge und Speziierung des Arsens in Gegenwart von Eisenmineralen. Es gelang der Nachweis einer As(III)-Oxidation zu As(V) in Fe(II)-Goethitsuspensionen, die erwartete Reduktion von As(V) zu As(III) war dagegen nicht zu beobachten. Auch mittels µ-XRD, SEM, TEM und Mössbauerspektroskopie konnte die redoxaktive oxidierende Eisenspezies nicht eindeutig identifiziert werden. Stattdessen konnte der Elektronentransfer von adsorbiertem Fe(II) auf das darunter liegende Goethit und die Umwandlung dieses Fe(II) in Goethit, wie in früheren Studien beschrieben, bestätigt werden. Während dieses Prozesses könnte ein instabiler Übergangs-zustand die Redoxtransformation des oberflächengebundenen Arsens verursacht haben.

Solche reaktiven Phasen konnten in biotischen Batchversuchen mit einer Mischung aus Goethit und 2-line Ferrihydrit nicht nachgewiesen werden. Anscheinend wirkte Goethit hier nicht als Adsorptionsmittel für Fe(II) vergleichbar zu den abiotischen Versuchen.

Dies war möglicherweise die Folge einer Oberflächenbelegung durch sekundär gebildete Eisenminerale, die Fe(II)-Sorption verhinderten. In Eisenreduktionskulturen, die ausschließlich Ferrihydrit als Fe(III)-Quelle enthielten wurde allerdings Reduktion von As(V) nachgewiesen, was den potenziellen Einfluss von biogenen, reaktiven Fe(II)-Fe(III)-Mineralsystemen auf die Redoxtransformation von Arsen zeigte.

Abschließend ist fest zu halten, dass diese Studie Limitierungen (Konzentration, Ionenstärke) und Effekte (Reduktionsraten, Mineral-bildung) von Huminstoffen auf die Stimulierung von mikrobieller Fe(III)-Reduktion durch Elektronenshuttling zeigt. Ins Besondere die Veränderung der Kristallinität, verursacht durch Huminsäure, kann die Reaktivität von Eisenmineralen in Hinsicht auf die Schadstoff-umwandlung (Arsen) beeinflussen. Da der Verbleib von Arsen unter anoxischen Bedingungen von vielen verschiedenen Faktoren abhängt kann die weitere Aufklärung von abiotischen Redoxreaktionen mit Fe(II)-Fe(III)-Mineralen zum Verständnis des natürlichen Verhaltens dieser Metalloidspezies beitragen. Ausgehend von diesen Ergebnissen folgt, dass Huminstoffe eine Schlüsselrolle in der mikrobiellen Eisenreduktion einnehmen, wenn sie in ausreichender Menge vorhanden sind um Elektronenshuttling zu unterstützen. Dann bestimmen sie Verbrauchsraten für schwach kristalline Fe(III)-Quellen wie Ferrihydrit und können durch den Einfluss auf die biogene Mineralbildung sogar natürliche Regenerationsprozesse in belasteten, anoxischen Aquiferen beeinflussen.

Table of Contents

1

Introduction

1. IRON AND IRON REDUCING BACTERIA

Iron is an important industrial raw material and a constituent of objects of daily use since centuries. It is a major element of the earth crust (2nd most abundant metal after Al), an essential trace element for organisms (hem-group, Fe-S-cluster) (Voet and Voet, 1992), shows catalytic functions under synthetic (ammonia synthesis) (Hollemann and Wiberg, 1985) and natural conditions (reactive iron barriers) and is used as color pigment (Cornell and Schwertmann, 2003). As a major constituent of primary minerals, like biotite, amphibole, pyroxene and olivine iron is present in soils and sediments in the form of weathering products of such minerals. The two environmentally most relevant redox states of iron, Fe(II) and Fe(III), are usually found as interstitial ions in clay minerals, in form of iron sulfides, sulfates, oxides, hydroxides and oxyhydroxides (Hollemann and Wiberg, 1985; Chernicoff, 1999; Cornell and Schwertmann, 2003).

Various mineralogical forms of Fe(III) can be utilized by a broad spectrum of bacterial strains as terminal electron acceptor (Weber et al., 2006). Although first discovered in the 1980s (Balashova and Zavarzin, 1979; Lovley and Phillips, 1988; Myers and Nealson, 1988) shortly after that dissimilatory iron reduction by microorganisms became an important research field and has been extensively studied in the past years (for review see Lovley et al., 2004; Kappler and Straub, 2005). Numerous studies investigated the impact of different properties of Fe(III) minerals on microbial reduction rates. One of them, is the redox potential of the different iron oxides for reduction to ferrous iron. The redox potentials at neutral pH (25°C) decrease from +/-0 to -314 mV in descending order for ferrihydrite > lepidocrocite > goethite > hematite > magnetite (Thamdrup, 2000). The minerals get more and more unfavorable towards microbial reduction. Furthermore, previous studies demonstrated the correlation between the surface area of utilized iron oxides and Fe(II) formation (Roden and Zachara, 1996; Roden, 2003), whereas another study showed the dependency of iron reduction rates on the solubility of the iron oxides (Bonneville et al., 2004).

The poorly crystalline mineral ferrihydrite $Fe(OH)_3$ turned out to be an important, easily accessible Fe(III) source for microbial iron reducers (Lovley and Phillips, 1988). However the defective structure makes it difficult to relate macroscopic oberservations e.g. in bacterial cultures to the physicochemical properties of ferrihydrite (surface area, redox potential, particle aggregation) (van der Giessen, 1966; Cornell and Schwertmann, 2003; Michel et al., 2007). In natural environments ferrihydrite is usually present in relatively young Holocene soils or sediments or at places where biogenic or rapid oxidation of Fe(II) takes place e.g. where anoxic Fe(II)-containing groundwater appears at the aerated surface. The iron concentrations vary between less than 1 g/kg and several hundred g/kg in soils, amongst others (soils on lava flows, gleys, podzols) ferrihydrite is found at the transition zone between oxic and anoxic conditions at the ground water level (Cornell and Schwertmann, 2003), where anaerobic Fe(III) reduction takes place. So far the two genera *Shewanella* and *Geobacter* have been found to dominate iron reducing environments (Thamdrup, 2000; Lovley et al., 2004). This observation could be due to isolation techniques which may selectively enrich these bacterial species in lab cultures and eliminate less adaptable strains. Therefore it is possible that the main representatives, capable of iron reduction, are still unknown. However, iron reducing bacteria accomplish a great effort in order to use the hardly soluble substrate Fe(III) at circumneutral conditions.

2. HUMIC SUBSTANCES AND THEIR ROLE IN MICROBIAL IRON REDUCTION

Considering the low solubility of ferrihydrite of $10^{-3.1}$ μM Fe at pH 7 (Schwertmann, 1991), bacteria had to develop special mechanisms in order to transfer electrons to the solid electron acceptor. Shuttling electrons via redox active soluble mediators is one of the possible mechanisms to compensate the very limited possibility to take up dissolved iron into the cell. Although some iron reducers are able to excrete and reduce redox active compounds like flavines (Marsili et al., 2008; von Canstein et al., 2008), it is more likely that bacteria choose a less energy consuming alternative if available. The utilization of ubiquitously present compounds like humic substances as electron carrier is a known pathway, which has been discovered approximately

ten years ago (Lovley et al., 1996; Coates et al., 1998; Royer et al., 2002b; Royer et al., 2002a). Nevertheless the knowledge about their role in mineral formation and transformation rates under environmental conditions, in particular low concentrations in solution, is limited.

Humic substances are degradation products of plant, animal and bacterial remains and contain a variety of different compound classes (carbohydrates, peptides, amino acids and aromatic compounds) originating in these sources and containing different functional groups (Stevenson, 1994). The percentage of specific functional groups can highly vary upon origin of the humic substance e.g. terrestrial or aquatic sources. Although quinone moieties have been identified as the responsible redox active groups involved in the electron transfer between cells and the mineral surface (Scott et al., 1998) the knowledge about the accessibility of these groups for bacteria and the actual transfer mechanism is very limited. In particular the effect of structural changes due to changes in geochemical conditions e.g. dissolved ions on the accessibility of redox active groups is unknown. Previous attempts to resolve the actual structure of humic substances quickly encountered difficulties due to the complexity of the heterogenic, polymeric and polydispersive nature of humic substances (Stevenson, 1994; Clapp and Hayes, 1999; Simpson et al., 2002). Therefore the structure of humic substances remains somewhat enigmatic and descriptions of changes keep being descriptive on a supramolecular scale (Ceccanti et al., 1989; Stevenson, 1994; Balnois et al., 1999; Conte and Piccolo, 1999; Hosse and Wilkinson, 2001).

3. IRON MINERAL TRANSFORMATION AND REACTIVITY

Iron minerals are exposed to influences such as thermal, oxidative, reductive, dissolving and precipitating processes. These either abiotic or biotic processes lead to changes in crystal structure, composition, surface area, morphology and porosity of the present minerals. The thermodynamically most stable iron (oxyhydr)oxides under oxic conditions are goethite and hematite, which are therefore common transformation products of many other iron (oxyhydr)oxides. However, under ambient natural conditions thermal conversions do not take place. In addition, the thermodynamically favoured transformation mechanism

can be influenced by kinetic constraints or foreign ions and lead to modified product properties or a mixture of minerals (Cornell and Schwertmann, 2003). As long as no abiotic reactants or iron metabolizing bacteria are present transformations of iron (oxyhydr)oxides at neutral, ambient conditions are slow and take place in time frames of years. They can be accelerated due to pH changes, the presence of oxygen (only Fe(II)-containing minerals), the influence of iron complexing compounds or under anoxic conditions in presence of reducing compounds, including oxalate and Fe(II) (Fischer, 1973; Fischer, 1983; Eick et al., 1999). The easy bioavailable Fe(III) source ferrihydrite sticks out due to its poorly ordered structure it can be basically transformed into most of the other iron (oxyhydr)oxides.

Iron metabolizing bacteria change the ratio of Fe(II) to Fe(III) and thereby determine the formation of a certain mineral (mixture) substantially. Besides the precipitation of Fe(II) containing minerals like siderite, vivanite or magnetite at high Fe(II) concentrations (Fredrickson et al., 1998), the transformation into other Fe(III) containing minerals depending on ferrihydrite reduction rates is either explained by recrystallization processes or topotactic conversion of the ferrihydrite (Ardizzone and Formaro, 1983; Gálvez et al., 1999; Zachara et al., 2002; Hansel et al., 2005; Coker et al., 2008). However, as soon as higher crystalline iron minerals and dissolved Fe(II) are present, formation of reactive iron species potentially occurs (Haderlein and Pecher, 1998), in which the identity of the crystalline mineral has been shown to determine the rate of reductive pollutant transformation (Elsner et al., 2004a). Laboratory studies conducted in recent years showed reductive transformation of pollutants as diverse as Cr, U, Tc, carbon tetrachloride or nitroaromatic compounds (Buerge and Hug, 1999; Liger et al., 1999; Elsner et al., 2004b; Fredrickson et al., 2004; Borch et al., 2005). Reduction of these compounds is equivalent to a detoxification process and consequently a potential mechanism for natural attenuation. However, this collection of target compounds may be incomplete and has to be extended in the further future. Arsenic may be another toxic element, which could be reduced in such systems, but has not been investigated in this context yet.

4. ARSENIC AND ITS ENVIRONMENTAL RELEVANCE

Redox changes of arsenic species strongly influence the fate of arsenic in the environment. In particular the interaction of arsenic with iron minerals depends on geochemical parameters like pH conditions, redox potential and the presence of foreign ions or organic compounds (Oscarson et al., 1980; Masscheleyn et al., 1991; Grafe et al., 2001; Dixit and Hering, 2003). Due to the strong sorption of arsenic to iron minerals it is not sufficient to quantify arsenic speciation in solution, but also to identify the surface-bound fraction in order to follow redox change reactions. Besides the two environmentally most relevant arsenic species, inorganic As(III) and As(V) oxyanions, also comparatively low concentrations of organo arsenicals (monomethylarsonic acid, dimethylarsinic acid and arseno betaine) are present in the environment, whereas the latter compounds are in general less toxic than the inorganic compounds. Chronical exposure to elevated levels of arsenic concentrations (World Health Organization drinking water limit 10 µg/l) can lead to skin, bladder, kidney or lung cancer as well as peripheral vascular disease or neuronal effects (for review see Francesconi and Kuehnelt, 2002; Hopenhayn, 2006).

Some arsenic contaminations are of anthropogenic origin (pesticides, coal combustion, mining sites) but a large number of sites exhibiting elevated arsenic contents are of geogenic origin (Nriagu, 2002; Smedley and Kinniburgh, 2002). Several hot-spots of naturally contaminated aquifers are located in Asia, in particular Southeast Asia and West-Bengal. In this region eroded, arsenic containing sediments (amongst others originating from the Himalayan mountain range) have been deposited in large amounts and represent a spatially widespread problem for the local drinking water supply (Smedley and Kinniburgh, 2002; Postma et al., 2007; Hug et al., 2008; Polizzotto et al., 2008). Although the geochemical processes have been intensely investigated since years there are still open questions regarding release mechanisms of arsenic especially in the afore mentioned regions (Sadiq, 1997; Swartz et al., 2004; Norra et al., 2005; Polizzotto et al., 2006; Tufano and Fendorf, 2008). In particular the presence of both arsenic redox states under natural conditions where just one of them is thermodynamically instable (e.g. As(V) under reducing conditions (Postma et al., 2007)) is not completely clarified based on laboratory studies. Without knowing

the actual mechanisms for arsenic release it is almost impossible to take preventing measures in order to reduce the aquifer contamination. For now supporting measures are mostly limited to the exploitation of uncontaminated aquifers or drinking water treatments, usually conducted on a local scale (Meng et al., 2001; Hug et al., 2008).

5. OBJECTIVES OF THIS STUDY

The environmental fate of arsenic is often related to the transformation of iron minerals, since both species are frequently associated with each other. In particular the biogenic reduction of Fe(III) minerals, the ensuing adsorption of Fe(II) and the subsequent formation of reactive iron species could potentially affect the redox state of arsenic in anoxic environments as illustrated in Figure 1. The role of humic substance in such reactive iron mineral systems has not been investigated so far. Evaluation of their effect on the mineral formation and transformation during microbial iron reduction may provide information about the potential reactivity of the biogenic precipitates.
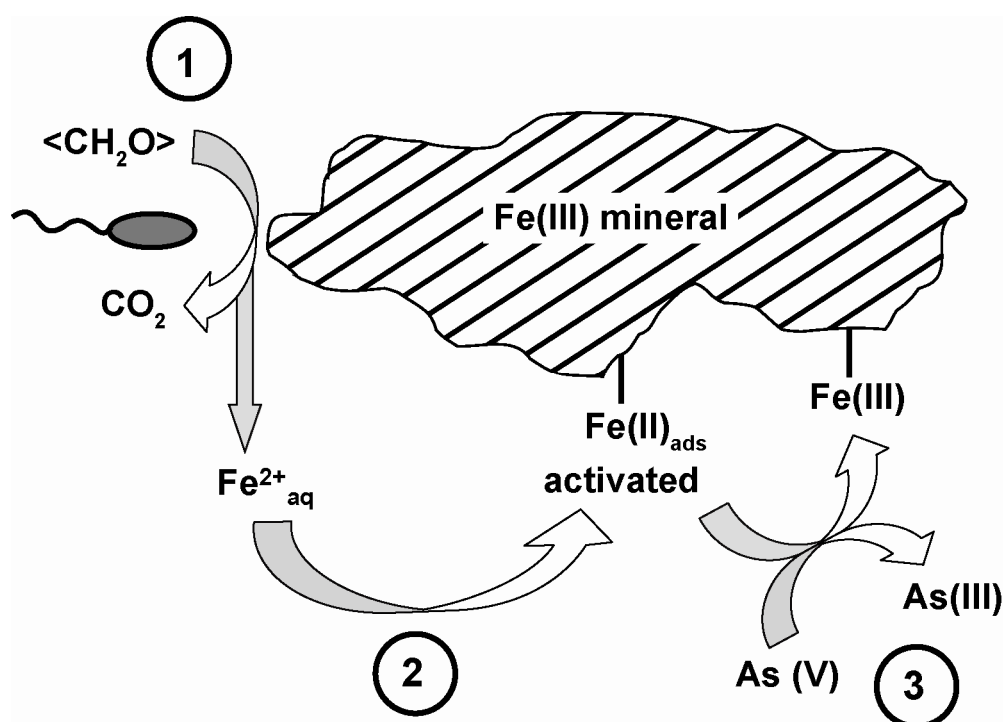

Fig. 1 Scheme of a possible pathway for the redox transformation of arsenic (reduction of As(V) to As(III)) in presence of biogenic reactive Fe(II)-Fe(III)-systems initiated by microbial iron reduction.

Therefore the aims of the present study were:

- Identification and quantification of factors influencing reduction rates and mineral formation during microbial reduction of 2-line ferrihydrite.
- Development of a method to prevent oxidation of Fe(II) in biogenic iron mineral precipitates for XRD analysis.
- Determination of the effect of variations in humic acid concentrations on electron shuttling during microbial iron reduction.
- Quantification of the impact of ionic strength on electron shuttling.
- Determination of the influence of humic substances on mineral product formation during microbial iron reduction and potential consequences for biogeochemical processes.
- Evaluation of extraction methods for quantification of arsenic adsorbed on iron minerals with special regard on the preservation of arsenic redox states.
- Quantification of arsenic redox transformations in abiotic and biotic mixed Fe(II) and Fe(III) mineral systems, including the identification of reactive iron phases.

6. REFERENCES

Ardizzone S. and Formaro L., 1983. Temperature induced phase transformation of metastable $Fe(OH)_3$ in the presence of ferrous ions. *Mater. Chem. Phys.* **8**, 125-133.

Balashova V. V. and Zavarzin G. A., 1979. Anaerobic reduction of ferric iron by hydrogen bacteria. *Microbiologiia* **48**, 773-778.

Balnois E., Wilkinson K. J., Lead J. R., and Buffle J., 1999. Atomic Force Microscopy of Humic Substances: Effects of pH and Ionic Strength. *Environ. Sci. Technol.* **33**, 3911-3917.

Bonneville S., Van Cappellen P., and Behrends T., 2004. Microbial reduction of iron(III) oxyhydroxides: effects of mineral solubility and availability. *Chem. Geol.* **212**, 255-268.

Borch T., Inskeep W. P., Harwood J. A., and Gerlach R., 2005. Impact of Ferrihydrite and Anthraquinone-2,6-Disulfonate on the Reductive Transformation of 2,4,6-Trinitrotoluene by a Gram-Positive Fermenting Bacterium. *Environ. Sci. Technol.* **39**, 7126-7133.

Buerge I. J. and Hug S. J., 1999. Influence of Mineral Surfaces on Chromium(VI) Reduction by Iron(II). *Environ. Sci. Technol.* **33**, 4285-4291.

Ceccanti B., Calcinai M., Bonmati-Pont M., Ciardi C., and Tarsitano R., 1989. Molecular size distribution of soil humic substances with ionic strength. *Sci. Total Environ.* **81-82**, 471-479.

Chernicoff S., 1999. *Geology.* Houghton Mifflin Company, Boston, New York.

Clapp C. E. and Hayes M. H. B., 1999. Sizes and Shapes of Humic Substances. *Soil Sci.* **164**, 777-789.

Coates J. D., Ellis D. J., Blunt-Harris E. L., Gaw C. V., Roden E. E., and Lovley D. R., 1998. Recovery of humic-reducing bacteria from a diversity of environments. *Appl. Environ. Microbiol.* **64**, 1504-1509.

Coker V. S., Bell A. M. T., Pearce C. I., Pattrick R. A. D., van der Laan G., and Lloyd J. R., 2008. Time-resolved synchrotron powder X-ray diffraction study of magnetite formation by the Fe(III)-reducing bacterium *Geobacter sulfurreducens. Am. Mineral.* **93**, 540-547.

Conte P. and Piccolo A., 1999. Conformational Arrangement of Dissolved Humic Substances. Influence of Solution Composition on Association of Humic Molecules. *Environ. Sci. Technol.* **33**, 1682-1690.

Cornell R. M. and Schwertmann U., 2003. *The Iron Oxides.* Wiley-VCH Verlag GmbH & Co. KGaA, Weinheim.

Dixit S. and Hering J. G., 2003. Comparison of Arsenic(V) and Arsenic(III) Sorption onto Iron Oxide Minerals: Implications for Arsenic Mobility. *Environ. Sci. Technol.* **37**, 4182-4189.

Eick M. J., Brady W. D., and Peak J. D., 1999. The Effect of Oxyanions on the Oxalate-Promoted Dissolution of Goethite. *Soil Sci. Soc. Am. J.* **63**, 113-1141.

Elsner M., Schwarzenbach R. P., and Haderlein S. B., 2004a. Reactivity of Fe(II)-Bearing Minerals toward Reductive Transformation of Organic Contaminants. *Environ. Sci. Technol.* **38**, 799-807.

Elsner M., Schwarzenbach R. P., Kellerhals T., Luzi S., Zwank L., Angst W., and Haderlein S. B., 2004b. Mechanisms and Products of Surface-Mediated Reductive Dehalogenation of Carbon Tetrachloride by Fe(II) on Goethite. *Environ. Sci. Technol.* **38**, 2058-2066.

Fischer W. R., 1973. Die Wirkung von zweiwertigem Eisen auf Lösung und Umwandlung von Eisen(III)-Hydroxiden. In: Schlichting E. and Schwertmann U. Eds.), *Pseudogley & Gley*. Verlag Chemie GmbH, Weinheim.

Fischer W. R., 1983. Theoretische Betrachtungen zur reduktiven Auflösung von Eisen(III)-oxiden. *Zeitschrift für Pflanzenernährung und Bodenkunde* **146**, 611-622.

Francesconi K. A. and Kuehnelt D., 2002. Arsenic Compounds in the Environment. In: Frankenberger J., William T. (Ed.), *Environmental Chemistry of Arsenic*. Marcel Dekker, Inc., New York.

Fredrickson J. K., Zachara J. M., Kennedy D. W., Dong H., Onstott T. C., Hinman N. W., and Li S.-m., 1998. Biogenic iron mineralization accompanying the dissimilatory reduction of hydrous ferric oxide by a groundwater bacterium. *Geochim. Cosmochim. Acta* **62**, 3239-3257.

Fredrickson J. K., Zachara J. M., Kennedy D. W., Kukkadapu R. K., McKinley J. P., Heald S. M., Liu C., and Plymale A. E., 2004. Reduction of TcO_4^- by sediment-associated biogenic Fe(II). *Geochim. Cosmochim. Acta* **68**, 3171-3187.

Gálvez N., Barrón V., and Torrent J., 1999. Effect of Phosphate on the Crystallization of Hematite, Goethite, and Lepidocrocite from Ferrihydrite. *Clays Clay Miner.* **47**, 304-311.

Grafe M., Eick M. J., and Grossl P. R., 2001. Adsorption of Arsenate (V) and Arsenite (III) on Goethite in the Presence and Absence of Dissolved Organic Carbon. *Soil Sci. Soc. Am. J.* **65**, 1680-1687.

Haderlein S. B. and Pecher K., 1998. Pollutant reduction in heterogeneous Fe(II)/Fe(III) systems. In: Sparks D. L. and Grundl T. Eds.), *Kinetics and Mechanisms of Reactions at the Mineral/Water Interface*. American Chemical Society, Washington, DC.

Hansel C. M., Benner S. G., and Fendorf S., 2005. Competing Fe(II)-Induced Mineralization Pathways of Ferrihydrite. *Environ. Sci. Technol.* **39**, 7147-7153.

Hollemann A. F. and Wiberg E., 1985. *Lehrbuch der Anorganischen Chemie*. Walter de Gruyter, Berlin, New York.

Hopenhayn C., 2006. Arsenic in Drinking Water: Impact on Human Health. *Elements* **2**, 103-107.

Hosse M. and Wilkinson K. J., 2001. Determination of Electrophoretic Mobilities and Hydrodynamic Radii of Three Humic Substances as a Function of pH and Ionic Strength. *Environ. Sci. Technol.* **35**, 4301-4306.

Hug S. J., Leupin O. X., and Berg M., 2008. Bangladesh and Vietnam: Different Groundwater Compositions Require Different Approaches to Arsenic Mitigation. *Environ. Sci. Technol.* **42**, 6318-6323.

Kappler A. and Straub K. L., 2005. Geomicrobiological cycling of iron. In: Banfield J. F., Cervini-Silva J., and Nealson K. M. Eds.), *Molecular Geomicrobiology*. The Mineralogical Society of America, Chantilly, Virginia, USA.

Liger E., Charlet L., and Van Cappellen P., 1999. Surface catalysis of uranium(VI) reduction by iron(II). *Geochim. Cosmochim. Acta* **63**, 2939-2955.

Lovley D. R. and Phillips E. J. P., 1988. Novel Mode of Microbial Energy Metabolism: Organic Carbon Oxidation Coupled to Dissimilatory Reduction of Iron or Manganese. *Appl. Environ. Microbiol.* **54**, 1472-1480.

Lovley D. R., Holmes D. E., and Nevin K. P., 2004. Dissimilatory Fe(III) and Mn(IV) Reduction, *Adv. Microb. Physiol.* Academic Press.

Lovley D. R., Coates J. D., Blunt-Harris E. L., Phillips E. J. P., and Woodward J. C., 1996. Humic substances as electron acceptors for microbial respiration. *Nature* **382**, 445-448.

Marsili E., Baron D. B., Shikhare I. D., Coursolle D., Gralnick J. A., and Bond D. R., 2008. *Shewanella* secretes flavins that mediate extracellular electron transfer. *Proc. Natl. Acad. Sci. USA* **105**, 3968–3973.

Masscheleyn P. H., Delaune R. D., and Patrick Jr. W. H., 1991. Effect of Redox Potential and pH on Arsenic Speciation and Solubility in a Contaminated Soil. *Environ. Sci. Technol.* **25**, 1414-1419.

Meng X., Korfiatis G. P., Christodoulatos C., and Bang S., 2001. Treatment of arsenic in Bangladesh well water using a household co-precipitation and filtration system. *Water Res.* **35**, 2805-2810.

Michel F. M., Ehm L., Antao S. M., Lee P. L., Chupas P. J., Liu G., Strongin D. R., Schoonen M. A. A., Phillips B. L., and Parise J. B., 2007. The Structure of Ferrihydrite, a Nanocrystalline Material. *Science* **316**, 1726-1729.

Myers C. R. and Nealson K. H., 1988. Bacterial Manganese Reduction and Growth with Manganese Oxide as the Sole Electron Acceptor. *Science* **240**, 1319-1321.

Norra S., Berner Z. A., Agarwala P., Wagner F., Chandrasekharam D., and Stüben D., 2005. Impact of irrigation with As rich groundwater on soil and crops: A geochemical case study in West Bengal Delta Plain, India. *Appl. Geochem.* **20**, 1890-1906.

Nriagu J. O., 2002. Arsenic Poisoning Through the Ages. In: Frankenberger W. T. J. (Ed.), *Environmental Chemistry of Arsenic*. Marcel Dekker, Inc., New York.

Oscarson D. W., Huang P. M., and Liaw W. K., 1980. The Oxidation of Arsenite by Aquatic Sediments. *J Environ Qual* **9**, 700-703.

Polizzotto M. L., Kocar B. D., Benner S. G., Sampson M., and Fendorf S., 2008. Near-surface wetland sediments as a source of arsenic release to ground water in Asia. *Nature* **454**, 505-508.

Polizzotto M. L., Harvey C. F., Li G., Badruzzman B., Ali A., Newville M., Sutton S., and Fendorf S., 2006. Solid-phases and desorption processes of arsenic within Bangladesh sediments. *Chem. Geol.* **228**, 97-111.

Postma D., Larsen F., Minh Hue N. T., Duc M. T., Viet P. H., Nhan P. Q., and Jessen S., 2007. Arsenic in groundwater of the Red River floodplain, Vietnam: Controlling geochemical processes and reactive transport modeling. *Geochim. Cosmochim. Acta* **71**, 5054-5071.

Roden E. E., 2003. Diversion of Electron Flow from Methanogenesis to Crystalline Fe(III) Oxide Reduction in Carbon-Limited Cultures of Wetland Sediment Microorganisms. *Appl. Environ. Microbiol.* **69**, 5702-5706.

Roden E. E. and Zachara J. M., 1996. Microbial Reduction of Crystalline Iron(III) Oxides: Influence of Oxide Surface Area and Potential for Cell Growth. *Environ. Sci. Technol.* **30**, 1618-1628.

Royer R. A., Burgos W. D., Fisher A. S., Unz R. F., and Dempsey B. A., 2002a. Enhancement of Biological Reduction of Hematite by Electron Shuttling and Fe(II) Complexation. *Environ. Sci. Technol.* **36**, 1939-1946.

Royer R. A., Burgos W. D., Fisher A. S., Jeon B. H., Unz R. F., and Dempsey B. A., 2002b. Enhancement of Hematite Bioreduction by Natural Organic Matter. *Environ. Sci. Technol.* **36**, 2897-2904.

Sadiq M., 1997. Arsenic chemistry in soils: An overview of thermodynamic predictions and field observations. *Water, Air, Soil Pollut.* **93**, 117-136.

Schwertmann U., 1991. Solubility and dissolution of iron oxides. *Plant Soil* **130**, 1-25.

Scott D. T., McKnight D. M., Blunt-Harris E. L., Kolesar S. E., and Lovley D. R., 1998. Quinone Moieties Act as Electron Acceptors in the Reduction of Humic Substances by Humics-Reducing Microorganisms. *Environ. Sci. Technol.* **32**, 2984-2989.

Simpson A., Kingery W., Hayes M., Spraul M., Humpfer E., Dvortsak P., Kerssebaum R., Godejohann M., and Hofmann M., 2002. Molecular structures and associations of humic substances in the terrestrial environment. *Naturwissenschaften* **89**, 84-88.

Smedley P. L. and Kinniburgh D. G., 2002. A review of the source, behaviour and distribution of arsenic in natural waters. *Appl. Geochem.* **17**, 517-568.

Stevenson F. J., 1994. *Humus Chemistry - Genesis, Composition, Reactions.* John Wiley & Sons, Inc., New York.

Swartz C. H., Blute N. K., Badruzzman B., Ali A., Brabander D., Jay J., Besancon J., Islam S., Hemond H. F., and Harvey C. F., 2004. Mobility of arsenic in a Bangladesh aquifer: Inferences from geochemical profiles, leaching data, and mineralogical characterization. *Geochim. Cosmochim. Acta* **68**, 4539-4557.

Thamdrup B., 2000. Bacterial manganese and iron reduction in aquatic sediments. In: Schink B. (Ed.), *Adv. Microb. Ecol.* Kluwer Academic/ Plenum Publishers, New York.

Tufano K. J. and Fendorf S., 2008. Confounding Impacts of Iron Reduction on Arsenic Retention. *Environ. Sci. Technol.* **42**, 4777-4783.

van der Giessen A. A., 1966. The structure of iron (III) oxide-hydrate gels. *Journal of Inorganic and Nuclear Chemistry* **28**, 2155-2156.

Voet D. and Voet J. G., 1992. *Biochemie*. VCH Verlagsgesellschaft mbH, Weinheim, New York, Basel, Cambridge, Tokyo.

von Canstein H., Ogawa J., Shimizu S., and Lloyd J. R., 2008. Secretion of Flavins by *Shewanella* Species and Their Role in Extracellular Electron Transfer. *Appl. Environ. Microbiol.* **74**, 615-623.

Weber K. A., Achenbach L. A., and Coates J. D., 2006. Microorganisms pumping iron: anaerobic microbial iron oxidation and reduction. *Nat. Rev. Microbiol.* **4**, 752-764.

Zachara J. M., Kukkadapu R. K., Fredrickson J. K., Gorby Y. A., and Smith S. C., 2002. Biomineralization of Poorly Crystalline Fe(III) Oxides by Dissimilatory Metal Reducing Bacteria (DMRB). *Geomicrobiol. J.* **19**, 179-207.

2

Influence of iron mineral concentrations and aggregate formation on 2-line ferrihydrite reduction by *Shewanella oneidensis* MR-1

ABSTRACT

Microbial iron reduction rates are determined by the provided mineral surface area, the redox potential of the mineral and its solubility. Ferrihydrite, a poorly ordered Fe(III) hydroxide and an easy available electron acceptor for bacteria makes an exception to this. The unsolved structure and the hydrated state of this iron mineral make predictions difficult which physicochemical properties determine microbial reduction rates and mineral transformation.

Estimations of aggregate dimensions revealed the transition from non-surface limited growth of the iron-reducing bacteria to the point where the available mineral surface area was completely covered with cells. The initially present amount of ferrihydrite determined whether this threshold value was crossed during Fe(III) consumption by bacteria. Furthermore the Fe(III) mineral concentration determined microbial reduction rates and thereby the identity of minerals formed and the extent of reduction. We observed that high concentrations of 2-line ferrihydrite (30 mM or higher) lead to magnetite and goethite formation, fast Fe(II) formation rates, and incomplete microbial reduction of Fe(III), whereas lower concentrations (approx. 5 mM) allowed complete reduction of the Fe(III) at slower rates and no precipitate formation. Time dependent μ-XRD analysis and sequential extractions showed no further mineral transformation once a certain mineral was formed.

In this study we demonstrate that the concentration of Fe(III) minerals during microbial Fe(III) reduction strongly influenced the reduction rates and the mineralogy of the reduction products. This suggests strong influence on the biogeochemical iron cycle in environmental systems not only depending on pH, solute chemistry, microbial strains, reduction mechanisms involved and the identity of initially present minerals.

1. INTRODUCTION

Iron is widely distributed in the environment and plays an important role in the biogeochemical cycling of nutrients (e.g. phosphate) and metal(loid) ions (e.g. arsenic). A large proportion of iron redox transformations is due to iron metabolizing microorganisms. Bacteria are capable of gaining energy by aerobic or anaerobic oxidation of Fe(II) as well as by reduction of Fe(III) (Straub et al., 2001; Lovley et al., 2004; Kappler and Straub, 2005; Weber et al., 2006). These redox processes lead either to the dissolution of iron minerals or to the formation of new iron mineral precipitates (Roden and Zachara, 1996; Kappler and Newman, 2004; Lovley et al., 2004). This in turn can promote either the release of bound nutrients and metal(loid) ions during mineral dissolution or the sequestration of these compounds during mineral formation. Members of the genera *Shewanella* and *Geobacter* have been found to be the dominating species in environments promoting microbial iron reduction (Thamdrup, 2000; Lovley et al., 2004). The metabolic versatility of the facultative anaerobic *Shewanella* strains makes them good candidates for environments with alterable natural conditions such as sediments or soils (Hau and Gralnick, 2007).

The microbial utilization of various Fe(III) oxides and hydroxides depends on their solubility and thus their crystallinity (Bonneville et al., 2004). While the more crystalline Fe(III) minerals such as goethite, akaganeite, hematite and magnetite are reduced at low rates and only to a smaller extent, the poorly crystalline ferric hydroxide, ferrihydrite, is reduced in substantial amounts, e.g. by *Geobacter metallireducens* (Lovley and Phillips, 1988). Directly correlated with crystallinity is the redox potential for different iron oxides at neutral pH (25°C) that decreases from +/-0 to -314 mV in descending order for ferrihydrite > lepidocrocite > goethite > hematite > magnetite (Thamdrup, 2000). As a consequence, these minerals become more and more unfavourable towards microbial reduction. Depending on the present electron donor, e.g. acetate (E_0'(CO_2/acetate) = -290 mV), thermodynamics can even preclude iron reduction coupled to the oxidation of a particular organic substrate because of the lacking electrochemical driving force.

The crystallinity of the iron oxides determines not only the redox potential but also the surface area available for microbial access. Previous studies demonstrated the correlation between the available surface area of utilized iron oxides and the rates of Fe(II) formation (Roden and Zachara, 1996). Especially in case of ferrihydrite the effectively accessible surface area for the bacteria in mineral suspension cultures is unknown. The assumed surface area spans from BET-measurements of the dehydrated mineral to theoretic, modelled values representing small nano particles (Roden and Zachara, 1996). It has been shown previously that even for goethite, a well crystalline iron oxyhydroxide, surface area determination of particles in the dry state cannot represent the conditions in suspended form (Liu et al., 2001; Cwiertny et al., 2008). The aggregation significantly influenced the number of available surface sites either for sorption of Fe(II) and reactive pollutant transformation (Cwiertny et al., 2008) or for the microbial Fe(III) reduction (Liu et al., 2001).

The identity and properties of the mineral products formed during microbial iron reduction are of interest because: (1) Fe(III) reduction leads to dissolution of nutrient- or toxic metal-bearing minerals (e.g. Cr, As, P (Arai and Sparks, 2001; Islam et al., 2004)), (2) Fe(III) reduction forms reactive iron minerals that have been shown to reduce inorganic (e.g. Cr, U (Buerge and Hug, 1999; Jeon et al., 2005)) and organic pollutants (e.g. carbon tetrachloride, nitro aromatic compounds (Elsner et al., 2004; Borch et al., 2005)) and (3) new formed precipitates can sequester toxic elements (e.g. As (Herbel and Fendorf, 2006; Kocar et al., 2006)). Fe(II)-bearing minerals form by a reaction of the microbially produced ferrous iron with available anions (e.g. carbonate or phosphate), or with remaining Fe(III) phases leading to the formation of mixed-valent Fe(II)-Fe(III) species such as magnetite or green rusts. The formation of certain mineral phases during microbial iron reduction is not depending on a specific microbial strain but rather on the geochemical conditions present during their formation (Konhauser, 1997; Mann, 2001). Presence of bicarbonate or phosphate either lead to preferential formation of siderite (Fredrickson et al., 1998) or green rust and vivianite (Hansel et al., 2003; Borch et al., 2007), depending on the concentration of these anions. In absence of these two anions additionally lepidocrocite (Fredrickson et al., 2003), goethite and

magnetite (Hansel et al., 2003; Kukkadapu et al., 2004; Borch et al., 2007), have been identified as products of microbial Fe(III) reduction. The rate of Fe(II) formation and therefore the amount of Fe(II) present triggers the solid transformation of ferrihydrite to either goethite or magnetite (Zachara et al., 2002; Coker et al., 2008). According to their mineralogy and surface area, iron oxides differ in reactivity and sorption capacity. Therefore identification of the mineral phases formed during microbial Fe(III) reduction is fundamental to predict possible secondary reactions in the environment such as pollutant degradation and nutrient sequestration. In most former studies, the mineral phases have been identified at the end points of reduction (Fredrickson et al., 1998; Fredrickson et al., 2003; Hansel et al., 2004; Behrends and Van Cappellen, 2007; Borch et al., 2007; Zegeye et al., 2007). However, in order to evaluate secondary processes potentially occurring as a consequence of microbial Fe(III) reduction in the environment, also transient mineral phases have to be identified.

The goal of our study therefore was to identify iron minerals at different stages of dissimilatory ferrihydrite reduction by *Shewanella oneidensis* MR-1 and identify rate- and mineralogy-determining factors. At the different time points, minerals were identified and quantified by sequential extractions, μ-XRD and Moessbauer measurements.

2. EXPERIMENTAL PROCEDURES

2.1. Bacterial cultures and experimental setup

Shewanella oneidensis strain MR-1, originally isolated from Oneida Lake, New York (Myers and Nealson, 1988) was provided by Jeff Gralnick (Univ. Minnesota). We chose this strain as our model strain since it is well characterized (full genome sequence available, see Heidelberg et al. (2002)), easy to cultivate and it is able to utilize a broad variety of different substrates (Nealson and Myers, 1990; Venkateswaran et al., 1999). Aerobic cultures on LB-medium agar plates were streaked out from a frozen stock kept at -80°C. LB-medium contained (per l): 10 g tryptone, 5 g yeast extract and 5 g NaCl (for LB plates 12 g agar was added). LB-plates were incubated at 28°C for approximately 24 h and afterwards kept at 4°C for up to 10 days. For liquid cultures, 50 ml of liquid LB medium in a 200 ml Erlenmeyer flask were inoculated with a single colony from the LB-plate. The capped flask was incubated oxically at 28°C on a rotary shaker at 150 rpm. Cell concentration in LB-cultures was determined by optical density (OD) measurements at 600 nm. OD_{600} was calibrated against cell counts obtained by direct counting with a Thoma-chamber by light microscopy (Axioscope 2, Zeiss, Germany) as well as against protein content (procedure see below). At the end of exponential growth, cells had consumed O_2 completely and switched to anaerobic metabolism (Lies et al., 2005).

Fe(III) reduction experiments were done in LML medium (Myers and Myers, 1994), containing 12 mM HEPES buffer and 30 mM lactate as electron donor, adjusted to pH 7 and prepared sterilely and anoxically using a Widdel flask. Inoculum for experiments was prepared as follows: 2 ml of LB-grown cell culture were harvested after 14 h at late exponential growth phase and centrifuged (5 min, 10 600 g). Cells were washed twice with LML medium, resuspended in 2 ml of medium and diluted to a final concentration of $2*10^5$ cells/ml in the culture tubes containing LML medium.

To monitor Fe(II) and mineral formation during microbial Fe(III) reduction, approximately 30 tubes per experiment were set up in parallel (depending on the determined parameters and test duration). Sterile culture tubes (total volume 23 ml) were filled with 9 ml (cultures

containing 5 mM ferrihydrite) or 6 ml (cultures containing 30 or 60 mM ferrihydrite) of anoxic LML-medium. The headspace was exchanged with N_2 and the tubes were sealed with butyl rubber stoppers. For sample treatments in the glove box (mineral preparation, sequential extraction) smaller culture tubes (total volume 17 ml) were used which were closed with a thin butyl rubber stopper and a screw cap. Finally, ferrihydrite suspension, HA solution or phosphate buffer solution, and the cells were injected with syringes and the tubes were incubated horizontally at 28°C in the dark.

At sampling time points selected tubes were sacrificed to determine the protein content, measure total Fe(II) and Fe(III) concentrations by acid digestion, to collect mineral samples or for sequential extraction of iron minerals. Complete digestion of the biogenic solids was necessary in order to determine the total iron amount including precipitates that stuck to the glass wall of the tubes and avoiding inhomogeneous sampling with syringes. Experiments were performed at least twice. In order to calculate the maximum reduction rates, total Fe(II) concentrations were plotted against time. A linear regression was calculated to derive the maximum slope for Fe(III) reduction rates.

2.2. Preparation of ferrihydrite

2-line ferrihydrite was synthesized according to Schwertmann and Cornell (2000) and Raven et al. (1998) using 40 g of $Fe(NO_3)_3*9H_2O$ per 500 ml water that was neutralized with 1 M KOH to a final pH not higher than 7.5. After centrifugation and 4 times washing with Millipore®-water, the wet solid was resuspended in water to an approximate concentration of 0.5 M Fe(III). This suspension was stored in the dark in serum bottles and tightly closed with a butyl rubber stopper. Deoxygenation under vigorous stirring was done by alternating application of vacuum and N_2 10 min each and in total three times. The mineral product was identified by μ-XRD after freeze-drying of an aliquot. Since we observed the formation of crystalline mineral phases (hematite) after autoclaving the ferrihydrite suspension or storing it for longer than 3 months (data not shown), suspensions used for this study were not sterilized and used within 2 months after synthesis for

experiments. N_2-BET measurements after freeze-drying yielded surface areas of the ferrihydrite between 240-280 m²/g.

2.3. Sampling

In order to determine total concentrations of Fe(III) and Fe(II) (see below) during microbial iron reduction, culture tubes were sacrificed at different time points and the minerals in the tubes were completely dissolved by adding 2.25 ml (cultures with 5 mM ferrihydrite) or 3 ml (30 or 60 mM ferrihydrite) of 12 M HCl to the culture.

Samples for Moessbauer spectroscopy, X-ray diffraction (XRD) and sequential extraction were prepared in an anoxic glove box (Braun, Germany; N_2 atmosphere) harvesting one screw-cap culture tube for each treatment. The samples were transferred stepwise into 2 ml-Eppendorf® tubes and centrifuged (2 min, 9 700 g). Subsamples of the supernatant were kept in the glove box and analyzed for dissolved Fe(II) and Fe(tot) (see below). The remaining solids were prepared for Moessbauer measurements, dried for XRD or treated with the sequential extraction method.

2.4. Sequential extraction

The protocol for sequential iron mineral extraction was modified after Roden and Zachara (1996). Loosely bound Fe(II) was extracted by a 1 M sodium acetate solution (pH 5). Vivianite and poorly crystalline ferrihydrite were dissolved in 0.5 M HCl whereas goethite, magnetite and hematite (crystalline minerals) were dissolved in 6 M HCl. Control experiments (data not shown) showed that siderite was dissolved already partly in the acetate extraction solution and gets completely dissolved in 0.5 M HCl.

Solutions for the extraction steps performed in the glove box were bubbled with N2 (30 min) before they were brought into the glove box. For the first extraction step 1.5 ml anoxic sodium acetate solution were added to the precipitates (separated by centrifugation) of one culture tube. The precipitates were resuspended using a vortexer and incubated for 24 h in the dark. The mixture was centrifuged (2 min, 9 700 g) and the supernatant was kept for Fe analysis (see below). Subsequently the residual solid was extracted with 1.5 ml of anoxic 0.5 M HCl. After 2 h

of incubation (in the dark) the mixture was centrifuged again and the supernatant was kept for Fe analysis (see below). The remaining solids were incubated in 1.5 ml of 6 M HCl at 70°C in a water bath for 30 min outside the glove box. The extract was then analyzed for the Fe content (see below).

2.5. Protein determination

For determination of protein contents 3 ml of culture were withdrawn sterile from tubes and kept at -28°C until measurement. After thawing, iron precipitates were dissolved by adding 600 µl of 6 M HCl and incubation at 37°C for 30 min or 10 min at 95°C according to the solubility of the formed precipitates. Protein was precipitated out adding 150 µl of 6 M trichloro acetic acid and incubation on ice for 30 min. After centrifugation (15 min, 20 800 g) the remaining pellet was dissolved in 500 µl 0.1 M NaOH and cooked for 5 min. These samples were analyzed using the Bradford method using the standard protocol of the BIORAD® micro assay for microtiter plates and determining the ratio of absorbances at 590 nm/450 nm measured with a plate reader (FlashScan 550 microplate reader, Analytik Jena AG, Germany).

2.6. Analytical methods

Dissolved Fe(II) was quantified using the ferrozine assay (Stookey, 1970). In order to measure total iron (Fe(tot)) concentrations, aliquots were reduced with 10% w/v $NH_2OH*HCl$ dissolved in 1 M HCl. Fe(II) and Fe(tot) samples were mixed with a 0.1% (w/v) solution of ferrozine in 50% (w/v) of ammonium acetate buffer. Absorbance was measured at 562 nm in microtiter plates with a plate reader (FlashScan 550 microplate reader, Analytik Jena AG, Germany).

Surface area of iron minerals was determined by the Brunau-Emmett-Teller (BET) method with a Gemini 2375 Surface Area Analyzer (Micromeritics, Germany) with N_2 as adsorbing gas. Dry mineral samples were degassed for 30 min under vacuum at 105°C, before measuring a five-point-BET-curve.

Size distribution of ferrihydrite aggregates was determined by a particle size analyzer (Mastersizer Micro, Malvern, UK), in a range from 0.3 μm to 300 μm. The volumetric particle size distribution of mineral suspensions was calculated from scatter patterns of a helium-neon laser.

For Moessbauer spectroscopic analysis, wet mineral samples were sealed between layers of Kapton® tape in the glove box. Samples were mounted in a close-cycle exchange-gas cryostat (Janis, USA) that allowed cooling of the sample to 4.2 K. Moessbauer spectra were collected with a constant acceleration drive system in transmission mode and with a ^{57}Co source. Spectra were calibrated against a spectrum of alpha-Fe metal foil collected at room temperature. Spectra calibration and fitting was performed with Recoil software (University of Ottawa, Canada) using Voight based spectral lines.

For μ-X-ray diffraction (μ-XRD) analyses, dried precipitates were prepared in the glove box. The solids were grinded in an agate mortar, suspended in approximately 50 μl of N_2-flushed ethanol and transferred with a glass pipette into small indentations (diameter 2 mm) on a silicon wafer. After evaporation of the ethanol, the samples were covered with a piece of clear plastic wrap (polyethylene) which remains oxygen tight for approximately 45 min. Samples were kept anoxic until measurement. The μ-XRD-device (Bruker D8 Discover X-ray diffraction instrument, Bruker AXS GmbH, Germany) consists of a Co K_α X-ray tube, operating at 30 kV, 30 mA, which is either connected to a polycapillary that allows measurements at a spot diameter of 50 μm or a monocapillary with a spot diameter of 300 μm. Each sample was measured in three overlapping frames of 30° 2θ, within 1 min measuring time for each frame, using a GADDS® area detector. The EVA® 10.0.1.0 software was used to merge the three measured frames of one sample and to identify the containing mineral phases using the PDF-database licensed by ICDD (International Centre for Diffraction Data). X-ray diffractograms show a broad signal in a 2θ range from 17° to 29°, originating from the foil which was used to protect the samples from oxidation. In this range and at smaller angels the intensity of the X-rays diffracted by the mineral lattice is reduced, due to the foil.

2.7. Electron microscopy

For scanning electron microscopy (SEM), subsamples from culture tubes were taken. Sample preparation including fixation and critical point drying were described elsewhere (Schadler et al., 2008). Samples were imaged with a Zeiss Gemini 1550VP FE-SEM and a Zeiss Gemini 1540XB FIB/FE-SEM.

3. RESULTS AND DISCUSSION

In order to investigate the influence of mineral concentration on reduction rates, extent of reduction and identity of mineral products formed during reduction, the iron reducing strain *Shewanella oneidensis* MR-1 was incubated with different concentrations of 2-line ferrihydrite.

3.1. Rates of microbial ferrihydrite reduction

Maximum rates of ferrihydrite reduction increased from 5 to 30 mM ferrihydrite and levelled off at higher concentrations with a maximum reduction rate of approx. 4 mmol Fe(II)/(l*d) (Fig. 1). The fact, that the maximum reduction rates increased with increasing ferrihydrite concentrations and levelled off at higher concentrations indicates a limitation by mineral surface area and allows conclusions about a possible reduction mechanism.
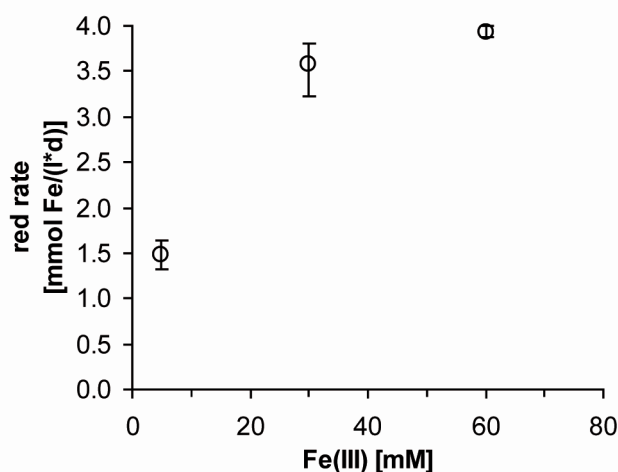

Fig. 1 Maximum Fe(III) reduction rates for *Shewanella oneidensis* MR-1 at different concentrations of 2-line ferrihydrite. Error bars indicate maximum and minimum rates of replicate experiments (n=4 for 5 mM, n=3 for 30 mM, n=2 for 60 mM).

In case of a mineral surface insufficiency the surface saturation by attached cells is reached during cell proliferation and the ongoing iron reduction. In this case the electron transfer from the cells to the mineral is limited to the number of cells in direct contact to the mineral surface. Then reduction rates do not reach maximum possible values. This effect was shown in our experiments (Fig. 1) by increasing the ferrihydrite concentration from 5 to 30, to 60 mM ferrihydrite. Finally one

conclusion would be the necessity of direct contact between cells and the mineral surface for the efficient electron transfer to Fe(III).

In contrast to this *Shewanella oneidensis* MR-1 was also described being able to reduce Fe(III) minerals at a distance (Lies et al., 2005). Newman and Kolter (2000) hypothesized that quinone compounds may be involved as electron shuttle between cells and Fe(III) minerals. This hypothesis was recently supplemented in studies by von Canstein et al. (2008) and Marsili et al. (2008) who demonstrated excretion of redox-active flavin compounds by a number of *Shewanella sp.* The ability to accelerate the reduction of poorly crystalline Fe(III) oxide was demonstrated in biotic and abiotic experiments (von Canstein et al., 2008).

In addition to the shuttling hypothesis, which was not supported by our own data, it was also suggested that in some cases direct contact of the cells to the mineral surface is necessary to reduce solid Fe(III) minerals. Ruebush et al. (2006) demonstrated the necessity of outer membrane cytochromes for iron mineral reduction by *Shewanella oneidensis* MR-1. These cytochromes may be localized at the cell surface or even included within conductive pili which were suggested to be used for the electron transfer between bacteria and the mineral surface (Gorby et al., 2006). These filament-like structures of about tens of microns length require at least close proximity of the cells to the mineral surface. If this is the case, the availability of sufficient surface area for the number of present cells would be a limiting factor for the reduction of the Fe(III) mineral, as it was shown under our experimental conditions.

Estimating the available surface area in microbial ferrihydrite reduction experiments, however, is not trivial. Surface area determination of ferrihydrite by methods like BET measurements or adsorption techniques in suspension depend on the accessibility of porous structures by adsorbents, on ferrihydrite synthesis, pretreatment (e.g. freeze drying, heating) and storage of the iron mineral before BET-measurements (Davis and Leckie, 1978; Stanjek and Weidler, 1992; Weidler, 1997; Cornell and Schwertmann, 2003). Surface areas determined for synthetic ferrihydrite show a wide distribution

(100-700 m²/g) and also natural ferrihydrite samples yield ranges of 200-400 m²/g (Cornell and Schwertmann, 2003). The highest values were obtained by mathematical derivation. Assuming a crystallite size of <10 nm for ferrihydrite (van der Giessen, 1966; Michel et al., 2007), a specific surface area of approximately 600 m²/g was estimated (Davis and Leckie, 1978). However, the nm-sized primary particles tend to form larger aggregates (Cornell and Schwertmann, 2003) especially under pH conditions close to the point of zero charge of the mineral (ferrihydrite: 7.9-7.8; Cornell and Schwertmann, 2003) which is actually the case under proper growth conditions for neutrophilic bacteria. The resulting porous structure of the aggregates provides limited access for μm-sized bacteria. Therefore not the nm-sized primary particles but rather these aggregates should be considered to estimate the bioavailable surface area for microbiological experiments like the ones presented in this study.

Size distribution of suspended ferrihydrite particles determined by laser scattering measurements showed a range of aggregate sizes with an average size of 20 μm (Fig. 2a). Using a ferrihydrite aggregate size of 20 μm and assuming a spherical shape, the surface area present in cultures containing 5, 30 or 60 mM ferrihydrite was calculated to be 4.0×10^{-2}, 2.4×10^{-1}, and 4.9×10^{-1} m²/l, respectively. This is equal to a surface area of 0.08 m²/g ferrihydrite and thus significantly lower than the usually estimated surface area of several hundred m²/g.

Surface area of ferrihydrite aggregates exemplary for a concentration of 5 mM ferrihydrite

    ϱ (Fe(OH)$_3$) = 3.96 g/cm³ (Cornell and Schwertmann, 2003)
    M (Fe(OH)$_3$) = 106.88 g/mol
    Size of the aggregates (determined by laser scattering Fig. 2a):
        d_{agr} = 20 μm; r_{agr} = 10 μm

    Surface area of a spherical aggregate:
        $A_{agr} = 4 \times r_{agr}^2 \times \pi = 1.26 \times 10^{-9}$ m²
    Volume of one aggregate:
        $V_{agr} = 4/3 \times r_{agr}^3 \times \pi = 4.19 \times 10^{-15}$ m³
    Weight of one aggregate:
        $m_{agr} = \varrho \times V_{agr} = 1.66 \times 10^{-8}$ g = 0.17 ng

Molar ferrihydrite concentration in cultures:
$$c_{FH} = 5 \times 10^{-3} \text{ mol/l}$$
Mass-related ferrihydrite concentration:
$$c_{FHm} = c_{FH} \times M_{FH} = 0.53 \text{ g/l}$$
Aggregate concentration:
$$c_{agr} = c_{FHm}/m_{agr} = 3.22 \times 10^{7} \text{ [agr]/l}$$
Surface area concentration:
$$c_A = c_{agr} \times A_{agr} = 4.0 \times 10^{-2} \text{ m}^2/l$$

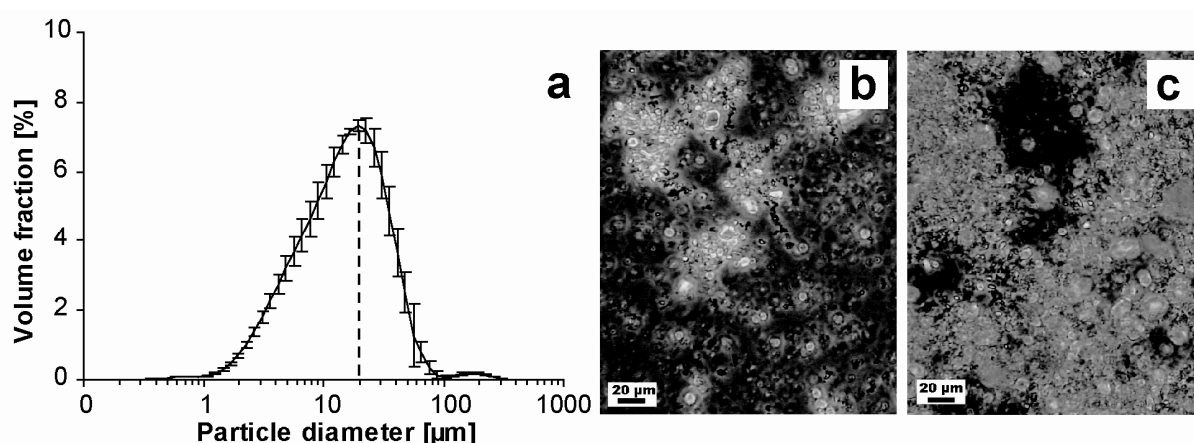**Fig. 2 (a) Size distribution of 2-line ferrihydrite aggregates in medium, determined by laser scattering, given in volume fractions [%]. (b, c) Light microscopy pictures of ferrihydrite aggregates (light, fuzzy particles) in medium with (b) 5 mM and (c) 30 mM. To preserve the shape of the aggregates no cover slide was used, resulting in multiple focusing planes.**

This approach still represents a rough estimation because aggregated particles show diverse sizes and have no smooth surface to which cells could easily attach (Fig. 2b and c), so the available surface area might be even smaller. These light microscopy pictures (Fig. 2b and c) and the sedimentation rate of the mineral aggregates (Fig. 3) in absence of cells suggest that depending on the ferrihydrite concentration the size of the aggregates varies. The interaction of cells and mineral aggregates in our experiments was investigated shortly after inoculation by staining the cells with a fluorescent dye and visualization by confocal laser microscopy (data not shown). The pictures showed that all cells were attached to the mineral surface and no planktonic cells were present.
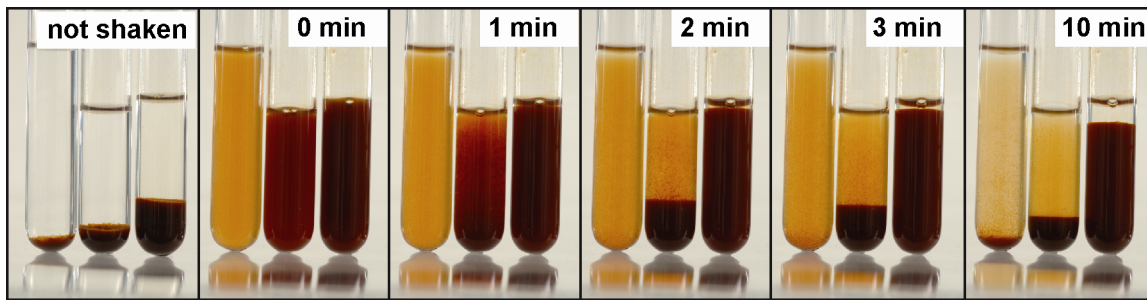
Fig. 3 Time series (0-10 min) of the sedimentation of 5 (left), 30(middle) and 60 mM 2-line ferrihydrite (right) in LML medium. Sedimentation in the 60 mM tube is slowest. The majority of the mineral aggregates settles down fast in the 30 mM setup. In presence of 5 mM ferrihydrite the particles sediment out slower, indicating a higher fraction of small particles.

In order to compare the available iron mineral surface area and the coverage by the initially present amount of cells we did the following calculation :

Calculation of the surface area possibly covered by cells
        Cell dimensions determined from an SEM-picture (Fig. 4a):
        length: 2 μm, width: 0.5 μm
        $A_{cell} = l \times w = 2 \, \mu m \times 0.5 \, \mu m = 1 \, \mu m^2 = 1 \times 10^{-12} \, m^2$
        $(1 \times 10^{-12} \, m^2/cell)$
        Cell number per ml: $n_{cells} = 2 \times 10^5$ cells/ml
        Surface area which potentially can be covered by cells:
        $c_A = A_{cells} \times n_{cells} = 2 \times 10^{-4} \, m^2/l$

With cell dimensions of $2 \times 0.5 \, \mu m$ (Fig. 4a) and an initial cell concentration of 2×10^5 cells/ml, a minimum surface area of $2 \times 10^{-4} \, m^2/l$ could be covered by MR-1 cells assuming a single layer coverage at the mineral surface. In reality this area might have been slightly larger because this does not include the possibility of contact between cell and mineral at more than one side of the cell. Nevertheless, when compared to the available mineral surface area, this calculation suggests that in all experiments (5, 30 and 60 mM ferrihydrite present initially) in the beginning, microbial Fe(III) reduction was not limited by available mineral surface area. Since the cell number increased due to cell growth and concomitantly ferrihydrite was consumed by reductive dissolution, the ratio of cell surface area per available ferrihydrite surface area changed over time.
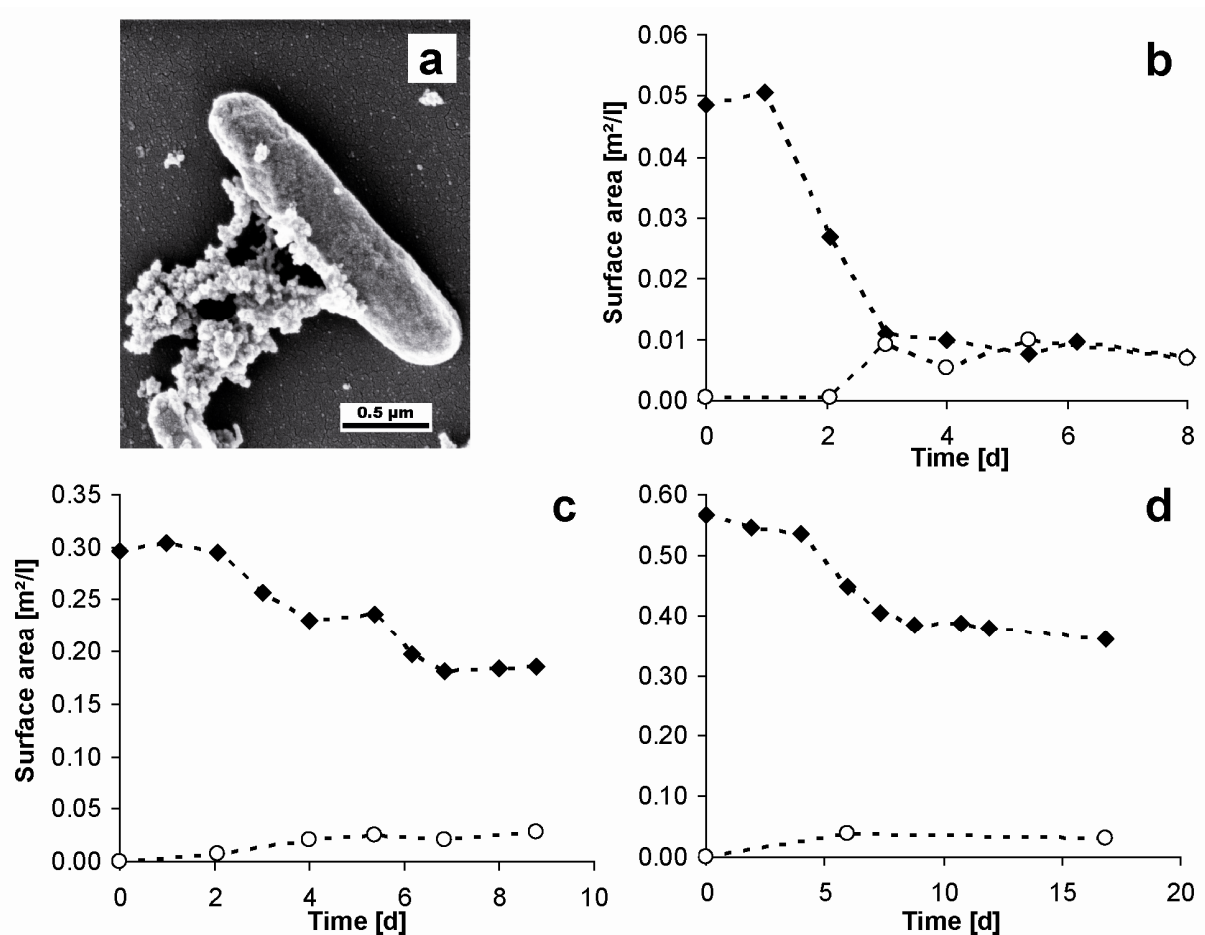
Fig. 4 (a) Representative SEM image of a fully grown cell after reduction of 2-line ferrihydrite. Temporal development of present surface area per volume [m²/l] of 2-line ferrihydrite aggregates (◆) and growing cells (○) during reduction of (b) 5 mM, (c) 30 and (d) 60 mM 2-line ferrihydrite by *Shewanella oneidensis* MR-1. Calculations were based on measured Fe(III) concentrations and cell numbers correlated to measured protein concentrations. Data points are connected as a guide to the eye.

An estimation of surface area development for ferrihydrite and cells, based on measured Fe(III) concentrations over time, showed that in experiments with 5 mM ferrihydrite after about three days (about 22% Fe(III) left, 9×10^5 cells/ml, calculated from protein measurements) the available mineral surface area equals the cell surface area leading to mineral surface area limitation (Fig. 4b). At ferrihydrite concentrations of 30 and 60 mM, no surface area limitation was reached during the reduction (Fig. 4c and d). As a consequence of the limiting mineral surface area in the 5 mM ferrihydrite experiment, assuming necessity of direct cell-mineral contact, the maximum reduction rate is

significantly lower compared to cultures with 30 and 60 mM ferrihydrite (Fig. 1).

However, it has to be considered that for experiments containing 30 or 60 mM ferrihydrite, the changes in mineral surface area cannot be simply derived from Fe(III) concentrations since for high ferrihydrite concentrations new Fe(III)-containing mineral phases were formed (e.g. magnetite, see section *3.4.*). In the presence of 5 mM ferrihydrite, however, Fe(III) was reduced and converted into dissolved Fe(II) by up to 80-90% without any secondary mineral formation (see section *3.3.*). Therefore the available surface area of the ferrihydrite decreased parallel to Fe(III) reduction. Additional evidence for the absence of a surface area limitation in cultures containing 30 or 60 mM ferrihydrite comes from the fact that despite the increase in ferrihydrite concentration we measured almost similar maximum reduction rates per day (Fig. 1).

This suggests that at these higher ferrihydrite concentrations not the mineral surface area but rather the number of cells is limiting. The effect of mineral surface saturation by attached cells has been described already by Roden (2003). Compared to the Fe(III) reduction rates determined in our study (1.5-4.0 mmol Fe(II)/(l*d)), Roden (2003) determined slightly lower rates (between 0.1-2.0 mmol Fe(II)/(l*d)), using 10 mM Fe(III) (surface areas of iron minerals: 10-600 m²/g) and demonstrated surface saturation at higher cell densities (5×10^8 cells/ml). However, it has to be considered that he used *Shewanella putrefaciens* strain CN32 in cell suspension experiments under non-growth conditions contrasting to our growth experiments with *Shewanella oneidensis* MR-1 where the number of cells increased during the course of the experiment.

3.2. Extent of microbial ferrihydrite reduction

Not only the rate but also the extent of mineral reduction showed a dependence on the initially present ferrihydrite concentration (Fig. 5). Providing low amounts of ferrihydrite (5 mM) and 2×10^5 cells/ml resulted in an almost complete (80-90%) reduction of Fe(III) to Fe(II) by the bacteria within 4 days. In contrast, the presence of 30 or 60 mM ferrihydrite led to incomplete reduction with approx. 40% total Fe(II) and 60% remaining Fe(III) after 5 and 9 days, respectively (Fig. 5).

These results confirm previous observations (Fredrickson et al., 2003) which also showed a decreasing extent of reduction for increasing ferrihydrite concentrations. However, in contrast to their study, our experiments showed a similar extent of reduction for 30 and 60 mM ferrihydrite whereas they observed a decrease in extent of reduction from 60 to 15% total Fe(II) formation (after 370 h) for increasing ferrihydrite concentrations from 25 to 100 mM. The fact that these authors used a different Fe(III)-reducing strain (*Shewanella putrefaciens* CN32), different cell numbers (2×10^8 cells/ml versus 2×10^5 cells/ml in our experiments), and a bicarbonate buffered medium (compared to the HEPES-buffered medium in our study) might be reasons for the observed differences. Another study with *Shewanella alga* BrY, incubated with tryptic soy broth, lactate and various iron oxides in different concentrations, showed after 30 days an extent of reduction between 40-50% in a concentration range of 1-200 mM amorphous Fe(III) gel (Roden and Zachara, 1996). This is in good agreement to our study (approx. 40% Fe(II) formation in 30 and 60 mM setups).
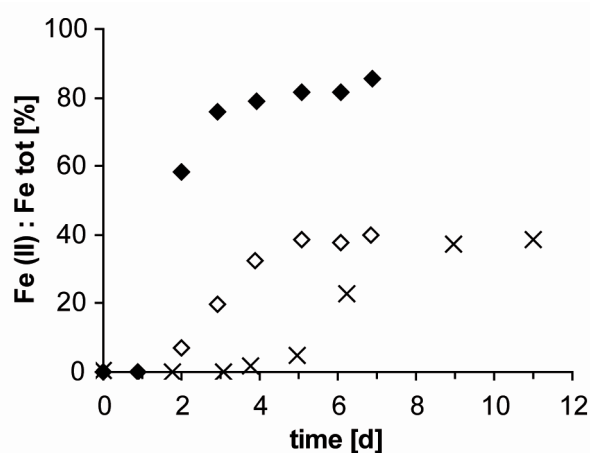

Fig. 5 Extent of Fe(III) reduction by *Shewanella oneidensis* MR-1 shown for representative experiments with 5 mM (◆), 30 mM (◇) and 60 mM (✕) 2-line ferrihydrite. Given in % of Fe(II) formed relative to total Fe.

Since different cell : mineral ratios lead to different surface coverage of the mineral particles the local concentration of cells differed with variation of the available mineral surface. Less coverage of the mineral surface has a "diluting effect" on the cell density in a local aspect. Due to a loss of direct contact between individual bacteria a threshold for quorum sensing mechanisms may be reached. The principle of quorum sensing is based on the excretion of signaling

compounds by the bacteria to sense each other. At increased concentrations of the signaling substance bacteria are aware of other cells nearby and initiate population beneficial processes, for example they can accelerate their metabolic activity. In our experiments an increase of the ferrihydrite concentration lead to longer lag phases before bacteria started reducing Fe(III) (Fig. 5). *Shewanella oneidensis* MR-1 was shown to be capable of quorum sensing (De Windt et al., 2003) and the sensing mechanisms between cells could either be hampered for example by the local "dilution effect". Adsorption of the signalling molecules to mineral surfaces was not shown in the literature so far (pers. communication with Jared Leadbetter 2007). Quorum sensing was intensively investigated in conjunction with formation of biofilms and especially its significance for pathogenic organisms (Keller and Surette, 2006). In contrast, there is very few know about the ecological significance and taxonomic distribution of this feature in the environment, as it influences metabolic activity of bacteria (Manefield and Turner, 2002).

3.3. Sequential extraction of minerals formed during microbial ferrihydrite reduction

To characterize the precipitates formed during biogenic Fe(III) reduction we focused on the two ferrihydrite concentrations which showed the greatest differences. A sequential extraction procedure was applied to quantify four different iron fractions: (I) dissolved, (II) loosely bound, (III) poorly crystalline precipitates and (IV) crystalline iron minerals. Fig. 6 shows concentrations normalized to the total iron concentration of sequential extractions of two microbial reduction experiments with 5 (Fig. 6a and b) and 30 mM (Fig. 6c and d) ferrihydrite, respectively. Fe(II) and Fe(III) recovery in the four different fractions at a certain time point correlated well with the total Fe(II) and Fe(III) concentrations determined in a separate tube, sacrificed in parallel (data not shown).

At a ferrihydrite concentration of 5 mM almost all formed Fe(II) remained in solution (82% of total iron) and was detectable in the supernatant (Fig. 6a). Finally, a minor fraction of 6% of the total iron was present as Fe(II) in the Na-acetate-extractable fraction. Residual Fe(III) (12%), representing ferrihydrite, was present in the fraction of

poorly crystalline iron minerals (Fig. 6b) after 6 days. During the course of reduction the Fe(III) concentration decreased in parallel to increasing Fe(II) concentrations. No formation of higher crystalline minerals was observed.
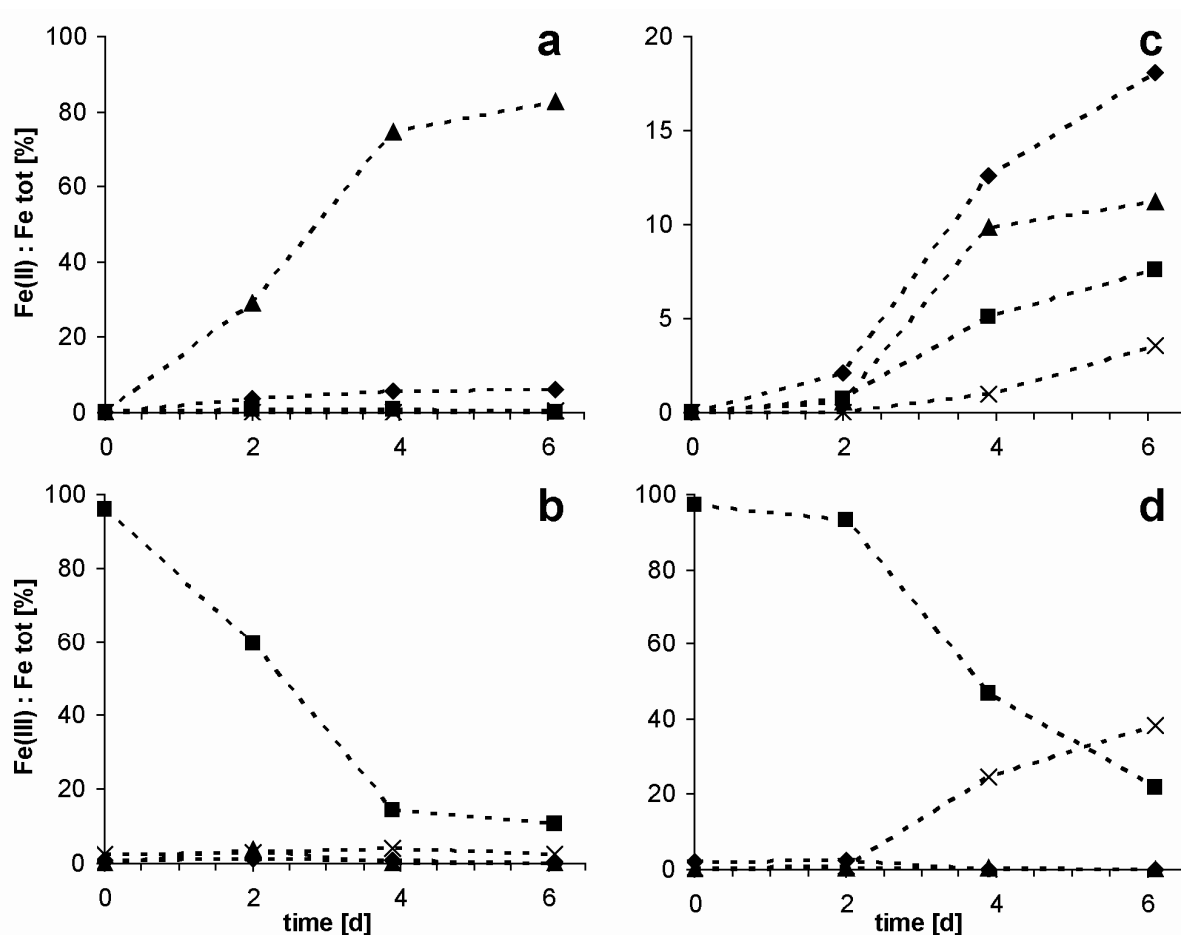

Fig. 6 Dissolved (▲), adsorbed (◆), poorly crystalline (■) and crystalline (✕) iron fractions separated by sequential extraction of precipitates formed during microbial reduction of (a, b) 5 mM and (c, d) 30 mM 2-line ferrihydrite in representative experiments. Concentrations are given in (a, c) percent of Fe(II) and (b, d) Fe(III) relative to the total iron concentration. Please note the different scale in panel c. Data points are connected as a guide to the eye.

In contrast to setups with 5 mM ferrihydrite, in experiments with 30 mM ferrihydrite, Fe(II) was detectable in all four fractions of dissolved, loosely bound, poorly crystalline and crystalline iron species (Fig. 6c), whereas Fe(III) (Fig. 6d) was detected in the poorly crystalline and crystalline mineral fraction only. The highest amount of Fe(II) (18%) after 6 days) was detectable in the fraction of loosely bound iron. 11%

of Fe(II) remained in solution, 8% were extracted with the poorly crystalline fraction and another 4% were detectable in the crystalline fraction. Fe(II) detection in all four extraction fractions suggests that secondary minerals of different crystallinity were formed during Fe(III) reduction. Fe(III) decreased in the poorly crystalline fraction parallel to Fe(II) formation, indicating ferrihydrite consumption. After 6 days, 22% of the Fe(III) were still present in the poorly crystalline fraction but total digestion tubes showed that the reduction did not continue (data not shown). The remaining amount is most likely present either in form of residual ferrihydrite or as poorly crystalline magnetite. The inaccessibility of the remaining Fe(III) could be due to blocking by adsorbed Fe(II) (Roden and Zachara, 1996) or by a coating with secondary precipitates. The measured Fe(II):Fe(III) ratio of 0.1 in the crystalline fraction does not correspond to the theoretical ratio of 0.5 in magnetite. This is probably due to the fact that in the crystalline fraction a mixture of minerals is present.

It has been suggested that the reduction of Fe(III) minerals (e.g. goethite) may be ceased by accumulation of aqueous Fe(II), due to a decrease of free energy and resulting thermodynamic constraints (Liu et al., 2001). However, an aqueous Fe(II) concentration of 10 mM, which was found to be critical for goethite reduction (Roden and Urrutia, 2002), was never exceeded in our 5 and 30 mM ferrihydrite experiments, where the greatest increase in maximum reduction rates was observed. In case of 10 mM Fe(II) present, 2-line ferrihydrite with a redox potential of +/- 0 mV (Thamdrup, 2000) would still be an energetically favourable electron acceptor for the oxidation of lactate to acetate (-470 mV, Thamdrup, 2000) compared to the higher crystalline Fe(III) mineral goethite (-274 mV, Thamdrup, 2000). As it will be discussed in the following section *3.4.*, in our experiments the cessation of Fe(III) reduction is rather due to secondary mineral formation processes.

3.4. Minerals formed during microbial ferrihydrite reduction

As shown by sequential extraction, there was just a very small amount of precipitates formed in cultures grown with initial ferrihydrite concentrations of 5 mM. This precipitate contains about 6% of the total amount of iron, potentially representing siderite formed by precipitation of Fe(II) with biologically produced CO_2 (from lactate oxidation). The

over all amount of solids was insufficient for analysis by XRD or Moessbauer spectroscopy. Therefore identification of mineral products for the 5 mM experiment was not possible. Similar problems were encountered already by other authors at low concentrations of ferrihydrite (Fredrickson et al., 2003).

In contrast, in microbial reduction experiments containing 30 mM ferrihydrite, formation of a black precipitate was observed which adhered to a magnetic stirring bar and was identified by XRD and Moessbauer spectroscopy as a mixture of magnetite and goethite (Fig. 7). XRD patterns of mineral samples taken directly after inoculation showed a broad signal of the initially present 2-line ferrihydrite between $2\theta = 35°$ to $45°$. The main magnetite reflection at a diffraction angle of $2\theta = 41.4°$ (lattice plain [311]) is visible already after 2 days of Fe(III) reduction. Starting with the fourth day, also the other characteristic reflections for magnetite appear in the diffractogram (Fig. 7a). Time dependent XRD-analysis showed in none of our experiments the formation of an intermediate mineral phase and a subsequent transformation of such an intermediate phase into another mineral phase. The broad reflections for magnetite (Fig. 7a and b) indicate a lower crystallinity or small crystallite size of the biogenic magnetite compared to well crystallized, synthetic magnetite.

The Fe(II) and Fe(III) concentrations detected in the poorly crystalline fraction during sequential extraction (Fig. 6) in combination with the XRD-measurements suggest the formation of poorly ordered magnetite. This seems to be (at least partially) dissolved already in the extraction step for poorly crystalline minerals (see section *3.3.*). In addition, a rapid increase of Fe(III) in the crystalline fraction was evident after 2 days which shows the simultaneous formation of crystalline Fe(III) phases such as magnetite or goethite.
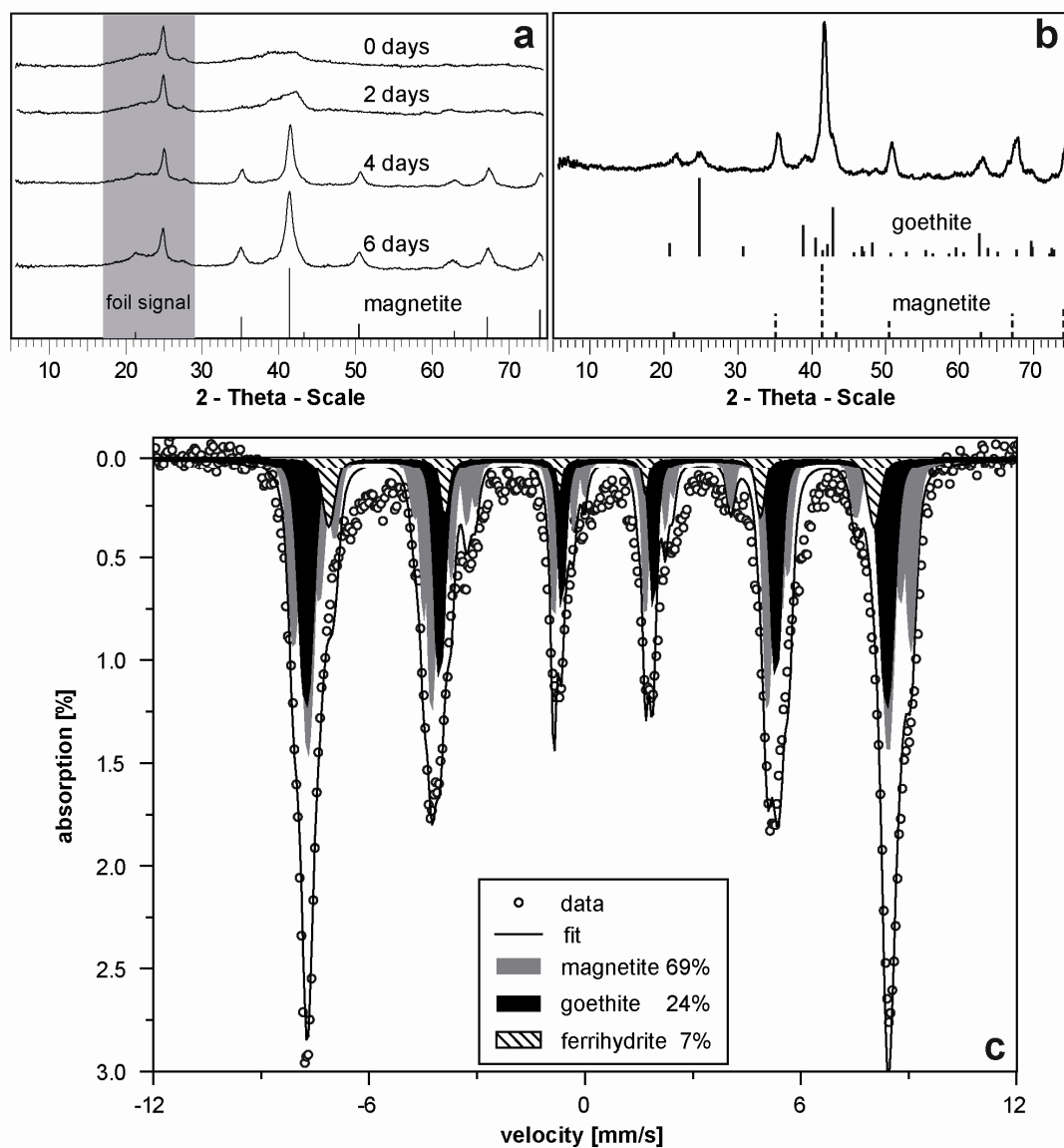
Fig. 7 Spectra of precipitates formed during reduction of 30 mM 2-line ferrihydrite by _Shewanella oneidensis_ MR-1 in representative experiments. (a) XRD spectra, samples were collected after 0, 2, 4 and 6 days of incubation (reference pattern: magnetite, grey bar indicates signal range of the foil, covering the sample). (b) XRD spectrum, sample collected after 9 days, measured without foil (reference patterns: goethite and magnetite). (c) Moessbauer spectrum at 4.2 K, sample collected after 9 days (open circles: measured data, solid line: fitted spectrum, filled areas: contained minerals and relative amount according to fitted line)

XRD measurements done with foil-covered samples to protect the minerals from air-oxidation did not indicate the presence of goethite since the background signal of the foil superimposes the strongest goethite reflection (2θ = 24.7°; lattice plane [101]). However, XRD measurements without the covering foil showed the presence of goethite

(Fig. 7b). Moessbauer analysis of a sample collected from a 30 mM ferrihydrite experiment after 9 days confirmed the presence of magnetite and goethite (Fig. 7c). The inner line broadening of the measured spectrum supported the conclusions drawn from XRD patterns indicating the presence of small-size or disordered crystal domains. Fitting the Moessbauer data with the Recoil software resulted in ratios of the different minerals of 69% magnetite, 24% goethite and 7% residual ferrihydrite with a possible deviation of 10%. Therefore the presence of a residual amount of ferrihydrite is questionable but not unlikely. Besides that the fitting showed that the formed magnetite contained a deficiency in Fe(II) with a resulting Fe(II):Fe(III) ratio of 0.2 instead of 0.5. These fitting results confirm the findings of the sequential extraction which showed incomplete consumption of ferrihydrite (poorly crystalline fraction) and a relative surplus of Fe(III) in the crystalline iron fraction (see section *3.3.*).

Transformation of Fe(III) minerals by microbial iron reduction has been extensively studied in the past. Depending on the geochemical conditions, microbial ferrihydrite reduction was described to form goethite, lepidocrocite, hematite, siderite, vivianite, green rusts and magnetite (Zachara et al., 2002; Fredrickson et al., 2003; Hansel et al., 2003; Kukkadapu et al., 2004; Borch et al., 2007). Based on these studies it was concluded that formation of biogenic minerals is controlled by factors like medium composition (in particular by the buffer system used), concentration of electron donor and acceptor, presence of phosphate, shuttling molecules such as AQDS, or mineral impurities like silicate, nickel or cobalt. Comparison of bicarbonate and complex organic buffers like PIPES or HEPES showed preferential formation of siderite, besides magnetite, goethite or lepidocrocite in presence of bicarbonate (Fredrickson et al., 1998; Fredrickson et al., 2003). In the absence of bicarbonate no siderite was formed but either magnetite at relatively high Fe(II) formation rates or goethite at low rates of Fe(II) formation (Zachara et al., 2002; Hansel et al., 2003; Kukkadapu et al., 2004). Our experiments at high ferrihydrite concentrations (30 and 60 mM ferrihydrite) confirm these observations as we used the organic buffer HEPES and detected approximately three times more magnetite than goethite at the highest determined Fe(II) formation rates (Fig. 1). However, in our experiments at low ferrihydrite concentrations (5 mM)

no magnetite was formed despite the relatively high rate of Fe(II) formation. Most likely the mineral surface available for Fe(II) adsorption was depleted too fast to promote solid phase conversion of ferrihydrite by adsorbed Fe(II). In our experiments CO_2 could only form by microbiological oxidation of lactate (30 mM) to acetate, which was obviously insufficient to excite the solubility product of siderite and form a detectable amount of the Fe(II) mineral. The majority of Fe(II) formed during microbial reduction of 5 mM ferrihydrite stayed in solution (Fig. 6a).

The dependency of mineral formation on Fe(II) formation rates is explained by two different mechanisms (Hansel et al., 2005; Coker et al., 2008). At low local Fe(II) concentrations, coverage of the residual ferrihydrite surface with adsorbed Fe(II) is low and a slow recrystallization (via a reductive dissolution-reprecipitation or structural rearrangement mechanism) of the Fe(III) mineral to goethite, lepidocrocite or hematite takes place (abiotic: Gálvez et al., 1999; biotic: Zachara et al., 2002; abiotic: Cornell and Schwertmann, 2003). With increasing reduction rates, more Fe(II) is produced which adsorbs to residual ferrihydrite and leads to magnetite formation by topotactic conversion of the ferrihydrite (Ardizzone and Formaro, 1983; Zachara et al., 2002). In presence of high Fe(II) concentrations in combination with carbonate or phosphate, the Fe(II) containing minerals siderite and vivianite are formed (Fredrickson et al., 1998).

4. SUMMARY AND CONCLUSIONS

In this study we followed the iron mineral phase development during microbial reduction of different concentrations of 2-line ferrihydrite by *Shewanella oneidensis* MR-1 over time. We showed the dependency of iron reduction rates on the surface area provided by the present Fe(III) mineral. The surface area is determined by the amount and the aggregate size of ferrihydrite.

The great versatility of Fe(III) concentrations in natural environments, for example in soil pores has to be considered when studying microbial iron transformation processes in nature e.g. at the transition zone between oxic and anoxic conditions at ground water level. The variation of the sedimentation behaviour showed that especially under neutral pH conditions the aggregation of ferrihydrite strongly influenced the size of ferrihydrite particles and thereby the accessibility for iron reducing bacteria. The exact dimensions of the aggregates are difficult to determine with common measurement techniques, which do alter the conditions under which the aggregates form. However this information is necessary to compare different iron minerals on a surface normalized basis and determine the rate determining physicochemical properties for microbial iron reduction. Additionally, the observed limitation of the microbial reduction by the provided mineral surface area indicated that under this experimental setup direct contact between cells and mineral was the predominant pathway for electron transfer to ferrihydrite. A change in iron reduction rates also causes a change in the resulting mineralogy. These minerals are potential electron donors for iron oxidizing bacteria or an iron source for plants. The bioavailability of iron bound in biogenic minerals is an important property in environmental systems e.g. in close vicinity to roots and influences the turnover rates for iron in anoxic environments.

5. ACKNOWLEDGEMENTS

6. REFERENCES

Arai Y. and Sparks D. L., 2001. ATR-FTIR Spectroscopic Investigation on Phosphate Adsorption Mechanisms at the Ferrihydrite-Water Interface. *J. Colloid Interface Sci.* **241**, 317-326.

Ardizzone S. and Formaro L., 1983. Temperature induced phase transformation of metastable $Fe(OH)_3$ in the presence of ferrous ions. *Mater. Chem. Phys.* **8**, 125-133.

Behrends T. and Van Cappellen P., 2007. Transformation of Hematite into Magnetite During Dissimilatory Iron Reduction - Conditions and Mechanisms. *Geomicrobiol. J.* **24**, 403-416.

Bonneville S., Van Cappellen P., and Behrends T., 2004. Microbial reduction of iron(III) oxyhydroxides: effects of mineral solubility and availability. *Chem. Geol.* **212**, 255-268.

Borch T., Inskeep W. P., Harwood J. A., and Gerlach R., 2005. Impact of Ferrihydrite and Anthraquinone-2,6-Disulfonate on the Reductive Transformation of 2,4,6-Trinitrotoluene by a Gram-Positive Fermenting Bacterium. *Environ. Sci. Technol.* **39**, 7126-7133.

Borch T., Masue Y., Kukkadapu R. K., and Fendorf S., 2007. Phosphate Imposed Limitations on Biological Reduction and Alteration of Ferrihydrite. *Environ. Sci. Technol.* **41**, 166-172.

Buerge I. J. and Hug S. J., 1999. Influence of Mineral Surfaces on Chromium(VI) Reduction by Iron(II). *Environ. Sci. Technol.* **33**, 4285-4291.

Coker V. S., Bell A. M. T., Pearce C. I., Pattrick R. A. D., van der Laan G., and Lloyd J. R., 2008. Time-resolved synchrotron powder X-ray diffraction study of magnetite formation by the Fe(III)-reducing bacterium *Geobacter sulfurreducens*. *Am. Mineral.* **93**, 540-547.

Cornell R. M. and Schwertmann U., 2003. *The Iron Oxides*. Wiley-VCH Verlag GmbH & Co. KGaA, Weinheim.

Cwiertny D. M., Handler R. M., Schaefer M. V., Grassian V. H., and Scherer M. M., 2008. Interpreting nanoscale size-effects in aggregated Fe-oxide suspensions: Reaction of Fe(II) with Goethite. *Geochim. Cosmochim. Acta* **72**, 1365-1380.

Davis J. A. and Leckie J. O., 1978. Surface ionization and complexation at the oxide/water interface II. Surface properties of amorphous iron oxyhydroxide and adsorption of metal ions. *J. Colloid Interface Sci.* **67**, 90-107.

De Windt W., Boon N., Siciliano S. D., and Verstraete W., 2003. Cell density related H_2 consumption in relation to anoxic Fe(0) corrosion and precipitation of corrosion products by *Shewanella oneidensis* MR-1. *Environ. Microbiol.* **5**, 1192-1202.

Elsner M., Schwarzenbach R. P., Kellerhals T., Luzi S., Zwank L., Angst W., and Haderlein S. B., 2004. Mechanisms and Products of Surface-Mediated

Reductive Dehalogenation of Carbon Tetrachloride by Fe(II) on Goethite. *Environ. Sci. Technol.* **38**, 2058-2066.

Fredrickson J. K., Kota S., Kukkadapu R. K., Liu C., and Zachara J. M., 2003. Influence of Electron Donor/Acceptor Concentrations on Hydrous Ferric Oxide (HFO) Bioreduction. *Biodegradation* **14**, 91-103.

Fredrickson J. K., Zachara J. M., Kennedy D. W., Dong H., Onstott T. C., Hinman N. W., and Li S.-m., 1998. Biogenic iron mineralization accompanying the dissimilatory reduction of hydrous ferric oxide by a groundwater bacterium. *Geochim. Cosmochim. Acta* **62**, 3239-3257.

Gálvez N., Barrón V., and Torrent J., 1999. Effect of Phosphate on the Crystallization of Hematite, Goethite, and Lepidocrocite from Ferrihydrite. *Clays Clay Miner.* **47**, 304-311.

Gorby Y. A., Yanina S., McLean J. S., Rosso K. M., Moyles D., Dohnalkova A., Beveridge T. J., Chang I. S., Kim B. H., Kim K. S., Culley D. E., Reed S. B., Romine M. F., Saffarini D. A., Hill E. A., Shi L., Elias D. A., Kennedy D. W., Pinchuk G., Watanabe K., Ishii S. i., Logan B., Nealson K. H., and Fredrickson J. K., 2006. Electrically conductive bacterial nanowires produced by *Shewanella oneidensis* strain MR-1 and other microorganisms. *Proc. Natl. Acad. Sci. USA* **103**, 11358-11363.

Hansel C. M., Benner S. G., and Fendorf S., 2005. Competing Fe(II)-Induced Mineralization Pathways of Ferrihydrite. *Environ. Sci. Technol.* **39**, 7147-7153.

Hansel C. M., Benner S. G., Nico P., and Fendorf S., 2004. Structural constraints of ferric (hydr)oxides on dissimilatory iron reduction and the fate of Fe(II). *Geochim. Cosmochim. Acta* **68**, 3217-3229.

Hansel C. M., Benner S. G., Neiss J., Dohnalkova A., Kukkadapu R. K., and Fendorf S., 2003. Secondary mineralization pathways induced by dissimilatory iron reduction of ferrihydrite under advective flow. *Geochim. Cosmochim. Acta* **67**, 2977-2992.

Hau H. H. and Gralnick J. A., 2007. Ecology and Biotechnology of the Genus *Shewanella. Annu. Rev. Microbiol.* **61**, 237-258.

Heidelberg J. F., Paulsen I. T., Nelson K. E., Gaidos E. J., Nelson W. C., Read T. D., Eisen J. A., Seshadri R., Ward N., Methe B., Clayton R. A., Meyer T., Tsapin A., Scott J., Beanan M., Brinkac L., Daugherty S., DeBoy R. T., Dodson R. J., Durkin A. S., Haft D. H., Kolonay J. F., Madupu R., Peterson J. D., Umayam L. A., Owen W., Wolf A. M., Vamathevan J., Weidman J., Impraim M., Lee K., Berry K., Lee C., Mueller J., Khouri H., Gill J., Utterback T. R., McDonald L. A., Feldblyum T. V., Smith H. O., Venter J. C., Nealson K. H., and Fraser C. M., 2002. Genome sequence of the dissimilatory metal ion−reducing bacterium *Shewanella oneidensis. Nat. Biotechnol.* **20**, 1118-1123.

Herbel M. and Fendorf S., 2006. Biogeochemical processes controlling the speciation and transport of arsenic within iron coated sands. *Chem. Geol.* **228**, 16-32.

Islam F. S., Gault A. G., Boothman C., Polya D. A., Charnock J. M., Chatterjee D., and Lloyd J. R., 2004. Role of metal-reducing bacteria in arsenic release from Bengal delta sediments. *Nature* **430**, 68-71.

Jeon B. H., Dempsey B. A., Burgos W. D., Barnett M. O., and Roden E. E., 2005. Chemical Reduction of U(VI) by Fe(II) at the Solid-Water Interface Using Natural and Synthetic Fe(III) Oxides. *Environ. Sci. Technol.* **39**, 5642-5649.

Kappler A. and Newman D. K., 2004. Formation of Fe(III)-minerals by Fe(II)-oxidizing photoautotrophic bacteria. *Geochim. Cosmochim. Acta* **68**, 1217-1226.

Kappler A. and Straub K. L., 2005. Geomicrobiological cycling of iron. In: Banfield J. F., Cervini-Silva J., and Nealson K. M. Eds.), *Molecular Geomicrobiology.* The Mineralogical Society of America, Chantilly, Virginia, USA.

Keller L. and Surette M. G., 2006. Communication in bacteria: an ecological and evolutionary perspective. *Nat. Rev. Microbiol.* **4**, 249-258.

Kocar B. D., Herbel M. J., Tufano K. J., and Fendorf S., 2006. Contrasting Effects of Dissimilatory Iron(III) and Arsenic(V) Reduction on Arsenic Retention and Transport. *Environ. Sci. Technol.* **40**, 6715-6721.

Konhauser K. O., 1997. Bacterial iron biomineralisation in nature. *FEMS Microbiol. Rev.* **20**, 315-326.

Kukkadapu R. K., Zachara J. M., Fredrickson J. K., and Kennedy D. W., 2004. Biotransformation of two-line silica-ferrihydrite by a dissimilatory Fe(III)-reducing bacterium: formation of carbonate green rust in the presence of phosphate. *Geochim. Cosmochim. Acta* **68**, 2799-2814.

Lies D. P., Hernandez M. E., Kappler A., Mielke R. E., Gralnick J. A., and Newman D. K., 2005. *Shewanella oneidensis* MR-1 Uses Overlapping Pathways for Iron Reduction at a Distance and by Direct Contact under Conditions Relevant for Biofilms. *Appl. Environ. Microbiol.* **71**, 4414–4426.

Liu C., Kota S., Zachara J. M., Fredrickson J. K., and Brinkman C. K., 2001. Kinetic Analysis of the Bacterial Reduction of Goethite. *Environ. Sci. Technol.* **35**, 2482-2490.

Lovley D. R. and Phillips E. J. P., 1988. Novel Mode of Microbial Energy Metabolism: Organic Carbon Oxidation Coupled to Dissimilatory Reduction of Iron or Manganese. *Appl. Environ. Microbiol.* **54**, 1472-1480.

Lovley D. R., Holmes D. E., and Nevin K. P., 2004. Dissimilatory Fe(III) and Mn(IV) Reduction, *Adv. Microb. Physiol.* Academic Press.

Manefield M. and Turner S. L., 2002. Quorum sensing in context: out of molecular biology and into microbial ecology. *Microbiology* **148**, 3762-3764.

Mann S., 2001. *Biomineralization: Principles and Concepts in Bioinorganic Materials Chemistry.* Oxford University Press, Inc., New York, Oxford.

Marsili E., Baron D. B., Shikhare I. D., Coursolle D., Gralnick J. A., and Bond D. R., 2008. *Shewanella* secretes flavins that mediate extracellular electron transfer. *Proc. Natl. Acad. Sci. USA* **105**, 3968–3973.

Michel F. M., Ehm L., Antao S. M., Lee P. L., Chupas P. J., Liu G., Strongin D. R., Schoonen M. A. A., Phillips B. L., and Parise J. B., 2007. The Structure of Ferrihydrite, a Nanocrystalline Material. *Science* **316**, 1726-1729.

Myers C. R. and Nealson K. H., 1988. Bacterial Manganese Reduction and Growth with Manganese Oxide as the Sole Electron Acceptor. *Science* **240**, 1319-1321.

Myers C. R. and Myers J. M., 1994. Ferric iron reduction-linked growth yields of *Shewanella putrefaciens* MR-1. *J. App. Bact.* **76**, 253-258.

Nealson K. H. and Myers C. R., 1990. Iron Reduction by Bacteria - a Potential Role in the Genesis of Banded Iron Formations. *Am. J. Sci.* **290A**, 35-45.

Newman D. K. and Kolter R., 2000. A role for excreted quinones in extracellular electron transfer. *Nature* **405**, 94-97.

Raven K. P., Jain A., and Loeppert R. H., 1998. Arsenite and Arsenate Adsorption on Ferrihydrite: Kinetics, Equilibrium, and Adsorption Envelopes. *Environ. Sci. Technol.* **32**, 344-349.

Roden E. E., 2003. Fe(III) Oxide Reactivity Toward Biological versus Chemical Reduction. *Environ. Sci. Technol.* **37**, 1319-1324.

Roden E. E. and Zachara J. M., 1996. Microbial Reduction of Crystalline Iron(III) Oxides: Influence of Oxide Surface Area and Potential for Cell Growth. *Environ. Sci. Technol.* **30**, 1618-1628.

Roden E. E. and Urrutia M. M., 2002. Influence of Biogenic Fe(II) on Bacterial Crystalline Fe(III) Oxide Reduction. *Geomicrobiol. J.* **19**, 209-251.

Ruebush S. S., Brantley S. L., and Tien M., 2006. Reduction of Soluble and Insoluble Iron Forms by Membrane Fractions of *Shewanella oneidensis* Grown under Aerobic and Anaerobic Conditions. *Appl. Environ. Microbiol.* **72**, 2925-2935.

Schadler S., Burkhardt C., and Kappler A., 2008. Evaluation of Electron Microscopic Sample Preparation Methods and Imaging Techniques for Characterization of Cell-Mineral Aggregates. *Geomicrobiol. J.* **25**, 228-239.

Schwertmann U. and Cornell R. M., 2000. *Iron Oxides in the Laboratory*. Wiley-VCH Verlag GmbH, Weinheim.

Stanjek H. and Weidler P. G., 1992. The effect of dry heating on the chemistry, surface area, and oxalate solubility of synthetic 2-line and 6-line ferrihydrites. *Clay Minerals* **27**, 397-412.

Stookey L. L., 1970. Ferrozine - A New Spectrophotometric Reagent for Iron. *Anal. Chem.* **42**, 779-781.

Straub K. L., Benz M., and Schink B., 2001. Iron metabolism in anoxic environments at near neutral pH. *FEMS Microbiol. Ecol.* **34**, 181-186.

Thamdrup B., 2000. Bacterial manganese and iron reduction in aquatic sediments. In: Schink B. (Ed.), *Adv. Microb. Ecol.* Kluwer Academic/ Plenum Publishers, New York.

van der Giessen A. A., 1966. The structure of iron (III) oxide-hydrate gels. *Journal of Inorganic and Nuclear Chemistry* **28**, 2155-2156.

Venkateswaran K., Moser D. P., Dollhopf M. E., Lies D. P., Saffarini D. A., MacGregor B. J., Ringelberg D. B., White D. C., Nishijima M., Sano H., Burghardt J., Stackebrandt E., and Nealson K. H., 1999. Polyphasic taxonomy of the genus *Shewanella* and description of *Shewanella oneidensis* sp. nov. *Int. J. Syst. Bacteriol.* **49**, 705-724.

von Canstein H., Ogawa J., Shimizu S., and Lloyd J. R., 2008. Secretion of Flavins by *Shewanella* Species and Their Role in Extracellular Electron Transfer. *Appl. Environ. Microbiol.* **74**, 615-623.

Weber K. A., Achenbach L. A., and Coates J. D., 2006. Microorganisms pumping iron: anaerobic microbial iron oxidation and reduction. *Nat. Rev. Microbiol.* **4**, 752-764.

Weidler P. G., 1997. BET Sample Pretreatment of Synthetic Ferrihydrite and its Influence on the Determination of Surface Area and Porosity. *Journal of Porous Materials* **4**, 165-169.

Zachara J. M., Kukkadapu R. K., Fredrickson J. K., Gorby Y. A., and Smith S. C., 2002. Biomineralization of Poorly Crystalline Fe(III) Oxides by Dissimilatory Metal Reducing Bacteria (DMRB). *Geomicrobiol. J.* **19**, 179-207.

Zegeye A., Ruby C., and Jorand F., 2007. Kinetic and thermodynamic analysis during dissimilatory gamma-FeOOH reduction: Formation of green rust 1 and magnetite. *Geomicrobiol. J.* **24**, 51-64.

3

Identification of biogenic iron minerals by X-ray diffraction

ABSTRACT

The mineral analysis of mineral precipitates with XRD is frequently used in geomicrobiological science. In particular the work with iron-reducing or iron-oxidizing cultures requires special sample treatments for oxygen-sensitive Fe(II)-containing minerals.

A Bruker D8 Discover GADDS XRD^2-microdiffractometer installed at the Institute for Geosciences at the University of Tuebingen was used to test three different sample preservation methods in order to prevent biogenic minerals from oxidation by air during the measurements. Preparation of small mineral samples on a Si-wafer and covering of the sample holder with a clear polyethylene foil were found to result in sufficient signal intensities for the identification of biogenic precipitates. Although color changes of potentially oxygen-sensitive Fe(II) minerals like siderite or vivianite exposed to air were observed, XRD measurements of these minerals did not show changes in the obtained XRD patterns after 19 or 30 h exposure to air, respectively. However, it cannot be excluded that biogenic minerals of small particle size may oxidize fast leading to changes in the crystal structure.

Future work should include detailed studies about the potential of biogenic precipitates to transform due to oxidation during measurements with XRD. Until these processes remain unclear it is recommended to use the covering foil in order to prevent unintended oxidation of oxygen-sensitive mineral samples.

1. INTRODUCTION

Microbial iron reduction is a widespread microbiological respiration pathway and a number of different studies investigated the mineral products formed during reduction of Fe(III) minerals to Fe(II). The end products of biogenic iron reduction vary from crystalline Fe(III) minerals (goethite, lepidocrocite), mixed-valent iron minerals (magnetite, green rusts) to Fe(II) minerals (siderite, vivianite) (Konhauser, 1997; Fredrickson et al., 1998; Zachara et al., 2002; Glasauer et al., 2003; Hansel et al., 2003; Kappler and Newman, 2004; Kukkadapu et al., 2004; Ferris, 2005; Borch et al., 2007). Several different techniques, like scanning/transmission electron microscopy (including energy-disperive X-ray spectroscopy or electron diffraction) Raman spectroscopy, X-ray photoelectron spectroscopy, synchrotron based X-ray absorption techniques or Moessbauer spectroscopy were applied in order to identify biogenic mineral precipitates in microbial cultures (for review see Geesey et al., 2002). However, some of these techniques may not be instruments of daily use for researchers, either due to restricted accessibility (synchrotron methods) or lacking local availability (Moessbauer spectroscopy).

One method which is usually frequently available in geoscience, material science or mineralogy departments is X-ray diffraction (XRD). Powder X-ray diffraction provides characteristic diffraction patterns of the analyzed mineral or mineral mixture. Scattering of an incident X-ray beam by the crystal lattice planes of a mineral leads to characteristic patterns caused by the differences in the spacing of lattice planes. Application of Rietveld refinement even allows the quantification of constituents of mineral mixtures and provides information about the crystallite size of the studied mineral. Detection limits for specific constituents in mineral mixtures can be around 5%. However the detection of amorphous mineral phases is not possible with XRD since a regular crystal structure is necessary to obtain defined scattering patterns.

Sample preparation for XRD measurements is relatively simple, a few grams of fine grained powder is spread on a sample holder considering a uniform, flat surface, but biogenic samples may need some special requirements. Especially Fe(II)-containing minerals may be

sensitive to oxidation if exposed to air. Furthermore, the yields of microbiological mineral transformation can be quite low in this case measurements on a μm scale are required. In particular the identification of iron minerals by XRD can be impeded by instruments equipped with Cu-K$_\alpha$ X-ray sources. Iron absorbs a considerable amount of X-ray energy resulting in a low detection signal and long measurement periods.

In this study we evaluate the advantages and limitations of a Bruker D8 Discover GADDS XRD²-microdiffractometer for the analysis of biogenic mineral precipitates from iron reducing cultures. In particular the sample preparation procedure for oxygen sensitive samples was tested.

2. MATERIALS AND METHODS

2.1. Chemicals and minerals

Goethite (α-FeOOH, Bayferrox 920 Z) was provided by LANXESS Deutschland GmbH. Hematite (α-Fe$_2$O$_3$) was tempered from magnetite (Fe$_3$O$_4$, Bayferrox E 8710) by heating up the powder within 1 h and keeping 900°C for 2 h.

Siderite was a gift from Martin Elsner (German Research Center for Environmental Health, Munich) to Andreas Kappler and stored under N$_2$ atmosphere. The mineral synthesis was described elsewhere (Elsner et al., 2004).

2-line ferrihydrite (Fe(OH)$_3$) was synthesized according to Schwertmann and Cornell (2000) and Raven et al. (1998) using 40 g of Fe(NO$_3$)$_3$*9H$_2$O per 500 ml water that was neutralized with 1 M KOH to a final pH not higher than 7.5. After centrifugation and 4 times washing with Millipore®-water, the wet solid was resuspended in water to an approximate concentration of 0.5 M Fe(III). For further use in bacteria cultures the mineral suspension was not autoclaved and stored in the dark in serum bottles and tightly closed with a butyl rubber stopper. Deoxygenation under vigorous stirring was done by alternating application of vacuum and N$_2$ 10 min each and in total three times. N$_2$-BET measurements after freeze-drying yielded surface areas of the ferrihydrite between 240-280 m²/g.

A 50 mM phosphate buffer was prepared by dissolution of Na$_2$HPO$_4$·2H$_2$O and KH$_2$PO$_4$ (analytical grade) in deionized water, filter-sterilized (cellulose acetate sterile filter unit, 0.2 µm, Fisher Scientific, Germany) into sterile, closed culture tubes and deoxygenated under sterile conditions by alternating application of vacuum and N$_2$ 5 min each and in total three times. Pahokee Peat Humic Acid Reference 1R103H2 was dissolved in 50 mM phosphate buffer (concentration 3 mg/ml). The solution was filter-sterilized (cellulose acetate sterile filter unit, 0.2 µm, Fisher Scientific, Germany) into sterile, closed culture tubes. The solution was deoxygenated as described above.

2.2. Formation of biogenic precipitates

Shewanella oneidensis strain MR-1 was provided by Jeff Gralnick (Univ. Minnesota). Aerobic cultures on LB-agar plates were streaked out from a frozen stock (-80°C) (incubation: 28°C, 24 h; kept for 10 days at 4°C). LB medium: 10 g tryptone, 5 g yeast extract, 5 g NaCl, 12 g agar (not for liquid medium). 50 ml of liquid LB medium in a 200 ml Erlenmeyer flask were inoculated with a single colony (incubation: 14 h, 28°C, shaken at 150 rpm, switched to anaerobic metabolism). Cell concentration in LB-cultures was determined by optical density measurements at 600 nm and calibrated against cell counts obtained by direct counting with a Thoma-chamber by light microscopy (Axioscope 2 from Zeiss, Germany). 2 ml of LB-grown cell culture were harvested and centrifuged (5 min, 10 600 g). Cells were washed twice with LML medium (Myers and Myers, 1994), containing 12 mM HEPES buffer and 30 mM lactate, set to pH 7 and used for inoculation. Cells were grown in serum bottles with 36 ml sterile, anoxic LML medium. The headspace was exchanged with N_2, 2-line ferrihydrite (5 mM), phosphate solution (0.8 mM) or humic acid solution (50mg/l) and finally the cells ($2*10^5$ cells/ml) were injected with syringes.

Mineral samples were prepared in an anoxic glove box (Braun, Germany; N_2 atmosphere) by stepwise transfer of the whole serum bottle content into 2 ml-Eppendorf® tubes and centrifugation (2 min, 9 700 g). The supernatant was decanted and the remaining solids were dried under N_2 atmosphere in the glove box.

2.3. Sample holder and preparation of oxygen sensitive iron minerals

The sample holder consists of an Al-disk (thickness app. 1 cm) with a diameter of 5 cm, a piece of a Si-single crystal wafer on top of it and an additional Al-ring which is used to tightly span a covering foil over the sample holder after sample preparation (Fig. 1). The Si-wafer has small indentations (diameter 2 mm) which are designated to fill in mineral samples.
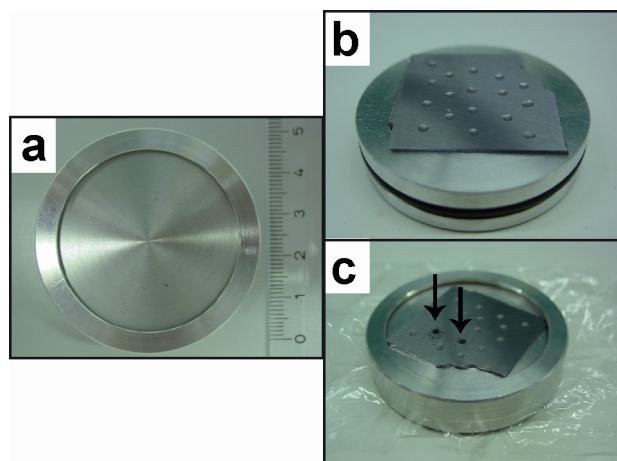
Fig. 1 Sample holder for anoxic preparation of mineral samples (a) without Si-wafer and foil, view from top, (b) with Si-wafer with indentations for samples, without fixation ring and (c) after sample preparation with fixed cover foil and two filled samples spaces (indicated by arrows).

The dry mineral sample (in the glove box) was transferred into an agate motar grinded carefully until a homogenous fine powder was achieved. The mineral powder was suspended to a slurry with a small volume of ethanol (<100 µl). The sample was transferred with a pasteur pipette into an indentation on the Si-wafer in small portions, letting the ethanol evaporate in between the application steps. Special care was taken that the indentations were completely filled with sample powder and an evenly, flat surface was achieved. After the samples were transferred into the indentations, a piece of clear plastic wrap (commercially available polyethylene house hold wrap) was carefully spanned over the sample holder without wrinkles by pressing down the fixation ring. Finally the sample holder was put into a jar, which was tightly closed and used to transport the samples under nitrogen atmosphere to the XRD instrument. From the point of opening the jar until the actual measurement was started it took approximately 3 minutes.

2.4. Instrumentation

The µ-XRD-device (Bruker D8 Discover GADDS XRD²-microdiffractometer, Bruker AXS GmbH, Germany) consists of a Co-K_α X-ray tube, operating at 30 kV, 30 mA, which is either connected to a polycapillary that allows measurements at a spot diameter of 50 µm or a monocapillary with a spot diameter of 300 µm (for detailed information about the equipment see Berthold et al., 2008). Each sample was measured in three overlapping frames of 30° 2θ, within 1 min

measuring time for each frame, using a GADDS® area detector. The EVA® 10.0.1.0 software was used to merge the three measured frames of one sample and to identify the containing mineral phases using the PDF-database licensed by ICDD (International Centre for Diffraction Data).

3. RESULTS AND DISCUSSION

3.1. Evaluation of sample protection measures

We evaluated the influence of different sample preparation methods on measurement parameters like identification of different minerals, signal intensity and shape. In particular previously applied methods like sample coverage with glycerol in order to preserve mineral samples from oxidation during XRD measurements were tested. The first attempts were done with the oxygen-insensitive minerals hematite and goethite and samples of biogenic vivianite. Figure 2 shows a comparison of the original hematite, and vivianite patterns and the different sample preservation methods tested in consideration of the signal yield.

The pure hematite and vivianite samples measured without any sample preservation matched well the reference patterns, without indications for impurities (Fig. 2). Measuring hematite through the glass window of a quartz glass cuvette did not yield any reflection signals. The glass window was obviously too thick for the X-ray radiation provided by our instrument and total absorption of the X-ray signals was observed. The same effect applies for measurements of vivianite covered with glycerol. The measurement of glycerol lead to a similarly undefined pattern as observed for the covered sample. This revealed one drawback of our instrumental setup. The Co-K_α X-ray source operates at a lower energy level (7.70 keV, from Lide (2008)) than the frequently used Cu-K_α X-ray sources (8.98 keV). Therefore, the X-ray radiation is more susceptible to absorption by viscous liquids or solid matter, e.g. glass. In previous studies samples were either mixed with glycerol and measured with Cu-K_α X-ray radiation (Fredrickson et al., 1998; Zachara et al., 1998), they were kept under a N_2-gas flow during measurement (Co-Kα radiation Glasauer et al., 2003) or were prepared in special sample holders in order to prevent them from oxidation (Kukkadapu et al., 2004; Behrends and Van Cappellen, 2007).
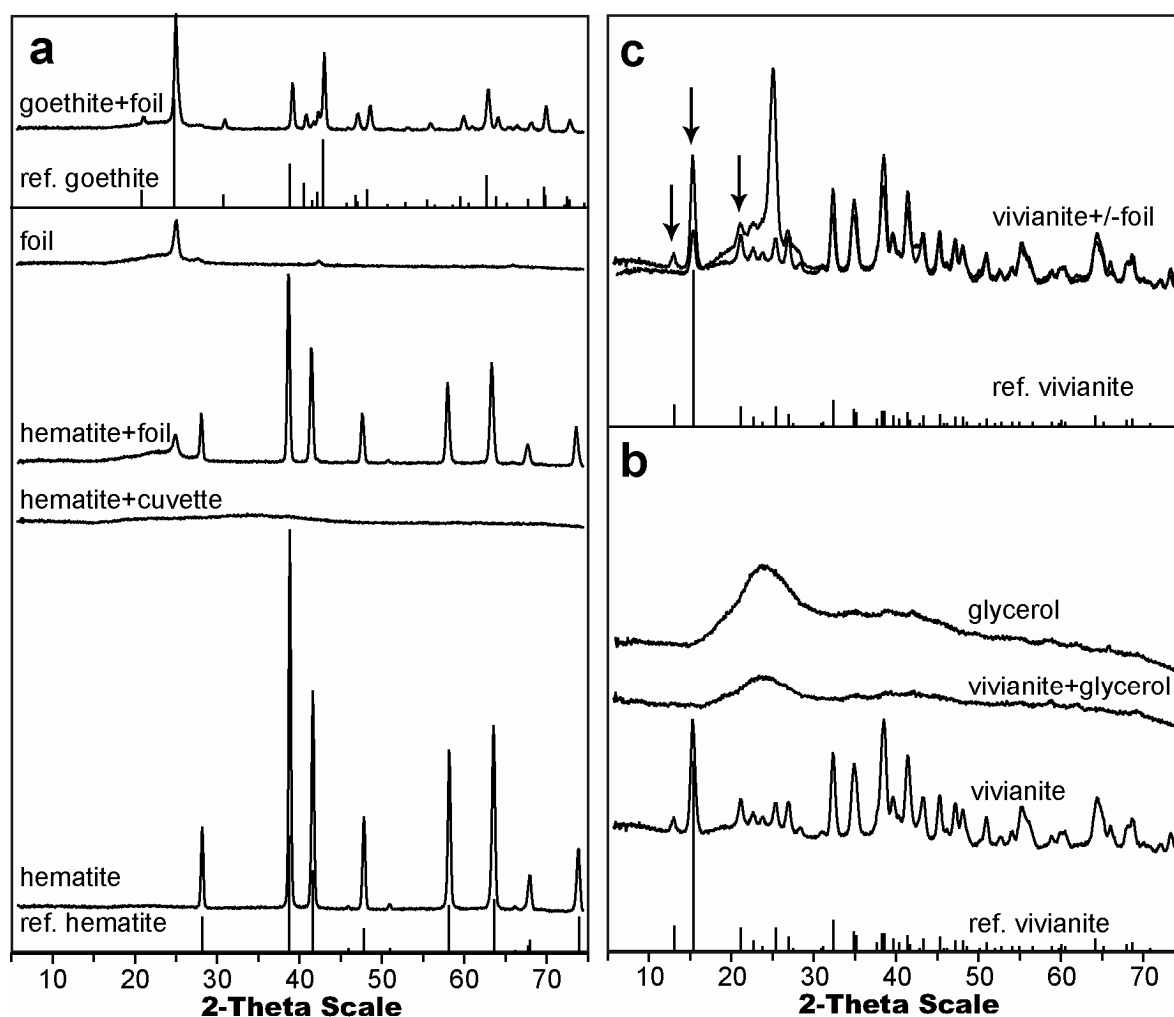
Fig. 2 Sample preparation methods for iron minerals showing XRD patterns of (a) hematite pure, filled into a quartz glass cuvette or covered with foil, the foil as reference and goethite covered with foil. XRD patterns of the right panel show biogenic vivianite formed after 13 d of reduction of 5 mM 2-line ferrihydrite in presence of 0.8 mM phosphate (b) pure, covered with glycerol compared to the glycerol signal and (c) a comparison of pure vivianite and vivianite coverd with foil; arrows indicate a decrease in signal intensity due to the covering foil. Reference patterns show hematite, goethite and vivianite.

On one hand the Co-K$_\alpha$ radiation was a drawback on the other hand the minimized fluorescence effect of iron (K$_\alpha$: 7.11 keV) at the lower Co-K$_\alpha$ energy level in combination with a 50 µm microlens provided a sufficient signal yield for extremely fast standard measurement periods of 3 min (even time steps of 6 sec are possible; see (Berthold et al., 2008)), compared to common measurement times of 30 min (depending on the measurement step rate). The small measurement spot of 50 µm represents another particular advantage of the applied instrument. The sample amount required for measurements providing the mineralogical information is extremely small (~50 mg, to

fill one indentation on the Si-wafer) and therefore particularly useful for the analysis of solids obtained from bacterial cultures with low precipitate yields. The installed video camera at the sample table of the instrument additionally facilitated focusing and selection of the measurement area.

Sample preparation using the clear plastic wrap provided the most satisfying results for identification of the present mineral phases (Fig. 2a and c). The reflection patterns of all three investigated minerals (hematite, goethite and vivianite) were displayed well in large parts. The foil featured a broad signal between a 2θ range from 17° to 29° and a minor reflection at 42°, which nevertheless made it possible to identify the minerals according to their reference patterns. In addition it has to be mentioned that although the foil was relatively thin it clearly affected reflection signals at low 2θ angles (Fig. 2c) where the pathway for the X-ray beam through the foil material was longer and the incident as well as the reflected beam were reduced in their intensity. Comparing the vivianite pattern with and without the covering foil reveals a decrease in reflection intensities at 2θ angles smaller than 28° in presence of the foil (Fig. 2c). This effect was also evident when comparing goethite patterns with and without foil (data not shown). However, the main goethite reflection at $2\theta = 25°$ coincided with the greatest intensity of the foil signal. This implicates that in particular at low concentrations where the other goethite reflections show low intensities the confirmation of the presence of goethite may be difficult if not impossible.

3.2. Oxygen sensitivity of Fe(II)-containing minerals

In order to determine the oxidation time for Fe(II) bound in minerals we measured time series of siderite and biogenic vivianite (Fig. 3).

Synthetic siderite did not show a change in the crystal structure after exposure to air for 19 h, although a color change from light yellow to light brown was clearly visible within one minute after the first exposure to air. Obviously the observed oxidation of the $FeCO_3$ powder was restricted to a thin layer at the surface of the mineral particles. The amount of the particle coating was too less to be detected with XRD. Additionally the formed mineral phase could be amorphous and would therefore not be detected by XRD. Measurements of biogenic vivianite

over a time period of 30 h did also not show a change in mineral structure indicating reasonably good stability of the mineral against oxidation at least for the time required to collect XRD patterns, even on standard instruments with longer measurement times.
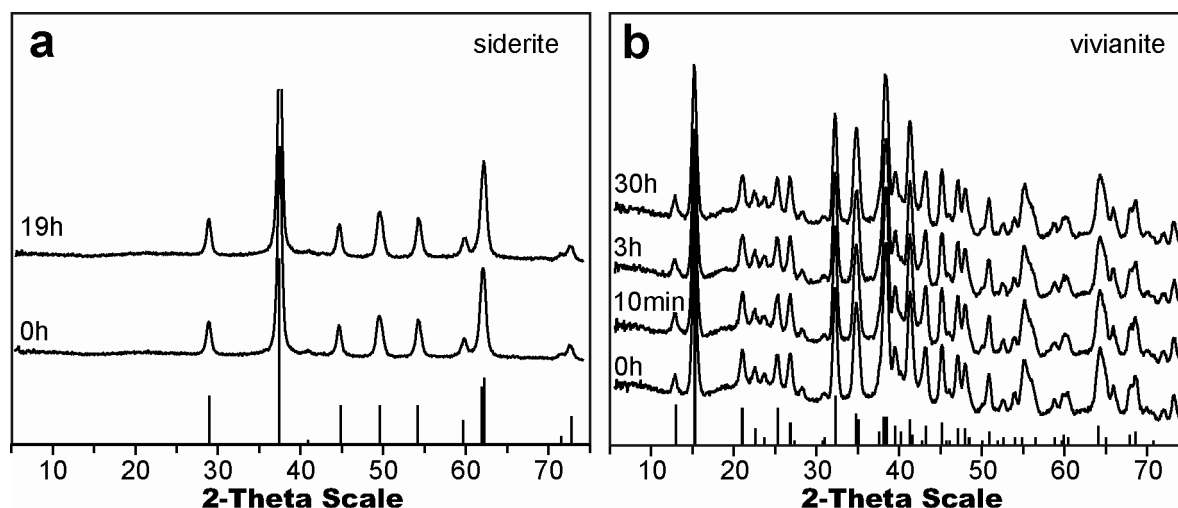

Fig. 3 Time dependent measurements of (a) synthetic siderite and (b) biogenic vivianite formed after 13 d of reduction of 5 mM 2-line ferrihydrite in presence of 0.8 mM phosphate. Samples were exposed to air for different time spans. Reference patterns show siderite and vivianite, respectively

However, the minerals formed by bacteria were not always well crystallized and most likely consisting of small particle sizes, depending on the culture conditions (Fig. 4). A decrease in particle and domain size of the minerals may facilitate a complete transformation of Fe(II) minerals. At small particle sizes the formation of a "thin" oxidized surface coating may represent a larger percentage of the particle volume. The oxidation could propagate through almost the whole volume of the small biogenic mineral particle. The structural information of the formed minerals would be changed to a large extent and identification of the initially present mineral may be impossible. A detailed evaluation of the effect of particle sizes with special regard to biogenic Fe(II) mineral precipitates on the measurability of mineral conversion by oxidation processes is required. As long as the oxidation of biogenic precipitates cannot be excluded the application of sample protecting measures is recommended.
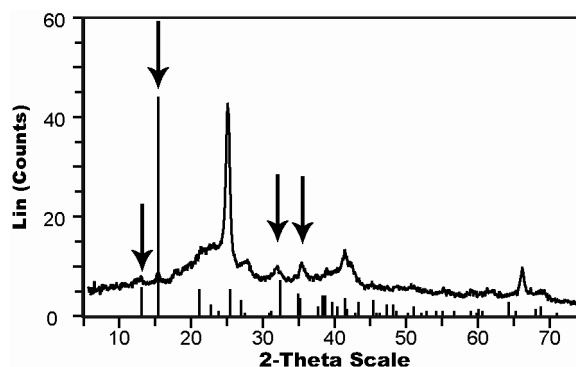
Fig. 4 Mineral precipitates formed after 11 d of reduction of 5 mM 2-line ferrihydrite in presence of 0.8 mM phosphate and 50 mg/l humic acid. The sample was covered with foil. The reference pattern shows vivianite. Arrows indicate remaining vivianite signals

Low crystalline vivianite showed a remainder of four somehow diffuse reflections. This is not enough for a clear identification of a mineral phase. In these cases complementary techniques like Moessbauer or X-ray absorption near-edge structure spectroscopy (XANES) are recommended to undoubtedly identify the present minerals. Since one major feature of XRD in general is the lacking possibility to detect poorly crystalline minerals, cross-checking the results obtained by XRD with other methods (e.g. XAS or Moessbauer) is recommended in all cases.

4. CONCLUSIONS

Depending on the particle size and crystallinity of Fe(II)-containing minerals the potential for oxidation by molecular oxygen and the measurability by XRD may be different. Biogenic minerals very often exhibit poor crystallinity, potentially leading to fast oxidation of Fe(II) during mineral analysis. In this study we demonstrated, that protection of oxygen-sensitive samples with a clear plastic wrap (polyethylene) provided satisfying results for the identification of Fe(II)-bearing biogenic iron minerals. However, at low 2θ angles the detected signal intensities were reduced due to the absorption of X-rays by the covering foil and therefore relative intensities of reflections are incorrect. The main reflection of the covering foil coincided with the main reflection of goethite, thus identification of goethite might be difficult at low concentrations. The special features of the applied XRD instrument provided several advantages based on the small measurement spots in combination with the video-supported focusing of the sample position, allowing high spatial resolution and the installed Co-K$_\alpha$ X-ray source. Small measurement spots reduce the required sample amount (~50 mg) and safe sample material for further analysis with other methods or allow a downsizing of culture setups and therefore saving of resources. The X-ray tube is especially suitable for iron containing samples because of the low fluorescent effect at the operation energies of the Co-K$_\alpha$ source.

5. ACKNOWLEGEMENTS

6. REFERENCES

Behrends T. and Van Cappellen P., 2007. Transformation of Hematite into Magnetite During Dissimilatory Iron Reduction - Conditions and Mechanisms. *Geomicrobiol. J.* **24**, 403-416.

Berthold C., Bjeoumikhov A., and Brügemann L., 2008. Fast XRD² Microdiffraction with Focusing X-Ray Microlenses. *Particle & Particle Systems Characterization*, submitted.

Borch T., Masue Y., Kukkadapu R. K., and Fendorf S., 2007. Phosphate Imposed Limitations on Biological Reduction and Alteration of Ferrihydrite. *Environ. Sci. Technol.* **41**, 166-172.

Elsner M., Schwarzenbach R. P., and Haderlein S. B., 2004. Reactivity of Fe(II)-Bearing Minerals toward Reductive Transformation of Organic Contaminants. *Environ. Sci. Technol.* **38**, 799-807.

Ferris F. G., 2005. Biogeochemical Properties of Bacteriogenic Iron Oxides. *Geomicrobiol. J.* **22**, 79-85.

Fredrickson J. K., Zachara J. M., Kennedy D. W., Dong H., Onstott T. C., Hinman N. W., and Li S.-m., 1998. Biogenic iron mineralization accompanying the dissimilatory reduction of hydrous ferric oxide by a groundwater bacterium. *Geochim. Cosmochim. Acta* **62**, 3239-3257.

Geesey G. G., Neal A. L., Suci P. A., and Peyton B. M., 2002. A review of spectroscopic methods for characterizing microbial transformations of minerals. *J. Microbiol. Methods* **51**, 125-139.

Glasauer S., Weidler P. G., Langley S., and Beveridge T. J., 2003. Controls on Fe reduction and mineral formation by a subsurface bacterium. *Geochim. Cosmochim. Acta* **67**, 1277-1288.

Hansel C. M., Benner S. G., Neiss J., Dohnalkova A., Kukkadapu R. K., and Fendorf S., 2003. Secondary mineralization pathways induced by dissimilatory iron reduction of ferrihydrite under advective flow. *Geochim. Cosmochim. Acta* **67**, 2977-2992.

Kappler A. and Newman D. K., 2004. Formation of Fe(III)-minerals by Fe(II)-oxidizing photoautotrophic bacteria. *Geochim. Cosmochim. Acta* **68**, 1217-1226.

Konhauser K. O., 1997. Bacterial iron biomineralisation in nature. *FEMS Microbiol. Rev.* **20**, 315-326.

Kukkadapu R. K., Zachara J. M., Fredrickson J. K., and Kennedy D. W., 2004. Biotransformation of two-line silica-ferrihydrite by a dissimilatory Fe(III)-reducing bacterium: formation of carbonate green rust in the presence of phosphate. *Geochim. Cosmochim. Acta* **68**, 2799-2814.

Lide D. R., 2008. *CRC Handbook of Chemistry and Physics*. CRC Press Taylor & Francis Group, Boca Raton.

Myers C. R. and Myers J. M., 1994. Ferric iron reduction-linked growth yields of *Shewanella putrefaciens* MR-1. *J. App. Bact.* **76**, 253-258.

Raven K. P., Jain A., and Loeppert R. H., 1998. Arsenite and Arsenate Adsorption on Ferrihydrite: Kinetics, Equilibrium, and Adsorption Envelopes. *Environ. Sci. Technol.* **32**, 344-349.

Schwertmann U. and Cornell R. M., 2000. *Iron Oxides in the Laboratory*. Wiley-VCH Verlag GmbH, Weinheim.

Zachara J. M., Kukkadapu R. K., Fredrickson J. K., Gorby Y. A., and Smith S. C., 2002. Biomineralization of Poorly Crystalline Fe(III) Oxides by Dissimilatory Metal Reducing Bacteria (DMRB). *Geomicrobiol. J.* **19**, 179-207.

Zachara J. M., Fredrickson J. K., Li S.-M., Kennedy D. W., Smith S. C., and Gassman P. L., 1998. Bacterial reduction of crystalline Fe^{3+} oxides in single phase suspensions and subsurface materials. *Am. Mineral.* **83**, 1462-1433.

4

Influence of humic substance concentration on electron shuttling and mineral transformation during microbial 2-line ferrihydrite reduction

ABSTRACT

Microbially catalyzed reduction of Fe(III) minerals plays an important role for C and Fe cycling and for the fate of (in)organic pollutants in the environment. Reduction of Fe(III) minerals can lead either to dissolution and/or (trans)formation of minerals and thus to a release or immobilization of sorbed compounds. Additionally, reactive iron mineral phases are formed that can undergo secondary redox reactions with other organic and inorganic compounds. The geochemical parameters controlling these processes, in particular, the effect of different concentrations of redox-active humic substances (HS) on electron transfer from the cells to the Fe(III) minerals (electron shuttling) and on mineral transformation are not fully understood.

In this study we demonstrated that depending on the ratio of humic acids (HA) to 2-line ferrihydrite, the Fe(III) reduction rates either increased via stimulation of electron transfer by HA electron shuttling, or decreased due to HA-ferrihydrite aggregate formation caused by sorption of HA to the ferrihydrite. Our experiments suggested that the degree of ferrihydrite surface coating by HA strongly influenced the aggregation of the iron hydroxide particles and thereby their accessible surface area for Fe(III)-reducing bacteria. We found that sorbed HA only (in the absence of detectable amounts of dissolved HA) did not stimulate electron transfer. Significant stimulation of Fe(III) reduction did not occur until a minimum concentration of 10 mg/l of dissolved HA was reached. Above 10 mg/l, reduction rates increased with increasing dissolved HA concentration of up to approximately 130 mg/l of dissolved HA, a concentration of dissolved HA being reached at about 200 mg/l total amount of HA when the ferrihydrite surface was saturated with HA molecules. A further increase in dissolved HA concentration did not further increase Fe(III) reduction rates. In addition, our results suggested that both Fe(II) complexation and Fe(III) solubilization by HA did not play a significant role for stimulation of Fe(III) reduction under our experimental conditions. Not only Fe(III) reduction rates but also the crystallinity of the mineral products formed during microbial Fe(III) reduction changed in the presence of HA. Generally, the crystal order and/or grain size of the magnetite produced

by Fe(III) reduction in the presence of HA was lower than the magnetite produced in the absence of HA.

In summary, this study shows that both the concentration of HA and Fe(III) minerals present during microbial Fe(III) reduction strongly influence the reduction rates and the mineralogy of the reduction products. This suggests that biogeochemical iron cycling in the environment not only depends on pH, solute chemistry, microbial strains, reduction mechanisms and the identity of initially present minerals but also on the concentrations and ratios of dissolved HA, sorbed HA and Fe(III) minerals.

1. INTRODUCTION

Fe(II) and Fe(III) minerals such as siderite ($Fe^{II}CO_3$), vivianite ($Fe_3^{II}(PO_4)_2*8H_2O$), magnetite ($Fe^{II}Fe^{III}_2O_4$), ferrihydrite ($Fe^{III}(OH)_3$), goethite (α-$Fe^{III}OOH$), lepidocrocite (γ-$Fe^{III}OOH$) or hematite (γ-$Fe^{III}_2O_3$) are subject to a large number of chemical and biological redox transformations in the environment. The biologically driven iron redox cycle includes Fe(III)-reducing as well as Fe(II)-oxidizing bacteria that inhabit a broad range of environments including, oxic, anoxic, microoxic, pH-neutral or acidic, ambient-temperature and hydrothermal conditions (Straub et al., 2001; Lovley et al., 2004; Kappler and Straub, 2005; Weber et al., 2006). Members of the genera *Shewanella* and *Geobacter* have been found to be the dominating species in pH-neutral environments promoting microbial iron reduction (Thamdrup, 2000; Lovley et al., 2004).

In order to use poorly soluble iron oxides as terminal electron acceptors which cannot pass the cell membrane, iron-reducing microorganisms developed three different strategies to transfer electrons to Fe(III): Electron transfer (1) by direct contact between cells and the mineral surface, (2) by reduction of complexed and thus solubilized Fe(III) facilitated by endogenous or exogenous chelating compounds and (3) by using redox-active electron shuttling molecules (for review see Lovley et al., 2004). Electron transfer via direct contact between cells and the mineral surface has been suggested to be mediated via conductive pili (Reguera et al., 2005; Gorby et al., 2006) and via outer membrane cytochromes (Ruebush et al., 2006). However, there is substantial evidence that microbial Fe(III) reduction does not necessarily need direct contact between cells and minerals (Nevin and Lovley, 2002a; Lies et al., 2005). The addition of Fe(III)-chelating compounds has been shown to enhance benzene reduction in contaminated soil samples, suggesting facilitated microbial access to Fe(III) by Fe(III) solubilization (Lovley et al., 1996a). Recently, flavin compounds, capable of electron shuttling and Fe(III) complexation, were shown to be produced and excreted by *Shewanella* strains (Marsili et al., 2008; von Canstein et al., 2008).

Besides these relatively simple and structurally defined organic molecules, heterogeneous humic substances (HS) can stimulate Fe(III) mineral reduction (Lovley et al., 1996b). HS are common constituents of soils and sediments, composed of detrital organic material and provide metal-ion-complexing and redox-active functional groups (Stevenson, 1994). Due to the heterogeneous, polymeric and polydispersive nature of HS, in many cases AQDS (9,10-anthraquinone-2,6-disulfonate), a simple model compound for quinone moieties in HS, was used in laboratory studies (Coates et al., 1998; Fredrickson et al., 1998; Kukkadapu et al., 2004; O'Loughlin, 2008). However, the significance of experiments in which HS are substituted by artificial electron shuttling compounds such as AQDS for understanding microbial electron transfer and mineral transformation is unclear. This is the case particularly since HS strongly sorb to Fe minerals and show a pH-dependent solubility behaviour. HS can be separated into three fractions with different solubility: fulvic acids (soluble at all pH values), humic acids (HA) (soluble at alkaline pH values) and humins (non-soluble). The structure of HS was shown to vary with geochemical conditions such as pH, ionic strength and HS redox state. As a consequence, the exposure and therefore the availability of redox active functional groups changes by molecule folding and unfolding mechanisms (Thieme et al., 2007). Additionally, HS are expected to block reactive sites on mineral surfaces by surface sorption although the role of sorbed HS for electron transfer between bacteria and minerals is not yet resolved.

Up to now HS are thought to stimulate microbial iron reduction in three ways: (1) by solubilization of Fe(III) minerals via iron complexation and transport of the Fe(III) to the cells (Lovley et al., 1996a; Nevin and Lovley, 2002b), (2) by complexation of Fe(II), thus preventing surface site blockage and providing thermodynamically favourable conditions for Fe(III) reduction (Royer et al., 2002b), or (3) via electron shuttling by transferring electrons from the cells to the Fe(III) minerals (Lovley et al., 1996b; Royer et al., 2002a). Studies investigating electron shuttling typically have been conducted using very high HS concentrations (up to 2 g/l) (Lovley et al., 1996b; Coates et al., 1998), compared to natural concentrations of HS between 0.4 mg/l in groundwater and 60 mg/l in surface water (Aiken, 1985) (0.2-60 mg C/l). Recently it has been shown that electron shuttling between

cells and 2-line ferrihydrite occurs if the dissolved HA concentration exceeds a minimum of 5 mg C/l (Jiang and Kappler, 2008). The stimulation by HA levelled off at a maximum reduction rate for HA concentrations of 25 mg C/l and higher (Jiang and Kappler, 2008). However, the influence of dissolved versus sorbed HS on the function of HS as electron shuttle and on the microbial transformation of iron minerals has not been determined thus far.

The mineralogy of precipitates formed by microbial iron reduction has a strong influence on biogeochemical processes. The rates of reductive transformation of hexachloroethane and 4-chloronitrobenzene have been shown to change, depending on the type of Fe(III) mineral in presence of dissolved Fe(II) (Elsner et al., 2004). Furthermore it is known, that for example iron reducing bacteria utilize dissolved or poorly crystalline Fe(III) sources faster than crystalline Fe(III) minerals like goethite, hematite or magnetite (Lovley and Phillips, 1988). This selectivity leads to a preferential consumption of poorly crystalline iron minerals like ferrihydrite. Additionally, biogenic Fe(II) promotes further formation of better crystalline and less bioavailable minerals like goethite, lepidocrocite or magnetite (Hansel et al., 2005; Pedersen et al., 2005; Coker et al., 2008). Therefore identification of the mineral phases formed during microbial Fe(III) reduction is fundamental to predict possible secondary reactions in the environment such as pollutant degradation and nutrient sequestration. The effect of HS on the identity of biogenic iron minerals formed during Fe(III) reduction is still unknown.

In summary, the effects of HS at naturally relevant HS concentrations on microbial iron reduction are sparsely studied. In particular, the effects of dissolved and sorbed HS on microbial reduction rates and mineral formation are unknown. Therefore, the goals of this study were to determine the influence of HS on microbial Fe(III) reduction rate, the extent of reduction, as well as on the identity and crystallinity of the minerals produced for two different 2-line ferrihydrite concentrations. Reduction rates were quantified by following Fe(II) formation over time. The minerals produced were identified and quantified by sequential extractions, µ-X-ray diffraction and Moessbauer spectroscopy.

2. EXPERIMENTAL PROCEDURES

2.1. Bacterial cultures and experimental setup

Shewanella oneidensis strain MR-1, originally isolated from Oneida Lake, New York (Myers and Nealson, 1988), was provided by Jeff Gralnick (Univ. Minnesota). We chose this strain as our model strain since it is well characterized (full genome sequence available, see Heidelberg et al. (2002)), easy to cultivate and for its ability to utilize a broad variety of different substrates (Nealson and Myers, 1990; Venkateswaran et al., 1999). Aerobic cultures on lysogeny broth (LB medium) agar plates were streaked out from a frozen stock kept at -80°C. LB-medium contained (per l): 10 g tryptone, 5 g yeast extract and 5 g NaCl (for LB-plates 12 g agar was added). LB-plates were incubated at 28°C for approximately 24 h and afterwards kept at 4°C for up to 10 days. For liquid cultures, 50 ml of liquid LB medium in a 200 ml Erlenmeyer flask were inoculated with a single colony from the LB-plate. The capped flask was incubated oxically at 28°C on a rotary shaker at 150 rpm. Cell concentration in LB-cultures was determined by optical density (OD) measurements at 600 nm. OD_{600} was calibrated against cell counts obtained by direct counting with a Thoma-chamber by light microscopy (Axioscope 2, Zeiss, Germany). At the end of exponential growth, cells had consumed O_2 completely and switched to anaerobic metabolism (Lies et al., 2005).

Fe(III) reduction experiments were conducted in LML medium (Myers and Myers, 1994), containing 12 mM HEPES buffer and 30 mM lactate as electron donor, adjusted to pH 7 and prepared sterilely and anoxically using a Widdel flask. Inoculum for experiments was prepared as follows: 2 ml of LB-grown cell culture were harvested after 14 h at late exponential growth phase and centrifuged (5 min, 10 600 g). Cells were washed twice with LML medium, resuspended in 2 ml of medium and diluted to a final concentration of 2×10^5 cells/ml in the culture tubes containing LML medium.

To monitor Fe(II) and mineral formation during microbial Fe(III) reduction, approximately 30 tubes were set up per experiment in parallel. Sterile culture tubes (total volume 23 ml) were filled with 9 ml (cultures containing 5 mM i.e. 0.5 g/l ferrihydrite) or 6 ml (cultures containing

30 mM i.e. 3.2 g/l ferrihydrite) of anoxic LML-medium. The headspace was exchanged with N_2 and the tubes were sealed with butyl rubber stoppers. For sample treatments in the glove box (mineral preparation, sequential extraction) smaller culture tubes (total volume 17 ml) were used which were closed with a thin butyl rubber stopper and a screw cap. Finally, ferrihydrite suspension, HA solution or phosphate buffer solution, and the cells were injected with syringes and the tubes were incubated horizontally at 28°C in the dark.

At sampling time points, several tubes (from the 30 parallel tubes) were selected to measure total Fe(II) and Fe(III) concentrations by acid digestion, to collect mineral samples and for sequential extraction of iron minerals. Complete digestion of the biogenic solids in one of the tubes was necessary at each time point in order to avoid inhomogeneous sampling with syringes and to determine the total amount of Fe(II) and Fe(III) including precipitates that stuck to the glass wall of the tubes.

All experiments testing different experimental conditions were performed at least twice. The experiment with 400 mg/l HA was performed once, but three tubes per sampling point were analyzed to get statistically significant values for the Fe(II) concentrations. In order to calculate the maximum reduction rates, total Fe(II) concentrations were plotted against time. A linear regression was used to derive the maximum slope for Fe(III) reduction rates.

2.2. Preparation of ferrihydrite suspensions and humic substance solutions

2-line ferrihydrite was synthesized according to Schwertmann and Cornell (2000) and Raven et al. (1998) using 40 g of $Fe(NO_3)_3 * 9H_2O$ per 500 ml water that was neutralized with 1 M KOH to a final pH of 7.2. After centrifugation and 4 times washing with Millipore®-water, the wet solid was resuspended in water to an approximate concentration of 0.5 M Fe(III). This suspension was stored in the dark in serum bottles and tightly closed with a butyl rubber stopper. Deoxygenation under vigorous stirring was done by alternating application of vacuum and N_2 for 10 min each and in total three times. The mineral product was identified by μ-X-ray diffraction (μ-XRD) after freeze-drying of an aliquot. Since we observed the formation of crystalline mineral phases

(hematite) after autoclaving the ferrihydrite suspension or storing it for longer than 3 months (data not shown), suspensions used for this study were not sterilized and used within 2 months after synthesis for experiments. N2-BET measurements after freeze-drying yielded surface areas of the ferrihydrite between 240-280 m2/g. 2-line ferrihydrite spiked with 20% of ^{57}Fe was synthesized to assure a sufficient signal yield for Moessbauer spectroscopy. Isotopic pure ^{57}Fe(0) was dissolved in 1 M HCl and kept anoxic. An aliquot equal to 20% Fe in our final mineral product was oxidized with H_2O_2 (35%). After addition of the remaining Fe(III) in the form of $Fe(NO_3)_3*9H_2O$ the ferrihydrite was synthesized as described before

For experiments with HA, IHSS (International Humic Substances Society) Pahokee Peat Humic Acid 1R103H2 was dissolved in 50 mM phosphate buffer (pH 7) to a concentration of up to 24 mg/ml. The final phosphate concentration in all humic acid containing experiments was 0.8 mM. After addition of HA to the phosphate buffer solution, in particular in the 24 mg/ml setups, the pH of the solution decreased slightly, leading to an incomplete dissolution of HA. In order to dissolve the HA completely, the pH was readjusted to 7 by dropwise addition of 2 M NaOH. The HA mixed with phosphate buffer was shaken for 1 h before filter-sterilization (cellulose acetate, 0.2 µm, Fisher Scientific, Germany) into autoclaved culture tubes closed with butyl rubber stoppers. After filtration the solution was deoxygenated under sterile conditions by alternating application of vacuum and N_2 for 5 min each and in total three times.

2.3. Sampling

In order to determine total concentrations of Fe(III) and Fe(II) (see below) during microbial iron reduction, culture tubes were sacrificed at different time points and the minerals in the tubes were completely dissolved by adding 2.25 ml (cultures with 5 mM ferrihydrite) or 3 ml (30 mM ferrihydrite) of 12 M HCl to the culture.

Samples for Moessbauer spectroscopy, µ-XRD and sequential extraction were prepared in an anoxic glove box (Braun, Germany; N_2 atmosphere) harvesting one screw-cap culture tube from each experimental setup. The samples were transferred stepwise into 2 ml-

Eppendorf® tubes and centrifuged (2 min, 9 700 g). Subsamples of the supernatant were kept in the glove box and analyzed for dissolved Fe(II) and Fe(tot). The remaining solids were prepared for Moessbauer measurements, dried for μ-XRD or treated with the sequential extraction method.

2.4. Sequential extraction

The protocol for sequential iron mineral extraction was modified after Roden and Zachara (1996). Loosely bound Fe(II) was extracted by a 1 M sodium acetate solution (pH 5). Vivianite and poorly crystalline minerals such as ferrihydrite were dissolved in 0.5 M HCl, whereas crystalline minerals such as goethite, magnetite and hematite were dissolved in 6 M HCl. Control experiments (data not shown) showed that synthetic siderite was dissolved partly in the acetate extraction solution and completely dissolved in 0.5 M HCl.

Solutions used for the extraction steps under anoxic conditions were bubbled with N_2 (30 min) before being brought into the glove box. For the first extraction step, 1.5 ml anoxic sodium acetate solution were added to the precipitates (that were separated by centrifugation) incubated for 24 h in the dark. The mixture was centrifuged (2 min, 9 700 g) and the supernatant was kept for Fe analysis. The residual solid was extracted with 1.5 ml of anoxic 0.5 M HCl. After 2 h of incubation (in the dark), the mixture was again centrifuged and the supernatant was kept for Fe analysis. The remaining solids were dissolved in 1.5 ml of 6 M HCl at 70°C in a water bath for 30 min outside the glove box. The extract was then analyzed for the Fe content.

2.5. Analytical methods

Dissolved HA were quantified by absorption measurements at 465 nm with a plate reader (FlashScan 550 microplate reader, Analytik Jena AG, Germany) of filtered samples (cellulose acetate, 0.2 μm, Fisher Scientific, Germany). LML-medium or phosphate buffer did not show significant interference at this wavelength. A filtered stock solution of IHSS standard Pahokee Peat Humic Acid 1R103H2 was diluted in 50 mM phosphate buffer to obtain a calibration curve between 0.03 and 0.3 mg/l.

Dissolved Fe(II) was quantified using the ferrozine assay (Stookey, 1970). In order to measure total iron (Fe(tot)) concentrations, aliquots were reduced with 10% w/v $NH_2OH*HCl$ dissolved in 1 M HCl. Fe(II) and Fe(tot) samples were mixed with a 0.1% (w/v) solution of ferrozine in 50% (w/v) of ammonium acetate buffer. Absorbance was measured at 562 nm in microtiter plates with a plate reader (FlashScan 550 microplate reader, Analytik Jena AG, Germany).

Surface area of iron minerals was determined by the Brunau-Emmett-Teller (BET) method with a Gemini 2375 Surface Area Analyzer (Micromeritics, Germany) with N_2 as adsorbing gas. Dry mineral samples were degassed for 30 min under vacuum at 105°C, before measuring a five-point-BET-curve.

For Moessbauer spectroscopic analysis, wet mineral samples were sealed between layers of Kapton® tape in the glove box. Samples were mounted in a close-cycle exchange-gas cryostat (Janis, USA) that allowed cooling of the sample to 4.2 K. Moessbauer spectra were collected with a constant acceleration drive system in transmission mode and with a ^{57}Co source. Spectra were calibrated against a spectrum of alpha-Fe metal foil collected at room temperature. Spectra calibration and fitting was performed with Recoil software (University of Ottawa, Canada) using Voigt based spectral lines.

For μ-XRD analyses, dried precipitates were prepared in the glove box. The solids were grinded in an agate mortar, suspended in approximately 50 μl of N_2-flushed ethanol and transferred with a glass pipette into small indentations (diameter 2 mm) on a silicon wafer. After evaporation of the ethanol, the samples were covered in the anoxic glovebox with a piece of clear plastic wrap (polyethylene) which remained oxygen tight for approximately 45 min and allowed XRD analysis outside the glovebox under anoxic conditions. The μ-XRD-device (Bruker D8 Discover X-ray diffraction instrument, Bruker AXS GmbH, Germany) consists of a Co K_α X-ray tube, operating at 30 kV, 30 mA, which is either connected to a polycapillary that allows measurements at a spot diameter of 50 μm or a monocapillary with a spot diameter of 300 μm. Each sample was measured in three overlapping frames of 30° 2θ, within 1 min measuring time for each

frame, using a GADDS® area detector. The EVA® 10.0.1.0 software was used to merge the three measured frames of one sample and to identify the containing mineral phases using the PDF-database licensed by ICDD (International Centre for Diffraction Data). X-ray diffractograms showed a broad signal in a 2θ range from 17° to 29°, originating from the foil which was used to protect the samples from oxidation. In this range and at smaller angels the intensity of the X-rays diffracted by the mineral lattice is reduced, due to the foil.

3. RESULTS AND DISCUSSION

3.1 Effect of phosphate and HA on Fe(III) reduction rates and extent

To determine the influence of HA on microbial reduction of ferrihydrite and mineral transformation, IHSS standard Pahokee Peat Humic Acid was added at different concentrations to cultures of Shewanella oneidensis MR-1 containing either 5 mM (0.53 mg/l) or 30 mM (3.21 mg/l) ferrihydrite. Since the HA were dissolved in phosphate buffer, control experiments containing medium, ferrihydrite, phosphate buffer, cells and no HA were set up. Compared to phosphate-free setups, these experiments allowed to determine the effect of phosphate present in the HA stock solutions on microbial ferrihydrite reduction and mineral transformation.

Phosphate binds strongly to iron oxide surfaces (Hongshao and Stanforth, 2001) and has been shown to hinder microbial Fe(III) reduction (Borch et al., 2007). Although we observed a decrease in reduction rates in the presence of 0.8 mM phosphate in both 5 and 30 mM ferrihydrite setups, we did not detect a significant change in the percentage of Fe(III) reduced at the end of microbial reduction, compared to phosphate-free setups (Fig. 1).

The extent of Fe(III) reduction reached up to 80-90% in all 5 mM ferrihydrite setups and was thus almost complete. Approximately 40% of Fe(III) were reduced in the 30 mM ferrihydrite setups. This is in contrast to the study by Borch et al. (2007), where Fe(II) formation decreased with increasing phosphate concentration and complete ferrihydrite reduction has not been observed even in absence of phosphate. However, it is not clear whether in their study microbial reduction was finished at the time point of analysis (after 7 days). Some of the differences observed could be due to the different medium composition (HEPES buffer and 30 mM lactate in our study vs. PIPES buffer and 3 mM lactate in the study by Borch and coauthors) and due to the different Fe(III) mineral substrates (pure ferrihydrite in our study vs. ferrihydrite-coated quartz sand used by Borch and coauthors) (see also discussion in section 3.5).
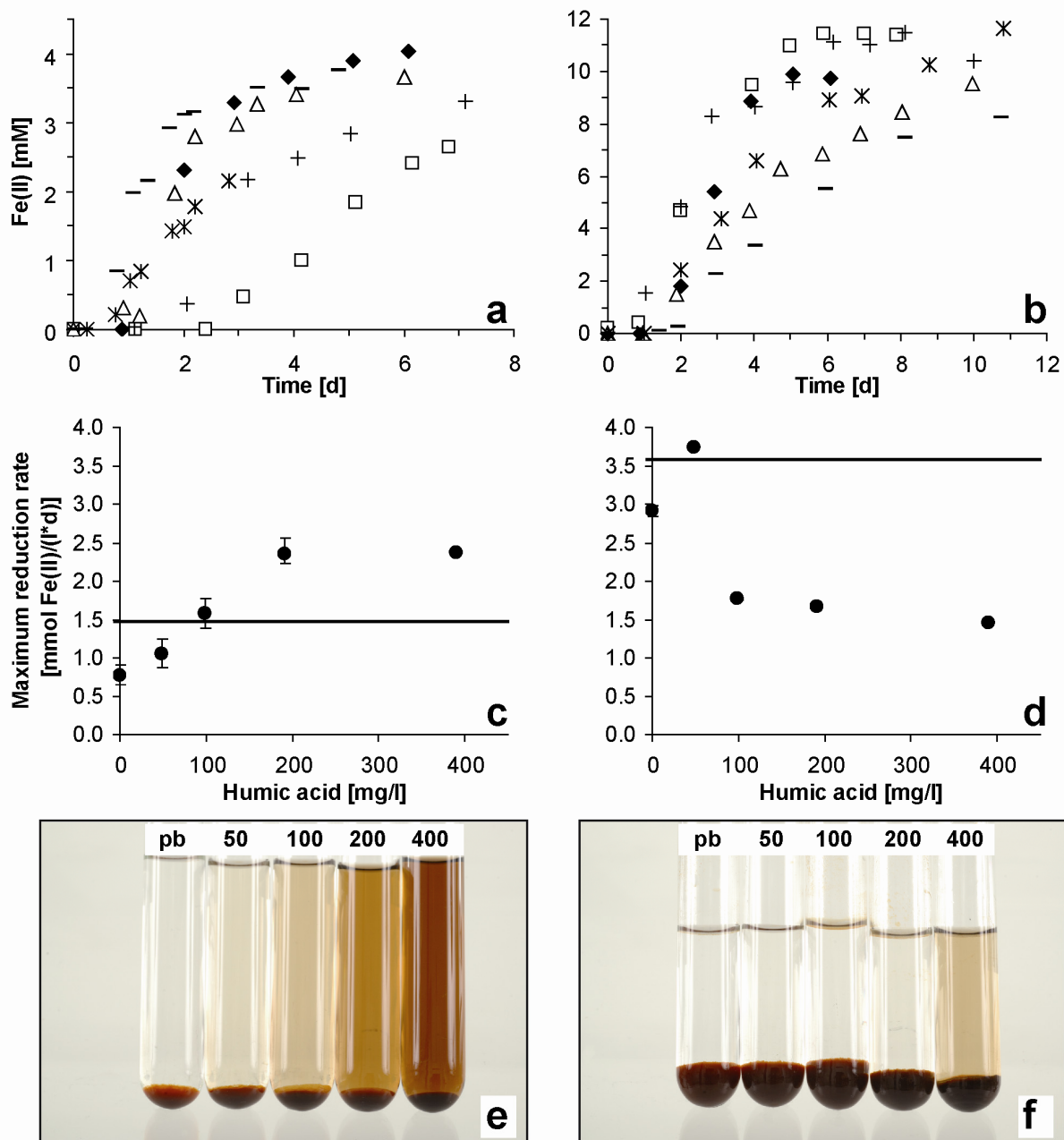
Fig. 1 Total Fe(II) formed over time by *Shewanella oneidensis* MR-1 in cultures (representative experiments shown) containing (a) 5 mM and (b) 30 mM 2-line ferrihydrite with no additions (◆), 0.8 mM phosphate (□), 50 mg/l HA (+), 100 mg/l HA (✳), 200 mg/l HA (△) and 400 mg/l HA (-) (all cultures amended with HA contained 0.8 mM phosphate). Maximum rates for microbial reduction of (c) 5 mM and (d) 30 mM 2-line ferrihydrite by *Shewanella oneidensis* MR-1 in cultures containing different concentrations of HA and in all cases 0.8 mM phosphate. Solid horizontal lines indicate maximum reduction rates of cultures that contained neither phosphate nor HA. Error bars indicate maximum and minimum rates of replicate experiments. In panel d error bars are smaller than the symbols. Images of culture supernatants after addition of different concentrations of HA in the presence of (e) 5 mM and (f) 30 mM 2-line ferrihydrite. Pictures show, from left to right, tubes containing 0.8 mM phosphate buffer (pb) or 50, 100, 200 and 400 mg/l HA (also containing 0.8 mM pb).

In their study, a sorption maximum of 0.8 mol phosphate per kg ferrihydrite was given. For comparison, we calculated the ratio of phosphate to the mass of ferrihydrite in our experiments and compared these values to the sorption values of phosphate to ferrihydrite given by Borch et al. (2007). In our experiments, in the presence of 5 mM ferrihydrite, the ratio of phosphate to ferrihydrite was almost twice (188%) as high as their sorption maximum, suggesting saturation of the mineral surface with adsorbed phosphate and excess dissolved phosphate. For experiments containing 30 mM ferrihydrite, the mineral surface was not completely saturated with phosphate (31% of their sorption maximum).

Nevertheless, the reduction rates decreased for both ferrihydrite concentrations (5 and 30 mM) in the presence of phosphate but the reduction extent remained constant (Fig. 1). Differences in Fe(III) reduction rates in the presence of phosphate were already described by Fredrickson et al. (1998) who compared hydrous ferric oxide (HFO) reduction in either bicarbonate- or PIPES-buffered medium, both with and without phosphate. They found that in bicarbonate-buffered medium, phosphate slowed down the reduction process, whereas in presence of PIPES buffer the Fe(III) reduction rates were similar with and without phosphate. In both buffer systems, they observed similar extents of Fe(III) reduction.

The addition of HA also did not change the extent of reduction but instead it increased the rate of Fe(III) reduction under certain conditions (Fig. 1). At the low ferrihydrite concentration (5 mM), stimulation of iron reduction by HA (compared to the HA-free but phosphate-containing setups) was observed at total HA concentrations ranging from 50 to 400 mg/l, although at 400 mg/l HA, iron reduction rates did not further increase compared to the 200 mg/l setup (Fig. 1c). In contrast, at 30 mM ferrihydrite only a HA concentration of 50 mg/l stimulated ferrihydrite reduction compared to the HA-free (but phosphate-containing) setup (Fig. 1d). At HA concentrations above 50 mg/l, the reduction rates decreased to values even lower than the rate determined in presence of only phosphate. At all HA concentrations tested, the Fe(III) reduction rates in 30 mM ferrihydrite setups did not

exceed significantly the reduction rates measured in absence of phosphate.

The acceleration of Fe(III) reduction observed in some of our experiments after HA addition could be due to electron shuttling via dissolved HA (Lovley et al., 1996b; Royer et al., 2002a), Fe(III) solubilization by complexation (Lovley et al., 1996a; Nevin and Lovley, 2002b), by scavenging of dissolved Fe(II) thereby maintaining the thermodynamic driving force for further Fe(III) reduction (Royer et al., 2002b) and decreasing Fe(II) sorption, or potentially even by facilitating electron transfer through sorbed HA (Marsili et al., 2008). In order to evaluate the actual mechanism which is responsible for the acceleration, first, we quantified the adsorbed and dissolved fractions of the HA present in our experiments. After adding HA at total concentrations from 50 to 400 mg/l to the Fe(III)-reducing cultures, quantification of HA in the culture supernatant showed that a significant fraction of the added HA was adsorbed to the mineral surface (Table 1).

Tab 1 Total and dissolved amount of Pahokee Peat Humic Acid (HA) and maximum amount of Fe(II) complexed by dissolved HA determined in cultures containing 5 mM or 30 mM of 2-line ferrihydrite (calculation of Fe(II) complexation see page 85).

HA total [mg/l]	5 mM ferrihydrite		30 mM ferrihydrite	
	HA dissolved [mg/l]	complexed Fe(II) [mM]	HA dissolved [mg/l]	complexed Fe(II) [mM]
48.9	14.4	0.11	n.d.	0.00
94.8	47.6	0.35	n.d.	0.00
191.7	126.6	0.93	n.d.	0.00
390.4	318.0	2.33	7.4	0.05

n.d.: not determinable = below detection limit of instrument (0.01 mg/l)

In the 5 mM ferrihydrite setups, dissolved HA concentrations between 14.4 and 318.0 mg/l were measured, indicating that in all 5 mM ferrihydrite setups dissolved HA was present (Table 1). In contrast, in the 30 mM setups complete HA adsorption was observed (dissolved HA concentrations below the detection limit) with the exception of the

experiment with an addition of 400 mg/l HA, where a small amount of HA (7.4 mg/l) remained in solution (Table 1). This sorption behavior could also be observed visually. The liquid phase in the culture tubes containing 30 mM ferrihydrite remained almost clear after ferrihydrite sedimentation (with the exception of the 400 mg/l setup), whereas in the 5 mM ferrihydrite setups a brownish-colored supernatant was observed at all HA concentrations (Fig. 1e and f).

In addition to these visual observations, we calculated the surface saturation of ferrihydrite by HA using the Langmuir parameters determined for HS adsorption on ferrihydrite by Tipping et al. (1981) (Table 2 and Fig. 2). These calculations showed that surface saturation of ferrihydrite (with a specific surface area of 255 m²/g determined by BET) by HA in presence of 30 mM ferrihydrite was not achieved at any HA concentration used in our experiments (Fig. 2 and Table 3). Consequently, in all 30 mM ferrihydrite setups there was an excess of mineral surface area compared to the amount of HA. The mineral surface was therefore just partially covered with HA molecules. Nevertheless, at the highest HA concentration of 400 mg/l added, we found that some HA (7.4 mg/l) remained in solution (Table 1). Similar to the 30 mM ferrihydrite setup with 400 mg/l HA, we found that also in the 5 mM ferrihydrite setup with 50 and 100 mg/l HA, dissolved HA was present (14.4 and 47.6 mg/l, respectively, Table 1), although surface saturation was not yet reached (<1.6 mg total HA/m² FH see Table 2 and Fig. 2). The corresponding calculations suggest that at HA concentrations of 200 mg/l or higher, the ferrihydrite surface is completely loaded with HA (>1.6 mg total HA/m² FH see Fig. 2 and Table 3). This confirms the experimental finding that increasing the total HA concentration by 200 mg/l from 200 mg/l to 400 mg/l lead to an almost equivalent increase of 191.4 mg/l in dissolved HA concentrations (from 126.6 to 318.0 mg/l Table 1), meaning that virtually no HA from this additional amount of HA were sorbed to the mineral surface.

Calculation of the sorption isotherm (HA on ferrihydrite) after Tipping et al. (1981)

- Data and equations given by Tipping et al. (1981):
α: loading of the adsorbent (mg adsorbed HS/g ferrihydrite)
n: maximum sorption capacity of the mineral ([mg/g])
K: sorption coefficient (affinity of the mineral for HS [l/mg])
c: remaining sorbent in solution (not sorbed HS in solution at equilibrium [mg/l])
Langmuir equation: $\alpha = nKc/(1+Kc)$

- Given parameters for sorption of HS on ferrihydrite:
$A_{FH} = 250$ m²/g
at pH 7: n = 224 mg/g; K = 0.5 l/mg
Solutions contained 0.1 g/l (m_{FH} = 0.1 g) iron oxide and HS concentrations in the range of 0-50 mg/l
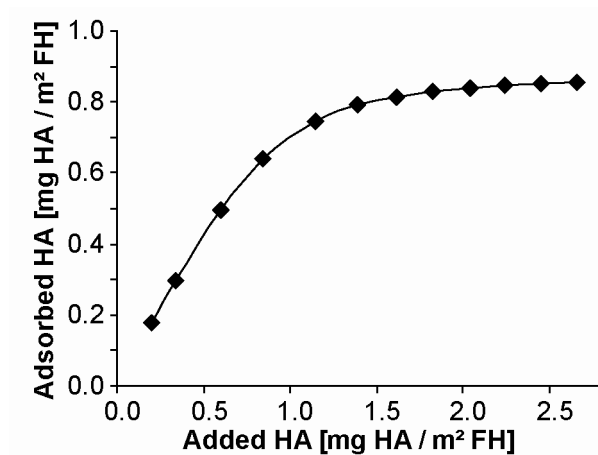
Fig. 2 Sorption of HA to ferrihydrite: data points represent calculated values for total amount of HA per m² mineral surface area added (from Table 2: column 7) plotted vs amount of HA sorbed per m² of ferrihydrite (FH) surface area (from Table 2: column 3)

Tab 2 Langmuir parameters and calculated values of the isotherm.

1	2	3	4	5	6	7
HS dissolved	HS sorbed fraction			HS total amount added		
c	α (calculated)	α/A	$\alpha \times m_{FH}$	$c+\alpha \times m_{FH}$	$(c+\alpha \times m_{FH})/m_{FH}$	$c+\alpha \times m_{FH}/(m_{FH}*A_{FH})$
[mg/l]	[mg/g]	[mg/m²]	[mg]	[mg/l]	[mg/g]	[mg/m²]
0.5	44.80	0.18	4.48	4.98	49.80	0.20
1	74.67	0.30	7.47	8.47	84.67	0.34
2.5	124.44	0.50	12.44	14.94	149.44	0.60
5	160.00	0.64	16.00	21.00	210.00	0.84
10	186.67	0.75	18.67	28.67	286.67	1.15
15	197.65	0.79	19.76	34.76	347.65	1.39
20	203.64	0.81	20.36	40.36	403.64	*1.61*
25	207.41	0.83	20.74	45.74	457.41	*1.83*
30	210.00	0.84	21.00	51.00	510.00	*2.04*
35	211.89	0.85	21.19	56.19	561.89	*2.25*
40	213.33	0.85	21.33	61.33	613.33	*2.45*
45	214.47	0.86	21.45	66.45	664.47	*2.66*

Content of the columns:

2: Calculation of α using some exemplary values for c (column 1)

3: α related to the mineral surface area A: α / A

4: total amount of HS adsorbed to the mineral surface: $\alpha \times m_{FH}$

5: total amount of HS in one liter: $c+\alpha \times m_{FH}$

6: mass ratio of total amount of HS to mass of ferrihydrite: $(c+\alpha \times m_{FH})/m_{FH}$

7: ratio of total amount of HS to surface area of ferrihydrite (italic/bold values indicate surface saturation; Fig. 2): $(c+\alpha \times m_{FH})/(m_{FH} \times A_{FH})$

HA sorption in own experiments (calculations)

Surface area mean value of five samples of synthesized, dried 2-line ferrihydrite surface area determined by BET-measurement (comparable to the study of Tipping): A_{FH} = 255 m²/g

Molecular weight of ferrihydrite: $M(Fe(OH)_3)$ = 106.88 g/mol
c_{FH} = 5 and 30 mmol/l

Mass-related ferrihydrite concentration: $c_{FHw} = c_{FH} \times M_{FH}$
c_{FHw} = 0.53 and 3.21 g/l

Surface saturation in our experiments was reached for experiments containing 5 mM ferrihydrite and 200 mg/l HA and higher (compare values given in bold/italic letters in Table 3 to the modelled data shown in Fig. 2).

Tab 3 Calculated values of HA sorption based on experimental data ($c_{HAtotal}$) for the total amount of HA related to the mass of ferrihydrite and the surface area of ferrihydrite (255 m²/g). Bold/italic values in the table indicate HA concentrations at which ferrihydrite surface saturation by HA is exceeded according to Fig. 2.

1	2	3	4	5
	total HA + 5 mM ferrihydrite		Total HA + 30 mM ferrihydrite	
$c_{HAtotal}$ HA				
[mg/l]	[mg/g]	[mg/m²]	[mg/g]	[mg/m²]
0.0	0.0	0.00	0.0	0.00
48.9	91.5	0.35	15.3	0.06
94.8	177.4	0.68	29.6	0.11
191.7	358.6	*1.38*	59.8	0.23
218.9	409.6	*1.58*	68.3	0.26
390.4	730.5	*2.81*	121.8	0.47

Content of the columns:
1: $c_{HAtotal}$ total concentration of HA added to the experiment [mg/l]
Experiments containing 5 mM (2+3) and 30 mM (4+5) ferrihydrite
2+4: mass of total HA per g ferrihydrite: $c_{HAtotal}/c_{FHw}$ [mg/g]
3+5: mass of total HA per surface area of ferrihydrite: $c_{HAtotal}/(c_{FHw} \times A_{FH})$ [mg/m²]

A stimulation of microbial reduction by dissolved HA can be observed in our 5 mM ferrihydrite setups where addition of HA increased Fe(III) reduction rates. The rates in presence of HA are not only higher than in phosphate-amended setups but also higher than in phosphate-free setups (Fig. 1c). The acceleration of Fe(III) reduction can be explained by the presence of significant concentrations of dissolved HA shuttling electrons from the cells to the Fe(III) minerals. In all 5 mM ferrihydrite setups the HA concentrations were above the lower limit of HA necessary for stimulation of Fe(III) reduction (10 mg/l HA) (Jiang and Kappler, 2008). From our data it can also be seen that after exceeding surface saturation of the mineral particles with adsorbed HA (5 mM ferrihydrite, 200 mg/l HA and above), no further acceleration of iron reduction rates occurred. The iron reduction rates remained at a constant elevated level, while the concentration of dissolved HA was still increasing (Table 1 and Fig. 1). Jiang and Kappler (2008) suggested an upper limit of dissolved HA concentration of 50 mg/l HA (in experiments using 1 mM ferrihydrite), above which no further stimulation of Fe(III) reduction occurred even in the presence of higher HA concentrations. Compared to their study, in our experiments five times as much ferrihydrite (5 mM) and consequently about five times as much surface area was present. Therefore, a five times as high HA concentration (250 mg/l) is expected to be necessary to reach the point at which no further stimulation of Fe(III) reduction occurs. Indeed, our experiments with 5 mM ferrihydrite showed no further increase of reduction rates at HA concentrations above 200 mg/l, a concentration close to the expected value based on the experiments from Jiang and Kappler (2008). Therefore, both studies support the hypothesis that an upper limit of HA concentration for stimulation of Fe(III) reduction by electron shuttling exists.

Above this concentration the electron transfer process may be limited either by the metabolic activity of the cells (oxidation of organic carbon and release of electrons) or by the electron transfer from dissolved (reduced) HA to the mineral surface (potentially via sorbed HA). The fact that the upper limit for stimulation of microbial iron reduction by HA occurs at the HA concentration where surface saturation of ferrihydrite is reached suggests that once the mineral surface is fully loaded with HA molecules, the maximum number of

sites available for electron transfer from dissolved HA to the mineral surface or to adsorbed HA at the mineral surface is reached. Consequently, electron transfer from dissolved (reduced) to adsorbed HA and/or to the mineral surface may control maximum reduction rates under these conditions.

In contrast to the 5 mM setups, in all 30 mM ferrihydrite setups the addition of HA (and 0.8 mM phosphate) did not stimulate Fe(III) reduction compared to the setups that contained neither HA nor phosphate. Only the addition of 50 mg/l HA lead to an increase of the reduction rates compared to phosphate-containing setups. The inhibiting effect of phosphate was most likely compensated by the added HA via complexation of some of the added phosphate by the HA (He et al., 2006; Guardado et al., 2008). The low reduction rates observed even at higher HA concentrations suggest that despite the presence of a significant amount of HA, these sorbed HA molecules did not stimulate microbial Fe(III) reduction (for detailed discussion of the 30 mM experiments see section 3.2). Even in 30 mM ferrihydrite setups with addition of 400 mg/l HA where 7.4 mg/l of HA remained in solution, this amount was not sufficient to significantly stimulate microbial iron reduction (Fig. 1d). This observation is again in agreement with the study from Jiang and Kappler (2008), who showed that a minimum concentration of 10 mg/l dissolved HA is necessary to stimulate microbial ferrihydrite reduction.

3.2 Fe(II) and Fe(III) complexation by HA

Besides facilitating electron transfer from cells to poorly soluble Fe(III) minerals, dissolved HS also have been suggested to stimulate microbial Fe(III) reduction by Fe(II) complexation and thus removal of the metabolic product, i.e. Fe(II), thereby increasing the thermodynamic driving force for further reduction (Royer et al., 2002b; Royer et al., 2002a). Consequently, with increasing concentrations of dissolved HA more Fe(II) is expected to be complexed, thus more Fe(III) is expected to be reduced and potentially even reduction rates increase. To determine whether this mechanism played a role in our experiments, we calculated the theoretical amount of Fe(II) that can be complexed by the dissolved HA present, based on the content of acidic functional groups given by the IHSS (Tab. 1).

Fe(II) complexation by IHSS Pahokee Peat HA (PPHA) 1R103H at pH 7

The data and equation used for the calculation are available on the homepage of the International Humic Substance Society IHSS (http://www.ihss.gatech.edu). For further information about the determination of acidic functional groups in HS, titration modelling, and the potential for iron complexation by HS see Ritchie and Perdue (2003) and Royer et al. (2002a).

Modified Henderson-Hasselbalch equation Ritchie and Perdue (2003):

$$Q_{tot} = \left(\frac{Q_1}{1 + \left(K_1 \left[H^+ \right] \right)^{1/n_1}} \right) + \left(\frac{Q_2}{1 + \left(K_2 \left[H^+ \right] \right)^{1/n_2}} \right)$$

Tab 4 Parameters given for PPHA 1R103H by IHSS

C content	Q_1	log K_1	n_1	Q_2	log K_2	n_2
56.84%	9.54	4.26	3.25	1.01	9.85	1.00

Calculation of the overall charge density for PPHA 1R103H at pH 7

$$Q_{tot} = \left(\frac{9.54}{1 + \left(10^{4.26} \cdot \left[10^{-7} \right] \right)^{1/3.25}} \right) + \left(\frac{1.01}{1 + \left(10^{9.85} \left[10^{-7} \right] \right)^{1/1.00}} \right)$$

$$Q_{tot} = \frac{9.54}{1.14} + \frac{1.01}{708.95} = 8.34 \, {mequ}/{gC}$$

Complexing capacity of PPHA 1R103H for Fe(II) in cultures:

One mole acidity binds 0.5 moles of Fe^{2+} (Royer et al., 2002a):
$C_{Fe(II)c} = Q_{tot}/2 = 4.17$ mmol Fe(II)/g C

Complexation capacity of PPHA 1R103H (C content: 56.84%):
$C_{Fe(II)HA} = C_{Fe(II)c}/0.5684 = 7.34$ mmol Fe(II)/g HA

Amount of Fe(II) complexed by dissolved HA in cultures (Tab. 1):
$c_{Fe(II)} = c_{HAdiss} \times C_{Fe(II)HA}$

According to these calculations, 126.6 and 318.0 mg/l dissolved HA should complex 0.93 and 2.33 mM Fe(II), respectively (Table 1). Consequently an increase of the total HA concentration from 200 to 400 mg/l in presence of 5 mM ferrihydrite should have a major effect on the Fe(II) complexation and thus on the iron reduction rates. However, the reduction rates were almost the same in the 200 and 400 mg/l setups and no further increase in total Fe(II) formed was observed. We therefore conclude that Fe(II) complexation played a minor role for stimulation of Fe(III) reduction in our experiments. In addition to complexation of Fe(II), HA can also complex and solubilize Fe(III). The lack of significant concentrations of dissolved Fe(III) in any of our experiments (see section 3.4.) suggests that Fe(III) complexation by HA also did not play an important role for stimulation of Fe(III) reduction, as suggested by Nevin and Lovley (2002b).

3.3 Effect of HA on HA-iron mineral aggregation and accessibility of iron minerals for microbial Fe(III) reduction

Our experiments showed that depending on the concentrations of ferrihydrite and HA, HA either stimulated microbial Fe(III) reduction by electron shuttling or inhibited Fe(III) reduction. The lack of correlation between Fe(III) reduction rates and HA concentration observed in the 30 mM ferrihydrite setups showed that another effect, besides surface blocking due to sorption, obviously played a role. Visual observation showed differences in particle sedimentation behaviour at different ferrihydrite and HA concentrations (Fig. 3), leading to the hypothesis that the ferrihydrite aggregate size and thus the surface area available for bacteria were different at the two different ferrihydrite concentrations. This is important since microbial Fe(III) reduction depends on the available surface area of the Fe(III) mineral (Roden and Zachara, 1996; Roden, 2003).

The size of the ferrihydrite aggregates differed already in the absence of HA at the two ferrihydrite concentrations used, with larger aggregates and faster sedimentation in the 30 mM compared to the 5 mM setup (Fig. 3a). However, not only ferrihydrite concentration but also the presence of HA influenced the aggregate formation. In all 5 mM ferrihydrite setups the HA-coated ferrihydrite particles were distributed almost homogeneously in the culture tube even after a few minutes and

settled very slowly (Fig. 3b). In contrast, with 30 mM ferrihydrite only after addition of 400 mg/l HA sedimentation was slow (comparable to the 5 mM setups), in all other 30 mM ferrihydrite tubes that contained less HA, the particles settled fast (Fig. 3c). When comparing these results to the concentrations of dissolved HA (Table 1), it can be seen that in all setups containing dissolved HA the sedimentation rates were slow, while in the absence of detectable amounts of dissolved HA, sedimentation was rapid. This suggests the presence of larger aggregates in the absence of dissolved HA. Such larger aggregates are expected to have lower surface/volume ratios, lower surface areas and therefore, a lower accessibility for the Fe(III)-reducing bacteria resulting in lower reduction rates as observed in our 30 mM ferrihydrite experiments (Fig. 1).
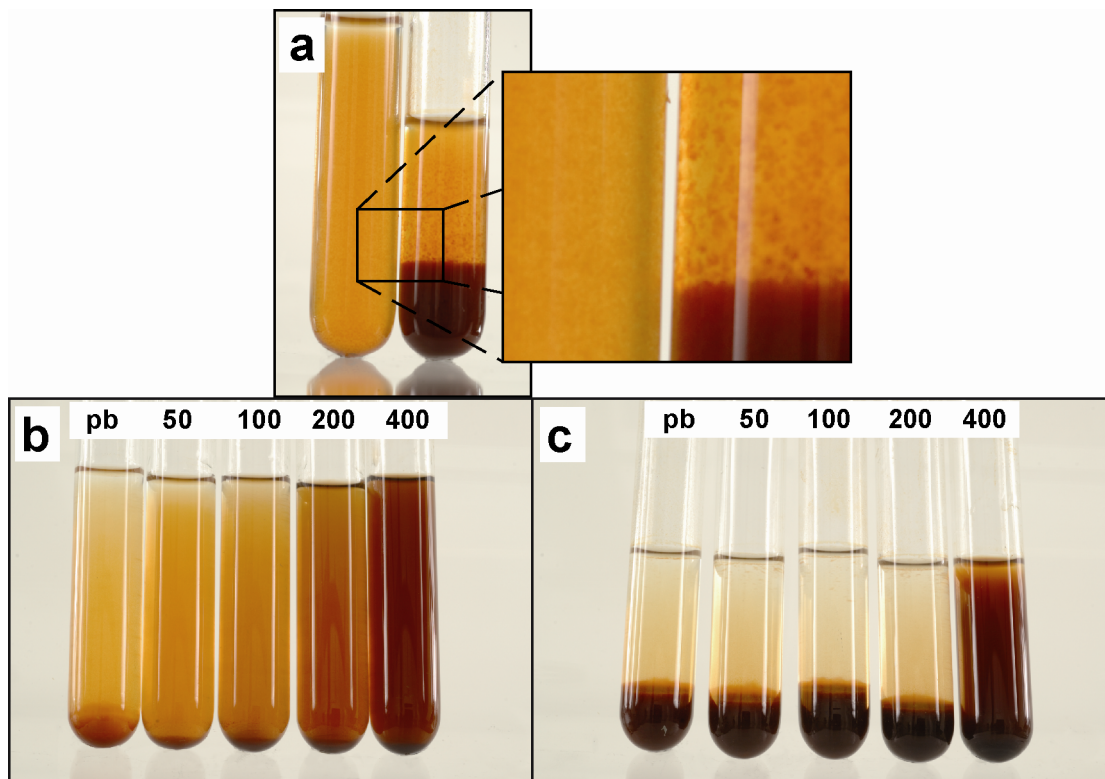
Fig. 3 **2-line ferrihydrite particle aggregation indicated by sedimentation behaviour of mineral particles before bacterial inoculation. Image (a) shows tubes that contain 5 mM (left tube) and 30 mM 2-line ferrihydrite (right tube) without any additions. Images were taken 2 minutes after shaking. Note the difference in ferrihydrite aggregate size visible in the close-up image. Image (b) shows tubes containing 5 mM and image (c) 30 mM 2-line ferrihydrite with and without addition of HA. Images were taken 10 minutes after shaking. Pictures show, from left to right, tubes containing 0.8 mM phosphate buffer (pb) or 50, 100, 200 and 400 mg/l HA (also containing 0.8 mM pb).**

Since our results suggest that the presence of sorbed HA influenced ferrihydrite aggregation and microbial electron transfer to ferrihydrite, it is necessary to understand the geochemical factors controlling the aggregation of these particles. Vermeer et al. (1998) showed that adsorption of negatively charged HA molecules to positively charged iron minerals changes the surface charge of the mineral particles depending on pH and present dissolved ions. They calculated the overall surface charge of hematite particles after adsorption of HA to be slightly negative at pH 6, in contrast to pure hematite (point of zero charge, pzc, of 8.9) which is positively charged at the above pH. They also observed less HA adsorption on smaller hematite particles compared to sorption to larger hematite particles at pH 6 with equal amounts of total surface area present. This was explained by a higher negative surface charge density at the small particles after HA adsorption compared to larger particles. The consequence of this is a strong repulsion between the negatively charged, small, HA-coated hematite particles and additional negatively charged dissolved HA molecules preventing further HA adsorption. Further, it has also been shown that the change in surface charge by adsorption of different amounts of HA to colloidal magnetite particles increased the stability of colloidal magnetite dispersions, probably due to repulsion of the negatively charged particles, preventing aggregation (Illés and Tombácz, 2006).

A similar stabilization of small mineral particles probably occurred in our 5 mM ferrihydrite experiments, where the ferrihydrite particles were relatively small in the absence of HA (Fig. 3a). Adsorption of HA to these small ferrihydrite aggregates lead to a high negative charge density on the aggregates, thus preventing further HA adsorption or coagulation (similar to the HA sorption experiments with small hematite particles described by Vermeer et al. (1998)). This clearly prevented further aggregation similarly as observed for the magnetite colloids (Illés and Tombácz, 2006) and lead to a high surface area per amount of ferrihydrite and good access for microbial Fe(III) reduction. The simultaneous presence of dissolved HA which we observed in our experiments with 5 mM ferrihydrite even promoted iron reduction by the dissolved HA acting as electron shuttle, (Fig. 1c) without the need of direct contact between the cells and the mineral surface. In presence of

30 mM ferrihydrite and HA concentrations >50 mg/l, reduction rates decreased to values even lower than in the absence or presence of phosphate (Fig. 1d), indicating that the ferrihydrite surface available for the Fe(III)-reducing bacteria decreased. This could be due to further aggregation instead of electrostatic repulsion of charged particles (as it was observed in the 5 mM ferrihydrite setups) after inhomogeneous sorption of negatively-charged HA to the positively-charged, larger primary particles. Illés and Tombácz (2006) described the non-uniform distribution of negatively charged HS on the positively charged magnetite surface as "patch-wise charge heterogeneity", leading to electrostatic attraction between the patches of opposite charge on the mineral surface and promoting aggregation of the particles. In this case, HA even act as bridging molecule between mineral particles. The particle aggregation leading to a decrease in available surface area for Fe(III) reduction, in combination with the lack of dissolved HA, probably explains the observed low reduction rates in presence of 100-400 mg/l HA (Fig. 1d). The fact that the reduction rate was slightly higher in presence of 50 mg/l HA suggests that at this HA concentration the amount of HA sorbed to mineral aggregates was probably not high enough to cause significant particle aggregation.

3.4 Consequences of HA-mineral aggregate formation on electron shuttling and Fe(III) reduction rates

HA can either stimulate Fe(III) reduction by electron shuttling or hinder electron transfer by sorption, surface blocking and/or aggregate formation leading to a smaller bioavailable mineral surface area. The scheme in Figure 4 illustrates and summarizes the complex interplay of the main components in our experimental system of iron minerals, HA and Fe(III)-reducing bacteria, considering the effects of phosphate and varying concentrations of HA and ferrihydrite.
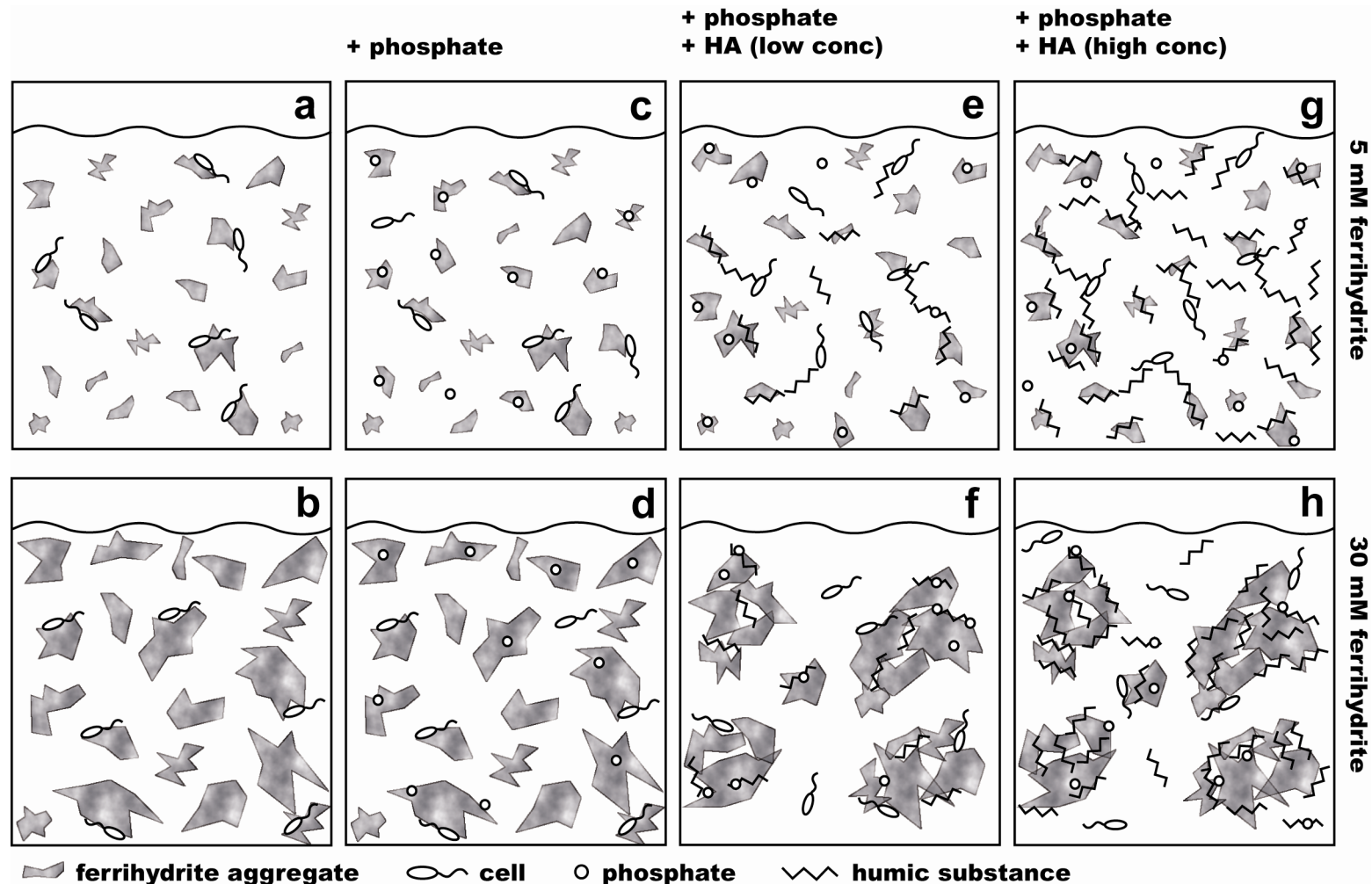
Fig. 3 Schematic illustration of changes in size of mineral aggregates, aggregate surface area and coverage of the aggregates by cells, phosphate and HA. The different panels illustrate cultures containing 5 mM (upper row) and 30 mM 2-line ferrihydrite (bottom row). All setups contain medium, ferrihydrite and cells. The concentrations of phosphate and humic acids (HA) vary in the different diagrams as indicated above the diagrams.

With increasing ferrihydrite concentrations the aggregate size of ferrihydrite increases, and thus the bioavailable surface area per mass ferrihydrite decreases as illustrated in Figure 4a and b for 5 and 30 mM ferrihydrite, respectively. Sorption of phosphate to the mineral surface blocks surface sites for electron transfer leading to decreased reduction rates (Fig. 1c and d, Fig. 4c and d). Additionally, negatively charged phosphate sorbed to ferrihydrite particles could cause repulsion of negatively charged cells, also leading to decreased reduction rates. The additional presence of HA seems to outweigh this inhibiting effect caused by phosphate, potentially due to binding of phosphate by the HA molecules (Fig. 4e and 4f). However, the presence of HA did not show an acceleration of microbial Fe(III) reduction under every condition investigated (Fig. 1c and d). In fact, HA sorption can block surface sites on the mineral and restrict the accessibility for bacteria. Additionally, and probably even more important, negatively charged adsorbed HA molecules bind to ferrihydrite particles, change the net surface charge of the iron mineral particles from positive to negative (at least partially) and depending on the size of the ferrihydrite particles, lead either to repulsion of the particles (Fig. 4e and 4g) or to formation of larger iron mineral aggregates (Fig. 4f and 4h). These larger ferrihydrite-HA aggregates provide even less access to the mineral surface for bacteria either due to their smaller surface area per mass ferrihydrite (in comparison to the non-aggregated ferrihydrite particles) or due to repulsion of negatively charged cells by the negatively charged mineral surface (Fig. 4f and h).

Both effects lead to lower reduction rates. This aggregation effect resulting in a lowered bioavailable surface area can be observed at low HA:ferrihydrite ratios (30 mM ferrihydrite experiments, Fig. 1d). In this case either none or only very few HA molecules are present in solution not supporting electron shuttling and requiring direct contact between cells and mineral surface for electron transfer. In the presence of lower ferrihydrite concentration (5 mM), a further increase of the HA:ferrihydrite ratio leads to the presence of significant concentrations of dissolved HA (Table 1). Once the minimum amount of 10 mg/l dissolved HA necessary for electron shuttling is reached, microbial reduction is stimulated (Fig. 1c and 4e). Dissolved HA effectively shuttle electrons between cells and ferrihydrite, which supersedes the need for

direct contact between cells and the mineral surface. However, the stimulating effect (indicated by increasing reduction rates) levels off as soon as the mineral surface is saturated with adsorbed HA in presence of 200 mg/l total HA (Fig. 1c and 4g). This suggests an upper limit of dissolved HA concentration above which the reduction rate is no longer limited by the electron transfer between cells and ferrihydrite via HA but rather by the release of electrons from the cells. In summary, we conclude that the rates of electron transfer from Fe(III)-reducing cells to ferrihydrite (including HA electron shuttling) strongly depend on the HA:ferrihydrite ratio, on the sorption capacity of ferrihydrite for HA, and thus on the proportions of dissolved and adsorbed HA.

3.5. Effect of HA on mineral formation during microbial Fe(III) reduction

The presence of both phosphate and HA are expected to influence the mineral formation during microbial Fe(III) reduction. We therefore quantified dissolved, loosely bound, poorly crystalline and crystalline Fe species by sequential extraction (Fig. 5) and identified the minerals produced by XRD, and for some experiments also by Moessbauer spectroscopy (Fig. 6 and 7).
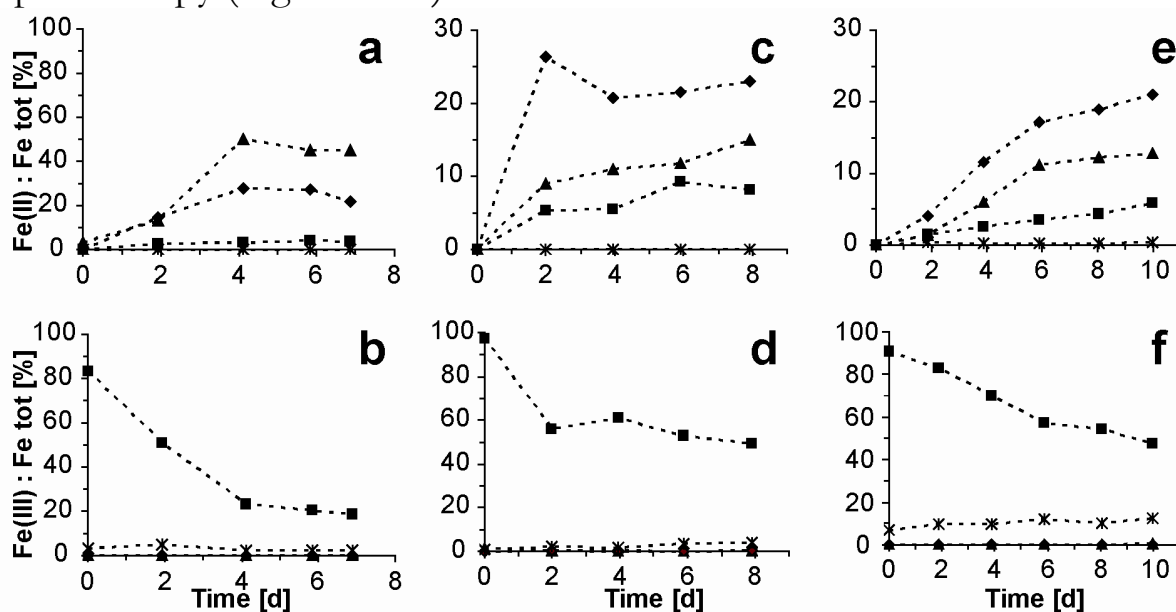
Fig. 5 Dissolved (▲), loosely bound (◆), poorly crystalline (■) and crystalline (✕) Fe(II) fractions (top row) and Fe(III) fractions (bottom row) quantified by sequential extraction of precipitates formed during microbial reduction of (a, b) 5 mM ferrihydrite+200 mg/l HA, (c, d) 30 mM ferrihydrite+0.8 mM phosphate buffer and (e, f) 30 mM ferrihydrite + 200 mg/l HA. Representative data from independent experiments are shown. Note the different scales (y-axis) in the two upper right panels. Data points are connected as a guide to the eye.

Sequential extraction of biogenic precipitates formed by *Shewanella onidensis* MR-1 at the lower ferrihydrite concentration (5 mM, with 200 mg/l HA; Fig. 5a) revealed a significantly higher extent of Fe(III) reduction and Fe(II) formation compared to all 30 mM ferrihydrite setups. Additionally, the amount of Fe(II) extracted in the loosely bound fraction of the HA-/ phosphate-containing 5 mM ferrihydrite cultures was significantly higher (27% of the total iron) compared to experiments with 5 mM ferrihydrite but without HA and phosphate (6%, chapter 2 Fig. 6). In the presence of HA/phosphate, some Fe(II) (4%) was present even in the poorly crystalline mineral fraction. These results suggest the formation of poorly crystalline minerals in presence of phosphate and HA, in contrast to phosphate- and HA-free setups where 5 mM ferrihydrite was completely converted into dissolved Fe(II) without any Fe(II) mineral precipitation (chapter 2 Fig. 6). Using XRD and Moessbauer spectroscopy, we identified vivianite as Fe(II) mineral in all experiments containing 5 mM ferrihydrite and either phosphate or HA dissolved in phosphate buffer after complete Fe(III) reduction (Fig. 6a, 7 und 8).
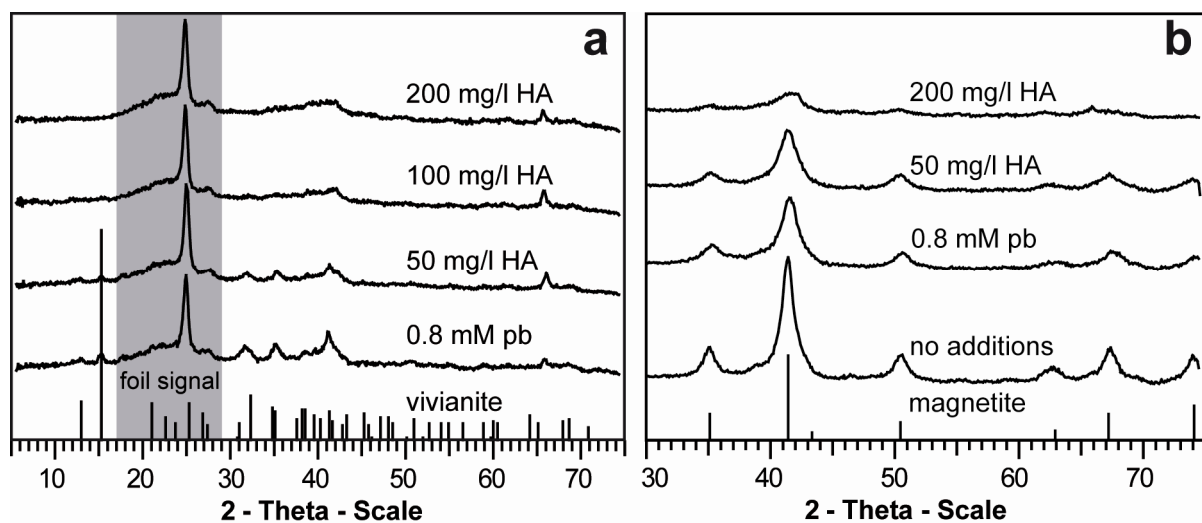
Fig. 6 X-ray diffractograms of precipitates formed during reduction of (a) 5 mM and (b) 30 mM 2-line ferrihydrite by *Shewanella oneidensis* MR-1 in presence of 50, 100 and 200 mg/l HA, respectively. Furthermore, reference experiments without additions and in the presence of 0.8 mM phosphate buffer (pb) are shown. Samples were collected after Fe(III) reduction stopped. Reference patterns of magnetite and vivianite are shown for comparison. The gray bar in panel b indicates the signal of the foil covering the sample holder to maintain anoxic conditions during measurements. Please note the different scale on the x-axis.
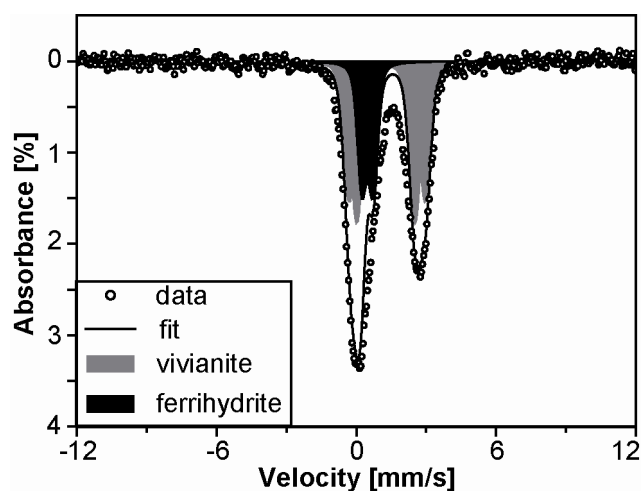
Fig. 7 Moessbauer spectrum (measured at 77K) of precipitates collected after 11 days of reduction of 5 mM 2-line ferrihydrite by *Shewanella oneidensis* MR-1 in presence of 0.8 mM phosphate. Open circles: measured data, filled areas: modelled relative amounts of identified minerals, solid line: fitted spectrum.

Reduction of 5 mM of 2-line ferrihydrite in presence of 0.8 mM phosphate and HA:

Vivianite could not be identified clearly from XRD patterns in experiments containing 5 mM ferrihydrite and HA. To verify the presence of vivianite, Moessbauer spectra of biogenic precipitates after complete reduction of 5 mM 2-line ferrihydrite were collected. The initial Fe(III) substrate was spiked with 20% of ^{57}Fe to assure a sufficient signal yield. XRD (Fig. 8a) and Moessbauer (Fig. 8b) measurements of the ^{57}Fe-labelled 2-line ferrihydrite showed traces of lepidocrocite and goethite as impurities in the synthesized ferrihydrite. After incubation of *Shewanella oneidensis* MR-1 with 5 mM ferrihydrite and 100 mg/l HA, the formation of vivianite was detected by XRD (Fig. 6b), and verified by Moessbauer spectroscopy (Fig. 8c and d). The incubation of the ^{57}Fe-labeled ferrihydrite with *Shewanella oneidensis* MR-1 did not lead to a transformation of the Fe(III) mineral impurities (goethite and lepidocrocite) indicated by the remaining sextet signals at 4.2 K and an additional dublett at 77 K. Vivianite was also identified in setups containing phosphate buffer, 50 and 200 mg/l HA.
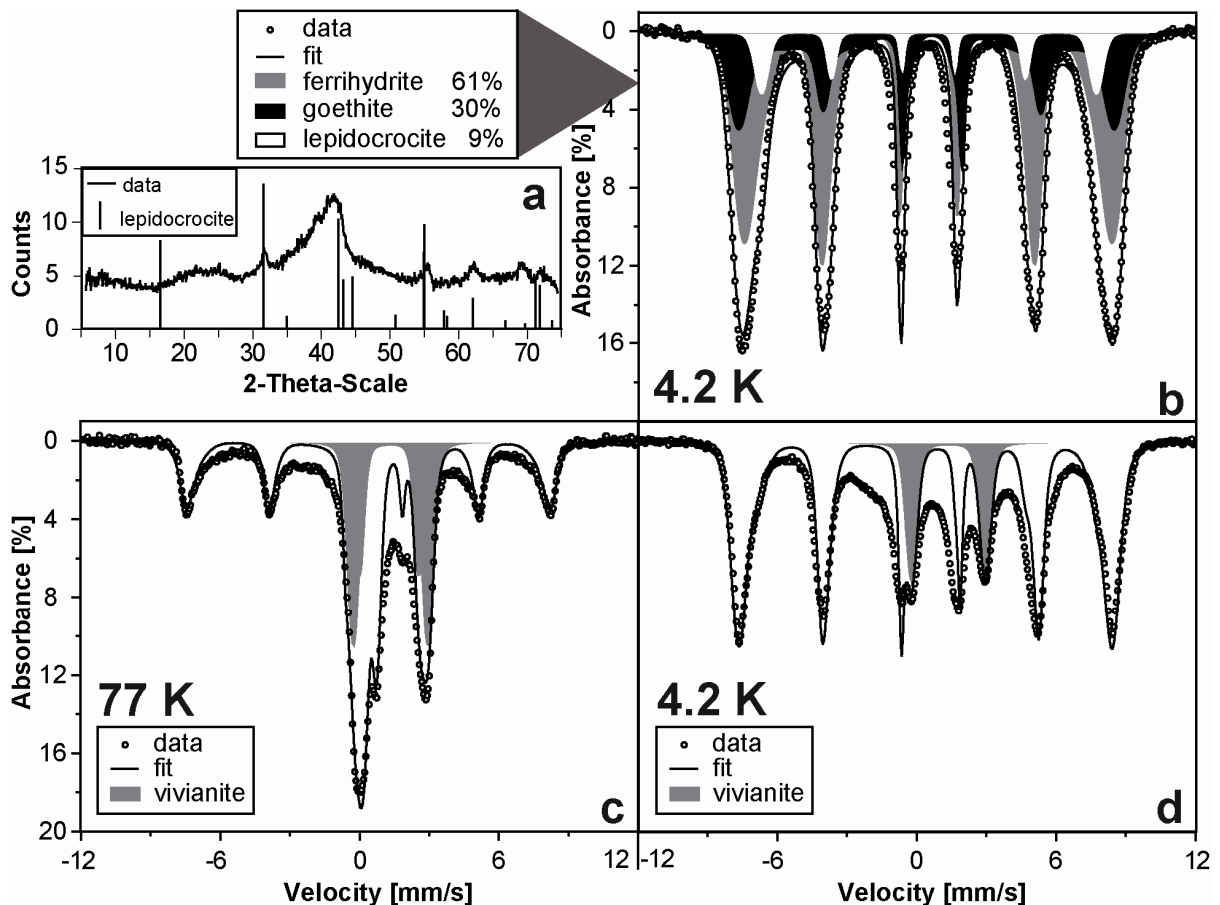
Fig. 8 (a) XRD diffractogram and (b) Moessbauer spectrum at 4.2 K of ^{57}Fe spiked 2-line ferrihydrite with lepidocrocite and goethite impurities. Open circles: measured data, solid line: fitted spectra, filled areas: modelled relative amounts of identified minerals. Moessbauer spectra (measured at (c) 77 K and (d) 4.2 K) of precipitates formed at the end of reduction in cultures containing 5 mM ^{57}Fe-labelled 2-line ferrihydrite and 100 mg/l HA. Open circles: measured data, solid line: fitted spectra, gray area: vivianite, remaining area of the fitted spectrum: mixture of goethite and lepidocrocite.

Previous studies showed a slow Fe(II)-induced recrystallization (via a reductive dissolution-reprecipitation or structural rearrangement mechanism) of ferrihydrite to goethite, lepidocrocite or hematite taking place at low local Fe(II) concentrations (abiotic: Gálvez et al., 1999; biotic: Zachara et al., 2002; abiotic: Cornell and Schwertmann, 2003). With increasing reduction rates, more Fe(II) is produced which adsorbs to residual ferrihydrite and leads to magnetite formation by topotactic conversion of the ferrihydrite (Ardizzone and Formaro, 1983; Zachara et al., 2002). In our experiments at low ferrihydrite concentrations (5 mM) neither magnetite nor goethite or lepidocrocite was formed. Most likely in these experiments the ferrihydrite surface available for

Fe(II) adsorption was depleted too fast to promote solid phase conversion of ferrihydrite to magnetite or recrystallization to goethite, lepidocrocite or hematite. Instead, the formed Fe(II) remained in solution as Fe^{2+} or precipitated out as vivianite in presence of phosphate.

In comparison to the 5 mM ferrihydrite setups, cultures containing 30 mM ferrihydrite showed different results for sequential extraction in presence of 0.8 mM phosphate without (Fig. 5c and d) or with 200 mg/l HA (Fig. 5e and f). The percentage of Fe(II) and Fe(III) present in the three extraction fractions of dissolved, loosely bound, and poorly crystalline iron determined in setups with 30 mM ferrihydrite in the presence of phosphate (Fig. 5c and d) was quite similar to the values obtained in experiments conducted in the absence of both phosphate and HA (capter 2 Fig. 6). The highest Fe(II) concentrations were detected in the fraction of loosely bound Fe(II), some Fe(II) stayed in solution and the lowest amount of Fe(II) was present in the poorly crystalline fraction (Fig. 5c and e). We did not detect significant amounts of Fe(III) in the fraction of dissolved iron. However, we observed significant differences in the crystalline fraction in the presence of 30 mM ferrihydrite amended with HA and/ or phosphate compared to HA-/ phosphate-free setups. XRD measurements showed formation of magnetite and goethite in phosphate- and HA-free cultures (chapter 2 Fig. 7), whereas formation of magnetite but not goethite was observed in the presence of HA and phosphate (Fig. 5).

Transformation of Fe(III) minerals by microbial iron reduction has been extensively studied in the past. It has been shown that depending on the geochemical conditions, microbial ferrihydrite reduction can form goethite, lepidocrocite, hematite, siderite, vivianite, green rusts and magnetite (Zachara et al., 2002; Fredrickson et al., 2003; Hansel et al., 2003; Kukkadapu et al., 2004; Borch et al., 2007). Based on these studies it was concluded that the formation of biogenic minerals during Fe(III) reduction is controlled by factors such as medium composition (in particular by the buffer system used), concentration of electron donor and acceptor, presence of phosphate, shuttling molecules such as AQDS, or mineral impurities such as silicate, nickel or cobalt. However, the effect of the presence of HA during microbial Fe(III) reduction on

mineral formation and transformation has not been previously investigated. In our experiments, no Fe(II) was detected in the sequentially extracted crystalline mineral fraction of the HA- and phosphate-amended cultures (Fig. 5c and e), although the presence of magnetite was demonstrated by XRD in both HA-free and HA-containing setups (Fig. 6b). There are two possible explanations for the absence of Fe(II) in the crystalline (6 M HCl extractable) Fe-fraction. The magnetite formed in the setups containing HA and phosphate may have been more soluble than the magnetite formed in HA-/ phosphate-free setups. This could be due to the formation of smaller particles or a decreased order in the crystal structure (supported by our XRD data, see below). Alternatively, the lack of Fe(II) in the 6 M HCl extract could be due to oxidation of Fe(II) in 6 M HCl under oxic conditions. Control experiments with Fe(II)Cl$_2$ solutions or Fe(II)-containing magnetite incubated at different HCl concentrations under oxic conditions showed Fe(II) oxidation to a significant extent (10-40%) in particular in 6 M but also in 5 M and 4 M HCl within a time range of minutes at 70°C.

Additionally, XRD analysis of precipitates formed in presence of HA and phosphate showed lower intensities and broader magnetite reflections than samples taken from HA- and phosphate-free cultures (Fig. 6b). The broadening of the reflections became even more pronounced with increasing HA concentrations. Again, this indicates more short range ordered and/ or smaller particle sized iron minerals. These conclusions are supported by the results of a recent study on abiotic precipitation of ferrihydrite in presence of organic matter (Eusterhues et al., 2008). These authors described a significant decrease in particle size and structural order of the ferrihydrite with increasing organic matter:iron ratios.

The decrease in crystal order and/ or grain size of the mineral products formed in our microbial Fe(III) reduction experiments in the presence of HA and phosphate (Fig. 6b) is most likely caused by adsorption of phosphate and/ or HA to the mineral surface. Abiotic studies showed that phosphate hinders the transformation of ferrihydrite to goethite or hematite (Gálvez et al., 1999). Magnetite crystallization can be inhibited by the presence of phosphate by blocking specific crystal faces (Couling and Mann, 1985). Blocking the ferrihydrite

surface prevents Fe(II) sorption, thus decreasing the density of sites occupied with Fe(II) and lowering the number of surface sites where conversion of ferrihydrite to magnetite can take place. Additionally, phosphate sorption to newly developed crystallites prevents the formation of well crystalline products. Previous studies investigating the effect of phosphate (Hansel et al., 2003; Borch et al., 2007) also showed formation of different minerals during ferrihydrite reduction by *Shewanella putrefaciens* strain CN32 in presence or absence of phosphate. They observed that higher crystalline phases like goethite were exclusively formed in absence of phosphate. Addition of phosphate in different ratios led to formation of magnetite, green rust or vivianite. These observations confirm our results showing the absence of higher crystalline minerals like goethite in presence of phosphate and decreasing crystallinity with increasing HA concentrations.

4. CONCLUSIONS

In this study we evaluated how the presence of HA influenced microbial reduction of the Fe(III) mineral 2-ferrihydrite at pH-neutral conditions. We found that electron shuttling via HA is restricted to a narrow range of dissolved HA concentrations (~10-130 mg/l HA). Natural HS concentrations between approximately 0.4 mg/l in groundwater and 60 mg/l in surface water (Aiken, 1985) suggest that anoxic groundwater aquifers contain HS concentrations mostly below the concentration range that can stimulate electron transfer from cells to Fe(III) minerals. This has to be taken into account in particular when considering HS as facilitators for electron transfer to Fe(III) minerals present in small pores of soils or sediments which are inaccessible for bacteria. We also found that depending on iron mineral and HS concentrations, HS can not only stimulate but also lower electron transfer to ferrihydrite via changes of aggregate sizes leading to a decreased bioavailable surface area. Obviously both dissolved and ferrihydrite-sorbed HA influence microbial electron transfer between cells to ferrihydrite. Therefore, seasonal changes of HS concentrations for example due to flooding events in rice paddy fields can have a large impact on iron mineral turnover rates and on the whole iron cycle.

The observed changes in mineral crystallinity in the presence of humic compounds have to be considered when discussing the reactivity of Fe minerals in the environment. The identity of the iron phases formed during microbial iron metabolism controls the further biogeochemical reactions of these iron minerals. It has been shown that crystalline Fe(III) minerals such as goethite, akaganeite, hematite and magnetite are reduced at much lower rates and only to a smaller extent compared to poorly crystalline ferrihydrite (Lovley and Phillips, 1988). Similar observations were made for the microbial oxidation of reduced iron minerals by iron-oxidizing bacteria. While more soluble minerals such as siderite were oxidized by anoxygenic phototrophic Fe(II)-oxidizing bacteria, more crystalline and less soluble minerals such as vivianite and magnetite were not oxidized by the same bacteria (Kappler and Newman, 2004). In addition, the crystallinity of the mineral products also controls the further reactivity of the minerals. Fe(II) sorbed to Fe(III) minerals with low crystallinity was less efficient

in the reductive transformation of organic pollutants under anoxic conditions than Fe(II) sorbed to highly crystalline Fe(III) minerals such as hematite (Elsner et al., 2004).

In summary our results suggest that biogeochemical iron cycling in environmental systems not only depends on pH, solute chemistry, microbial strains, reduction mechanisms involved and the identity of initially present minerals, but also on the presence of dissolved HS and on the ratio of HS to Fe(III) mineral. Therefore, the effect of HS on microbial iron mineral transformation and reactivity has to be included in the framework of environmental iron biogeochemistry.

5. ACKNOWLEDGEMENTS

6. REFERENCES

Aiken G. R., 1985. *Humic substances in soil, sediment, and water: geochemistry, isolation, and characterization.* Wiley, New York.

Ardizzone S. and Formaro L., 1983. Temperature induced phase transformation of metastable $Fe(OH)_3$ in the presence of ferrous ions. *Mater. Chem. Phys.* **8**, 125-133.

Borch T., Masue Y., Kukkadapu R. K., and Fendorf S., 2007. Phosphate Imposed Limitations on Biological Reduction and Alteration of Ferrihydrite. *Environ. Sci. Technol.* **41**, 166-172.

Coates J. D., Ellis D. J., Blunt-Harris E. L., Gaw C. V., Roden E. E., and Lovley D. R., 1998. Recovery of humic-reducing bacteria from a diversity of environments. *Appl. Environ. Microbiol.* **64**, 1504-1509.

Coker V. S., Bell A. M. T., Pearce C. I., Pattrick R. A. D., van der Laan G., and Lloyd J. R., 2008. Time-resolved synchrotron powder X-ray diffraction study of magnetite formation by the Fe(III)-reducing bacterium *Geobacter sulfurreducens. Am. Mineral.* **93**, 540-547.

Cornell R. M. and Schwertmann U., 2003. *The Iron Oxides.* Wiley-VCH Verlag GmbH & Co. KGaA, Weinheim.

Couling S. B. and Mann S., 1985. The influence of inorganic phosphate on the crystallization of magnetite (Fe_3O_4) from aqueous solution. *J. Chem. Soc., Chem. Commun.*, 1713 - 1715.

Elsner M., Schwarzenbach R. P., and Haderlein S. B., 2004. Reactivity of Fe(II)-Bearing Minerals toward Reductive Transformation of Organic Contaminants. *Environ. Sci. Technol.* **38**, 799-807.

Eusterhues K., Wagner F. E., Häusler W., Hanzlik M., Knicker H., Totsche K. U., Kögel-Knabner I., and Schwertmann U., 2008. Characterization of Ferrihydrite-Soil Organic Matter Coprecipitates by X-ray Diffraction and Mössbauer Spectroscopy. *Environ. Sci. Technol.* **42**, 7891-7897.

Fredrickson J. K., Kota S., Kukkadapu R. K., Liu C., and Zachara J. M., 2003. Influence of Electron Donor/Acceptor Concentrations on Hydrous Ferric Oxide (HFO) Bioreduction. *Biodegradation* **14**, 91-103.

Fredrickson J. K., Zachara J. M., Kennedy D. W., Dong H., Onstott T. C., Hinman N. W., and Li S.-m., 1998. Biogenic iron mineralization accompanying the dissimilatory reduction of hydrous ferric oxide by a groundwater bacterium. *Geochim. Cosmochim. Acta* **62**, 3239-3257.

Gálvez N., Barrón V., and Torrent J., 1999. Effect of Phosphate on the Crystallization of Hematite, Goethite, and Lepidocrocite from Ferrihydrite. *Clays Clay Miner.* **47**, 304-311.

Gorby Y. A., Yanina S., McLean J. S., Rosso K. M., Moyles D., Dohnalkova A., Beveridge T. J., Chang I. S., Kim B. H., Kim K. S., Culley D. E., Reed S. B., Romine M. F., Saffarini D. A., Hill E. A., Shi L., Elias D. A., Kennedy D. W., Pinchuk G., Watanabe K., Ishii S. i., Logan B., Nealson K. H., and

Fredrickson J. K., 2006. Electrically conductive bacterial nanowires produced by *Shewanella oneidensis* strain MR-1 and other microorganisms. *Proc. Natl. Acad. Sci. USA* **103**, 11358-11363.

Guardado I., Urrutia O., and Garcia-Mina J. M., 2008. Some Structural and Electronic Features of the Interaction of Phosphate with Metal-Humic Complexes. *J. Agric. Food Chem.* **56**, 1035-1042.

Hansel C. M., Benner S. G., and Fendorf S., 2005. Competing Fe(II)-Induced Mineralization Pathways of Ferrihydrite. *Environ. Sci. Technol.* **39**, 7147-7153.

Hansel C. M., Benner S. G., Neiss J., Dohnalkova A., Kukkadapu R. K., and Fendorf S., 2003. Secondary mineralization pathways induced by dissimilatory iron reduction of ferrihydrite under advective flow. *Geochim. Cosmochim. Acta* **67**, 2977-2992.

He Z., Ohno T., Cade-Menun B. J., Erich M. S., and Honeycutt C. W., 2006. Spectral and Chemical Characterization of Phosphates Associated with Humic Substances. *Soil Sci. Soc. Am. J.* **70**, 1741-1751.

Heidelberg J. F., Paulsen I. T., Nelson K. E., Gaidos E. J., Nelson W. C., Read T. D., Eisen J. A., Seshadri R., Ward N., Methe B., Clayton R. A., Meyer T., Tsapin A., Scott J., Beanan M., Brinkac L., Daugherty S., DeBoy R. T., Dodson R. J., Durkin A. S., Haft D. H., Kolonay J. F., Madupu R., Peterson J. D., Umayam L. A., Owen W., Wolf A. M., Vamathevan J., Weidman J., Impraim M., Lee K., Berry K., Lee C., Mueller J., Khouri H., Gill J., Utterback T. R., McDonald L. A., Feldblyum T. V., Smith H. O., Venter J. C., Nealson K. H., and Fraser C. M., 2002. Genome sequence of the dissimilatory metal ion−reducing bacterium *Shewanella oneidensis*. *Nat. Biotechnol.* **20**, 1118-1123.

Hongshao Z. and Stanforth R., 2001. Competitive Adsorption of Phosphate and Arsenate on Goethite. *Environ. Sci. Technol.* **35**, 4753-4757.

Illés E. and Tombácz E., 2006. The effect of humic acid adsorption on pH-dependent surface charging and aggregation of magnetite nanoparticles. *J. Colloid Interface Sci.* **295**, 115-123.

Jiang J. and Kappler A., 2008. Kinetics of Microbial and Chemical Reduction of Humic Substances: Implications for Electron Shuttling. *Environ. Sci. Technol.* **42**, 3563-3569.

Kappler A. and Straub K. L., 2005. Geomicrobiological cycling of iron. In: Banfield J. F., Cervini-Silva J., and Nealson K. M. Eds.), *Molecular Geomicrobiology*. The Mineralogical Society of America, Chantilly, Virginia, USA.

Kukkadapu R. K., Zachara J. M., Fredrickson J. K., and Kennedy D. W., 2004. Biotransformation of two-line silica-ferrihydrite by a dissimilatory Fe(III)-reducing bacterium: formation of carbonate green rust in the presence of phosphate. *Geochim. Cosmochim. Acta* **68**, 2799-2814.

Lies D. P., Hernandez M. E., Kappler A., Mielke R. E., Gralnick J. A., and Newman D. K., 2005. *Shewanella oneidensis* MR-1 Uses Overlapping Pathways

for Iron Reduction at a Distance and by Direct Contact under Conditions Relevant for Biofilms. *Appl. Environ. Microbiol.* **71**, 4414–4426.

Lovley D. R. and Phillips E. J. P., 1988. Novel Mode of Microbial Energy Metabolism: Organic Carbon Oxidation Coupled to Dissimilatory Reduction of Iron or Manganese. *Appl. Environ. Microbiol.* **54**, 1472-1480.

Lovley D. R., Woodward J. C., and Chapelle F. H., 1996a. Rapid anaerobic benzene oxidation with a variety of chelated Fe(III) forms. *Appl. Environ. Microbiol.* **62**, 288-291.

Lovley D. R., Holmes D. E., and Nevin K. P., 2004. Dissimilatory Fe(III) and Mn(IV) Reduction, *Adv. Microb. Physiol.* Academic Press.

Lovley D. R., Coates J. D., Blunt-Harris E. L., Phillips E. J. P., and Woodward J. C., 1996b. Humic substances as electron acceptors for microbial respiration. *Nature* **382**, 445-448.

Marsili E., Baron D. B., Shikhare I. D., Coursolle D., Gralnick J. A., and Bond D. R., 2008. *Shewanella* secretes flavins that mediate extracellular electron transfer. *Proc. Natl. Acad. Sci. USA* **105**, 3968–3973.

Myers C. R. and Nealson K. H., 1988. Bacterial Manganese Reduction and Growth with Manganese Oxide as the Sole Electron Acceptor. *Science* **240**, 1319-1321.

Myers C. R. and Myers J. M., 1994. Ferric iron reduction-linked growth yields of *Shewanella putrefaciens* MR-1. *J. App. Bact.* **76**, 253-258.

Nealson K. H. and Myers C. R., 1990. Iron Reduction by Bacteria - a Potential Role in the Genesis of Banded Iron Formations. *Am. J. Sci.* **290A**, 35-45.

Nevin K. P. and Lovley D. R., 2002a. Mechanisms for Accessing Insoluble Fe(III) Oxide during Dissimilatory Fe(III) Reduction by *Geothrix fermentans*. *Appl. Environ. Microbiol.* **68**, 2294-2299.

Nevin K. P. and Lovley D. R., 2002b. Mechanisms for Fe(III) Oxide Reduction in Sedimentary Environments. *Geomicrobiol. J.* **19**, 141-159.

O'Loughlin E. J., 2008. Effects of Electron Transfer Mediators on the Bioreduction of Lepidocrocite (γ-FeOOH) by *Shewanella putrefaciens* CN32. *Environ. Sci. Technol.* **42**, 6876-6882.

Pedersen H. D., Postma D., Jakobsen R., and Larsen O., 2005. Fast transformation of iron oxyhydroxides by the catalytic action of aqueous Fe(II). *Geochim. Cosmochim. Acta* **69**, 3967-3977.

Raven K. P., Jain A., and Loeppert R. H., 1998. Arsenite and Arsenate Adsorption on Ferrihydrite: Kinetics, Equilibrium, and Adsorption Envelopes. *Environ. Sci. Technol.* **32**, 344-349.

Reguera G., McCarthy K. D., Mehta T., Nicoll J. S., Tuominen M. T., and Lovley D. R., 2005. Extracellular electron transfer via microbial nanowires. *Nature* **435**, 1098-1101.

Ritchie J. D. and Perdue E. M., 2003. Proton-binding study of standard and reference fulvic acids, humic acids, and natural organic matter. *Geochim. Cosmochim. Acta* **67**, 85-96.

Roden E. E., 2003. Fe(III) Oxide Reactivity Toward Biological versus Chemical Reduction. *Environ. Sci. Technol.* **37**, 1319-1324.

Roden E. E. and Zachara J. M., 1996. Microbial Reduction of Crystalline Iron(III) Oxides: Influence of Oxide Surface Area and Potential for Cell Growth. *Environ. Sci. Technol.* **30**, 1618-1628.

Royer R. A., Burgos W. D., Fisher A. S., Unz R. F., and Dempsey B. A., 2002a. Enhancement of Biological Reduction of Hematite by Electron Shuttling and Fe(II) Complexation. *Environ. Sci. Technol.* **36**, 1939-1946.

Royer R. A., Burgos W. D., Fisher A. S., Jeon B. H., Unz R. F., and Dempsey B. A., 2002b. Enhancement of Hematite Bioreduction by Natural Organic Matter. *Environ. Sci. Technol.* **36**, 2897-2904.

Ruebush S. S., Brantley S. L., and Tien M., 2006. Reduction of Soluble and Insoluble Iron Forms by Membrane Fractions of *Shewanella oneidensis* Grown under Aerobic and Anaerobic Conditions. *Appl. Environ. Microbiol.* **72**, 2925-2935.

Schwertmann U. and Cornell R. M., 2000. *Iron Oxides in the Laboratory*. Wiley-VCH Verlag GmbH, Weinheim.

Stevenson F. J., 1994. *Humus Chemistry - Genesis, Composition, Reactions*. John Wiley & Sons, Inc., New York.

Stookey L. L., 1970. Ferrozine - A New Spectrophotometric Reagent for Iron. *Anal. Chem.* **42**, 779-781.

Straub K. L., Benz M., and Schink B., 2001. Iron metabolism in anoxic environments at near neutral pH. *FEMS Microbiol. Ecol.* **34**, 181-186.

Thamdrup B., 2000. Bacterial manganese and iron reduction in aquatic sediments. In: Schink B. (Ed.), *Adv. Microb. Ecol.* Kluwer Academic/ Plenum Publishers, New York.

Thieme J., McNulty I., Vogt S., and Paterson D., 2007. X-ray Spectromicroscopy - A Tool for Environmental Sciences. *Environ. Sci. Technol.* **41**, 6885-6889.

Tipping E., 1981. The adsorption of aquatic humic substances by iron oxides. *Geochim. Cosmochim. Acta* **45**, 191-199.

Venkateswaran K., Moser D. P., Dollhopf M. E., Lies D. P., Saffarini D. A., MacGregor B. J., Ringelberg D. B., White D. C., Nishijima M., Sano H., Burghardt J., Stackebrandt E., and Nealson K. H., 1999. Polyphasic taxonomy of the genus *Shewanella* and description of *Shewanella oneidensis* sp. nov. *Int. J. Syst. Bacteriol.* **49**, 705-724.

Vermeer A. W. P., van Riemsdijk W. H., and Koopal L. K., 1998. Adsorption of Humic Acid to Mineral Particles. 1. Specific and Electrostatic Interactions. *Langmuir* **14**, 2810-2819.

von Canstein H., Ogawa J., Shimizu S., and Lloyd J. R., 2008. Secretion of Flavins by *Shewanella* Species and Their Role in Extracellular Electron Transfer. *Appl. Environ. Microbiol.* **74**, 615-623.

Weber K. A., Achenbach L. A., and Coates J. D., 2006. Microorganisms pumping iron: anaerobic microbial iron oxidation and reduction. *Nat. Rev. Microbiol.* **4**, 752-764.

Zachara J. M., Kukkadapu R. K., Fredrickson J. K., Gorby Y. A., and Smith S. C., 2002. Biomineralization of Poorly Crystalline Fe(III) Oxides by Dissimilatory Metal Reducing Bacteria (DMRB). *Geomicrobiol. J.* **19**, 179-207.

5

Ionic strength influences redox activity of humic acids

ABSTRACT

Humic substances (HS) are redox-active polymeric compounds present in soils and sediments and are involved in abiotic and biotic redox processes. They can mediate electron transfer from microorganisms to poorly soluble electron acceptors such as Fe(III) minerals, but the geochemical parameters controlling these redox processes are mostly unknown.

In order to evaluate the effect of ionic strength on the redox activity of HS, we incubated nonreduced and reduced HS at different ionic strength with dissolved and solid Fe(III) compounds and quantified the amount of electrons transferred from HS to Fe(III). Additionally, we determined microbial Fe(III) reduction rates in the presence of HS (dissolved at different ionic strength before addition to the experiments) as electron shuttles using the Fe(III)-reducing strain *Shewanella oneidensis* MR-1.

The amount of electrons transferred from reduced HS to Fe(III) strongly depended on ionic strength. More electrons were transferred from HS to Fe(III) with increasing ionic strength. This effect was observed for solid as well as for dissolved Fe(III) compounds (ferrihydrite, goethite, hematite, Fe(III) citrate) suggesting that differences in redox activity depend on changes of HS redox properties rather than on Fe(III) mineral surface effects. In contrast to HS a quinone model compound (AQDS, 9,10-anthraquinone-2,6-disulfonate) showed no difference in redox activity at different ionic strengths suggesting that the ionic strength-dependent change in redox behaviour of HS was related to changes in HS structure. Not only abiotic electron transfer from HS to Fe(III) but also biotic electron transfer from Fe(III)-reducing bacteria to Fe(III) via HS electron shuttling changed with ionic strength. Most remarkably not the ionic strength in the experiment itself but rather the ionic strength present during dissolution of the HS before addition to the experiment controlled the redox activity of the HS.

To identify the underlying mechanisms for the observed behaviour, we determined HS sizes and found that nonreduced HS showed only minor changes in molecular size at different ionic strengths

whereas reduced HS seemed to aggregate and form larger particles in an extended size range with particle sizes up to 4 μm at high ionic strength. Aggregation of reduced HS at high ionic strength was probably triggered by decreasing HS charges which we quantified via zeta potential measurements. Potentiometric titration experiments of reduced HS showed that neither identity nor quantity of functional sites exposed depended on ionic strength.

Our results suggest that during reduction, HS molecules expand due to an increase in intramolecular electrostatic repulsion caused by increased charge densities (uptake of electrons). This process in combination with decreasing zeta potentials at high ionic strengths favours aggregation of reduced HS molecules. The resulting large, network-like HS structures then offer an improved access of reactive sites in HS for dissolved Fe(III) (compared to reduced molecules at low ionic strength) leading to increased electron transfer at higher ionic strength.

We conclude that the contribution of HS to redox processes in the environment strongly depends on geochemical conditions such as ionic strength. In aquifers, for example, where low ionic strengths prevail, HS might play a minor role for electron shuttling processes compared to high ionic strength systems such as freshwater or in particular marine environments.

1. INTRODUCTION

Humic substances (HS) are polymeric degradation products of biopolymers such as lignin, proteins and carbohydrates (Stevenson, 1994). Due to their redox activity they can be involved in a variety of geochemical processes such as pollutant degradation or reduction of Fe(III) and other metal ions thereby influencing environmental element cycling and transformation (Lovley et al., 1998; Gu and Chen, 2003; Kappler and Haderlein, 2003). The functional moieties mostly responsible for their redox behavior are quinones (Scott et al., 1998), N- and S-containing functional groups and complexed metal ions such as iron (Stevenson, 1994; Fimmen et al., 2007; Einsiedl et al., 2008).

Microorganisms of different metabolic groups (e.g. methanogens, Fe(III)- and SO_4^{2-}-reducers, fermenting and even halorespiring bacteria) can use HS as terminal electron acceptors (Lovley et al., 1996; Benz et al., 1998; Coates et al., 1998; Cervantes et al., 2002). The microbially reduced HS can then transfer electrons to a different electron acceptor (for example to solid Fe(III) phases) thus acting as so-called electron-shuttles. Microorganisms can thereby bridge spatial gaps limiting the bioavailability of Fe(III) minerals. The transfer of electrons from reduced HS to e.g. Fe(III) minerals is a chemical reaction influenced by mineral crystallinity and identity (Bauer and Kappler, 2009).

The HS electron shuttling mechanism may represent an essential pathway for the reduction of Fe(III) minerals and for electron flux in anoxic environments in general since HS are ubiquitously present and can be reduced by a broad variety of different bacteria as mentioned above. Support for this hypothesis comes from Kappler et al. (2004) who showed that the fraction of reduced HS extracted from a sediment increased with depth demonstrating that in anoxic environments a significant fraction of HS is present in a reduced state and at the same time possibly involved in electron transfer processes.

In order to fully evaluate the potential of HS to contribute to the redox cascade in anoxic environments, it is necessary to determine the geochemical parameters influencing HS redox processes. In this context, Jiang and Kappler (2008) evaluated minimum HS concentrations required for electron shuttling and found that shuttling occurs only if

concentrations of dissolved HS exceed 5-10 mg C/L. However, more research is required in order to identify and assess geochemical factors influencing HS reactivity.

In laboratory experiments investigating interactions between Fe(III), HS and microorganisms a compound often present is phosphate either as a buffer or serving as a nutrient for microbes. However, the use of phosphate is critical since it can undergo various reactions with Fe(III) and HS. The formation of ternary complexes with HS-bound metal ions was observed (Guardado et al., 2007) as well as adsorption to Fe(III) mineral surfaces (Borggaard et al., 2005; Jiao et al., 2008). As a result of increasing phosphate concentrations, electron transfer processes can be inhibited as was shown by Borch et al. (2007) in biotic reduction experiments using ferrihydrite as a terminal electron acceptor. Our initial goal therefore was to quantify the inhibiting effect of phosphate adsorption on Fe(III) mineral surfaces during Fe(III) mineral reduction by reduced HS. This also included control experiments where phosphate buffer was replaced by NaCl solution in order to follow a general effect of ionic strength.

It is known that parameters such as salt concentrations and redox state can influence the spatial structure of HS. Nonreduced HS tend to form small humic molecule associations or collapsed humic macromolecules with increasing ionic strength in phosphate or NaCl solutions, depending on the pH and the fraction of HS investigated (humic acids, fulvic acids or humins) (Ceccanti et al., 1989; Balnois et al., 1999). However, it is still unknown to which extent a structural change due to e.g. varying ionic strength affects the redox activity and therefore the electron transfer to and from HS.

In order to evaluate the effect of ionic strength on the redox activity of nonreduced as well as reduced HS, we quantified the extent of Fe(III) reduction by HS at different ionic strength. To identify the factors responsible for changes in redox activity, we measured particle sizes of HS at different ionic strength and conducted potentiometric titrations in order to quantify site densities of functional groups potentially involved in Fe(III) reduction. Charges of HS were determined via zeta potential measurements. In addition to the abiotic experiments the potential impact of varying ionic strength on microbial

electron shuttling via HS was tested. Therefore, we used HS that were dissolved in solutions of different ionic strength (before addition to the experiments) as electron shuttles during reduction of 2-line ferrihydrite by *Shewanella oneidensis* strain MR-1.

2. METHODS

2.1 Solutions

KH_2PO_4 and $Na_2HPO_4 \cdot 2H_2O$ (analytical grade) were used as phosphate sources. NaCl (analytical grade) was used to prepare sodium chloride solutions. Salts were dissolved in Millipore® water, autoclaved (121°C, ~2 bar) and stored in the dark for further use. Final salt concentrations were 0, 3 and 33 mM for phosphate buffer and 0, 6 and 60 mM for NaCl-solutions which refer to identical ionic strengths in phosphate buffer and NaCl setups.

A 10 mM stock solution of AQDS (Na_2-9,10-anthraquinone-2,6-disulfonate, Sigma Aldrich, 98%) was dissolved in Millipore®-water and reduced chemically in the presence of H_2 and a Pd catalyst as described in Jiang et al. (2009). AQDS-solutions were prepared freshly before each experiment and kept in the dark.

2.2 Preparation of Fe(III) compounds

Ferric citrate ($FeC_6H_5O_7 \cdot H_2O$, 0.5 M) was dissolved in boiling Millipore®-water and adjusted to pH 7 with 10 M NaOH. The solution was autoclaved and stored under N_2 at room temperature in the dark.

2-line ferrihydrite ($Fe(OH)_3$) was prepared according to Schwertmann and Cornell (2000) and Raven et al. (1998) by neutralization of a 200 mM $Fe(NO_3)_3$ solution with 1 M KOH (final pH 7-7.5). The end product was identified as 2-line ferrihydrite ($Fe(OH)_3$) by X-ray diffraction (XRD, data not shown). N_2-BET measurements of a freeze dried aliquot yielded surface areas of the mineral between 240-280 m²/g. N_2-bubbled anoxic ferrihydrite suspensions used for this study were stored in the dark and used within 2 months after synthesis.

Goethite (α-FeOOH, Bayferrox 920 Z) was provided by LANXESS (Leverkusen, Germany). Hematite (α-Fe_2O_3) was tempered (1 h heating up, 2 h at 900°C) from magnetite (Fe_3O_4, Bayferrox E 8710). Purity (>99%) of goethite and hematite was confirmed via XRD-measurements (not shown). All minerals were suspended in Millipore® water to a concentration of 5 mM (diluted to 1.7 mM in abiotic experiments), washed with Millipore® water three times, air-dried

and stored at room temperature in the dark until further use. For long-term experiments (>1 week) with highly crystalline mineral phases (goethite, hematite), all laboratory equipment and mineral suspensions were autoclaved (121°C, ~ 2 bar) or sterilized in an oven at 180°C for 4 h. XRD measurements after autoclaving showed that goethite did not change its mineralogical identity (data not shown). Mineral changes of hematite due to autoclaving were not expected (Cornell and Schwertmann, 2003). Samples were taken sterilely under anoxic conditions and the absence of microorganisms in the abiotic experiments was confirmed by light microscopy of DAPI (4',6-Diamidino-2-phenylindol)-stained aliquots of selected samples.

2.3 Preparation of HS solutions

Pahokee Peat humic acid (PPHA) Reference 1R103H2 and IHSS Suwannee River humic acid Standard II 2S101H (SRHA) were purchased from the International Humic Substance Society (IHSS) as well as Natural humic acids (HOHA) were extracted from Lake Hohloh, a bog lake in the Black Forest in Southwestern Germany and provided by Dr. C Zwiener (University of Karlsruhe, Germany). For detailed extraction procedures, please see Kumke et al (1999). For the abiotic Fe(III) mineral reduction experiments in phosphate buffer, HA stock solutions (0.5 g/l) were prepared freshly for each experiment according to Jiang and Kappler (2008). The final HA concentration in the experiments was 0.3 g/l. HA solutions were chemically reduced by incubation with H_2/Pd (0.5% Pd, Acros Organics) as described previously (Benz et al., 1998; Kappler et al., 2004). After complete reduction, Pd-pellets were removed by filtration (cellulose acetate sterile filter unit, 0.2 μm, Fisher Scientific, Germany). In unbuffered setups (experiments with NaCl instead of phosphate buffer), the pH of HA solutions was adjusted to 7 with NaOH and stayed stable throughout the experiment which can be attributed to the intrinsic buffering capacity of the HA or it even increased in some experiments (~1 pH unit in the unbuffered systems) meaning that at all timepoints a complete dissolution of HA was guaranteed.

For biotic shuttling experiments, PPHA was dissolved at varying concentrations of up to 24 mg/ml either in water, 12.5 or 50 mM phosphate buffer. Due to the high initial PPHA concentration (24 mg/ml), the pH dropped slightly even in the buffered systems and

was readjusted to pH 7 with NaOH if necessary. The PPHA solutions were filter-sterilized (cellulose acetate sterile filter unit, 0.2 μm, Fisher Scientific, Germany) into sterile, closed culture tubes. The solutions were deoxygenated sterilely by alternating application of vacuum and N_2 for 5 min each (3 times).

Precipitation of HS during preparation or runtimes of the experiments was not observed at any times.

2.4 Abiotic Fe(III) reduction: Quantification of HS reducing capacities

For quantification of their reducing capacities (RC, amount of electrons transferred from HA to Fe(III) compounds), nonreduced and reduced HA solutions were incubated with Fe(III) compounds in phosphate buffer and NaCl solutions of different concentrations. Fe(III) compounds were added to HA solutions under anoxic and if necessary under sterile conditions (experiments with a run time >1 week). After closing the bottles with O_2-tight butyl rubber stoppers they were placed on an overhead shaker (10 rpm) in the dark at room temperature. Control experiments were run in parallel with HS or Fe(III) compounds only in order to quantify any Fe(II) leaching from HS or Fe(II) present in the Fe(III) compounds. Samples were taken at selected time points under anoxic (and sterile) conditions and analyzed for Fe(II) and dissolved organic carbon (DOC, see below). RC was determined at the end points of the reactions when no further Fe(II) formation could be observed by the spectrophotometric ferrozine assay (see below). RC were normalized to the mass of HA present in the experiments.

2.5 Electron-shuttling effect of HS dissolved at different ionic strengths during microbial reduction of Fe(OH)$_3$

Shewanella oneidensis strain MR-1 was provided by Jeff Gralnick (Univ. Minnesota). Aerobic cultures on LB-agar plates were streaked out from a frozen stock (-80°C) (incubation: 28°C, 24 h). LB medium consisted of 10 g tryptone, 5 g yeast extract, 5 g NaCl, 12 g agar (not for liquid medium). 50 ml of liquid LB medium were inoculated with a single colony (incubation: 14 h, 28°C, shaken at 150 rpm). 2 ml of LB-grown cell culture were harvested and centrifuged (5 min, 10 600 g). Cells were washed twice with LML medium (Myers and Myers, 1994), containing 12 mM HEPES buffer and 30 mM lactate, set

to pH 7, and used for inoculation. 20 to 30 sterile culture tubes (23 ml) were filled with 9 ml of anoxic LML-medium under N_2 headspace and sealed with sterile rubber stoppers Ferrihydrite in suspension was added to the medium yielding a final concentration of 5 mM. In order to rule out a possible influence of phosphate on our results (e.g. due to interactions between phosphate and Fe(III) mineral surfaces) we kept the final phosphate concentration in the experiments constant (0.8 mM). Therefore, aliquots of 12.5 mM phosphate buffer PPHA stock solutions added to the microbial cultures were fourfold larger than the ones from the 50 mM phosphate buffer stock solution. The PPHA concentration in the stock solution of different phosphate concentration was varied in order to keep the final HS concentrations in the experiments identical. HA and cells (2×10^5 cells/ml) were injected anoxically with syringes and the tubes were incubated horizontally at 28°C in the dark. For sampling, three selected tubes were sacrificed by acid digestion to measure the total Fe(II) and Fe(III) concentration by the ferrozine assay (see below). In order to calculate the maximum reduction rate of an experiment, total Fe(II) concentrations were plotted against time. A linear regression was calculated to derive the maximum slope for Fe(II) formation.

2.6 Analytical methods

In order to measure total iron (Fe_{tot}) concentrations, a sample aliquot was reduced with 10% w/v $NH_2OH \cdot HCl$ dissolved in 1 M HCl before adding the ammonium acetate (50% w/v) buffered ferrozine solution (Stookey, 1970). Absorbance was measured at 562 nm in microtiter plates with a plate reader (FlashScan 550 microplate reader, Analytik Jena AG, Germany). Dissolved organic carbon (DOC) was quantified using a TOC/DOC analyzer (Elementar High TOC, Germany, detection limit 1 mg C/l). We could not detect a correlation between amount of DOC sorbed to Fe(III) minerals and phosphate buffer concentrations (not shown) neither for nonreduced nor for reduced PPHA.

2.7 Particle size measurements

Particle sizes of (non-)reduced PPHA solutions (pH 7) in phosphate buffer and NaCl solutions of different ionic strengths were measured under a constant stream of N_2 via dynamic light scattering with a Microtrac Zetatrac (ParticleMetrix, Meerbusch, Germany).

Thereby, the sample was irradiated by light from a laser light diode through an optical power splitter. The Doppler-shifted light from the particles caused by Brownian motion was mixed with coherent un-shifted light in a silicon photo-detector and converted to the audio range. After amplification, filtration, digitalization and a mathematical analysis by the Microtra® Windows Software a particle size distribution was obtained. For data presentation, representative intensity-weighed measurements were selected.

2.8 Zeta potential measurements

Zeta potential measurements of (non-)reduced PPHA solutions (pH 7) in phosphate buffer and NaCl solutions at different ionic strengths were carried out with a Zetaview Laser Electrophoresis Microscope (Particle Metrix, Meerbusch, Germany). Thereby, an electric field is applied across the sample solutions in an electrophoresis chamber. Charged particles in the sample then migrate towards the oppositely charged electrode with a velocity proportional to the magnitude of the Zeta potential. The movement of the particles creates a frequency shift of an incident laser beam which is measured as the particle mobility. After consideration of dispersant viscosity and application of the Smochulowski theory this mobility can be converted to the zeta potential using the Henry equation:

$$U_E = \frac{2\varepsilon z f(ka)}{3\eta}$$

with z: zeta potential, U_E: electrophoretic mobility, ε: dielectric constant of the medium, η: viscosity of the medium and $f(ka)$: Henry´s function using a value of 1.5 referring to the Smoluchowski approximation (k: inverse double layer thickness, a: particle radius). Measurements were carried out under strictly anoxic conditions.

2.9 Titration of functional groups in HS

Titration of reduced PPHA solutions (0.3 mg/ml) with background electrolyte concentrations of 1, 6 and 60 mM NaCl were carried out with the titrating unit Titrando 836 (Metrohm, Herisau, Switzerland) equipped with a control unit (840 Touch Control), a rod stirrer (802 rod stirrer with Ti Stand 804) and a 20 ml-buret (Dosino 800 dosing unit). HS Samples (~30 ml) were filled into a glass container

closed with a lid holding the stirrer, the pH electrode and a tube for addition of 0.1 M anoxic NaOH. Samples were first adjusted to pH 3.5 by manual addition of anoxic 1 M HCl followed by automatic stepwise addition of NaOH up to a final pH of 12.5 (titration time about 4 h). The titrator was set up to perform a "monotonic equivalence point titration" (MET). A detailed description of the method can be found in Brassard et al. (1990) . All measurements were carried out in an anoxic glovebox (Braun, Germany; 100 % N_2). Titration data were analyzed with the linear programming method (LPM, (Brassard et al., 1990)). All calculations were carried out using Matlab (The MathWorks Inc.).

3. RESULTS

3.1 Fe(III) reduction by nonreduced and reduced HA at different ionic strength

In order to assess the impact of ionic strength on the redox activity of HA, we quantified their reducing capacities (RC, amount of electrons transferred from HA to an electron acceptor). To this end, we incubated nonreduced and reduced HA with a variety of solid-phase Fe(III) compounds as electron acceptors at varying phosphate buffer concentrations. We then quantified Fe(II) formation representing the amount of electrons transferred from HA to Fe(III) minerals.
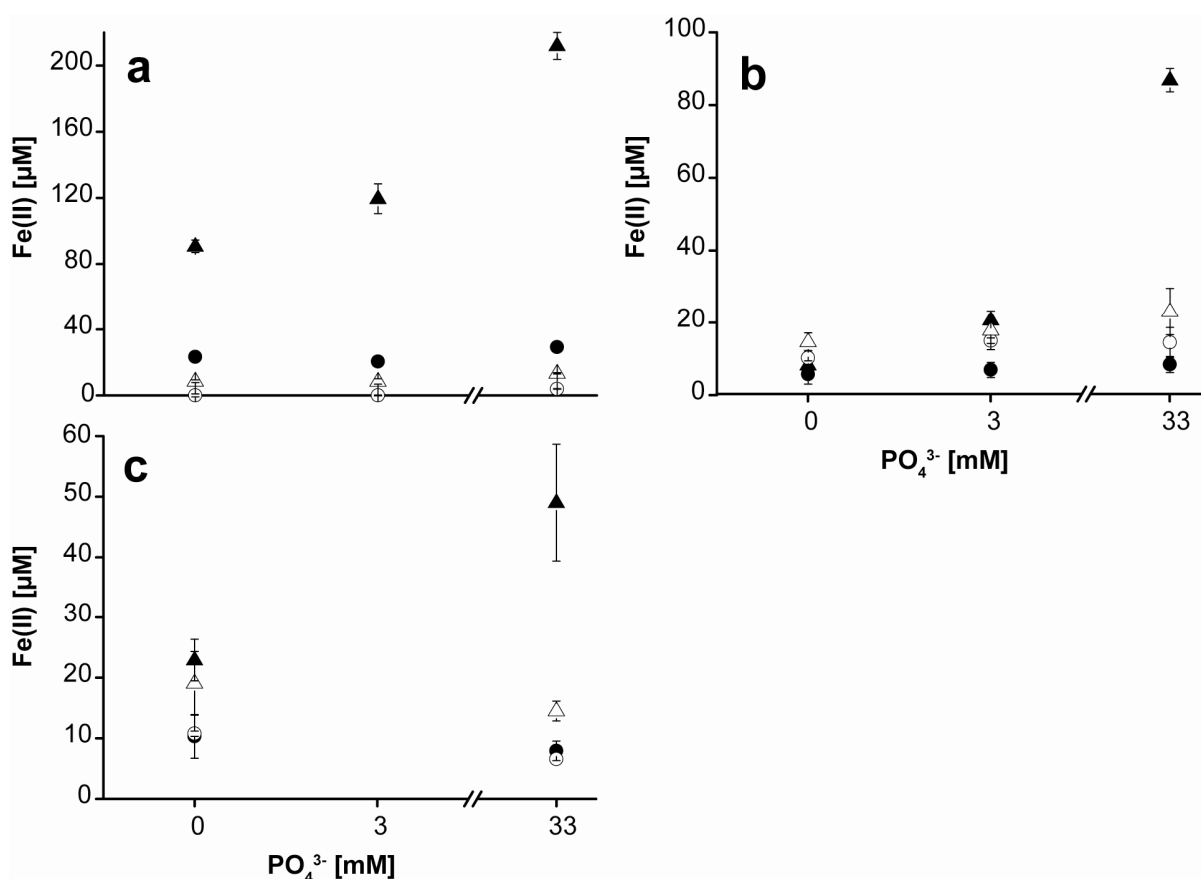
Figure 1: Fe(II) produced during abiotic reduction of (a) 2-line ferrihydrite, (b) goethite and (c) hematite by reduced (▲) and nonreduced (●) PPHA dissolved in different phosphate buffer concentrations (0-33 mM). Open symbols represent PPHA control experiments where no Fe(III) compound was added in order to quantify Fe(II) leaching out of reduced (△) and nonreduced (○) PPHA. Experiments were carried out in triplicates or duplicates (control experiments). Note the varying scales on the y-axis.

We found that nonreduced Pahokee Peat HA (PPHA) transferred only small amounts of electrons to Fe(III) minerals. The extent of electron transfer did not vary significantly at different phosphate buffer concentrations (Fig. 1). In contrast, reduced PPHA transferred significantly more electrons to Fe(III) with increasing ionic strength for all Fe(III) minerals tested (Fig. 1). In comparison to experiments in water, in setups with the highest phosphate buffer concentration (33 mM), Fe(II) production increased by a factor of two (ferrihydrite, hematite) or even ten (goethite). When Fe(II) concentrations remained stable (after 1 day for ferrihydrite, 8 days for hematite and 20 days for goethite), absolute amounts of Fe(II) produced at constant ionic strength (33 mM phosphate buffer) increased in the order hematite < goethite < ferrihydrite (Fig. 1). Such a dependence of extent of Fe(III) reduction on iron mineral identity was already shown previously in a recent study from our group (Bauer and Kappler, 2009).

In order to rule out that the observed changes in electron transfer from HS to Fe(III) are caused by mineral surface effects due to the phosphate present in the setups, we modified our experiments as follows: First, we replaced Fe(III) minerals by dissolved Fe(III) citrate thus eliminating the influence of Fe(III) mineral surface processes. Second, we substituted phosphate salts by NaCl at identical ionic strengths (6 and 60 mM NaCl solutions corresponding to 3 and 33 mM phosphate buffer, respectively). When using dissolved Fe(III) citrate for reduction by reduced PPHA in phosphate buffer, we also saw a significant increase in Fe(II) formation with increasing phosphate buffer concentrations (Fig. 2). At concentrations higher than 33 mM no significant further increase in electron transfer from HS to Fe(III) citrate could be observed (Fig. 2). When using NaCl solutions instead of phosphate buffer, we also found an increase in the amount of electrons transferred from reduced PPHA, SRHA and also from HOHA to Fe(III) citrate with increasing NaCl concentrations by a factor of 1.4 (PPHA) or 1.2 (SRHA and HOH), respectively (Fig. 3). These experiments additionally showed that not only PPHA but also other HS exhibit this ionic strength-dependent changes in redox behavior.
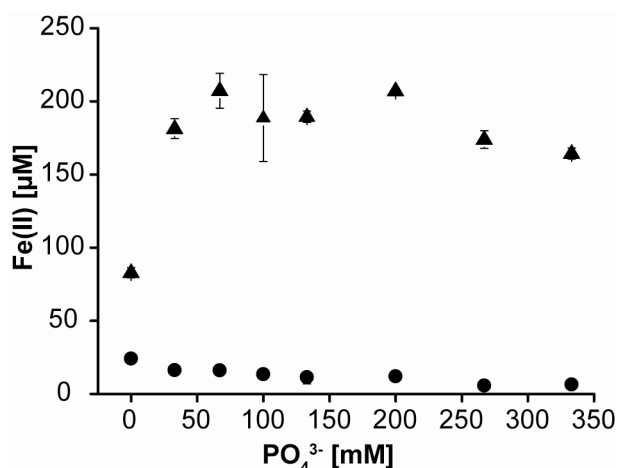
Fig. 2 Fe(II) produced during abiotic reduction of Fe(III) citrate by reduced (▲) and nonreduced (●) PPHA in the presence of increasing phosphate buffer concentrations (0-333 mM). Experiments were carried out in triplicates. Control experiments showed a constant concentration of Fe(II) leached from PPHA of $2.8\pm1.6\,\mu M$ (reduced) and $0.4\pm1.1\,\mu M$ (nonreduced), respectively, which was independent from phosphate buffer concentrations.
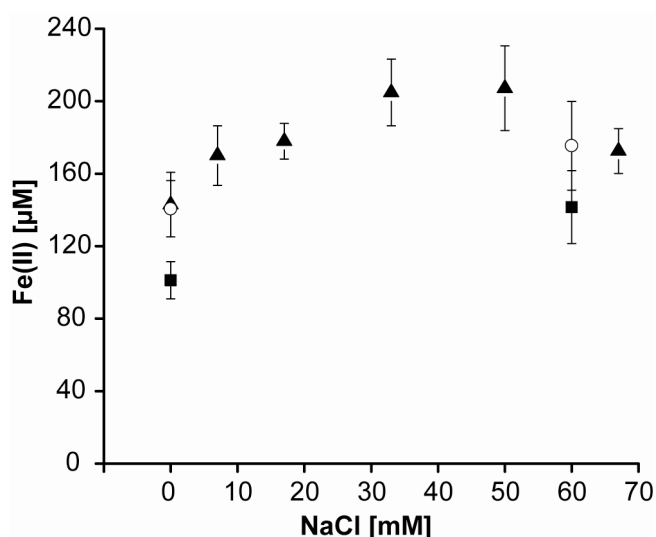

Fig. 3 Fe(II) produced during abiotic reduction of Fe(III) citrate by reduced PPHA (▲), HOH (■) and SRHA (○) at different NaCl concentrations. No significant amount of Fe(II) was leached out of (non-) reduced PPHA and no Fe(II) was leached out of (non-)reduced HOH and SRHA which was checked in control experiments where no Fe(III) was added (not shown). Experiments were carried out in triplicates or duplicates (control experiments).

In order to find out whether the observed ionic strength-dependent changes in redox activity were related to structural changes in HA molecules or rather due to some effects of the added ions on the reactivity of quinoid functional groups in HA, humics were replaced by AQDS (9,10-anthraquinone-2,6-disulfonate), a commonly used model

compound for quinoid groups in HS. However, when we repeated our Fe(III) citrate reduction experiments using reduced AQDS instead of reduced HA, we did not observe a change in redox behaviour of AQDS at different concentrations of phosphate buffer or NaCl (data not shown). The amount of electrons transferred from reduced AQDS to Fe(III) citrate remained constant under all phosphate buffer and NaCl concentrations tested (0-33 mM phosphate buffer and 0-60 mM NaCl, respectively), indicating that ionic strength did not influence the redox activity of quinoid moieties themselves. However, one distinct physicochemical parameter of HA known to change with ionic strength is their spatial structure. From our results so far we hypothesize that the reason for the change in redox activities at different ionic strengths might be due to conformational changes of HA molecules.

3.2 Particle size distributions of nonreduced and reduced HA

The spatial structure of HS potentially determines the accessibility of redox-active moieties and thereby electron transfer reactions of HS. Changes in spatial structure can be detected by particle size measurements of HA. We therefore measured sizes of nonreduced and reduced PPHA in water as well as in NaCl solutions and phosphate buffer at a low (6 mM NaCl vs 3 mM phosphate buffer) and a high (60 mM NaCl vs. 33 mM phosphate buffer) salt concentration each representing identical ionic strength.

We observed that nonreduced PPHA did not change their particle size significantly with increasing salt concentrations (Fig. 4). The size range of nonreduced HA stayed constant in 6 and 60 mM NaCl solutions (150-350 nm) as well as in 3 and 33 mM phosphate buffer (150-300 nm). Only in the absence of salts (in pure water) particle size distributions of nonreduced PPHA varied with a fraction of very small particles additionally appearing in the size range of 1-2 nm (Fig. 4a).
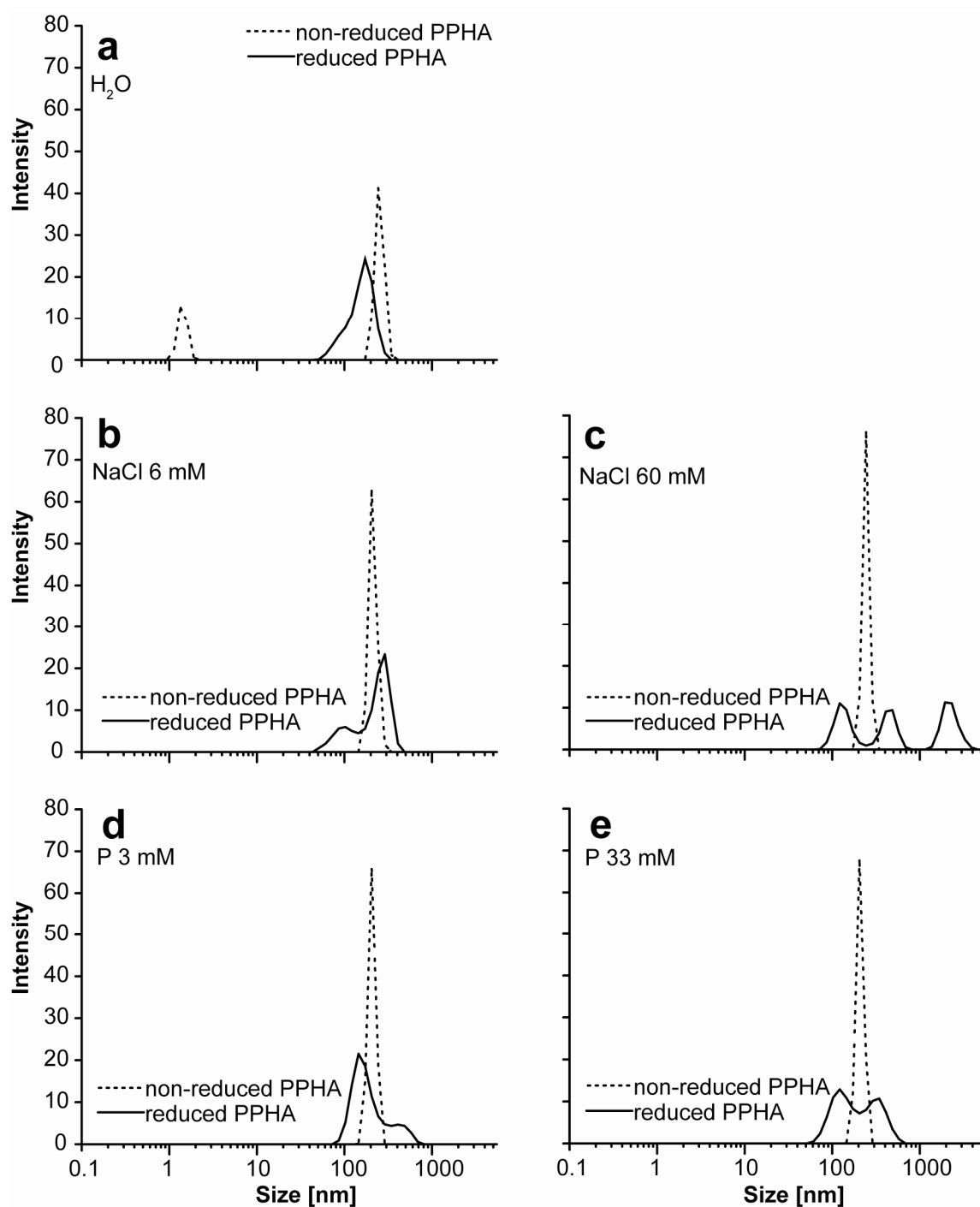
Fig. 4 Particle size distributions of nonreduced (dashed line) and reduced (solid line) PPHA in (a) water and (b and c) in different NaCl (6 and 60 mM) and (d and e) phosphate buffer (3 and 33 mM) concentrations. Samples were set up and analyzed in parallels (i.e., two (non-)reduced samples per ionic strength and ion identity) and measured several times. For data presentation, one representative distribution per setup was chosen. Please note the logarithmic scale on the x-axis.

However, in contrast to the nonreduced samples, reduced PPHA showed distinctly different particle sizes at different ionic strengths. In water (Fig. 4a), a monomodal distribution of reduced PPHA molecules

covering a size range between 50-350 nm was present. When we increased the salt concentrations to a low ionic strength (6 mM NaCl or 3 mM phosphate buffer), the distribution function changed to a bimodal shape (Fig. 4b and d). For NaCl solutions, particles ranging from 40-500 nm with a small peak around 90 nm and a main peak around 300 nm were observed whereas in phosphate buffer, the size range shifted to larger particles (80-800 nm) with a main peak around 150 nm and a side peak at 500 nm. At high salt concentrations (60 mM NaCl or 33 mM phosphate buffer), bi- or even trimodal particle size distributions were detected for reduced PPHA and the total size range extended significantly (Fig. 4c and e). Particularly in the setup with 60 mM NaCl three peaks appeared depicting particles of three different size ranges scattering around values of 150, 450 and 2000 nm (total size range from 70-4000 nm). In the 33 mM phosphate buffer setups, within a total size range between 60-700 nm two fractions emerged with maxima at approximately 130 and 350 nm.

3.3 Zeta potential measurements of nonreduced and reduced HA

The charge of a molecule can influence its aggregation behavior and therefore, also its size. We carried out zeta potential measurements to detect changes in HS charges at different ionic strength which could possibly explain the size variation that we observed (described above).

Quantification of zeta potentials of PPHA molecules in NaCl solutions and phosphate buffer showed a dependence of HA charges on ionic strength while the redox state of HA had no influence on HA zeta potential (Fig. 5). As expected, HA particles were negatively charged in all setups except for the highest NaCl concentration (60 mM), where reduced PPHA even showed a small fraction of positively charged particles (data not shown). For both nonreduced and reduced HA, with increasing ionic strength zeta potentials decreased (became less negative) from -67 mV in water to -58 (nonreduced) and -61 mV (reduced) at 6 mM and -53 (nonreduced) and -46 mV (reduced) at 60 mM NaCl solutions (Figure 5). In phosphate buffer, zeta potentials decreased to -65 mV (nonreduced and reduced) at 3 mM and -44 (nonreduced) and -52 mV (reduced) at 33 mM (Fig. 5).
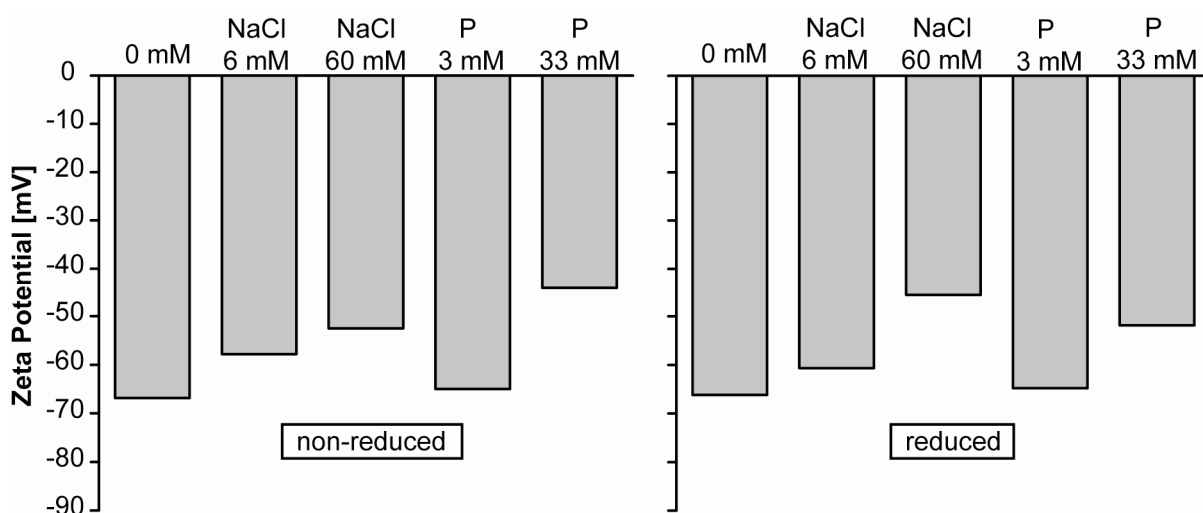
**Fig. 5 Zeta potential measurements of nonreduced and reduced PPHA at pH 7
and 25°C at different ionic strengths. Measurements were carried out in
NaCl solutions (6 and 60 mM) as well as in phosphate buffer (abbreviated
by P, 3 and 33 mM).**

There was no obvious difference between nonreduced and reduced PPHA. Also the identity of ions obviously did not play a role for these changes since the average zeta potentials of samples in NaCl solutions and phosphate buffer of the same ionic strength were similar (Fig. 5 a and b). However, it has to be mentioned that for each sample we observed a rather broad distribution of zeta potentials for PPHA at the different salt concentrations which even broadened with increasing ionic strength (data not shown).

3.4 Identification and quantification of surface site density of reduced HA.

The reactivity of HS strongly depends on the identity and also the quantity of functional groups accessible during redox reactions. We carried out potentiometric titrations to quantify reactive sites in PPHA at different ionic strength and to potentially detect a correlation between reactivity of PPHA and reactive sites quantified.

By titration experiments covering a pH range from 3.5-12.5, we quantified five different functional groups (surface sites) in nonreduced and reduced PPHA at three ionic strengths (1, 6, 60 mM NaCl) indicating the presence of five different pK_a values. The measured pK_a values scattered closely around pH 5.3 (site 1), 6.5 (site 2), 7.5 (site 3), 8.5 (site 4) and 9.6 (site 5) (Fig. 6). At low pH values (sites 1 and 2), site densities varied slightly at different ionic strengths while at high pH

values (sites 3-5), no significant differences were observed. However, the changes in site density for low pH values showed no clear trend depending on ionic strength.
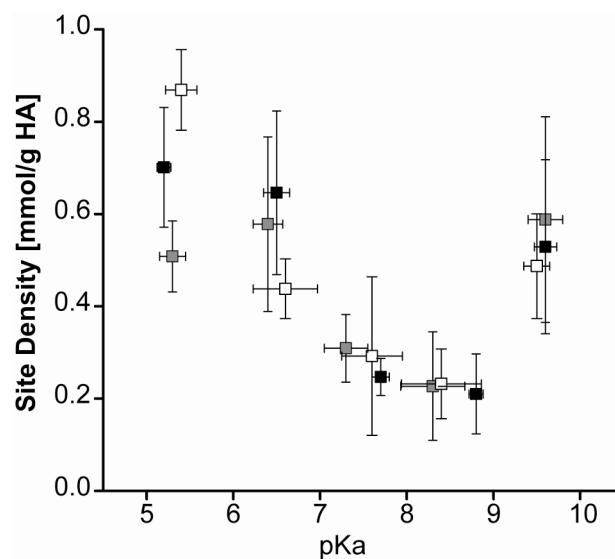

Fig. 6 Site densities of reduced PPHA (0.3 mg/ml) dissolved in NaCl solutions of different concentrations (1 mM (■), 6 mM (▦), 60 mM (□)). Site densities (y-axis) are assigned to corresponding pK_a-values (x-axis). Error bars represent standard deviations calculated from three independent parallels

3.5 Influence of ionic strength on the function of HA as electron shuttles for Fe(III) reducing bacteria

The iron-reducing strain *Shewanella oneidensis* MR-1 was incubated with 5 mM 2-line ferrihydrite and PPHA as an electron shuttle. PPHA stock solutions were prepared at different ionic strengths (0, 12.5 or 50 mM phosphate buffer) before addition to the experiments while phosphate buffer concentrations in the experiments were adjusted to identical ionic strength. We quantified maximum Fe(III) reduction rates in presence of three different PPHA concentrations (0.05, 0.2 and 0.4 mg/ml).

The maximum rates of biotic ferrihydrite reduction with 0.2 and 0.4 mg/ml PPHA as an electron shuttle increased with increasing concentrations of phosphate buffer in which PPHA were dissolved before addition to the experiments (Fig. 7) whereas stimulation of electron shuttling by increased pre-incubation phosphate buffer concentrations was less pronounced for cultures containing 0.05 mg/ml PPHA.
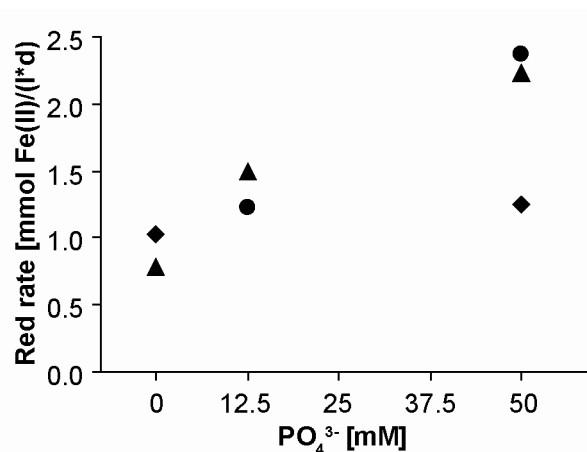
Fig. 7 Maximum rates for microbial reduction of 5 mM 2-line ferrihydrite by *Shewanella oneidensis* MR-1 in cultures containing 0.05 (◆), 0.2 (▲) and 0.4 mg/ml (●) PPHA which were prepared at different phosphate concentrations (0, 12.5 or 50 mM; please note that the final phosphate concentration in the setups was always the same, 0.8 mM). Reduction rates were calculated by linear regression of the maximum increase in total Fe(II) concentrations.

4. DISCUSSION

The discussion part is structured as follows: It begins with information about general influences of ionic strength on molecular properties of HS (paragraph 4.1). We then connect the ionic strength-induced changes of molecular properties to the variations in HS particle sizes (paragraph 4.2). After that, we draw conclusions on how ionic strength and structural changes affect HS redox activity (paragraph 4.3) and finally transfer our results to the environment (paragraph 4.4).

4.1 Influence of ionic strength on molecular properties of HS

Zeta potential measurements of nonreduced and reduced PPHA showed a decrease in PPHA surface charges with increasing ionic strength (Fig. 5) which is confirmed by a study of Hosse and Wilkinson (2001) who measured electrophoretic mobilities (proportional to zeta potentials) of three different purified IHSS humic substances (including PPHA). They also showed a clear dependence on ionic strength indicated by decreasing mobilities of HS with increasing ionic strength. In natural samples, similar correlations between decreasing electrophoretic mobility and increasing ionic strength were detected for estuarine colloids and isolated estuarine HA (Muller, 1996). The decrease in electrophoretic mobility with increasing ionic strength is caused by neutralization of HA surface charges by ions present. Consequently, the migration of charged HA molecules in an electric field is slowed down.

When we quantified surface site densities of reduced PPHA at different ionic strength, we detected no distinct trends with increasing ionic strength (Fig. 6). The functional sites we found were similar to studies of Bratskaya et al. (2008) who found up to four pK_a values scattering around similar values than ours for different humic and fulvic acids. HA molecules feature a heterogeneous structure and composition including a wide variety of functional groups such as phenolic or carboxylic groups. Atoms of varying electronegativity (i.e., electron-withdrawing or -donating groups) in vicinity of functional groups can influence physicochemical properties such as pK_a values of the reactive sites significantly. Therefore an assignment of the detected pK_a values to defined functional groups in HA is quite challenging which is the reason why functional groups in HA determined by titration are commonly

divided into fractions reacting below and above pH 7 corresponding to carboxylic and phenolic groups, respectively (Abbt-Braun et al., 2004). Transferring this approach to our results, we can assign about 56% of the functional groups to the fraction <pH 7 and 44% to the fraction >pH 7 which means that there were almost as many phenolic groups present as carboxylic functional groups. This is in good agreement with results from Milne et al. (2001) who found a ratio of 54:46 for carboxylic vs. phenolic groups in PPHA.

Finally we can conclude that ionic strength influenced zeta potentials and therefore charges of PPHA molecules but not their accessibility (for hydroxyl ions and protons) or identity of the reactive functional sites.

4.2 Structural rearrangements of HS caused by changing zeta potentials at varying ionic strength

Various studies analyzing changes in HA size related to changes in ionic strength have been performed before. At high ionic strength the presence of small HS molecules has been observed due to repelling forces between the ions in solution and charged groups of HS which can lead to the formation of a collapsed, folded structure (max. 100 mM P Ceccanti et al., 1989; Stevenson, 1994; max. 1 mM NaCl Kucerik et al., 2007). Alternatively, associations of small HA molecules that have been described to be present in larger HA molecules (Hayes and Clapp, 2001; Piccolo, 2001; Simpson et al., 2002; Sutton and Sposito, 2005) would break apart due to repelling forces between ions and charged functional groups in HS. However, in our experiments with nonreduced HA, neither break-up of molecules nor molecule folding (both potentially leading to signals of smaller molecules in the light diffraction experiments) occurred to a significant extent. Except for the small fraction in the 1-2 nm size only present in water, no further significant decrease in particle sizes became evident when ionic strength was increased from low to high concentrations (Fig. 4). A similar behavior was observed by Hosse and Wilkinson (2001) in experiments with nonreduced PPHA which also showed only very slight changes in hydrodynamic radii at different concentrations of malonate buffer (0-1000 mM) which was explained by the authors with a small swelling and shrinking potential of the used humics due to structural limitations. Also for two other nonreduced HS (IHSS fulvic avid and IHSS aquatic humic

acid) they could not detect any structural changes with increasing ionic strength. As a consequence, they supported a humic structure model of rigid spheres.

In contrast to nonreduced HS, not much is known about the structure of reduced HS. In a study of Coates et al. (2001) it was stated that reduced HS are present as small dense particles whereas after reoxidation large loose aggregates could be found. This is in contrast to Thieme et al. (2007) who showed X-ray tomography images in which reduced HS exhibit a network-like structure with large intramolecular spaces and more heterogeneous particle size distributions compared to reoxidized HS which appear more compact. These latter observations are in agreement with our data obtained in water where we also detected slightly larger particles for the nonreduced HA compared to reduced HA. A reason for this difference between reduced and nonreduced HA could be that due to the chemical reduction of HA by H_2/Pd (electron transfer into HA molecules) the charge density within the reduced humic molecule is much higher than in nonreduced molecules. As a consequence, larger repulsive forces exist which might lead to intramolecular repulsion within the HA molecule leading to expansion and a more porous structure. Furthermore, our measurements revealed that reduced HA exhibited a much more sensitive behaviour towards ionic strength than nonreduced HA with particle size distributions becoming more heterogeneous and wide-ranged with increasing NaCl and phosphate buffer concentrations. For nonreduced HA, the opposite effect was described before, i.e., coiling of nonreduced HS with increasing ionic strength (Ceccanti et al., 1989; Hayes and Clapp, 2001).

In salt solutions, dissolved ions interact with functional groups of HS and change HS molecule charges due to charge neutralization by counter ions which decreases electrostatic repulsion between HA molecules (Tipping, 2002). This in turn influences aggregation behavior leading to larger particles and therefore greater sizes of HA. Thereby the detection of HA molecules with particle sizes >0.22 μm (Fig. 4d, f) can be explained although all HA samples were filtered (mesh size 0.22 μm) during the preparations of HA solutions before the experiments (see methods part). Furthermore, the increased heterogeneity in particle size distributions with increasing ionic strength is probably caused by formation of HS molecule associations of irregular shape. Since dynamic

light scattering only allows determination of molecule diameters the measured particle size distributions become more heterogeneous the more particles deviate from spherical shape.

Alvarez-Puebla and Garrido (2005) suggested a close correlation between zeta potentials and HA sizes. They found a linear relationship when they plotted sizes of a gray HA against zeta potentials showing increasing sizes of HA with decreasing (less negative) zeta potentials. Indeed we could confirm these observations for reduced PPHA which showed the same behavior exhibiting particle sizes of up to 4 µm with increasing salt concentrations (Fig. 4). In fact, it is very unlikely that ~50 nm sized particles (in water), already expanded due to intramolecular repulsion after reduction, would expand further to a diameter of 4 µm (at high ionic strength) supporting the assumption that the size increase is rather caused by aggregation. This is in agreement with the Schulze-Hardy rule which relates the aggregate formation by colloides to the addition of oppositely charged ions. With higher ion concentration the tendency for molecule aggregation increases. In contrast, nonreduced PPHA did not always show changes in sizes despite the changes in zeta potentials. An exception was the small fraction of particles in a size range of 1-2 nm which we detected exclusively in samples of nonreduced PPHA in water (Fig. 4a). The reason for this behaviour is not clear, but Hosse and Wilkinson (2001) found the same behavior of PPHA and two other IHSS humic substances (all nonreduced) exhibiting decreasing charges with increasing ionic strength but no increased aggregation. For reduced PPHA, however, the spatial structure is much more rugged in contrast to nonreduced HA (Thieme et al., 2007) and it is thus expected that also the amount of pores increases with increasing aggregation and increasing ionic strength, respectively. De Jonge and Mittelmeijer-Hazeleger (1996) state that 95-99% of soil organic matter surface area is formed by micropores. The more rugged and porous the reduced HA molecules become with increasing ionic strength the easier they can get caught by each other due to structural reasons leading to the formation of larger particles.

4.3 Consequences of ionic strength effects on the electron transfer from HS to Fe(III) (redox activity)

It can be expected that reduced PPHA exhibiting a more open structure with increasing ionic strength are also more permeable than nonreduced PPHA for small components such as Fe(III) citrate molecules or Fe(III) mineral nanoparticles which could explain the increasing RCs of reduced HA with increasing ionic strength. Although in our titration experiments we did not observe a strong correlation between surface site density and ionic strength (Fig. 6), it has to be considered that the accessibility of functional moieties was determined with H^+ and OH^- ions. In contrast, in our experiments quantifying RCs of HA we used Fe(III) as a reactant. It is possible that for Fe(III) the access to reactive sites was limited compared to H^+/OH^- since Fe(III) citrate or Fe(III) mineral nanoparticles are larger than H^+/OH^- and it can also be complexed more strongly thus being less "mobile" within the HA structure. Therefore, it seems possible that functional groups in very small pores (pm range) might not have been accessible for Fe(III) but for H^+/OH^-. An increase in porosity in reduced HA with increasing salt concentrations might not have been detected via titration experiments because the majority of sites was accessible for H^+/OH^- at all times. The overall amount of pores exhibiting more functional sites which potentially react with Fe(III) is likely to increase due to the enhanced aggregation of multiple particles which can be seen in Figure 4 at high ionic strength. It is expected that the amount of positively charged complexed metal ions and also the binding strength decreases with increasing ionic strength as it was shown by Rate et al. (1993) for Cu^{2+}. Our hypothesis assuming more reactive sites accessible for Fe(III) at higher ionic strength is confirmed in the abovementioned study of Coates et al. (2001) who quantified an increase of 15% in binding capacity of reduced HA for heavy metals compared to the oxidized state. Combining their and our results we suggest the following mechanism for the increased Fe(III) reduction with increasing ionic strength: reduction of HS leads to an expansion of HS molecules due to a high electron density. With increasing ionic strength, the rugged molecules aggregate and become larger and more heterogeneous in size. If then Fe(III) (either as Fe(III) citrate or Fe(III) ions leached from Fe(III) mineral particles by HS) gets into contact with these large conductive networks, the metal ions can percolate more easily, displace loosely attached K^+ and Na^+ ions due to their higher affinity in

particular to carboxylic functional groups and be complexed momentarily. This processes are followed by a fast reduction of the Fe(III) via a rapid electron transport within the HS molecule and subsequently the produced Fe(II) is leached because it is bound less strongly than Fe(III) (Emmenegger et al., 2001). Then the reactive site is available again for another Fe(III) ion and this process is repeated until the HS are depleted in electrons or until a thermodynamic equilibrium is reached. We observed long time periods (days to weeks) until a stable Fe(II) concentration was reached specifically for experiments containing highly crystalline Fe(III) minerals (goethite, hematite). This may indicate additionally a role of dissolved Fe(III) ions and their availability depending on Fe(III) mineral solubility.

The effect of ionic strength on physicochemical properties of HS is obviously not only a temporary effect but rather permanent. Evidence for this can be found in our biotic experiments. There, maximum microbial Fe(III) reduction rates clearly depended on the phosphate buffer concentration present in the PPHA stock solutions (in which they were dissolved before addition to the experiments) with higher reduction rates for the HA dissolved at higher ionic strength (Fig. 7). In our 0.05 mg/ml PPHA-containing experiments after immediate, partly sorption of PPHA to the mineral the amount of dissolved PPHA (<0.015 mg/ml) was close to or even below the lowest concentration (0.01 mg/ml) necessary for electron shuttling (Jiang and Kappler, 2008), which lead to a rather small increase of reduction rates when phosphate buffer concentrations for dissolution of PPHA were increased from 0 to 50 mM. In contrast, experiments containing 0.2 or 0.4 mg/ml PPHA lead to dissolved HA concentrations in the saturation range for electron shuttling (0.08 to 0.32 mg/l respectively), where maximum stimulation was reached independently from the HA concentration (chapter 4, Jiang and Kappler, 2008). Any effects due to different amounts of phosphate sorbed to iron mineral surfaces can be excluded since the phosphate concentration was identical in all setups (0.8 mM).

We know from our zeta potential measurements that HA molecule charges decrease with increasing salt concentrations as discussed above. In our biotic system containing Fe(III) minerals, microbial cells and nutrients, complex interactions of sorption and electrostatic repulsion take place. If HA are added to such a system they usually show a strong

affinity for Fe(III) mineral surfaces (Tipping, 1981) and less adsorption to negatively charged cells because HA are also negatively charged. However, from our zeta potential measurements we can assume that HA zeta potentials and therefore charges in our shuttling experiments were less negative when the phosphate buffer concentration was increased during dissolution of PPHA before addition to the experiments. Obviously this effect was sustained (e.g., by non-specific adsorption of K^+ and Na^+) even after addition of HA to the experimental medium-mineral mixture. HA particles maintained their charge, built up during dissolution, and kept this property even after introduction into a solution with a different ionic strength indicating a "memory effect". This effect possibly lead to a facilitated electron transfer from microbial cells to PPHA due to less electrostatic repulsion and enhanced contact between cells and HA. More reducing equivalents could then be transferred to Fe(III) minerals after fast microbial reduction of PPHA resulting in an increase of maximum reduction rates, independent from the liberation of Fe(III) ions into solution. The increased redox activity of PPHA in our microbial experiments was therefore caused by a different mechanism than described above for the abiotic setups where HA structure and mineral solubility seemed to be crucial.

4.4 Effect of varying ionic strength on HS redox activity and electron shuttling in the environment

Our results suggest that not only the presence of microorganisms capable to reduce HS, the presence of adequate electron acceptors or the concentration of dissolved HS but also ionic strength present determines the significance of HS as electron shuttles in the environmental redox cascade. Therefore, the impact of HS might differ substantially depending on the environment in which they occur. Marine or freshwater systems exhibit an average salinity of ~3.5% and <0.1%, respectively. If we use the simplified assumption that all ions are present as NaCl, these values equal molar concentrations of 602 mM and 17.2 mM NaCl, respectively. In artificial freshwater medium commonly used for microbial experiments, ionic strength is in the same range (18.4 mM in Straub et al., 1998). In comparison, ionic strength in artificial groundwater medium is much lower (1.7 mM in Hansel et al., 2004). This leads to the suggestion that the redox activity of HS in aquifers might be of minor relevance. In contrast, in freshwater, marine

water and sediment porewater, HS might represent highly redox-active electron transferring compounds.

For lab experiments focusing on redox activity of HS using them either as sole electron transferring agent or in shuttling experiments involving microorganisms, the choice of solute for HS is crucial for the results. Depending on the natural scenario that is supposed to be mimicked in vitro, salt solutions of adequate concentrations should be used for dissolution of HS as well as in the actual experiments. Furthermore, it has to be considered that the medium used for dissolution of HS might influence HS redox activity at a later stage in the experiment.

To date, profound knowledge about nonreduced HS is available. However, since it is likely that in the environment HS are present in a reduced state to a significant extent (Kappler et al., 2004), more research is needed focusing on HS in a reduced state under anoxic conditions. Only after we have understood the factors influencing the redox activity of not only nonreduced, but also of reduced HS, we will be able to fully evaluate the significance of HS in the electron transfer chain in different environments.

6. REFERENCES

Abbt-Braun G., Lankes U., and Frimmel F. H., 2004. Structural characterization of aquatic humic substances - The need for a multiple method approach. *Aquatic Sciences - Research Across Boundaries* **66**, 151-170.

Alvarez-Puebla R. A. and Garrido J. J., 2005. Effect of pH on the aggregation of a gray humic acid in colloidal and solid states. *Chemosphere* **59**, 659-667.

Balnois E., Wilkinson K. J., Lead J. R., and Buffle J., 1999. Atomic Force Microscopy of Humic Substances: Effects of pH and Ionic Strength. *Environ. Sci. Technol.* **33**, 3911-3917.

Bauer I. and Kappler A., 2009. Rates and extend of reduction of Fe(III) compounds and O_2 by humic substances. *Environ. Sci. Technol.*, in press.

Benz M., Schink B., and Brune A., 1998. Humic acid reduction by *Propionibacterium freudenreichii* and other fermenting bacteria. *Appl. Environ. Microbiol.* **64**, 4507-4512.

Borch T., Masue Y., Kukkadapu R. K., and Fendorf S., 2007. Phosphate Imposed Limitations on Biological Reduction and Alteration of Ferrihydrite. *Environ. Sci. Technol.* **41**, 166-172.

Borggaard O. K., Raben-Lange B., Gimsing A. L., and Strobel B. W., 2005. Influence of humic substances on phosphate adsorption by aluminium and iron oxides. *Geoderma* **127**, 270-279.

Brassard P., Kramer J. R., and Collins P. V., 1990. Binding site analysis using linear programming. *Environ. Sci. Technol.* **24**, 195-201.

Bratskaya S., Golikov A., Lutsenko T., Nesterova O., and Dudarchik V., 2008. Charge characteristics of humic and fulvic acids: Comparative analysis by colloid titration and potentiometric titration with continuous pK-distribution function model. *Chemosphere* **73**, 557-563.

Ceccanti B., Calcinai M., Bonmati-Pont M., Ciardi C., and Tarsitano R., 1989. Molecular size distribution of soil humic substances with ionic strength. *Sci. Total Environ.* **81-82**, 471-479.

Cervantes F. J., de Bok F. A. M., Duong-Dac T., Stams A. J. M., Lettinga G., and Field J. A., 2002. Reduction of humic substances by halorespiring, sulphate-reducing and methanogenic microorganisms. *Environ. Microbiol.* **4**, 51-57.

Coates J. D., Chakraborty R., O'Connor S., Schmidt C., and Thieme J., 2001. The Geochemical Effects of Microbial Humic Substances Reduction. *Acta Hydrochim. Hydrobiol.* **28**, 420-427.

Coates J. D., Ellis D. J., Blunt-Harris E. L., Gaw C. V., Roden E. E., and Lovley D. R., 1998. Recovery of humic-reducing bacteria from a diversity of environments. *Appl. Environ. Microbiol.* **64**, 1504-1509.

Cornell R. M. and Schwertmann U., 2003. *The Iron Oxides.* Wiley-VCH Verlag GmbH & Co. KGaA, Weinheim.

de Jonge H. and Mittelmeijer-Hazeleger M. C., 1996. Adsorption of CO_2 and N_2 on Soil Organic Matter: Nature of Porosity, Surface Area, and Diffusion Mechanisms. *Environ. Sci. Technol.* **30**, 408-413.

Einsiedl F., Mayer B., and Schäfer T., 2008. Evidence for Incorporation of H$_2$S in Groundwater Fulvic Acids from Stable Isotope Ratios and Sulfur K-edge X-ray Absorption Near Edge Structure Spectroscopy. *Environ. Sci. Technol.* **42**, 2439-2444.

Emmenegger L., Schönenberger R., Sigg L., and Sulzberger B., 2001. Light-induced redox cycling of iron in circumneutral lakes. *Limnol. Oceanogr.* **46**, 49-61.

Fimmen R. L., Cory R. M., Chin Y.-P., Trouts T. D., and McKnight D. M., 2007. Probing the oxidation-reduction properties of terrestrially and microbially derived dissolved organic matter. *Geochim. Cosmochim. Acta* **71**, 3003-3015.

Gu B. and Chen J., 2003. Enhanced microbial reduction of Cr(VI) and U(VI) by different natural organic matter fractions. *Geochim. Cosmochim. Acta* **67**, 3575-3582.

Guardado I., Urrutia O., and Garcia-Mina J. M., 2007. Size Distribution, Complexing Capacity, and Stability of Phosphate-Metal-Humic Complexes. *J. Agric. Food Chem.* **55**, 408-413.

Hansel C. M., Benner S. G., Nico P., and Fendorf S., 2004. Structural constraints of ferric (hydr)oxides on dissimilatory iron reduction and the fate of Fe(II). *Geochim. Cosmochim. Acta* **68**, 3217-3229.

Hayes M. H. B. and Clapp C. E., 2001. Humic Substances: Considerations of Compositions, Aspects of Structure, and Environmental Influences. *Soil Sci.* **166**, 723-737.

Hosse M. and Wilkinson K. J., 2001. Determination of Electrophoretic Mobilities and Hydrodynamic Radii of Three Humic Substances as a Function of pH and Ionic Strength. *Environ. Sci. Technol.* **35**, 4301-4306.

Jiang J. and Kappler A., 2008. Kinetics of Microbial and Chemical Reduction of Humic Substances: Implications for Electron Shuttling. *Environ. Sci. Technol.* **42**, 3563-3569.

Jiang J., Bauer I., Paul A., and Kappler A., 2009. Arsenic redox changes by microbially and chemically formed semiquinone radicals and hydrochinones in a humic substance model quinone. *Environ. Sci. Technol.*, in press.

Jiao Y., Hendershot W. H., and Whalen J. K., 2008. Modeling Phosphate Adsorption by Agricultural and Natural Soils. *Soil Sci. Soc. Am. J.* **72**, 1078-1084.

Kappler A. and Haderlein S. B., 2003. Natural Organic Matter as Reductant for Chlorinated Aliphatic Pollutants. *Environ. Sci. Technol.* **37**, 2714-2719.

Kappler A., Benz M., Schink B., and Brune A., 2004. Electron shuttling via humic acids in microbial iron(III) reduction in a freshwater sediment. *FEMS Microbiology Ecology* **47**, 85-92.

Kucerik J., Smejkalova D., Cechlovska H., and Pekar M., 2007. New insights into aggregation and conformational behaviour of humic substances: Application of high resolution ultrasonic spectroscopy. *Org. Geochem.* **38**, 2098-2110.

Kumke M. U., Zwiener C., Abbt-Braun G., and Frimmel F. H., 1999. Spectroscopic Characterization of Fulvic Acid Fractions of a Contaminated Groundwater. *Acta Hydrochim. Hydrobiol.* **27**, 409-415.

Lovley D. R., Coates J. D., Blunt-Harris E. L., Phillips E. J. P., and Woodward J. C., 1996. Humic substances as electron acceptors for microbial respiration. *Nature* **382**, 445-448.

Lovley D. R., Fraga J. L., Blunt-Harris E. L., Hayes L. A., Phillips E. J. P., and Coates J. D., 1998. Humic Substances as a Mediator for Microbially Catalyzed Metal Reduction. *Acta hydrochimica hydrobiologica* **26**, 152-157.

Milne C. J., Kinniburgh D. G., and Tipping E., 2001. Generic NICA-Donnan Model Parameters for Proton Binding by Humic Substances. *Environ. Sci. Technol.* **35**, 2049-2059.

Muller F. L. L., 1996. Measurement of electrokinetic and size characteristics of estuarine colloids by dynamic light scattering spectroscopy. *Anal. Chim. Acta* **331**, 1-15.

Myers C. R. and Myers J. M., 1994. Ferric iron reduction-linked growth yields of *Shewanella putrefaciens* MR-1. *J. App. Bact.* **76**, 253-258.

Piccolo A., 2001. The Supramolecular Structure of Humic Substances. *Soil Sci.* **166**, 810.

Rate A. W., McLaren R. G., and Swift R. S., 1993. Response of copper (II) humic acid dissociation kinetics to factors influencing complex stability and macromolecular conformation. *Environ. Sci. Technol.* **27**, 1408-1414.

Raven K. P., Jain A., and Loeppert R. H., 1998. Arsenite and Arsenate Adsorption on Ferrihydrite: Kinetics, Equilibrium, and Adsorption Envelopes. *Environ. Sci. Technol.* **32**, 344-349.

Schwertmann U. and Cornell R. M., 2000. *Iron Oxides in the Laboratory*. Wiley-VCH Verlag GmbH, Weinheim.

Scott D. T., McKnight D. M., Blunt-Harris E. L., Kolesar S. E., and Lovley D. R., 1998. Quinone Moieties Act as Electron Acceptors in the Reduction of Humic Substances by Humics-Reducing Microorganisms. *Environ. Sci. Technol.* **32**, 2984-2989.

Simpson A., Kingery W., Hayes M., Spraul M., Humpfer E., Dvortsak P., Kerssebaum R., Godejohann M., and Hofmann M., 2002. Molecular structures and associations of humic substances in the terrestrial environment. *Naturwissenschaften* **89**, 84-88.

Stevenson F. J., 1994. *Humus Chemistry - Genesis, Composition, Reactions*. John Wiley & Sons, Inc., New York.

Stookey L. L., 1970. Ferrozine - A New Spectrophotometric Reagent for Iron. *Anal. Chem.* **42**, 779-781.

Straub K. L., Hanzlik M., and Buchholz-Cleven B. E. E., 1998. The use of biologically produced ferrihydrite for the isolation of novel iron reducing bacteria. *Syst. Appl. Microbiol.* **21**, 442-449.

Sutton R. and Sposito G., 2005. Molecular Structure in Soil Humic Substances: The New View. *Environ. Sci. Technol.* **39**, 9009-9015.

Thieme J., McNulty I., Vogt S., and Paterson D., 2007. X-ray Spectromicroscopy - A Tool for Environmental Sciences. *Environ. Sci. Technol.* **41**, 6885-6889.

Tipping E., 1981. The adsorption of aquatic humic substances by iron oxides. *Geochim. Cosmochim Acta* **45**, 191-199.

Tipping E., 2002. *Cation binding by humic substances*. Cambridge University Press, Cambridge.

6

Redox transformation of arsenic by Fe(II)-activated goethite (α-FeOOH)

ABSTRACT

The redox state and speciation of the metalloid arsenic (As) determine its environmental fate and toxicity. Knowledge about biogeochemical processes influencing arsenic redox state is therefore necessary to understand and predict its environmental behaviour. Here we quantified arsenic redox changes by pH-neutral goethite [α-FeIIIOOH] mineral suspensions amended with Fe(II) using wet-chemical and synchrotron X-ray absorption (XANES) analysis. Goethite itself did not oxidize As(III) and, in contrast to thermodynamic predictions, Fe(II)-goethite systems did not reduce As(V). However, we observed rapid oxidation of As(III) to As(V) in Fe(II)-goethite systems followed by slow re-reduction of some of the As(V) produced. Moessbauer spectroscopy showed initial formation of [57]Fe-goethite after [57]Fe(II) addition plus a so far unidentified additional Fe(II) phase. No other Fe(III) phase could be detected by Moessbauer, EXAFS, SEM, XRD or HR-TEM. This suggests that reactive Fe(III) species form as an intermediate Fe(III) phase upon Fe(II) addition and electron transfer into bulk goethite but before crystallisation of the newly formed Fe(III) as goethite. In summary this study suggests that in the simultaneous presence of Fe(III) oxyhydroxides and Fe(II), as commonly observed in environments inhabited by iron-reducing microorganisms, As(III) oxidation can occur. This potentially explains the presence of As(V) in reduced groundwater aquifers.

1. INTRODUCTION

Arsenic (As) is a health threat in many countries all over the world. About 150 million people world-wide are estimated to be exposed to elevated arsenic concentrations in drinking water (Nriagu, 2002). Anthropological and geological sources affect arsenic concentrations in soils, sediments, surface water and ground water. The mechanisms controlling retention and release of arsenic at the solid-water interface had been subject to extensive studies (Smedley and Kinniburgh, 2002; Polizzotto et al., 2006). However, the relevant processes are often site-specific and controlled by the present aqueous geochemistry, hydrology or anthropogenic impact (Polizzotto et al., 2008). This has led to contrary findings in the literature about the mechanisms responsible for arsenic release/ sorption and for arsenic redox reactions both in the environment but also in laboratory systems. For a long time it has been suggested for example that reductive dissolution of arsenic-bearing Fe(III) minerals in groundwater aquifers leads to a release of the adsorbed arsenic (Postma et al., 2007). However, as recently shown, microbial iron(III) reduction can also lead to the formation of stable Fe(II)-containing mineral phases and thus to arsenic sorption and immobilization (Islam et al., 2004; Kocar et al., 2006; Tufano and Fendorf, 2008). Bacteria can also change arsenic mobility by As(V) reduction as well as by As(III) oxidation (Oremland and Stolz, 2005; Kulp et al., 2008). Reduction of As(V) to As(III) for example leads to enhanced mobility and toxicity of the reduced species (Masscheleyn et al., 1991; Dixit and Hering, 2003; Oremland and Stolz, 2005).

The differences in mobility and toxicity of the two most environmentally relevant arsenic species, As(III) and As(V) oxyanions, make an in-depth understanding of arsenic redox chemistry important. Abiotic oxidation of dissolved As(III) has been observed in presence of oxygen combined with Fe(II) and oxygen in combination with MnO_2 (Oscarson et al., 1980; Sun and Doner, 1998; Daus et al., 2000). Chemical oxidation of As(III) has also been observed on the solid phase of reactive iron barriers (Su and Puls, 2004), in the presence of Fe(IV) formed by H_2O_2-dependent Fenton reactions (Hug and Leupin, 2003), under alkaline conditions in presence of Fe(0) or Fe(III) oxyhydroxides (Manning et al., 2002) and by lake sediments (Oscarson et al., 1980).

Although thermodynamically unfavourable, As(V) was also found under anoxic conditions in natural groundwater samples (Postma et al., 2007).

Recently it was shown that the Fe(II)-bearing minerals magnetite, siderite and carbonate green rust were unable to reduce As(V) to As(III) (Jönsson and Sherman, 2008). To our knowledge no detailed studies have been published on the redox interaction of arsenic with green rusts or systems containing Fe(III) mineral and aqueous/sorbed Fe(II) although such systems showed reduction of organic compounds (Haderlein and Pecher, 1998; Borch et al., 2005) as well as heavy metals (Liger et al., 1999; Williams and Scherer, 2001) . Especially goethite interacting with dissolved Fe(II) showed high redox activity in comparison to the other Fe(III) (oxy)hydroxides (Elsner et al., 2004).

Based on the knowledge gaps outlined above, the goal of this study was to quantify the redox transformation of As(V) and As(III) in systems containing goethite and aqueous Fe(II). Dissolved and sorbed arsenic species were quantified by wet-chemical analysis and synchrotron-based X-ray absorption techniques (XANES). The mineral phases were characterized by scanning electron microscopy (SEM), high-resolution transmission electron microscopy (HR-TEM), μ-X-ray diffraction (μ-XRD), Fe extended X-ray absorption fine structure (Fe-EXAFS) and by Moessbauer spectroscopy.

2. EXPERIMENTAL SECTION

2.1. Chemicals and minerals

All chemicals used in this study were of analytical grade. Arsenic solutions were prepared from sodium salts ($NaAsO_2$, Na_2HAsO_4).

The Fe(II) stock solution was prepared by adding 3.63 g (0.065 mmol) metal iron (Fe(0)) to 100 mL anoxic 1 M HCl in a screw cap serum bottle with a rubber septum under anoxic conditions. The suspension was heated to 80°C while gently stirring. After 2 hours no more hydrogen evolution was observed indicating that Fe(0) oxidation stopped. The suspension was filtered in an anoxic glove box with a 0.2 µm PTFE filter to remove any residual metal iron. The concentration of Fe(II) was determined colorimetrically by the ferrozine assay (see below). An isotopically pure $^{57}Fe(II)$ solution was prepared similarly from $^{57}Fe(0)$ (Fe(0) 96% pure, ChemGas) according to Williams and Scherer (2004).

Goethite (Bayferrox 920 Z) was provided by LANXESS Deutschland GmbH. Isotopically pure ^{56}Fe-goethite was synthesized using isotopically pure $^{56}Fe(0)$ (99.9% pure, ChemGas) according to Williams and Scherer (2004) and heated in aqueous suspension for 4 days at 60°C. The mineral purity and absence of significant amounts of organic or inorganic contaminations were verified by TOC (total organic carbon), XRF (X-ray fluorescence), SEM, XRD and, in case of minerals with natural abundance of Fe-isotopes, also by Moessbauer analysis. The mineral specific surface area was determined by N_2-BET measurements (Bayferox 920 Z goethite: 9.2 m²/g, ^{56}Fe-goethite: 44 m²/g).

2.2. Fe(II)-goethite arsenic redox transformation experiments

Goethite suspensions with a goethite concentration of 50 m²/l (5.4 g/l, a_s=9.2 m²/g) were prepared anoxically in screw cap bottles with a Teflon coated rubber septum. The mineral powder was suspended in DI water, homogenized for 24 h in an overhead shaker and washed twice with DI water. The stirred suspension was purged with N_2 for 1 h and transferred into an anoxic chamber (Braun, Germany; 100% N_2 atmosphere). Dissolved Fe(II) (0.7 M stock solution, prepared as described above) and 0.2 M NaOH were added alternating with

equilibration periods of several hours between the additions until an Fe(II) concentration in solution of 1 mM and a pH of 7 was reached. Aliquots of 25 ml suspension were distributed into 50 ml serum bottles. After addition of As(III) or As(V) to a final concentration of 1.2 mg/l, the bottles were shaken in the dark (to prevent photochemical reactions) at room temperature. After sampling at 0 h, 6 h and 7 d, the content of one bottle was filtered through a syringe filter (0.45 µm, nitrocellulose acetate, Millipore). The homogenously distributed Fe-layer on the filter was dried (~2 min), then sealed between two pieces of Kapton polyimide film to prevent oxidation while minimizing X-ray absorption, and packed in anoxic vials individually until measurement at the Stanford Synchrotron Radiation Lightsource (SSRL) or with the Moessbauer spectrometer. Subsamples for SEM and XRD analysis were collected as well as liquid samples for Fe(II) and arsenic identification and quantification.

2.3. Analytical methods

Separation of the aqueous arsenic species was done using an anion exchange cartridge according to Meng et al. (2001). This cartridge retains As(V) but not As(III) within the pH range of 4-9. After separation, aqueous arsenic was quantified by inductively coupled plasma mass spectroscopy, ICP-MS, (Elan 600, PE SCIEX, Perkin Elmer). Detection limit for arsenic was 1 µg/l. Samples were stabilized in 0.1 M HNO_3 and stored in the fridge until measurement. Rhodium was added as internal standard to each sample to a final concentration of 1 ppm Rh.

Dissolved iron was quantified using the ferrozine assay (Stookey, 1970). In order to measure total iron (Fe(tot)) concentrations, aliquots were reduced with 10% w/v $NH_2OH*HCl$ dissolved in 1 M HCl. Fe(II) and Fe(tot) samples were mixed with a 0.1% w/v solution of ferrozine in 50% ammonium acetate buffer. Absorbance was measured at 562 nm in microtiter plates with a plate reader (FlashScan 550 microplate reader, Analytik Jena AG, Germany).

The specific surface area of iron minerals was determined by the BET method with a Gemini 2375 Surface Area Analyzer with N_2 as adsorbing gas. Mineral samples were degassed and dried for 30 min under vacuum at 105°C, before measuring a five-point-BET-curve.

Moessbauer spectra were collected with a constant acceleration drive system in transmission mode and with a [57]Co source at room temperature. Samples were mounted in a close-cycle exchange-gas cryostat (Janis, USA) that allowed cooling of the sample to 4.2 K. Spectra were calibrated against a spectrum of alpha-Fe metal foil collected at room temperature. Spectra calibration and fitting was performed with Recoil software (University of Ottawa, Canada) using Voigt based spectral lines.

For micro-X-ray diffraction (μ-XRD), samples were grinded in an agate mortar, prepared on a Si single crystal silicon wafer and covered with a polyethylene foil to prevent oxidation. The samples were kept anoxic in a tightly closed glass jar until analysis. The μ-XRD-device (Bruker D8 Discover X-ray diffraction instrument, Bruker AXS GmbH, Germany) with a Co K_α X ray tube, operating at 30 kV, 30 mA, allows measurements at a spot diameter of 50 μm or 300 μm (Berthold et al., 2008). Each 3-min-measurement consists of three overlapping frames of 30° 2θ, using a GADDS® area detector. The EVA® 10.0.1.0 software was used to merge the three measured frames and identify the containing mineral phases using the PDF-database licensed by the International Centre for Diffraction Data (ICDD).

Extended X-ray absorption fine structure (EXAFS) and X-ray absorption near-edge structure (XANES) spectroscopy was performed at the Stanford Synchrotron Radiation Lightsource (SSRL) on beamlines 10-2 and 11-2, respectively. The storage ring was operated at 3.0 GeV and at currents between 60 and 100 mA. The Fe-EXAFS analytical procedures used here were similar to those described previously (Borch et al., 2007). Energy selection was accomplished with a Si(111) monochromator, and spectra were recorded in transmission mode using ion chambers. A set of iron reference compounds was used to perform linear combination k^3-weighted EXAFS spectral fitting using the SIXPACK interface to IFEFIT (Webb, 2005). A Si(220) monochromator was utilized for energy selection at the arsenic K-edge. Incident and transmitted intensities were measured with 15-cm N_2-filled ionization chambers. Sample fluorescence was measured with a 30-element Ge detector containing a 6-μm Ge filter. Higher harmonic components in the X-ray beam were minimized by a harmonic rejection mirror. The samples were maintained at 5 K during the data collection

to prevent sample beam damage (i.e., beam induced redox reactions) using an Oxford Instruments CF1208 continuous flow liquid helium cryostat. Arsenic K-edge spectra were internally calibrated with sodium arsenate (11,874 eV). XANES spectra were collected by scanning across the K-edge (11,867 eV) using 0.2-eV steps. Spectral processing and data analyses were conducted with the program SixPack (Webb, 2005). The background was removed from the spectrum before normalization using a Gaussian fit for the pre-edge and a quadratic fit for the postedge. Arsenic speciation was done by comparing white line features of the model compounds arsenate (as Na_2HAsO_4 or AsO_4^{3-} adsorbed to goethite) and arsenite (as $NaAsO_2$ or AsO^{2-} adsorbed to goethite), as previously shown valid for identifying arsenic oxidation states (Toevs et al., 2008). Linear combination fitting (LCF) of the sample spectra was performed using the arsenic model compounds. Precision of fitting arsenic species from XANES spectra is estimated to be 5% (Bostick et al., 2004).

Mineral samples for scanning electron microscopy (SEM) were prepared under anoxic conditions on an Al-stub covered with a conductive graphite tape. The sample was coated with a 45 nm Au coating (SCD 005/CEA 035 sputter, BAL-TEC). Images were obtained with an electron microscope (SEM LEO-1450VP, LEO electron microscopy) with an acceleration voltage of 15-20 kV at a working distance of 5-12 mm.

For high resolution transmission electron microscopy (HR-TEM) aliquots of a goethite and a Fe(II)-goethite suspension were taken. After centrifugation the solids were washed twice with anoxic water and dried. Minerals were resuspended in methanol and placed on a holey carbon grid. HR-TEM images were taken at a JEOL 2100-F electron microscope (Handler et al., 2009).

2.4. Thermodynamic calculations

Arsenic redox potentials were calculated at pH 6, 7 and 8 for a total arsenic concentration of 16 μM (experimental conditions) using Geochemist's Workbench (React, version 6.05, RockWare) and the database therein. Within the redox transition range both As(III) and As(V) are thermodynamically stable. The according E_h limits were set at the point where the concentration of either As(III) or As(V) at a certain

pH fell below the detection limit of our ICP-MS method (1 µg/l). The iron redox potential was calculated using the Nernst equation and the redox potential of goethite -274 mV (pH 7) given by (Thamdrup, 2000).

3. RESULTS

3.1. Arsenic redox changes in Fe(II)-goethite systems

Arsenic redox changes were followed and quantified both in solution and at the mineral surface after incubation of As(III) or As(V) with goethite and Fe(II)-goethite. X-ray absorption near edge spectroscopy (XANES) was used for speciation and quantification of mineral surface-associated arsenic (Fig. 1).
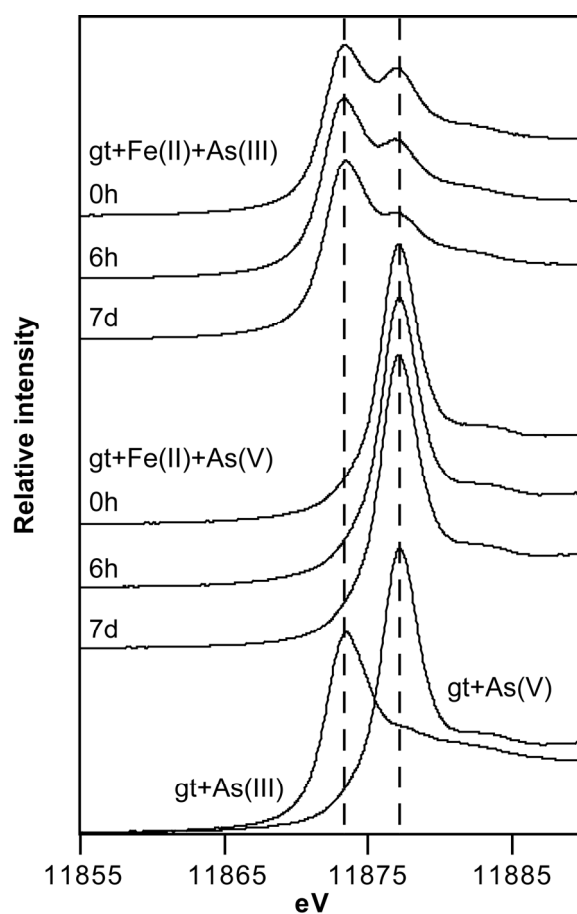
Fig. 1 **As-XANES spectra showing arsenic redox transformation by reactive iron species at time point zero (directly after mixing), after 6 hours and after 7 days. The experiments contained goethite (gt) and Fe(II) with either As(III) or As(V). For comparison As(V) and As(III) adsorbed to goethite without Fe(II) are shown at the bottom.**

Tab 1 Redox speciation of sorbed arsenic in the solid phase and in solution for abiotic experiments with goethite (gt) and As(III)/As(V) or goethite, Fe(II) and As(III)/As(V).

		Solid phase[1]				Concentration in solution[2]			
		As(III) [%]	As(V) [%]	As(III) [ppm]	As(V) [ppm]	As(III) [%]	As(V) [%]	As(III) [µg/l]	As(V) [µg/l]
gt+Fe(II)+As(III)	0h	79	21	119	32	86	14	324	53
	6h	84	16	154	29	94	6	187	12
	7d	88	12	173	24	89	11	114	14
gt+Fe(II)+As(V)	0h	-	100	-	221	-	-	-	-
	6h	-	100	-	221	-	-	-	-
	7d	-	100	-	221	-	-	-	-
gt+As(III)	7d	100	-	208	-	100	-	69	-
gt+As(V)	7d	-	100	-	221	-	-	-	-

1) determined by XANES
2) determined by ICP-MS
-) concentration below detection limit (1µg/l)

Both XANES analysis (Fig. 1) and quantification of arsenic in solution (Table 1) showed neither As(III) oxidation nor As(V) reduction by pure goethite. When adding Fe(II) to goethite suspensions we did not observe As(V) reduction even after 7 days of incubation indicating that the Fe(II)-goethite system was unable to reduce As(V) to As(III) under these conditions (Fig. 1, Table 1). However, when adding As(III) to a Fe(II)-goethite suspension we observed rapid oxidation of As(III), both in solution and in the solid phase (Fig. 1, Table 1). XANES analysis showed 21, 16 and 12% oxidized As(III) (i.e. As(V)) at the mineral surface directly after mixing (0 h), after 6 h and after 7 d, respectively. The total amount of arsenic in solution decreased from 377 to 128 µg/l after 7 d of reaction (Table 1), indicating increasing adsorption over time. During the same time period the dissolved concentration of As(V) decreased from 53 to 14 µg/l. Since the amount of As(V) bound to the solid phase did also decrease from 32 to 24 ppm, this suggests a re-reduction of previously formed As(V) back to As(III).

3.2. Mineral formation and transformation in Fe(II)-goethite systems

To understand the arsenic redox changes observed in our experiments it is necessary to identify the reactive iron species responsible for the As(III) oxidation and the following As(V) re-reduction in these systems. We therefore performed Moessbauer spectroscopy, Fe-EXAFS, XRD, SEM and HR-TEM analysis in an attempt to elucidate the structure of the minerals present. In order to identify potentially reactive iron phases formed upon addition of Fe(II), we used the advantage of Moessbauer spectroscopy to specifically detect the ^{57}Fe isotope. We prepared a goethite/Fe(II) suspension using ^{56}Fe-goethite and aqueous ^{57}Fe(II) (without addition of arsenic). The transformation of the added ^{57}Fe(II) at the goethite surface was then selectively detected by Moessbauer spectroscopy without the background signal of the underlying ^{56}Fe-goethite. Fitting of the obtained spectrum (measured at 77K) resulted in a sextet (95%) indicating the presence of ^{57}Fe-goethite that is probably formed by oxidation of the ^{57}Fe(II) by the underlying goethite but also by atom exchange between Fe(II) in the aqueous phase and structural Fe(III) in goethite (as described recently by Handler et al. (2009)) (Fig. 2).

In addition to the goethite sextet, we observed a doublet (5%), indicating the presence of a [57]Fe(II) species, which could possibly represent Fe(II) hydroxide, green rust or adsorbed Fe(II). However, the presence of Fe(II) hydroxide could be ruled out due to a decrease of 0.4 mm/s in the quadrupole splitting distribution of the Fe(II) signal from 3.0 mm/s (given for Fe(II) hydroxide) (Miyamoto, 1976) to 2.6 mm/s.
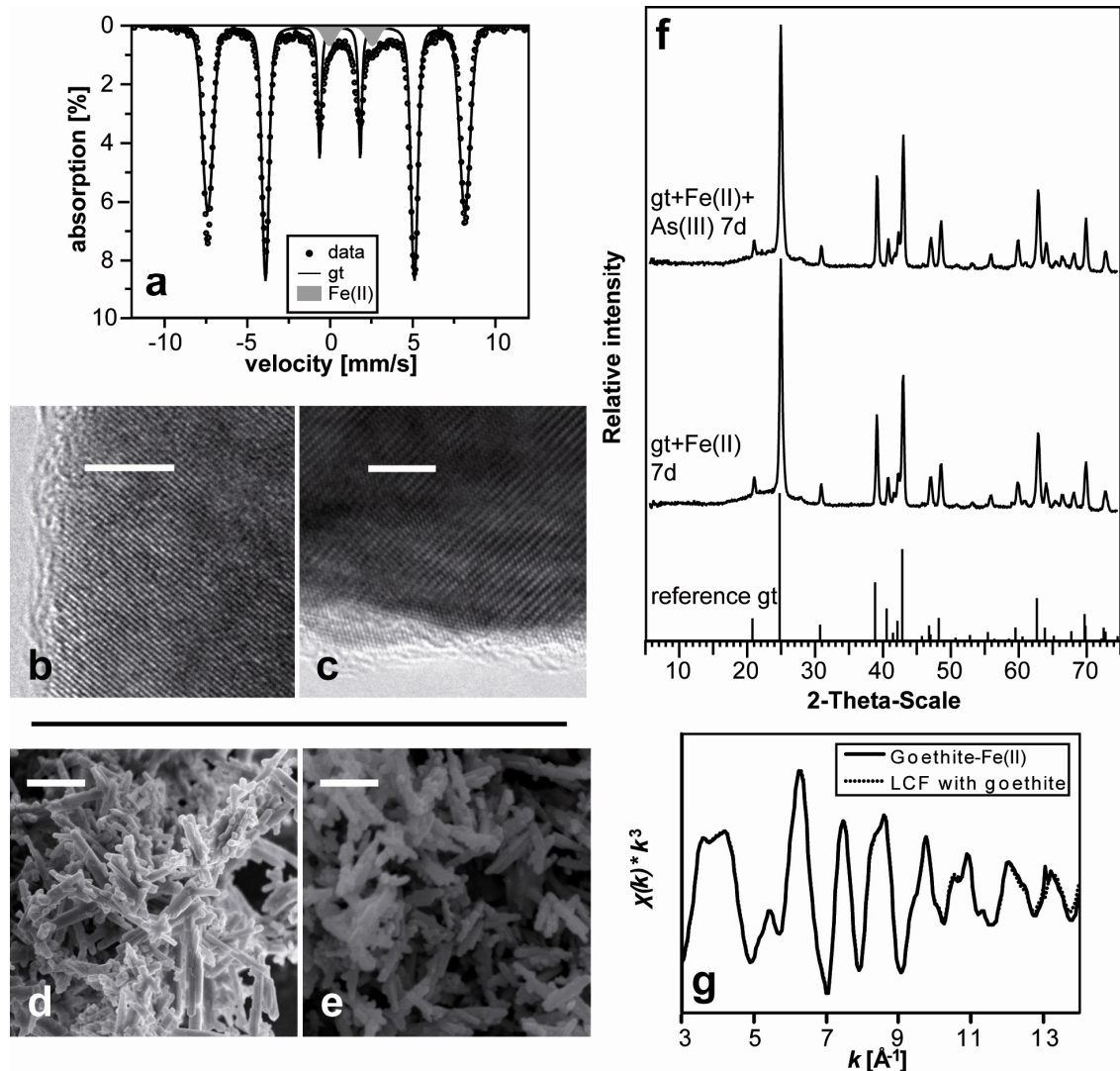

Fig. 2 (a) Moessbauer spectrum of [56]goethite with adsorbed [57]Fe(II) measured at 77 K showing a Fe(III) goethite sextet and a Fe(II) doublet. **(b, c)** HR-TEM images of **(b)** goethite and **(c)** Fe(II)-goethite systems after 4 d of incubation (size bar 5 nm). **(d, e)** SEM images of **(d)** goethite or **(e)** Fe(II)-goethite systems after 7 d of incubation (size bar 1 μm). **(f)** XRD patterns of Fe(II)-goethite and Fe(II)-goethite + As(III) after 7 d of incubation, showing reflections only for goethite. **(g)** k[3]-weighted Fe-EXAFS spectrum of goethite reacted with Fe(II) and As(III) for 7 d (solid line) and linear combination fit (LCF; dotted line) using pure goethite with adsorbed As(III).

HR-TEM images of pure goethite compared to Fe(II)-treated goethite rods showed no distinct changes in crystal structure (Fig. 2). This confirms a previous TEM study (Handler et al., 2009) where the authors also saw no differences between pure goethite and Fe(II)-treated goethite although they speculated that differences might be seen by HR-TEM. XRD, Fe-EXAFS and SEM analysis of the Fe(II)-goethite mixture after 7 d of incubation with and without added As(III) showed reflections (XRD), spectra (Fe-EXAFS) and structures (SEM) typical for goethite (Fig. 2). No secondary iron minerals were observed or identified by SEM, XRD and Fe-EXAFS. However, the amount of the Fe(II) phase (5% of the added dissolved ^{57}Fe(II)) detected by Moessbauer spectroscopy is very low and most likely not detectable by the other analytical methods used (due to the-Fe EXAFS and XRD detection limits of approximately 5 mol % Fe and 5 wt %, respectively).

4. DISCUSSION

The main goal of our study was to quantify arsenic redox transformation by reactive iron phases. However, As(V) and As(III) both have a high binding affinity for iron minerals that is controlled by the arsenic redox state, ionic strength and the prevailing pH conditions (Masscheleyn et al., 1991; Bowell, 1994; Raven et al., 1998; Dixit and Hering, 2003). Since wet-chemical extraction methods are either incomplete or lead to arsenic redox changes (Jackson and Miller, 2000), we followed the arsenic redox state by independent analysis of aqueous and sorbed arsenic species.

4.1. Arsenic redox transformation by Fe(II)-activated goethite

Quantification of dissolved arsenic species separated by an ion exchange cartridge followed by ICP-MS analysis and of mineral-bound arsenic by synchrotron based X-ray absorption spectroscopy (XAS) allowed analysis and quantification of the arsenic redox speciation in our arsenic-iron systems. Based on thermodynamic considerations for Fe(II)/goethite in comparison to the As(V)/As(III) redox couple, reduction of As(V) to As(III) is expected to occur at neutral pH (Fig. 3).
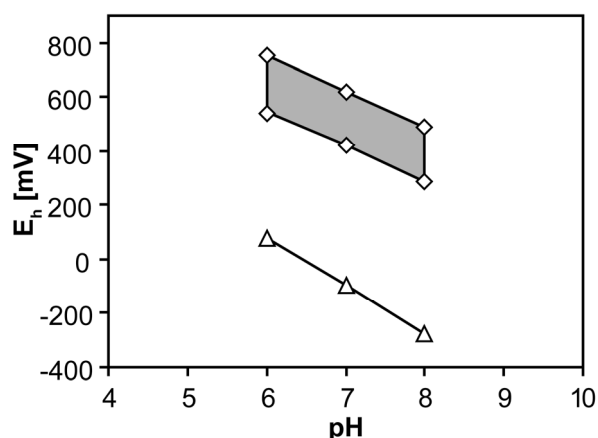
Fig. 3 E_h-pH diagram showing the E_h range for As(V)/As(III) at pH 6, 7 and 8 (diamonds, gray field). Triangles indicate E_h for the goethite/Fe(II) couple at a Fe(II) concentration of 1 mM.

Similar experiments with reactive Fe(II)-bearing mineral systems demonstrated reduction of heavy metals by such reactive iron minerals. Reduction of Cr(VI) was shown in abiotic experiments in the presence of the mixed-valent iron mineral carbonate green rust (Williams and Scherer, 2001), whereas U(VI) reduction was found in Fe(II)-hematite

systems and in the presence of natural iron-containing particles from iron rich coastal sediment (Liger et al., 1999). In contrast to reduction of the dissolved chromate and uranyl which leads to formation of less toxic and immobile oxides and hydroxides, reduction of As(V) would enhance the risk potential of this metalloid due to the higher mobility and toxicity of As(III) (Smedley and Kinniburgh, 2002). However, in our experiments we did not observe As(V) reduction by abiotic Fe(II)-goethite systems but rather As(III) oxidation in both the solid and the liquid phase (Fig. 1; Table 1).

Several potential mechanisms for arsenic oxidation were suggested in the literature (Fig. 4a). Since we observed no redox transformation in experiments with goethite in the absence of Fe(II), we can rule out the direct oxidation of As(III) by goethite in our systems, as it was suggested by Sun and Doner to occur in particular at lower pH values (pH 5) (1998). Direct oxidation of As(III) by O_2 can also be excluded in our experiments due to strict anoxic experimental conditions. The oxidation of As(III) by O_2 is a relatively slow process (Oscarson et al., 1980), even trace amounts of O_2 can therefore not explain the fast oxidation of As(III) observed in samples obtained right after As(III) addition to the Fe(II)-goethite mineral suspension. Additionally, the absence of O_2 in our experiments excludes the previously described As(III) oxidation in presence of O_2 and Fe(II) (Daus et al., 2000; Hug and Leupin, 2003; Katsoyiannis et al., 2008).

The potential for a Fenton's reaction induced oxidation of As(III) by reactive hydroxyl radicals was also considered since aqueous systems exposed to ultraviolet and visible light can cause the formation of hydrogen peroxide (i.e., H_2O_2) (Zuo and Hoigne, 1993). However, Fenton's reaction does not seem to be a plausible explanation for the oxidation of As(III) since the experiments were conducted under strictly anoxic conditions and in the dark thereby eliminating photochemical formation of H_2O_2. The potential for synchrotron radiation induced oxidation of As(III) was also tested by comparing multiple rapid XANES scans performed on the same sample location but no beam-induced redox change was observed when analyzed at 5K. We therefore conclude that the As(III) oxidation observed in our experiments was caused by a reactive Fe(III) species or secondary iron mineral phase that was formed by interaction of Fe(II) with goethite.
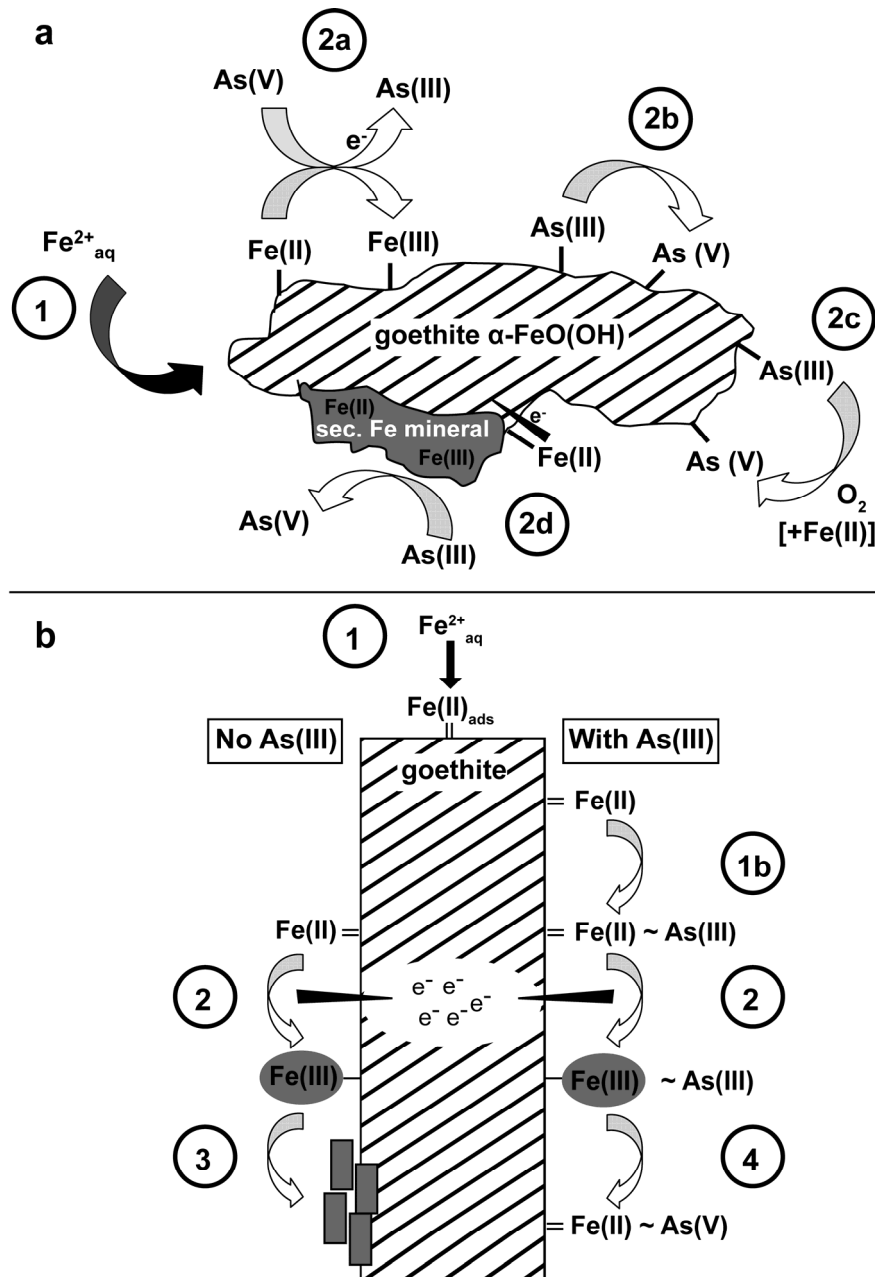
Fig. 4 (a) Scheme summarizing possible redox reactions in a system containing dissolved Fe(II), goethite and As(III) or As(V). (1) Adsorption of dissolved Fe(II), (2a) reduction of As(V) by adsorbed Fe(II), (2b) direct oxidation of As(III) at the goethite surface, (2c) oxidation of As(III) by O_2 and (2d) As(III) oxidation by secondary mixed-valent iron mineral phases. (b) Suggested mechanism of formation of a reactive Fe(III) intermediate phase formed upon (1) adsorption of dissolved Fe^{2+}, (1b) binding of As(III) to sorbed Fe(II), (2) electron transfer into the bulk goethite phase forming the reactive Fe(III) intermediate. This intermediate either (3) transforms/crystallizes into goethite or (4) oxidizes As(III) that is bound via an Fe(II)-bridge (before e-transfer to the bulk goethite) and via the reactive Fe(III)-intermediate (after e-transfer to the bulk goethite).

4.2. Identity of reactive iron phases formed in the Fe(II)-goethite system

Fe-EXAFS, XRD and SEM analysis did not indicate the presence of any crystalline or amorphous mineral phase other than goethite (Fig. 2). There was also no evidence for the formation of a new iron phase based on HR-TEM imaging after 4 d of reaction of goethite with aqueous Fe(II) (Fig. 2). However, Moessbauer spectroscopy analysis of a system containing isotopically pure ^{56}Fe-goethite and ^{57}Fe(II) allowed us to selectively trace the fate of the initially present dissolved ^{57}Fe(II). Upon addition of aqueous ^{57}Fe(II), we detected a so far unidentified ^{57}Fe(II)-containing compound, possibly a green rust phase or sorbed Fe(II)-species. The lack of another Fe(III) signal in addition to the Fe(III)-goethite signal questions the presence of the mixed Fe(II)-Fe(III) phase green rust, but does not necessarily exclude it. The expected Fe(III) signal for green rust could be masked by the dominant goethite signal and the broad Fe(II) signal and may not be resolved in the spectrum due to its low content. Although green rusts formed in oxic and anoxic Fe(0)-containing systems have been shown to oxidize As(III) (Su and Puls, 2004; Lien and Wilkin, 2005; Su and Wilkin, 2005), a very recent lab study demonstrated that carbonate green rust neither caused reduction of As(V) nor oxidation of As(III) (Jönsson and Sherman, 2008). Therefore the influence of green rust on the redox state of arsenic remains controversial.

In addition to the ^{57}Fe(II)-signal, we also observed the formation of a ^{57}Fe(III)-mineral phase, namely goethite (although it cannot be excluded that other Fe(III) phases were present in amounts below the Moessbauer detection limit of approx. 2%). Similar to previous studies (Williams and Scherer, 2004; Larese-Casanova and Scherer, 2007; Cwiertny et al., 2008), this can be interpreted as a result of electron transfer from surface bound ^{57}Fe(II) to the underlying goethite and crystallization of the formed ^{57}Fe(III) as goethite. Recently, even a complete atom exchange between the aqueous Fe(II) and goethite was described and indicated some recrystallization of the goethite particles (Handler et al., 2009). The fact that goethite is formed from the added Fe(II) and no other Fe(III) mineral phases were detected suggests that the reactive Fe(III) phase that is responsible for As(III) oxidation in our experiments is formed as a reactive intermediate phase. This species could have formed immediately after As(III) addition to the

Fe(II)-goethite system and electron transfer from sorbed Fe(II) to the bulk goethite and before the structural reorientation of this Fe(III) (the original Fe(II)) and its final crystallization as goethite (Fig. 4b). Evidence for such a short-lived but very reactive intermediate comes from the observation that the kinetics of As(III) oxidation in our system obviously is very fast. Specifically, we observed the highest extent of As(III) oxidation immediately after mixing of all components (Fig. 1, Table 1).

4.3. Role of ternary goethite-Fe(II)-As(III) complexes

Model calculations of Fe(II) sorption to goethite by Hiemstra and van Riemsdijk (2007) suggested a combination of Fe(II) sorption and Fe(II) surface oxidation. This is in agreement with our experiments which led to the presence of adsorbed ^{57}Fe(II) and ^{57}Fe-goethite formation, respectively. According to their calculations, the predominance of one or the other mechanism depends mainly on pH variations just around pH 7. Hiemstra and van Riemsdijk (2007) and Dixit and Hering (2006) also found that more As(III) is adsorbed by goethite in presence of increasing amounts of Fe(II). They suggested the formation of ternary binuclear-bidentate complexes either in the form of goethite-As(III)-Fe(II) (Hiemstra and van Riemsdijk, 2007) or goethite-Fe(II)-As(III) (Dixit and Hering, 2006). Such complexes may even facilitate electron transfer in-between the three reactants. Although both studies did not consider redox transformations of arsenic in their calculations, it would be conceivable that in our as well as in their experiments the presence of an inner-sphere complex of goethite-Fe(II)$_2$-As(III) could have led to a transfer of two electrons from the two Fe(II) atoms to goethite followed by the formation of a reactive intermediate goethite-Fe(III)$_2$-As(III) complex (Fig. 4b). The formed Fe(III) with a potentially enhanced redox activity could now act as an oxidant for As(III) forming a goethite-Fe(II)$_2$-As(V) complex (Fig. 4b). Since more As(III) sorption to goethite in the presence of Fe(II) was determined based on ICP analysis of the total soluble arsenic concentration in the supernatant (Dixit and Hering, 2006), it is likely that the increased As(III) sorption observed by these authors was due to As(III) oxidation (in the goethite-Fe(III)$_2$-As(III) complex) and thus As(V) adsorption rather than formation of ternary goethite-Fe(II)-As(III) complexes per se. It is widely recognized that As(V) and As(III) predominantly form inner-sphere complexes on iron (hydr)oxides,

however, it is still not clear what structural arrangement predominates (Gustafsson and Bhattacharya, 2007). The type of inner-sphere complex formed between As(V) and goethite (e.g., bidentate binuclear, bidentate mononuclear or monodentate) will likely influence the sorption capacity of goethite. If the structural arrangement of As(V) adsorption is different than for As(III) then oxidation of As(III) could explain the observed increased As(III) adsorption in the presence of Fe(II).

4.4. Environmental implications

Understanding the implications of mixed valent iron systems including the identification of redox active phases will help to describe arsenic redox changes under natural conditions. Several studies have already described the occurrence of thermodynamically instable As(V) under reducing conditions in natural environments (Swartz et al., 2004; de Mello et al., 2007). Oxidation of As(III) by a Fe(II)-goethite mixture similar to our experimental conditions may be an important mechanism that could be responsible for As(V) formation in anoxic aquifers.

5. ACKNOWLEDGMENTS

6. REFERENCES

Berthold C., Bjeoumikhov A., and Brügemann L., 2008. Fast XRD² Microdiffraction with Focusing X-Ray Microlenses. *Particle & Particle Systems Characterization*, submitted.

Borch T., Inskeep W. P., Harwood J. A., and Gerlach R., 2005. Impact of Ferrihydrite and Anthraquinone-2,6-Disulfonate on the Reductive Transformation of 2,4,6-Trinitrotoluene by a Gram-Positive Fermenting Bacterium. *Environ. Sci. Technol.* **39**, 7126-7133.

Borch T., Masue Y., Kukkadapu R. K., and Fendorf S., 2007. Phosphate Imposed Limitations on Biological Reduction and Alteration of Ferrihydrite. *Environ. Sci. Technol.* **41**, 166-172.

Bostick B. C., Chen C., and Fendorf S., 2004. Arsenite Retention Mechanisms within Estuarine Sediments of Pescadero, CA. *Environ. Sci. Technol.* **38**, 3299-3304.

Bowell R. J., 1994. Sorption of arsenic by iron oxides and oxyhydroxides in soils. *Appl. Geochem.* **9**, 279-286.

Cwiertny D. M., Handler R. M., Schaefer M. V., Grassian V. H., and Scherer M. M., 2008. Interpreting nanoscale size-effects in aggregated Fe-oxide suspensions: Reaction of Fe(II) with Goethite. *Geochim. Cosmochim. Acta* **72**, 1365-1380.

Daus B., Mattusch J., Paschke A., Wennrich R., and Weiss H., 2000. Kinetics of the arsenite oxidation in seepage water from a tin mill tailings pond. *Talanta* **51**, 1087-1095.

de Mello J., Talbott J., Scott J., Roy W., and Stucki J., 2007. Arsenic Speciation in Arsenic-rich Brazilian Soils from Gold Mining Sites under Anaerobic Incubation. *Environ. Sci. Poll. Res.* **14**, 388-396.

Dixit S. and Hering J. G., 2003. Comparison of Arsenic(V) and Arsenic(III) Sorption onto Iron Oxide Minerals: Implications for Arsenic Mobility. *Environ. Sci. Technol.* **37**, 4182-4189.

Dixit S. and Hering J. G., 2006. Sorption of Fe(II) and As(III) on goethite in single- and dual-sorbate systems. *Chemical Geology - Controls on Arsenic Transport in Near-Surface Aquatic Systems* **228**, 6-15.

Elsner M., Schwarzenbach R. P., and Haderlein S. B., 2004. Reactivity of Fe(II)-Bearing Minerals toward Reductive Transformation of Organic Contaminants. *Environ. Sci. Technol.* **38**, 799-807.

Gustafsson J. P. and Bhattacharya P., 2007. *Geochemical modelling of arsenic adsorption to oxide surfaces*. Elsevier.

Haderlein S. B. and Pecher K., 1998. Pollutant reduction in heterogeneous Fe(II)/Fe(III) systems. In: Sparks D. L. and Grundl T. Eds.), *Kinetics and Mechanisms of Reactions at the Mineral/Water Interface*. American Chemical Society, Washington, DC.

Handler R. M., Beard B. L., Johnson C. M., and Scherer M. M., 2009. Atom Exchange between Aqueous Fe(II) and Goethite: An Fe Isotope Tracer Study. *Environ. Sci. Technol.* **43**, 1102-1107.

Hiemstra T. and van Riemsdijk W. H., 2007. Adsorption and surface oxidation of Fe(II) on metal (hydr)oxides. *Geochim. Cosmochim. Acta* **71**, 5913-5933.

Hug S. J. and Leupin O., 2003. Iron-Catalyzed Oxidation of Arsenic(III) by Oxygen and by Hydrogen Peroxide: pH-Dependent Formation of Oxidants in the Fenton Reaction. *Environ. Sci. Technol.* **37**, 2734-2742.

Islam F. S., Gault A. G., Boothman C., Polya D. A., Charnock J. M., Chatterjee D., and Lloyd J. R., 2004. Role of metal-reducing bacteria in arsenic release from Bengal delta sediments. *Nature* **430**, 68-71.

Jackson B. P. and Miller W. P., 2000. Effectiveness of Phosphate and Hydroxide for Desorption of Arsenic and Selenium Species from Iron Oxides. *Soil Sci. Soc. Am. J.* **64**, 1616-1622.

Jönsson J. and Sherman D. M., 2008. Sorption of As(III) and As(V) to siderite, green rust (fougerite) and magnetite: Implications for arsenic release in anoxic groundwaters. *Chem. Geol.* **255**, 173-181.

Katsoyiannis I. A., Ruettimann T., and Hug S. J., 2008. pH Dependence of Fenton Reagent Generation and As(III) Oxidation and Removal by Corrosion of Zero Valent Iron in Aerated Water. *Environ. Sci. Technol.* **42**, 7424-7430.

Kocar B. D., Herbel M. J., Tufano K. J., and Fendorf S., 2006. Contrasting Effects of Dissimilatory Iron(III) and Arsenic(V) Reduction on Arsenic Retention and Transport. *Environ. Sci. Technol.* **40**, 6715-6721.

Kulp T. R., Hoeft S. E., Asao M., Madigan M. T., Hollibaugh J. T., Fisher J. C., Stolz J. F., Culbertson C. W., Miller L. G., and Oremland R. S., 2008. Arsenic(III) Fuels Anoxygenic Photosynthesis in Hot Spring Biofilms from Mono Lake, California. *Science* **321**, 967-970.

Larese-Casanova P. and Scherer M. M., 2007. Fe(II) Sorption on Hematite: New Insights Based on Spectroscopic Measurements. *Environ. Sci. Technol.* **41**, 471-477.

Lien H. L. and Wilkin R. T., 2005. High-level arsenite removal from groundwater by zero-valent iron. *Chemosphere* **59**, 377-386.

Liger E., Charlet L., and Van Cappellen P., 1999. Surface catalysis of uranium(VI) reduction by iron(II). *Geochim. Cosmochim. Acta* **63**, 2939-2955.

Manning B. A., Hunt M. L., Amrhein C., and Yarmoff J. A., 2002. Arsenic(III) and Arsenic(V) Reactions with Zerovalent Iron Corrosion Products. *Environ. Sci. Technol.* **36**, 5455-5461.

Masscheleyn P. H., Delaune R. D., and Patrick Jr. W. H., 1991. Effect of Redox Potential and pH on Arsenic Speciation and Solubility in a Contaminated Soil. *Environ. Sci. Technol.* **25**, 1414-1419.

Meng X., Korfiatis G. P., Christodoulatos C., and Bang S., 2001. Treatment of arsenic in Bangladesh well water using a household co-precipitation and filtration system. *Water Res.* **35**, 2805-2810.

Miyamoto H., 1976. The magnetic properties of Fe(OH)$_2$. *Mater. Res. Bull.* **11**, 329-335.

Nriagu J. O., 2002. Arsenic Poisoning Through the Ages. In: Frankenberger W. T. J. (Ed.), *Environmental Chemistry of Arsenic.* Marcel Dekker, Inc., New York.

Oremland R. S. and Stolz J. F., 2005. Arsenic, microbes and contaminated aquifers. *Trends Microbiol.* **13**, 45-49.

Oscarson D. W., Huang P. M., and Liaw W. K., 1980. The Oxidation of Arsenite by Aquatic Sediments. *J Environ Qual* **9**, 700-703.

Polizzotto M. L., Kocar B. D., Benner S. G., Sampson M., and Fendorf S., 2008. Near-surface wetland sediments as a source of arsenic release to ground water in Asia. *Nature* **454**, 505-508.

Polizzotto M. L., Harvey C. F., Li G., Badruzzman B., Ali A., Newville M., Sutton S., and Fendorf S., 2006. Solid-phases and desorption processes of arsenic within Bangladesh sediments. *Chem. Geol.* **228**, 97-111.

Postma D., Larsen F., Minh Hue N. T., Duc M. T., Viet P. H., Nhan P. Q., and Jessen S., 2007. Arsenic in groundwater of the Red River floodplain, Vietnam: Controlling geochemical processes and reactive transport modeling. *Geochim. Cosmochim. Acta* **71**, 5054-5071.

Raven K. P., Jain A., and Loeppert R. H., 1998. Arsenite and Arsenate Adsorption on Ferrihydrite: Kinetics, Equilibrium, and Adsorption Envelopes. *Environ. Sci. Technol.* **32**, 344-349.

Smedley P. L. and Kinniburgh D. G., 2002. A review of the source, behaviour and distribution of arsenic in natural waters. *Appl. Geochem.* **17**, 517-568.

Stookey L. L., 1970. Ferrozine - A New Spectrophotometric Reagent for Iron. *Anal. Chem.* **42**, 779-781.

Su C. and Puls R. W., 2004. Significance of Iron(II,III) Hydroxycarbonate Green Rust in Arsenic Remediation Using Zerovalent Iron in Laboratory Column Tests. *Environ. Sci. Technol.* **38**, 5224-5231.

Su C. M. and Wilkin R. T., 2005. Arsenate and arsenite sorption on and arsenite oxidation by iron(II, III) hydroxycarbonate green rust, *Advances in Arsenic Research.*

Sun X. and Doner H. E., 1998. Adsorption and oxidation of arsenite on goethite. *Soil Sci.* **163**, 278-287.

Swartz C. H., Blute N. K., Badruzzman B., Ali A., Brabander D., Jay J., Besancon J., Islam S., Hemond H. F., and Harvey C. F., 2004. Mobility of arsenic in a Bangladesh aquifer: Inferences from geochemical profiles, leaching data, and mineralogical characterization. *Geochim. Cosmochim. Acta* **68**, 4539-4557.

Thamdrup B., 2000. Bacterial manganese and iron reduction in aquatic sediments. In: Schink B. (Ed.), *Adv. Microb. Ecol.* Kluwer Academic/ Plenum Publishers, New York.

Toevs G., Morra M. J., Winowiecki L., Strawn D., Polizzotto M. L., and Fendorf S., 2008. Depositional Influences on Porewater Arsenic in Sediments of a Mining-Contaminated Freshwater Lake. *Environ. Sci. Technol.* **42**, 6823-6829.

Tufano K. J. and Fendorf S., 2008. Confounding Impacts of Iron Reduction on Arsenic Retention. *Environ. Sci. Technol.* **42**, 4777-4783.

Webb S. M., 2005. SIXpack: a graphical user interface for XAS analysis using IFEFFIT. *Phys. Scr.*, 1011.

Williams A. G. B. and Scherer M. M., 2001. Kinetics of Cr(VI) Reduction by Carbonate Green Rust. *Environ. Sci. Technol.* **35**, 3488-3494.

Williams A. G. B. and Scherer M. M., 2004. Spectroscopic Evidence for Fe(II)-Fe(III) Electron Transfer at the Iron Oxide-Water Interface. *Environ. Sci. Technol.* **38**, 4782-4790.

Zuo Y. and Hoigne J., 1993. Evidence for Photochemical Formation of H_2O_2 and Oxidation of SO_2 in Authentic Fog Water. *Science* **260**, 71-73.

7

Arsenic redox transformations in biogenic Fe(III) mineral-Fe(II) systems

ABSTRACT

Redox changes of arsenic in anoxic, iron reducing environments can be influenced by microbial activity, either by direct oxidation or reduction of arsenic species or indirectly via the change of redox conditions. Although the main geochemical processes are frequently investigated several effects observed under natural conditions remain unclear up to now. In particular the role of reactive iron systems of biogenic origin for the redox state of arsenic was not investigated so far.

In order to quantify arsenic redox changes in presence of iron minerals wet-chemical extraction reagents were applied on arsenic-amended goethite suspensions at neutral pH. As we observed redox transformation as well as incomplete desorption of arsenic from the mineral phase with the reagents used, we analyzed liquid and solid phase of the biogenic experiments separately using ICP-MS and synchrotron-based X-ray absorption spectroscopy. Incubation of the iron reducing strain *Shewanella oneidensis* MR-1 with a mixture of goethite and 2-line ferrihydrite did not lead to any As(III) oxidation or As(V) reduction, respectively. Goethite or other microbiologically formed minerals did not function as an adsorption template for dissolved Fe(II), at least it had no influence on the redox state of the added arsenic species. In contrast to these results we observed reduction of As(V) to As(III) in a system of microbiologically reduced 2-line ferrihydrite only. Besides formation of magnetite and small amounts of goethite no other potentially reactive iron phases could be identified with the applied methods.

The results of this study suggest that the redox state of arsenic in anoxic environments may be determined by the formation of biogenic, mixed-valent iron mineral precipitates. However the exact mechanism remains unclear and seems to depend sensitively on the ratio of dissolved Fe(II) to the specific Fe(III) mineral phase.

1. INTRODUCTION

Microorganisms are thought to strongly influence the fate of arsenic in anoxic environments. Either directly via utilization of arsenic as electron acceptor or donor, respectively, or indirectly via transformation of arsenic bearing host minerals. It has been shown for example that bacteria can change the redox state of arsenic by As(V) reduction as well as by As(III) oxidation (Oremland and Stolz, 2005; Kulp et al., 2008). In addition, several studies investigated the impact of iron-reducing bacteria on the retention behaviour of arsenic in anoxic aquifers. Tufano and Fendorf (2008) for example were able to support previous findings (Islam et al., 2005; Herbel and Fendorf, 2006; Kocar et al., 2006) of arsenic retention in iron reducing environments just partly. After an initial increase in arsenic retention they observed prolonged release of arsenic after long term incubation of the Fe(III) minerals with iron reducers in a flow-through column.

Similar to the confounding findings about the retention of arsenic during microbial iron mineral reduction, the mechanisms causing redox transformation of arsenic in natural systems are still not completely understood. Several studies described already the occurrence of both arsenic redox states under reducing conditions in natural environments (Hamon et al., 2004; Kent and Fox, 2004; Swartz et al., 2004; de Mello et al., 2007; Postma et al., 2007), although As(V) is thermodynamically instable under reducing conditions (Masscheleyn et al., 1991; Smedley and Kinniburgh, 2002). Knowledge about redox transformation processes is fundamental in particular because the two most environmentally relevant arsenic species, As(III) and As(V) oxyanions show differences in toxicity and mobility. The more toxic, reduced species (As(III)) has been shown to be in general more mobile than As(V) (Masscheleyn et al., 1991; Bowell, 1994; Dixit and Hering, 2003; Antelo et al., 2005; Oremland and Stolz, 2005).

Besides its role in arsenic retention microbial iron reduction could also indirectly influence the redox state of arsenic. Previous studies showed the potential of biogenic, mixed-valent Fe(II)-Fe(III) mineral systems for the reductive transformation of organic and inorganic pollutants (Heijman et al., 1993; Fredrickson et al., 2004; Williams et al., 2005). Similar effects could be expected in Presence of arsenic. Previous

studies showed that a combination of different Fe(III) minerals even enhanced the remediation potential of biogenic precipitates (Tobler et al., 2007). Ferrihydrite, a poorly crystalline Fe(III) mineral, was reduced by *Geobacter metallireducens* during toluene oxidation and lepidocrocite was added to function as an adsorption template for biogenic Fe(II). The formed reactive minerals reductively degraded nitroaromatic compounds. This approach of using mineral mixtures was also applied in the present study.

We investigated the potential of biogenic Fe(II)-Fe(III) mineral mixtures on the redox transformation of arsenic under anoxic conditions. In order to quantify the two redox states we evaluated different extraction reagents which finally turned out to be inadequate for a quantitative analysis of the potential redox transformation reactions. The arsenic species were analyzed separately in the liquid (ICP-MS after ion exchange separation) and the solid phase. Furthermore we followed microbial Fe(II) formation by complete acid digestion of the solid phase and iron mineral (trans)formation by XRD and Moessbauer spectroscopy.

2. MATERIALS AND METHODS

2.1. Chemicals and minerals

All chemicals used in this study were of analytical grade. Arsenic solutions were prepared from sodium salts ($NaAsO_2$, Na_2HAsO_4).

2-line ferrihydrite was synthesized according to Schwertmann and Cornell (2000) and Raven et al. (1998) using 40 g of $Fe(NO_3)_3 \cdot 9H_2O$ per 500 ml water that was pH adjusted with 1 M KOH to a final pH not higher than 7.5. After centrifugation and 4 times washing with DI water, the wet solid was resuspended in water to an approximate concentration of 0.5 M Fe(III). This suspension was deoxygenated by alternating application of vacuum and N_2 flushing for 10 min each for a total of three times. The suspension was stored up to 10 days in the dark in serum bottles. The mineral was identified by XRD analysis after freeze drying an aliquot and the specific surface area was determined by N_2-BET measurements (a_S=270 m²/g).

Goethite (Bayferrox 920 Z) was provided by LANXESS Deutschland GmbH. The mineral purity was verified by XRD analysis and the mineral specific surface area was determined by N_2-BET measurements (a_S=9.2 m²/g). Purified goethite particles were suspended in Millipore®-water to achieve the final concentration of 0.5 M Fe(III). The suspension was deoxygenated in butyl rubber stopper closed bottle (see above). For comparison the goethite suspension was also not sterilized.

2.2. Arsenic-goethite extraction experiments

Arsenic containing goethite suspensions were prepared under oxic conditions in screw cap bottles. Goethite with a concentration of 50 m²/l (3.16 g/l, a_S=15.8 m²/g) was suspended in bicarbonate buffer (5 mM) and spiked with 500 µg/l As(III) or As(V). The suspension was shaken for 2 h at room temperature in the dark and subsequently separated into 50 ml aliquots under continuous stirring. The arsenic loaded goethite was centrifuged (30 min 4500 rpm), the supernatant decanted and analyzed for dissolved As by FI-HG-AAS (Flow injection hydride generating atom absorption spectroscopy). The remaining solid was treated with the different extractants that were prepared according to Keon et al. (2001), Wenzel et al. (2001) and Samanta and Clifford

(2005) with analytical grade chemicals in bi-destilled water. Aliquots of the following extractants (50 ml each) were added to the arsenic loaded goethite to extract the following target species of arsenic: (i) loosely bound As with 1.34 mM EDTA (ethylene diamine tetraacetic acid) + 87 mM acetic acid, shaken for 1 h at room temperature, (ii) amorphous iron oxyhydroxides with 1 M HCl, shaken for 1 h at room temperature, (iii) amorphous/ poorly crystalline iron hydroxides with 0.2 M oxalate buffer (pH 3.2), shaken for 2 h in the dark at room temperature, (iv) well crystalline iron hydroxides with 0.2 M oxalate buffer + 0.1 M ascorbic acid (pH 3.2), 30 min at 95°C and (v) crystalline iron oxyhydroxides with 5.7 M subboiled HCl, 1 h shaken in the dark at room temperature + 45 min at 95°C until complete dissolution of goethite was observed. After extraction, the suspensions were centrifuged (30 min 4500 rpm), the supernatant was decanted and analyzed for dissolved As by FI-HG-AAS.

2.3. Biogenic arsenic redox transformation experiments

Shewanella oneidensis strain MR-1, originally isolated from Oneida Lake, New York (Myers and Nealson, 1988) was provided by Dr. Jeff Gralnick (Univ. Minnesota). Aerobic cultures on LB-agar plates were streaked out from a frozen stock kept at -80°C. LB-medium contained (per 1 l): 10 g tryptone, 5 g yeast extract, 5 g NaCl (for LB plates 12 g agar was added). LB-plates were incubated at 28°C for approximately 24 h and afterwards kept at 4°C up to 10 days. For liquid culture preparation, 50 ml of liquid LB medium in a 200 ml Erlenmeyer flask were inoculated with a single colony form the LB-plate. The capped flask was incubated at 28°C on a rotary shaker at 150 rpm. Cell concentration in LB-cultures was determined by optical density (OD) measurements at 600 nm. OD_{600} was calibrated against cell counts obtained by direct counting with a Thoma-chamber by light microscopy (Axioscope 2 from Zeiss, Germany). At the end of exponential growth, cells had consumed O_2 completely and switched to anaerobic metabolism (Lies et al., 2005).

For further experiments, cells were cultured in sterile and anoxic LML medium (Myers and Myers, 1994), containing 12 mM HEPES buffer and 30 mM lactate, set to pH 7 and prepared using a Widdel flask. Inoculum for experiments was prepared as follows: 2 ml of LB-grown cell culture were harvested after 14 h at late exponential growth

phase and centrifuged (5 min, 10 600 g). Cells were washed twice with LML medium, resuspended in 2 ml of medium and diluted to a final concentration of 2×10^5 cells/ml for the experiments.

To monitor microbial Fe(III)-reduction rates, numerous tubes (~30) were set up in parallel for one experiment and incubated lying horizontally at 28°C in the dark. Sterile culture tubes (total volume 23 ml) were filled with 9 ml of anoxic LML-medium. The headspace was exchanged with N_2 and tubes were sealed with butyl rubber stoppers. For sample treatments in the glove box (Braun, Germany; N_2 atmosphere) smaller culture tubes (total volume 17 ml) were used which were closed with a thin butyl rubber stopper and a screw cap. Ferrihydrite or goethite in suspension was added to the medium for a final concentration of 5 mM each and finally the cells were injected with syringes. At sampling time points selected tubes were sacrificed to measure the total Fe(II) and Fe(III) concentration by acid digestion (6 ml 12 M HCl, 3:5 dilution), to take mineral samples for XRD measuremens or to apply the sequential extraction protocol. Complete digestion of the culture tubes was necessary to include precipitates that formed at the glass wall of the tubes and to avoid inhomogeneous sampling with syringes. In order to calculate the maximum reduction rate of an experiment, total Fe(II) concentration determined with the ferrozine assay (see below) was plotted against time. A linear regression was calculated to derive the maximum slope for Fe(II) formation.

For experiments proving reactivity of biogenic iron minerals for arsenic species cells were grown in serum bottles with 25 ml sterile, anoxic LML medium. 2-line ferrihydrite served as the primary Fe(III) source (terminal electron acceptor) for the bacteria, either alone (30 mM, 3.2 g/l) or in a mixture of ferrihydrite (15 mM, 1.6 g/l) and goethite (15 mM, 1.3 g/l). Goethite was added as adsorption template for biogenic Fe(II). The bottles were sampled with a syringe during iron reduction for Fe(II) and Fe(tot) (100 μl aliquot dissolved in 900 μl 1 M HCl) measurements (Fe(tot) sample preparation for goethite containing cultures: 100 μl aliquot dissolved in 900 μl 6 M HCl). At time point zero and two more time points of microbial reduction a few serum bottles were pasteurized (10 min, 80°C) in order to eliminate microbial activity (tested in control experiments) and 280 μg/l As(III) or As(V) were added to follow arsenic redox transformation by the microbially

produced reactive iron minerals. Spiked bottles were incubated on a shaker in the dark for 0 h, 6 h and 7 d. Bottles were sacrificed in the anoxic glove box after incubation. Solids were separated from the solution using syringe filters (0.45 μm, nitrocellulose acetate, Millipore). Samples were taken for X-ray absorption near edge structure (XANES) spectroscopy, Moessbauer spectroscopy and μ-X-ray diffraction (μ-XRD) of the solid and inductively coupled plasma mass spectroscopy (ICP-MS) measurements of As(III) and As(tot) (anion exchanger cartridge) and the ferrozine assay for Fe(II) in the permeate (methods see below).

2.4. Sequential extraction

Samples for sequential extraction were prepared in an anoxic glove box (Braun, Germany; N_2 atmosphere) harvesting one screw-cap culture tube for each treatment. The samples were transferred stepwise into 2 ml-Eppendorf® tubes and centrifuged (2 min, 9 700 g) the remaining solids were treated with the sequential extraction method.

The protocol for sequential iron mineral extraction was modified after Roden and Zachara (1996). Loosely bound Fe(II) was extracted by a 1 M sodium acetate solution (pH 5). Vivianite and poorly crystalline ferrihydrite were dissolved in 0.5 M HCl whereas goethite, magnetite and hematite (crystalline minerals) were dissolved in 6 M HCl. Control experiments (data not shown) showed that siderite was dissolved already partly in the acetate extraction solution and gets completely dissolved in 0.5 M HCl.

Solutions for the extraction steps performed in the glove box were bubbled with N_2 (30 min) before they were brought into the glove box. For the first extraction step 1.5 ml anoxic sodium acetate solution were added to the precipitates (separated by centrifugation) of one culture tube. The precipitates were resuspended using a vortexer and incubated for 24 h in the dark. The mixture was centrifuged (2 min, 9 700 g) and the supernatant was kept for Fe analysis (see below). Subsequently the residual solid was extracted with 1.5 ml of anoxic 0.5 M HCl. After 2 h of incubation (in the dark) the mixture was centrifuged again and the supernatant was kept for Fe analysis (see below). The remaining solids were incubated in 1.5 ml of 6 M HCl at 70°C in a water bath for 30 min

outside the glove box. The extract was then analyzed for the Fe content (see below).

2.5. Analytical methods

Dissolved iron was quantified using the ferrozine assay (Stookey, 1970). In order to measure total iron (Fe(tot)) concentrations, aliquots were reduced with 10% w/v $NH_2OH*HCl$ dissolved in 1 M HCl. Fe(II) and Fe(tot) samples were mixed with a 0.1% w/v solution of ferrozine in 50% ammonium acetate buffer. Absorbance was measured at 562 nm in microtiter plates with a plate reader (FlashScan 550, Analytik Jena AG, Germany).

Separation of the arsenic species in solutions was done using an anion exchanger cartridge according to Meng et al. (2001). This cartridge retained As(V) but not As(III) within the pH range of 4-9. For the extraction experiments the pH of the samples was adjusted to 6 by addition of concentrated NaOH (32%) before separation.

Arsenic in the aqueous phase was analyzed by inductively coupled plasma mass spectroscopy, ICP-MS, (Elan 600, PE SCIEX, Perkin Elmer). Detection limit for As was 1 µg/l. Samples were stabilized in 0.1 M HNO_3 and stored in the fridge until measurement. Rhodium was added to each sample to a final concentration of 1 ppm Rh. Additionally, As(III) and As(tot) samples from extraction experiments were analyzed by flow injection hydride generating atomic absorption spectroscopy (FI-HG-AAS) consisting of a FI-HG system (FIAS 200, Perkin Elmer) coupled to an AAS (AAS 4100, Perkin Elmer). All samples were acidified with 0.2 M HCl and for As(tot) measurements the samples were additionally reduced with a mixture 1% KI-1% ascorbic acid. For the measurements the samples were automatically hydrogenated with a 0.2% NaBH4-0.2% NaOH solution according to the method described in Rüde (1996).

The specific surface area of iron minerals was determined by the BET method with a Gemini 2375 Surface Area Analyzer (Micromeritics, Germany) with N_2 as adsorbing gas. Dry mineral samples were degassed for 30 min under vacuum at 105°C, before measuring a five-point-BET-curve.

Wet mineral samples were sealed for Moessbauer spectroscopy between layers of Kapton® tape in the glove box. Moessbauer spectra were collected with a constant acceleration drive system in transmission mode and with a ^{57}Co source at room temperature. Samples were mounted in a close-cycle exchange-gas cryostat (Janis, USA) that allowed cooling of the sample to 4.2K. Spectra were calibrated against a spectrum of α-Fe metal foil collected at room temperature. Spectra calibration and fitting was performed with Recoil software (University of Ottawa, Canada) using Voight based spectral lines.

For micro-X-ray diffraction (μ-XRD), samples were grinded in an agate mortar, prepared on a Si single crystal silicon wafer and kept anoxic in a tightly closed glass jar upon measurement. The μ-XRD-device (Bruker D8 Discover X-ray diffraction instrument, Bruker AXS GmbH, Germany) with a Co K_α X ray tube, operating at 30 kV, 30 mA, allows measurements at a spot diameter of 50 μm or 300 μm. Each 3-min-measurement consists of three overlapping frames of 30° 2θ, using a GADDS® area detector. The EVA® 10.0.1.0 software was used to merge the three measured frames and identify the containing mineral phases using the PDF-database licensed by the International Centre for Diffraction Data (ICDD).

X-ray absorption near-edge structure (XANES) spectroscopy was performed at the Stanford Synchrotron Radiation Laboratory on beamline 11-2. The storage ring was operated at 3.0 GeV and at currents between 60 and 100 mA. A Si(220) monochromator was utilized for energy selection at the As K-edge. Incident and transmitted intensities were measured with 15-cm N_2-filled ionization chambers. Sample fluorescence was measured with a 13-element Ge detector containing a 6-μm Ge filter. The monochromator was detuned 20% to minimize higher harmonic components in the X-ray beam or a harmonic rejection mirror was present. The samples were maintained at 5 K during the data collection to prevent sample beam damage (i.e., beam induced redox reactions) using an liquid nitrogen cryostat (~70 K). As K-edge spectra were internally calibrated with sodium arsenate (11 874 eV). XANES spectra were collected by scanning across the K-edge (11 867 eV) using 0.2-eV steps. Spectral processing and data analyses were conducted with the program SixPack (Webb, 2005). The background was removed from the spectrum before normalization using a Gaussian fit for the pre-edge

and a quadratic fit for the postedge. As speciation was done by comparing white line features of the model compounds arsenate (as Na_2HAsO_4 or AsO_4^{3-} adsorbed to goethite/ferrihydrite) and arsenite (as $NaAsO_2$ or AsO_2^- adsorbed to goethite/ferrihydrite), as shown valid for identifying As oxidation states (Toevs et al., 2008). Linear combination fitting (LCF) of each unknown spectrum was performed using the model compounds adsorbed to either goethite or ferrihydrite and fit results were normalized to unity. Precision of fitting As species from XANES spectra is estimated to be 5% (de Lemos et al., 2006).

3. RESULTS AND DISCUSSION

The main goal of our study was to follow arsenic redox transformation by reactive iron phases. However, As(V) and As(III) both have a high binding affinity for iron minerals and their affinity is influenced by the arsenic redox state and the prevailing pH conditions (Pierce and Moore, 1980; Pierce and Moore, 1982; Masscheleyn et al., 1991; Bowell, 1994; Raven et al., 1998; Dixit and Hering, 2003). Therefore arsenic in presence of iron minerals can be quantified and specified in three different ways: (i) complete desorption of both arsenic species from the solid phase followed by analysis of the liquid phase, (ii) dissolution of the arsenic loaded iron minerals and solution analysis and (iii) independent analysis of the arsenic species in solid and liquid phase.

3.1. Arsenic redox changes during As extraction

Various sequential extraction procedures have been suggested and applied for soils and sediments to quantify arsenic bearing fractions such as adsorbed and coprecipitated arsenic as well as recalcitrant arsenic minerals such as arsenopyrite or realgar in natural samples, usually without considering the arsenic speciation (Keon et al., 2001; Wenzel et al., 2001).

Different extraction reagents for arsenic were evaluated by determining the recovery of initially added arsenic and the preservation of its redox state. After goethite was loaded with arsenic the decanted supernatants did not show a redox transformation of arsenic (data not shown) in any batch before the extraction reagents were added. The extraction recovery of arsenic was generally higher for goethite suspensions initially spiked with As(III) (Fig. 1a) compared to the ones spiked with As(V) (Fig. 1b), especially when using the less harsh extraction reagents where the Fe(III) mineral was not completely dissolved compared to the 6 M HCl treatment that lead to complete goethite dissolution. This was due to a lower adsorption affinity of As(III) (adsorption maximum pH 8) and an increasing amount of adsorbed As(V) (adsorption maximum <pH 4) at low pH on the goethite surface (Manning et al., 1998; Dixit and Hering, 2003).
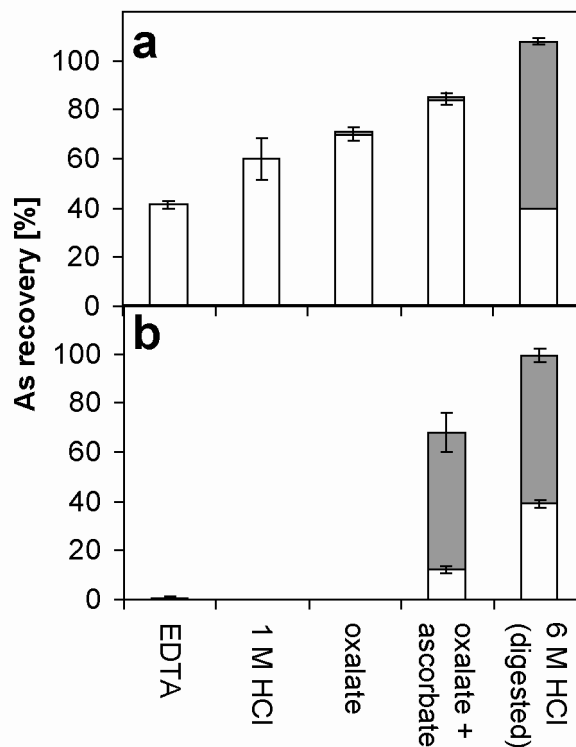
Fig. 1 Arsenic recovery in mixtures of (a) goethite + As(III) and (b) goethite + As(V) after treatment with different reagents that lead to either extraction (EDTA, 1 M HCl, oxalate or oxalate/ ascorbate) or complete dissolution of the solid (6 M HCl). Gray bars indicate As(V), white bars As(III), error bars represent standard deviation of two or three parallel batches.

Although the use of EDTA/acetic acid solution, 1 M HCl, oxalate buffer (pH 3.2) or the mixture of oxalate buffer and ascorbic acid (pH 3.2) did not lead to significant oxidation of As(III), these reagents were not satisfying since in all cases desorption of arsenite from goethite was incomplete. Extractions of As(V) with the four reagents that did not dissolve goethite completely either did not release bound arsenic into solution (with EDTA, 1 M HCl or oxalate) or in case of the reductive organic acid-containing oxalate/ascorbate solution even reduced a significant amount of As(V) to As(III). The only extractant yielding full recovery of the added arsenic was 6 M HCl that lead to complete dissolution of the goethite irrespective of the initial arsenic species. Unfortunately, treatment with this concentrated boiling acid under oxic conditions lead to As(III) oxidation, most likely by O_2 and surprisingly even to some As(V) reduction. Previous studies already showed accelerated As(III) oxidation with decreasing pH in oxic goethite-As(III) systems (Sun and Doner, 1998). In contrast, the reduction of As(V) observed after complete dissolution of the As(V)-bearing goethite by

6 M HCl cannot be explained easily. From the main components present, O_2, 6 M HCl, dissolved Fe(III) and As(V) a reduction of As(V) to As(III) cannot be expected. Comparable to our results also other extraction reagents (hydroxyl ions or phosphate) showed incomplete extraction from amorphous Fe(III) hydroxide and goethite or caused redox changes of the initially present arsenic species (Jackson and Miller, 2000).

Since the mild reagents EDTA, 1 M HCl and oxalate did not extract any As(V) at all and the harsh reagents changed the redox state of As, a quantitative analysis of As(III) oxidation or As(V) reduction at goethite surfaces by these extraction methods was not possible. These observations suggest that results of previous extration studies with natural arsenic-containing samples lead to operationally defined arsenic fractions that contain only limited information about the redox distribution of the arsenic in the samples.

3.2. Goethite reduction by *Shewanella oneidensis* MR-1

Since it has been shown in a previous study (Elsner et al., 2004) that the Fe(II)-goethite system has the highest potential for reductive transformation of pollutants compared to the other iron (oxy)hydroxides we setup cultures containing 5 mM goethite with the iron reducing strain *Shewanella oneidensis* MR-1. During a time span of 22 d we observed no formation of Fe(II) in these setups (Fig. 2a). Therefore we do not expect formation of reactive Fe(II)-goethite species just in presence of *Shewanella oneidensis* MR-1 and goethite.

In a further experiment we added 5 mM ferrihydrite to the culture, which served as easily available Fe(III) source for the bacteria. Although goethite was not reduced by the bacteria it was added in order to function as adsorption template for the formed biogenic Fe(II) similar to the mixed mineral experiments by Tobler et al. (2007). After the microbial reduction of the mineral mixture was finished there was still a significant amount of Fe(III) present in the cultures (Fig. 2b), indicating that goethite also remained unchanged in these setups. This observation is further supported by extraction data which clearly showed Fe(II) formation almost exclusively in dissolved form (up to 45% of the total iron) (Fig. 2c). This pool of dissolved Fe(II) could potentially serve as source for the regeneration of reactive sites at the goethite mineral

surface during reductive pollutant transformation (Haderlein and Pecher, 1998). Fe(III) concentrations of the extraction fractions showed almost equal amounts of poorly crystalline (52% ferrihydrite) and crystalline Fe(III) (48% goethite) in the beginning (Fig. 2d). During the course of reduction the fraction of poorly crystalline Fe(III) constantly decreased and the amount of goethite stayed stable. As the total amount of Fe(II) which was formed stayed in solution no secondary Fe(II) mineral phase was formed. Accordingly, the XRD pattern exclusively showed reflections for goethite (data not shown).
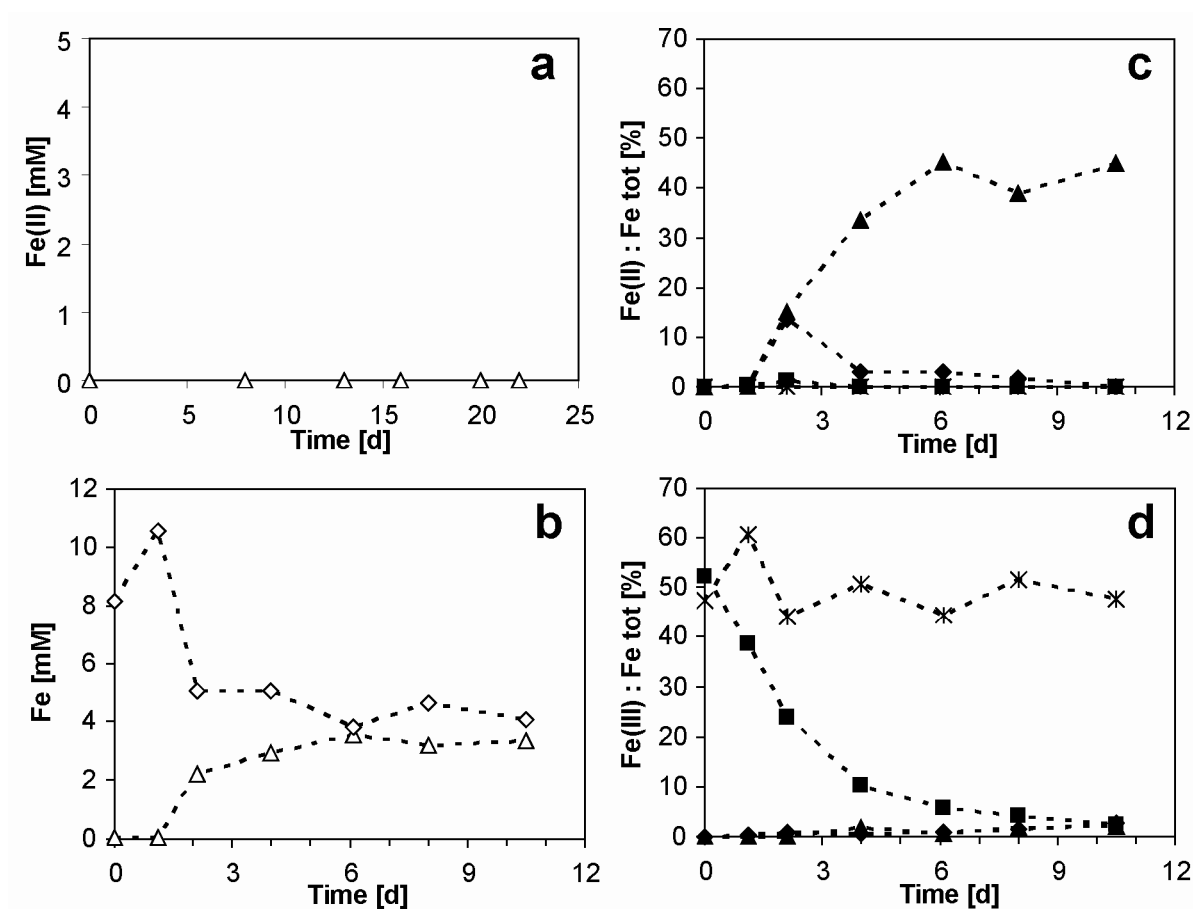
Fig. 2 (a) Fe(II) (Δ) formation by *Shewanella oneidensis* MR-1 in presence 5 mM goethite. (b) Fe(II) (Δ) formation and Fe(III) (◊) consumption by *Shewanella oneidensis* MR-1 in presence of 5 mM 2-line ferrihydrite and goethite, respectively. (c, d) Dissolved (▲), adsorbed (◆), poorly crystalline (■) and crystalline (✕) iron fractions separated by sequential extraction of precipitates formed during microbial reduction of 5 mM 2-line ferrihydrite and goethite, respectively. Concentrations are given in (c) percent of Fe(II) and (d) Fe(III) relative to the total iron concentration.

3.3. Arsenic redox changes during microbial Fe(III) reduction

In order to determine the reactivity of secondary, biogenic minerals formed by iron reducing bacteria we set up experiments with *Shewanella oneidensis* MR-1 and Fe(III) minerals. We compared the reduction products of the easy bioaccessible Fe(III) source 2-line ferrihydrite (30 mM) and a mixture of 2-line ferrihydrite (15 mM) and goethite (15 mM; higher concentrations than in previous experiments to gain enough material for all analyses). The higher crystalline goethite potentially served as adsorption template for biogenic Fe(II) leading to reactive Fe(II) species.

Figure 3 shows the reduction of Fe(III) and the Fe(II) formation as well as the mineral analysis results over the course of 9 days in the mixed mineral setups. The bacteria reduced 15 mM ferrihydrite rapidly producing 5.3 mM Fe(II) within 9 days. We measured 2 mM dissolved Fe(II) after 4 days and 3 mM after 9 days and calculated the remaining amount of Fe(II), that can theoretically sorb to mineral surfaces or form secondary minerals, by subtracting dissolved from total Fe(II) (see zoom-in Fig. 3a). XRD and Moessbauer analyses (Fig. 3b) showed the biogenic transformation of the present ferrihydrite to magnetite within 9 days, whereas goethite remained unchanged. Synchrotron analysis of the sorbed As (data not shown) and quantification of arsenic in solution with ICP-MS (Table 1) indicated that at none of the sampled time points during microbial iron reduction redox transformation of arsenic took place after 0 h, 6 h or 7 d of incubation of the biogenic iron minerals with As(III) or As(V).

Although biogenic Fe(II) was consumed by the transformation of ferrihydrite into magnetite and probably goethite, the remaining concentration of Fe(II) in solution was still plenty enough to serve as regeneration source for reactive sites. A limitation due to a lack of dissolved Fe(II) was therefore not the reason for the inactivity of our biotic system. Obviously goethite did not function as an adsorption template for Fe(II) probably due to blocking of initially present goethite towards Fe(II) adsorption by surface coating with the secondary formed iron minerals. Moessbauer spectra (Fig. 3b) did not show formation of green rust or adsorbed Fe(II) supporting the assumption that no reactive mixed-valent iron phase was formed.
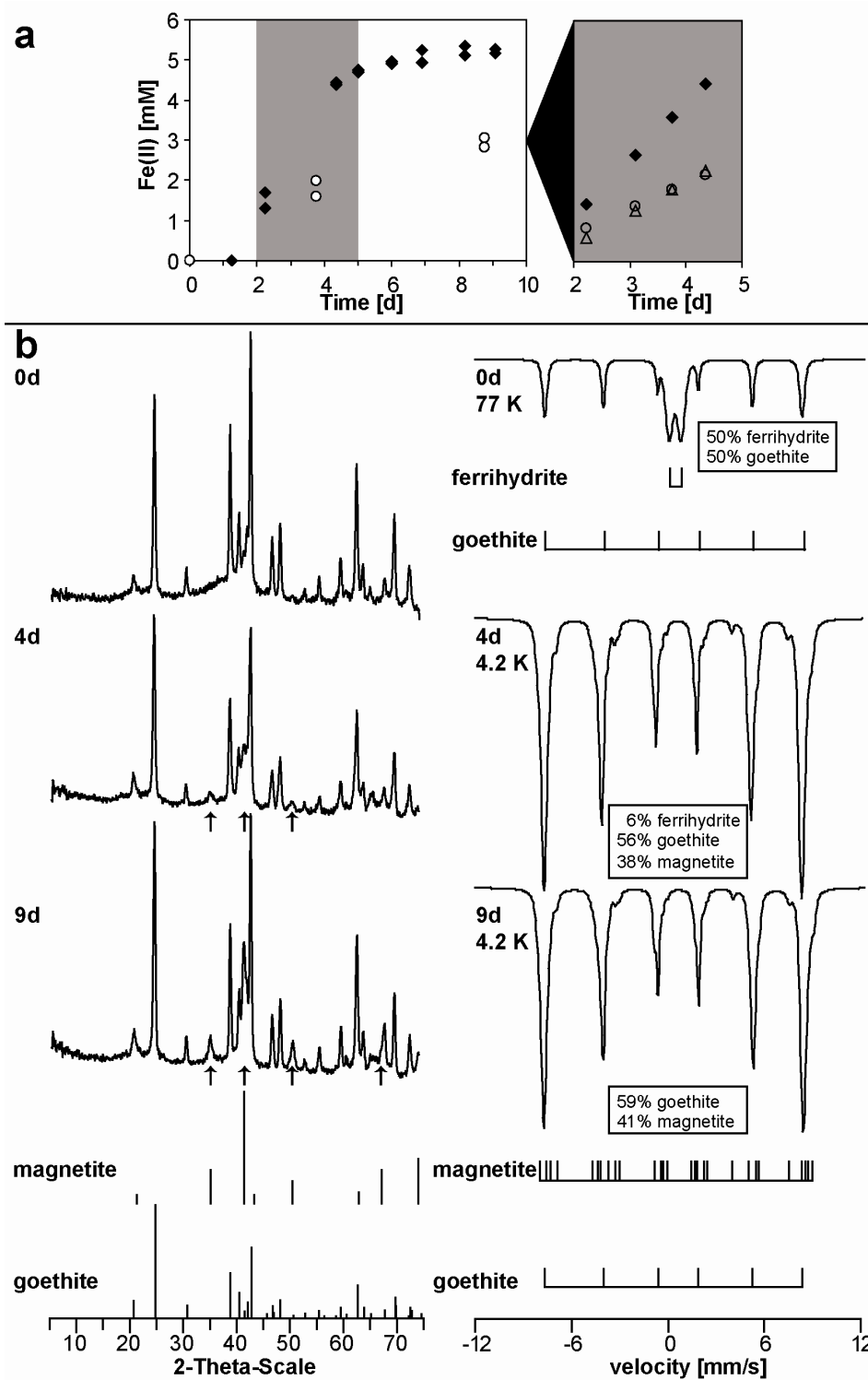
Fig. 3 (a) Fe(II) formation by *Shewanella oneidensis* MR-1 in (15 mM 2-line ferrihydrite and 15 mM goethite). The graphs show Fe(II)$_{tot}$ (♦) and Fe(II)$_{diss}$ (○) of duplicate experiments. Fe(II)$_{diss}$ was determined in supernatants of XRD and Moessbauer samples. Enlargement: calculated values using linear regressions of Fe(II)$_{tot}$ (♦) and Fe(II)$_{diss}$ (○) data and their difference: Fe(II)$_{ads}$ (Δ). (b) XRD patterns and Moessbauer spectra (at 77 and 4.2 K) of incubated minerals after 0d, 4d and 9d with reference patterns of goethite, magnetite and ferrihydrite. Note for XRD pattern: at time point zero: ferrihydrite appears as broad bump of the base line between 2θ = 35° to 45°; the appearance of magnetite reflections is indicated by arrows.

1   **Table 1 Arsenic concentrations in solution for biogenic transformation experiments, determined by ICP-MS**

Samples[1]	As(V) added			As(III) added			Controls			
	As(III)	[μg/l] As(tot)	As(V)[2]	As(III)	[μg/l] As(tot)	As(V)[2]		As(III)	[μg/l] As(tot)	As(V)[2]
Gt Fh 0d A	-	1.1	0.0	2.0	2.6	0.6	Gt Fh AsV	-	-	-
Gt Fh 0d B	-	1.1	0.0	2.0	2.1	0.1	Gt Fh AsIII	1.1	1.1	0.0
Gt Fh 0d C	-			1.1	1.1	0.0	Gt Fh AsV AsIII	1.0	1.3	0.3
Gt Fh 4d A	-	-	-	3.2	3.0	0.0	Gt Fh	-	-	-
Gt Fh 4d B	-	-	-	1.5	1.6	0.0				
Gt Fh 4d C	-	-	-	1.2	1.2	0.0	Fh AsV	-	-	-
Gt Fh 9d A	-	-	-	8.0	7.4	0.6	Fh AsIII	1.0	1.0	0.0
Gt Fh 9d B	-	-	-	2.4	2.6	0.3	Fh AsV AsIII	-	-	-
Gt Fh 9d C	-	-	-	-	1.3	0.0	Fh	-	-	-
Fh 0d A	-	-	-	1.5	1.5	0.0	FeII AsV	2.4	353.5	351.1
Fh 0d B	-	1.0	1.0	1.1	1.2	0.2	FeII AsIII	285.5	288.5	3.0
Fh 0d C	-	-	-	-	-	-				
Fh 3d A	-	-	-	1.6	1.5	0.0	MR-1 AsV	291.0	301.0	10.0
Fh 3d B	-	-	-	1.1	1.2	0.1	MR-1 AsIII	293.0	310.0	17.0
Fh 3d C	-	-	-	-	-	-				
Fh 6d A	-	-	-	2.5	2.6	0.1				
Fh 6d B	-	-	-	1.3	1.4	0.1				
Fh 6d C	-	-	-	-	-	-				

1) Capital letters indicate incubation time of biogenic precipitates with As(III) or As(V), A: 0 h, B: 6 h, C: 7 d
2) As(V) concentrations are calculated by subtraction of As(III) from As(tot)
-) Concentrations below detection limit (1 μg/l)

2

The arsenic concentrations in solution of samples containing iron minerals were all close to the detection limit of the ICP-MS method, indicating almost quantitative adsorption of As(III) and As(V) to the solid phase (Table 1). Furthermore, the speciation of dissolved arsenic (if present) approved the findings of the solid phase analysis. Small amounts of dissolved arsenic detected in As(III) containing setups confirmed the known effect of weaker binding of As(III) to iron minerals compared to As(V) (Masscheleyn et al., 1991; Bowell, 1994; Dixit and Hering, 2003). As(V) seems to adsorb quantitatively and very fast, whereas As(III) setups show a continuous decrease in total dissolved arsenic concentrations throughout the 7 days of incubation. Control setups showed no redox transformation of arsenic by the initially present iron minerals or in presence of dissolved Fe(II) only. Detection of small amounts of the opposite redox state which was initially added could be caused by incomplete separation of the arsenic species by the ion exchanger cartridges, but again these values are close to the detection limit of the instrument. In contrast we observed significant reduction of As(V) by viable *Shewanella oneidensis* MR-1 cells, grown on lactate/fumerate instead of iron. We excluded the effect of this microbiological detoxification mechanism in our iron reducing experiments by pasteurization of the actively metabolizing cultures before adding the arsenic species. Residual organic matter of cells did not cause arsenic redox transformation in a sufficient amount, because in several biogenic mineral batches no arsenic transformation was detectable.

Figure 4a shows the Fe(II) formation in batch cultures containing 30 mM 2-line ferrihydrite over the course of 7 days and Table 1 the according arsenic concentrations. *Shewanella oneidensis* MR-1 reduced ferrihydrite within 6 days producing ~10 mM Fe(II). After 3 days ~15% (4.5 mM) of the total Fe(III) were reduced to Fe(II) which is approximately half of the total amount of Fe(II) formed at the end of reduction. At the same time point ~1.6 mM Fe(II) were detectable in solution and this amount increased up to ~2.2 mM Fe(II) after 6 days of microbial reduction. The formation of biogenic Fe(II) also lead to the mineralogical transformation of ferrihydrite to magnetite and a small fraction of goethite, as proved by XRD and Moessbauer measurements after 3 and 6 days (Fig 4b).
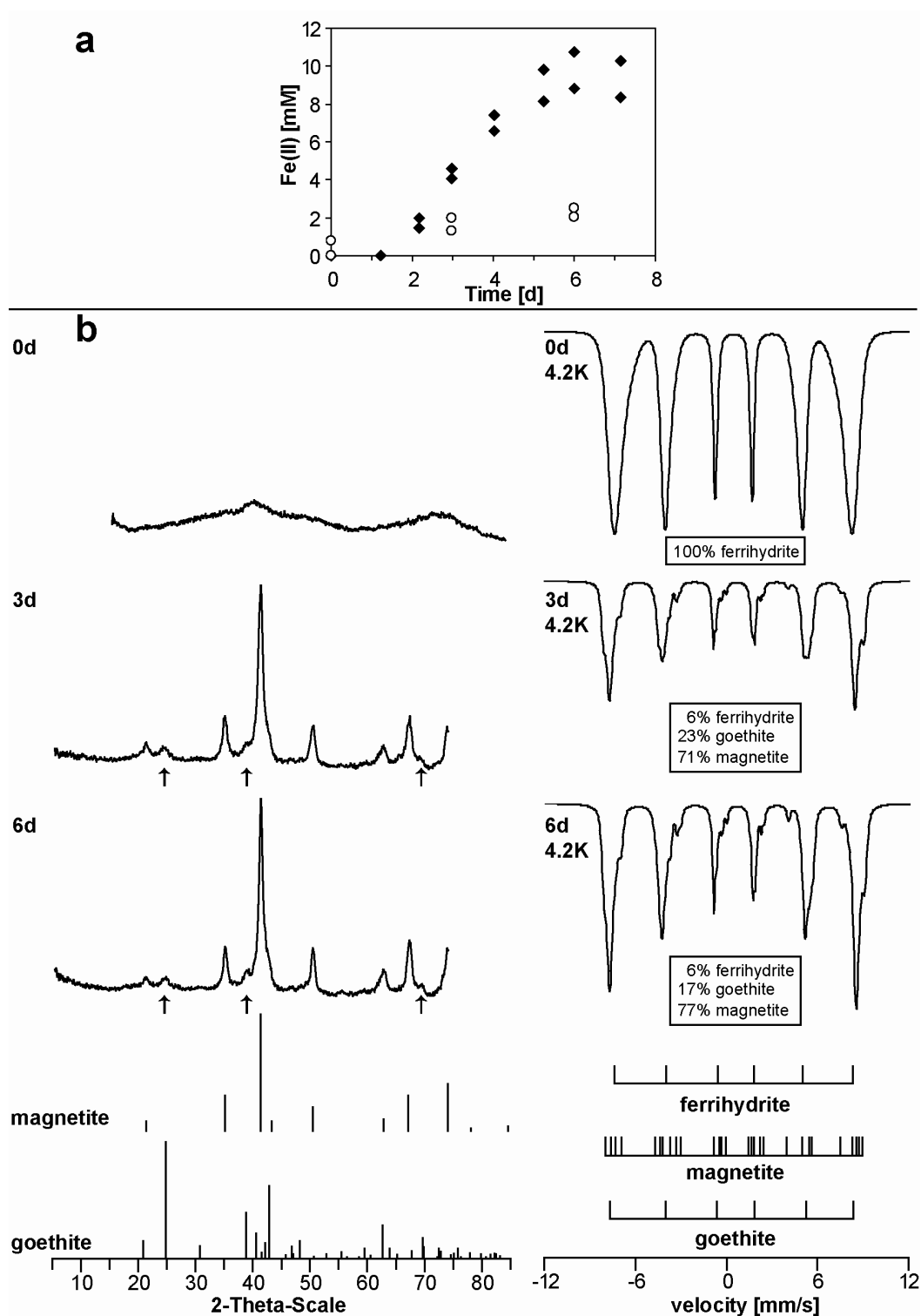
Fig. 4 (a) Fe(II) formation by *Shewanella oneidensis* MR-1 in presence of 30 mM 2-line ferrihydrite. The graphs show Fe(II)$_{tot}$ (♦) and Fe(II)$_{diss}$ (○) of duplicate experiments. Fe(II)$_{diss}$ was determined in supernatants of XRD and Moessbauer samples. (b) XRD patterns and Moessbauer spectra (at 4.2 K) of the incubated minerals after 0d, 3d and 6d of incubation with reference patterns of goethite, magnetite and ferrihydrite. The XRD patterns at time point zero shows two broad bumps $2\theta = 35°$ to 45°indicating the presence of 2-line ferrihydrite; the appearance of goethite refletions is indicated by arrows.

Although the intensities of XRD reflections were still slightly increasing from 3 to 6 days and the iron reduction was just at an intermediate stage after 3 days we detected almost similar ratios of magnetite and goethite by Moessbauer spectroscopy for the 3 and 6 d samples. This inconsistency remains unclear but could be due to insufficient mixing during sample preparation.

XANES analysis of the As redox state in solid phase (Fig. 5) revealed reduction of a small amount of As(V) to As(III) in biogenic mineral mixtures after 3 days of reduction for all three time points (0 h, 6 h and 7 d) sampled after arsenic addition, but no oxidation. The change of the redox state was hardly detectable but data transformation using the first derivative of the spectrum revealed the presence of As(III) in the mineral samples. This redox transformation could not be verified by the liquid phase analysis (Table 1). Since arsenic sorbed strongly to the iron minerals dissolved arsenic concentrations were below the detection limit.
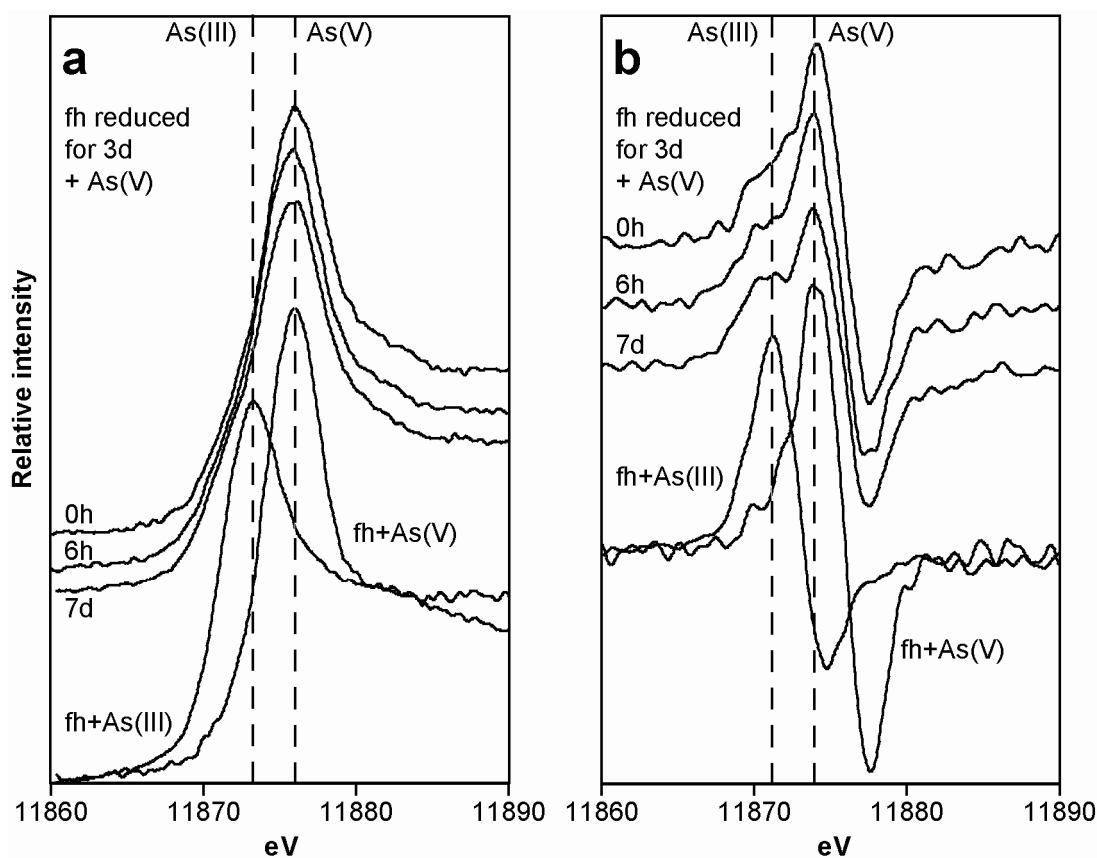
Fig. 5 (a) As-XANES spectra and (b) first derivative of the XANES spectra of biogenic precipitates formed after 3 d of reduction by *Shewanella oneidensis* **MR-1 in presence of 30 mM 2-line ferrihydrite (fh) and** subsequent incubation with As(V) for 0 h, 6 h and 7 d

In contrast to the mixed mineral setups, we observed partially reduction of As(V) to As(III), but only at an intermediate stage of iron reduction, after 3 days. The mineral analysis with XRD and Moessbauer spectroscopy did not reveal the presence of green rust or adsorbed Fe(II) but only magnetite and goethite which is in agreement with former studies considering biogenic mineral transformation (Zachara et al., 2002; Hansel et al., 2003; Borch et al., 2007; Coker et al., 2008). The reactivity of the intermediate reduction stage is somewhat surprising, because the mineral composition and the concentration of dissolved Fe(II) shows no significant differences between day 3 and day 6 of microbial reduction. Therefore the identity of the reactive species remains unclear.

4. CONCLUSIONS

We were not able to simulate the formation of reactive iron species with the biogenic reduction of a mineral mixture of 2-line ferrihydrite and goethite, at least the redox state of arsenic was not affected. However, in presence of biotically reduced 2-line ferrihydrite only we observed reduction of As(V), but only limited to an intermediate stage of reduction.

The redox potential of the Fe(III) mineral-Fe(II) system is variable in a range of more than 1000 mV (Haderlein and Pecher, 1998). Since we were not able to identify a reactive species in our experimental setups it is almost impossible to predict the potential redox reactions of arsenic in our system. Factors like mineral composition and crystallinity as well as the concentration of dissolved Fe(II) depend on the influence of microbial iron reduction and may change fast, according to our experimental observations. Our results suggest a sensitive balance between the Fe(III)/Fe(II) and the As(V)/As(III) redox pairs under anoxic conditions. Future experiments with other combinations of Fe(III) minerals in different ratios may lead to thermodynamically favourable conditions which lead to redox changes between As(III) and As(V). The co-existence of both arsenic redox states As(III) and As(V) in natural iron-containing environments was shown in previous studies (Hamon et al., 2004; Kent and Fox, 2004; Swartz et al., 2004; de Mello et al., 2007). So far thermodynamic non-equilibrium distribution of the arsenic species was attributed to slow transformation kinetics (Oscarson et al., 1980; Cullen and Reimer, 1989), but our results give reason that specific mixtures of Fe(III) and Fe(II) in dissolved and solid state (probably of biological origin) can cause abiotic arsenic redox transformations. In order to identify such reactive conditions further investigation is needed.

5. ACKNOWLEDGEMENTS

6. REFERENCES

Antelo J., Avena M., Fiol S., Lopez R., and Arce F., 2005. Effects of pH and ionic strength on the adsorption of phosphate and arsenate at the goethite-water interface. *J. Colloid Interface Sci.* **285**, 476-486.

Borch T., Masue Y., Kukkadapu R. K., and Fendorf S., 2007. Phosphate Imposed Limitations on Biological Reduction and Alteration of Ferrihydrite. *Environ. Sci. Technol.* **41**, 166-172.

Bowell R. J., 1994. Sorption of arsenic by iron oxides and oxyhydroxides in soils. *Appl. Geochem.* **9**, 279-286.

Coker V. S., Bell A. M. T., Pearce C. I., Pattrick R. A. D., van der Laan G., and Lloyd J. R., 2008. Time-resolved synchrotron powder X-ray diffraction study of magnetite formation by the Fe(III)-reducing bacterium *Geobacter sulfurreducens*. *Am. Mineral.* **93**, 540-547.

Cullen W. R. and Reimer K. J., 1989. Arsenic Speciation in the Environment. *Chem Rev* **89**, 713-764.

de Lemos J. L., Bostick B. C., Renshaw C. E., Sturup S., and Feng X., 2006. Landfill-Stimulated Iron Reduction and Arsenic Release at the Coakley Superfund Site (NH). *Environ. Sci. Technol.* **40**, 67-73.

de Mello J., Talbott J., Scott J., Roy W., and Stucki J., 2007. Arsenic Speciation in Arsenic-rich Brazilian Soils from Gold Mining Sites under Anaerobic Incubation. *Environ. Sci. Poll. Res.* **14**, 388-396.

Dixit S. and Hering J. G., 2003. Comparison of Arsenic(V) and Arsenic(III) Sorption onto Iron Oxide Minerals: Implications for Arsenic Mobility. *Environ. Sci. Technol.* **37**, 4182-4189.

Elsner M., Schwarzenbach R. P., and Haderlein S. B., 2004. Reactivity of Fe(II)-Bearing Minerals toward Reductive Transformation of Organic Contaminants. *Environ. Sci. Technol.* **38**, 799-807.

Fredrickson J. K., Zachara J. M., Kennedy D. W., Kukkadapu R. K., McKinley J. P., Heald S. M., Liu C., and Plymale A. E., 2004. Reduction of TcO_4^- by sediment-associated biogenic Fe(II). *Geochim. Cosmochim. Acta* **68**, 3171-3187.

Haderlein S. B. and Pecher K., 1998. Pollutant reduction in heterogeneous Fe(II)/Fe(III) systems. In: Sparks D. L. and Grundl T. Eds.), *Kinetics and Mechanisms of Reactions at the Mineral/ Water Interface.* American Chemical Society, Washington, DC.

Hamon R. E., Lombi E., Fortunati P., Nolan A. L., and McLaughlin M. J., 2004. Coupling Speciation and Isotope Dilution Techniques To Study Arsenic Mobilization in the Environment. *Environ. Sci. Technol.* **38**, 1794-1798.

Hansel C. M., Benner S. G., Neiss J., Dohnalkova A., Kukkadapu R. K., and Fendorf S., 2003. Secondary mineralization pathways induced by dissimilatory iron reduction of ferrihydrite under advective flow. *Geochim. Cosmochim. Acta* **67**, 2977-2992.

Heijman C. G., Holliger C., Glaus M. A., Schwarzenbach R. P., and Zeyer J., 1993. Abiotic Reduction of 4-Chloronitrobenzene to 4-Chloroaniline in a

Dissimilatory Iron-Reducing Enrichment Culture. *Appl. Environ. Microbiol.* **59**, 4350–4353.

Herbel M. and Fendorf S., 2006. Biogeochemical processes controlling the speciation and transport of arsenic within iron coated sands. *Chem. Geol.* **228**, 16-32.

Islam F. S., Pederick R. L., Gault A. G., Adams L. K., Polya D. A., Charnock J. M., and Lloyd J. R., 2005. Interactions between the Fe(III)-Reducing Bacterium *Geobacter sulfurreducens* and Arsenate, and Capture of the Metalloid by Biogenic Fe(II). *Appl. Environ. Microbiol.* **71**, 8642-8648.

Jackson B. P. and Miller W. P., 2000. Effectiveness of Phosphate and Hydroxide for Desorption of Arsenic and Selenium Species from Iron Oxides. *Soil Sci. Soc. Am. J.* **64**, 1616-1622.

Kent D. B. and Fox P. M., 2004. The influence of groundwater chemistry on arsenic concentrations and speciation in a quartz sand and gravel aquifer. *Geochemical Transactions* **5**.

Keon N. E., Swartz C. H., Brabander D. J., Harvey C., and Hemond H. F., 2001. Validation of an Arsenic Sequential Extraction Method for Evaluating Mobility in Sediments. *Environ. Sci. Technol.* **35**, 2778-2784.

Kocar B. D., Herbel M. J., Tufano K. J., and Fendorf S., 2006. Contrasting Effects of Dissimilatory Iron(III) and Arsenic(V) Reduction on Arsenic Retention and Transport. *Environ. Sci. Technol.* **40**, 6715-6721.

Kulp T. R., Hoeft S. E., Asao M., Madigan M. T., Hollibaugh J. T., Fisher J. C., Stolz J. F., Culbertson C. W., Miller L. G., and Oremland R. S., 2008. Arsenic(III) Fuels Anoxygenic Photosynthesis in Hot Spring Biofilms from Mono Lake, California. *Science* **321**, 967-970.

Lies D. P., Hernandez M. E., Kappler A., Mielke R. E., Gralnick J. A., and Newman D. K., 2005. *Shewanella oneidensis* MR-1 Uses Overlapping Pathways for Iron Reduction at a Distance and by Direct Contact under Conditions Relevant for Biofilms. *Appl. Environ. Microbiol.* **71**, 4414–4426.

Manning B. A., Fendorf S. E., and Goldberg S., 1998. Surface Structures and Stability of Arsenic(III) on Goethite: Spectroscopic Evidence for Inner-Sphere Complexes. *Environ. Sci. Technol.* **32**, 2383-2388.

Masscheleyn P. H., Delaune R. D., and Patrick Jr. W. H., 1991. Effect of Redox Potential and pH on Arsenic Speciation and Solubility in a Contaminated Soil. *Environ. Sci. Technol.* **25**, 1414-1419.

Meng X., Korfiatis G. P., Christodoulatos C., and Bang S., 2001. Treatment of arsenic in Bangladesh well water using a household co-precipitation and filtration system. *Water Res.* **35**, 2805-2810.

Myers C. R. and Nealson K. H., 1988. Bacterial Manganese Reduction and Growth with Manganese Oxide as the Sole Electron Acceptor. *Science* **240**, 1319-1321.

Myers C. R. and Myers J. M., 1994. Ferric iron reduction-linked growth yields of *Shewanella putrefaciens* MR-1. *J. App. Bact.* **76**, 253-258.

Oremland R. S. and Stolz J. F., 2005. Arsenic, microbes and contaminated aquifers. *Trends Microbiol.* **13**, 45-49.

Oscarson D. W., Huang P. M., and Liaw W. K., 1980. The Oxidation of Arsenite by Aquatic Sediments. *J Environ Qual* **9**, 700-703.

Pierce M. L. and Moore C. B., 1980. Adsorption of Arsenite on Amorphous Iron Hydroxide from Dilute Aqueous Solution. *Environ. Sci. Technol.* **14**, 214-216.

Pierce M. L. and Moore C. B., 1982. Adsorption of arsenite and arsenate on amorphous iron hydroxide. *Water Res.* **16**, 1247-1253.

Postma D., Larsen F., Minh Hue N. T., Duc M. T., Viet P. H., Nhan P. Q., and Jessen S., 2007. Arsenic in groundwater of the Red River floodplain, Vietnam: Controlling geochemical processes and reactive transport modeling. *Geochim. Cosmochim. Acta* **71**, 5054-5071.

Raven K. P., Jain A., and Loeppert R. H., 1998. Arsenite and Arsenate Adsorption on Ferrihydrite: Kinetics, Equilibrium, and Adsorption Envelopes. *Environ. Sci. Technol.* **32**, 344-349.

Roden E. E. and Zachara J. M., 1996. Microbial Reduction of Crystalline Iron(III) Oxides: Influence of Oxide Surface Area and Potential for Cell Growth. *Environ. Sci. Technol.* **30**, 1618-1628.

Rüde T. R., 1996. Beiträge zur Geochemie des Arsens. PhD-Thesis, University of Karlsruhe.

Samanta G. and Clifford D. A., 2005. Preservation of Inorganic Arsenic Species in Groundwater. *Environ. Sci. Technol.* **39**, 8877-8882.

Schwertmann U. and Cornell R. M., 2000. *Iron Oxides in the Laboratory*. Wiley-VCH Verlag GmbH, Weinheim.

Smedley P. L. and Kinniburgh D. G., 2002. A review of the source, behaviour and distribution of arsenic in natural waters. *Appl. Geochem.* **17**, 517-568.

Stookey L. L., 1970. Ferrozine - A New Spectrophotometric Reagent for Iron. *Anal. Chem.* **42**, 779-781.

Sun X. and Doner H. E., 1998. Adsorption and oxidation of arsenite on goethite. *Soil Sci.* **163**, 278-287.

Swartz C. H., Blute N. K., Badruzzman B., Ali A., Brabander D., Jay J., Besancon J., Islam S., Hemond H. F., and Harvey C. F., 2004. Mobility of arsenic in a Bangladesh aquifer: Inferences from geochemical profiles, leaching data, and mineralogical characterization. *Geochim. Cosmochim. Acta* **68**, 4539-4557.

Tobler N. B., Hofstetter T. B., Straub K. L., Fontana D., and Schwarzenbach R. P., 2007. Iron-Mediated Microbial Oxidation and Abiotic Reduction of Organic Contaminants under Anoxic Conditions. *Environ. Sci. Technol.*

Toevs G., Morra M. J., Winowiecki L., Strawn D., Polizzotto M. L., and Fendorf S., 2008. Depositional Influences on Porewater Arsenic in Sediments of a Mining-Contaminated Freshwater Lake. *Environ. Sci. Technol.* **42**, 6823-6829.

Tufano K. J. and Fendorf S., 2008. Confounding Impacts of Iron Reduction on Arsenic Retention. *Environ. Sci. Technol.* **42**, 4777-4783.

Webb S. M., 2005. SIXpack: a graphical user interface for XAS analysis using IFEFFIT. *Phys. Scr.*, 1011.

Wenzel W. W., Kirchbaumer N., Prohaska T., Stingeder G., Lombi E., and Adriano D. C., 2001. Arsenic fractionation in soils using an improved sequential extraction procedure. *Anal. Chim. Acta* **436**, 309-323.

Williams A. G. B., Gregory K. B., Parkin G. F., and Scherer M. M., 2005. Hexahydro-1,3,5-trinitro-1,3,5-triazine Transformation by Biologically Reduced Ferrihydrite: Evolution of Fe Mineralogy, Surface Area, and Reaction Rates. *Environ. Sci. Technol.* **39**, 5183-5189.

Zachara J. M., Kukkadapu R. K., Fredrickson J. K., Gorby Y. A., and Smith S. C., 2002. Biomineralization of Poorly Crystalline Fe(III) Oxides by Dissimilatory Metal Reducing Bacteria (DMRB). *Geomicrobiol. J.* **19**, 179-207.

8

Discussion and Outlook

The results of the studies presented in this thesis provide detailed insight into the effect of humic substances on microbial iron reduction, the biogenic precipitates formed and their potential bioavailability and reactivity in the geochemical iron cycle. Furthermore, first results attempting to quantify the redox transformation of arsenic in abiotic and biotic reactive Fe(II)-Fe(III) mineral systems are shown.

The redox chemistry of iron is known to cover a broad range of redox potentials (-500 to 1100 mV), due to the versatile speciation of iron in natural environments. Transformation processes between these different species influence a broad variety of different biochemically relevant elements (Stumm and Sulzberger, 1992). The geochemical cycling of iron by iron metabolizing bacteria plays a substantial role in the phase transformation of iron species (Fredrickson et al., 1998; Zachara et al., 2002; Kappler and Newman, 2004; Weber et al., 2006). Throughout the last decades studies concerning microbial iron reduction exhibited the influence of different properties of Fe(III) minerals, such as redox potentials or solubility on microbial reduction rates. In this context the relation between reduction rates and the surface area of the Fe(III) substrates has been shown (Roden and Zachara, 1996; Roden, 2003). However, the determination of the surface area of the Fe(III) mineral with the highest bioavailability, 2-line ferrihydrite, is complicated due to its hydrated, poorly ordered structure (van der Giessen, 1966; Cornell and Schwertmann, 2003; Michel et al., 2007).

A new approach for mineral surface area determination based on the formation of ferrihydrite aggregates in microbial cultures at circumneutral pH showed the influence of surface area limitation on microbial reduction rates. Although the primary nanometer-sized particles suggested a much higher available surface area this aggregate formation decreased the bioavailable surface area substantially. In addition it was shown qualitatively that the size of mineral aggregates was related to the concentration of Fe(III) mineral in suspension. The lack of appropriate analytical methods for undisturbed measurements of the formed aggregates however did not allow accurate determination of the aggregate sizes and could be subject for further research. The application of ultrasonic spectroscopy methods might be a way to obtain size distribution spectra, but requires knowledge of many parameters

(e.g. specific density) of the particle suspension investigated (Babick and Ripperger, 2004; Richter et al., 2007). The particle size of ferrihydrite aggregates is in particular important for the cultivation of iron-reducing strains which require direct contact to the Fe(III) mineral for electron transfer (e.g. *Geobacter* sp.).

Besides electron transfer via direct contact between cells and mineral surface, redox active compounds like humic substances can be used by iron reducing bacteria in order to reduce Fe(III) minerals indirectly via electron shuttling (Lovley et al., 1998; Nevin and Lovley, 2000). Herein concentration limits for the stimulating effect of dissolved humic acid on microbial iron reduction by *Shewanella oneidensis* MR-1 were determined under growth conditions. Furthermore, a model concept for mineral aggregate formation in presence of humic acid was developed, describing inhibiting and stimulating effects of humic acid. This model suggests a correlation between the surface saturation of iron minerals with adsorbed humic acid and the upper concentration limit for enhancement of the stimulating effect of dissolved humic acid. In order to reveal the potential role of adsorbed humic substance in the electron transfer mechanism future experiments should be conducted attempting to investigate adsorbed and dissolved humic substance separately. This may be possible by coating the mineral surface with a non-redox active polymeric compound (e.g. cellulose) to avoid direct contact of humic substance with the mineral surface. In the optimal case microbial reduction rates of coated mineral particles should be comparable to non-coated mineral cultures providing similar surface accessibility. If then the shuttling effect of dissolved humic substance is diminished due to sorbed cellulose, this would be an indication for the necessity of adsorbed humic substance for efficient electron transfer to solid electron acceptors. Further experiments could include other microbial strains and medium compositions and their influence on the concentration range of humic substances for effective shuttling in microbial iron reduction.

The influence of these parameters is especially interesting concerning the mineral formation during biogenic iron reduction. Such reduction products can contain oxygen sensitive Fe(II) species. In order to prevent biogenic minerals from oxidation during measurements a

sample protection procedure using a covering foil was developed and successfully applied for μ-XRD measurements. Further studies are needed to evaluate which biogenic precipitates are actually oxygen sensitive, how does the particle size of precipitates affect the oxidation and whether expected mineral transformations can be detected by XRD measurements. The minerals formed in presence of humic acid were shown to be less crystalline than in absence of humic acid, for both ferrihydrite concentrations investigated. This has fundamental impact on the bioavailability of iron for plants or other microorganisms as it has been shown before that higher crystalline iron minerals were less susceptible for transformation by iron-oxidizers and iron-reducers (Lovley and Phillips, 1988; Kappler and Newman, 2004).

Results of the studies herein further demonstrated the influence of ionic strength on the redox activiy of humic substances in abiotic and biotic experiments. The observed increase in transferred electrons with increasing ionic strength was correlated to a change in molecular structure of reduced humic acids. The electrostatic repulsion between charged ions and reduced humic acids caused a larger, likely porous structure (Thieme et al., 2007) and provided more reactive sites for electron transfer to Fe(III). Next steps include the application of synchrotron based X-ray tomography in order to image the potentially changed 3-D structure of humic acid depending on the ionic strength. The electron shuttling by humic acids was enhanced at higher ionic strength due to facilitated interaction between bacteria and less charged humic substances particles. Based on the observation that dilution did not alter the impact of phosphate which was applied to humic acid in different concentrations before addition to bacterial cultures, a partly irreversible change of the humic acid structure is suggested. In order to determine the possible (irreversible) uptake of ions by humic acids (covalent binding, complexation, electrostatic binding) synchrotron soft X-ray absorption spectroscopy, scanning transmission X-ray microscopy or element specific NMR could be applied (Prietzel et al., 2003).

The observed lower crystallinity of biogenic iron minerals in particular in presence of humic acid potentially has influence on the reactivity of the formed mixed-valent iron minerals, which have been shown to reduce heavy metal ions and organic pollutants (Buerge and

Hug, 1999; Liger et al., 1999; Fredrickson et al., 2004; Borch et al., 2005). It has been shown for example that lower crystalline Fe(III) minerals mixed with dissolved Fe(II) were less efficient in the reductive transformation of organic pollutants in anoxic setups (Elsner et al., 2004). Extending the current knowledge about these natural attenuation processes, it was shown herein for the first time that abiotic and biotic mixed-valent iron minerals lead to a redox transformation of arsenic. In this regard the separate quantification of the arsenic speciation in liquid and solid phase proved to be an appropriate approach in order to follow redox transformation of arsenic in presence of iron minerals. Extraction reagents which were applied in order to either quantitatively desorb the arsenic species from goethite or completely dissolve the Fe(III) mineral were insufficient with regard to the recovery of the previously adsorbed amount of arsenic and the preservation of arsenic redox states.

The studies carried out on abiotic goethite-Fe(II) systems did not show the thermodynamically expected reduction of As(V) to As(III). Instead, As(III) oxidation by a so far unidentified iron species was observed. Results of previous studies demonstrating electron transfer from adsorbed Fe(II) to the bulk Fe(III) mineral (Williams and Scherer, 2004; Larese-Casanova and Scherer, 2007) by formation of goethite after Fe(II) sorption to goethite could be verified in our experiments using Moessbauer spectroscopy. With this method we detected goethite and an unidentified Fe(II) mineral phase. We suggest a reactive short-living intermediate stage of adsorbed Fe(II) during electron transfer to the bulk mineral phase responsible for arsenic oxidation. Application of SEM, μ-XRD, EXAFS or HR-TEM was not sufficient to clearly identify the reactive species. However, identification of such reactive iron phases and determination of its redox potential is a prerequisite for the prediction and interpretation of arsenic redox transformation in anoxic environments. Furthermore, information about the abiotic reactive iron system considering variations in pH conditions, dissolved Fe(II) concentrations, incubation times and applied minerals is needed.

Compared to results of the abiotic experiments, reduction of As(V) by microbially reduced 2-line ferrihydrite was shown. Additionally, no redox transformation of arsenic was detected for biogenic precipitates formed in cultures containing equal amounts of

2-line ferrihydrite and goethite. Although the formation of Fe(II) and the development of iron mineral phases were carefully followed, the mechanistic basis for these observations remained unclear. As this experimental study represents a first attempt to transform arsenic abiotically with biotic mineral precipitates numerous variations of the experimental conditions are possible for future experiments. Since goethite did not form reactive phases similar to the ones in abiotic setups and was also shown to be not usable as Fe(III) source for *Shewanella oneidensis* MR-1, under the chosen conditions, for example the amount of ferrihydrite should be reduced or added in small portions. This could probably prevent magnetite formation at the surface of the goethite particles and support exclusively the formation of dissolved Fe(II) providing optimized conditions for the adsorption of Fe(II) to goethite similar to the abiotic experiments.

The provided results of this study regarding redox changes of arsenic by biogenic iron mineral precipitates show the potential of these mineral phases for the expected transformations. The further role of humic substances in such systems should be subject to future investigations based on the demonstrated decrease in crystallinity in presence of humic substances and thereby concomitant decrease in reactivity of the formed iron minerals.

REFERENCES

Babick F. and Ripperger S., 2004. Schallspektroskopische Charakterisierung konzentrierter Emulsionen. *Chemie Ingenieur Technik* **76**, 30-40.

Borch T., Inskeep W. P., Harwood J. A., and Gerlach R., 2005. Impact of Ferrihydrite and Anthraquinone-2,6-Disulfonate on the Reductive Transformation of 2,4,6-Trinitrotoluene by a Gram-Positive Fermenting Bacterium. *Environ. Sci. Technol.* **39**, 7126-7133.

Buerge I. J. and Hug S. J., 1999. Influence of Mineral Surfaces on Chromium(VI) Reduction by Iron(II). *Environ. Sci. Technol.* **33**, 4285-4291.

Cornell R. M. and Schwertmann U., 2003. *The Iron Oxides*. Wiley-VCH Verlag GmbH & Co. KGaA, Weinheim.

Elsner M., Schwarzenbach R. P., and Haderlein S. B., 2004. Reactivity of Fe(II)-Bearing Minerals toward Reductive Transformation of Organic Contaminants. *Environ. Sci. Technol.* **38**, 799-807.

Fredrickson J. K., Zachara J. M., Kennedy D. W., Dong H., Onstott T. C., Hinman N. W., and Li S.-m., 1998. Biogenic iron mineralization accompanying the dissimilatory reduction of hydrous ferric oxide by a groundwater bacterium. *Geochim. Cosmochim. Acta* **62**, 3239-3257.

Fredrickson J. K., Zachara J. M., Kennedy D. W., Kukkadapu R. K., McKinley J. P., Heald S. M., Liu C., and Plymale A. E., 2004. Reduction of TcO_4- by sediment-associated biogenic Fe(II). *Geochim. Cosmochim. Acta* **68**, 3171-3187.

Kappler A. and Newman D. K., 2004. Formation of Fe(III)-minerals by Fe(II)-oxidizing photoautotrophic bacteria. *Geochim. Cosmochim. Acta* **68**, 1217-1226.

Larese-Casanova P. and Scherer M. M., 2007. Fe(II) Sorption on Hematite: New Insights Based on Spectroscopic Measurements. *Environ. Sci. Technol.* **41**, 471-477.

Liger E., Charlet L., and Van Cappellen P., 1999. Surface catalysis of uranium(VI) reduction by iron(II). *Geochim. Cosmochim. Acta* **63**, 2939-2955.

Lovley D. R. and Phillips E. J. P., 1988. Novel Mode of Microbial Energy Metabolism: Organic Carbon Oxidation Coupled to Dissimilatory Reduction of Iron or Manganese. *Appl. Environ. Microbiol.* **54**, 1472-1480.

Lovley D. R., Fraga J. L., Blunt-Harris E. L., Hayes L. A., Phillips E. J. P., and Coates J. D., 1998. Humic Substances as a Mediator for Microbially Catalyzed Metal Reduction. *Acta hydrochimica hydrobiologica* **26**, 152-157.

Michel F. M., Ehm L., Antao S. M., Lee P. L., Chupas P. J., Liu G., Strongin D. R., Schoonen M. A. A., Phillips B. L., and Parise J. B., 2007. The Structure of Ferrihydrite, a Nanocrystalline Material. *Science* **316**, 1726-1729.

Nevin K. P. and Lovley D. R., 2000. Potential for Nonenzymatic Reduction of Fe(III) via Electron Shuttling in Subsurface Sediments. *Environ. Sci. Technol.* **34**, 2472-2478.

Prietzel J., Thieme J., Neuhäusler U., Susini J., and Kögel-Knabner I., 2003. Speciation of sulphur in soils and soil particles by X-ray spectromicroscopy. *Eur. J. Soil Sci.* **54**, 423-433.

Richter A., Voigt T., and Ripperger S., 2007. Ultrasonic attenuation spectroscopy of emulsions with droplet sizes greater than 10 μm. *J. Colloid Interface Sci.* **315**, 482-492.

Roden E. E., 2003. Fe(III) Oxide Reactivity Toward Biological versus Chemical Reduction. *Environ. Sci. Technol.* **37**, 1319-1324.

Roden E. E. and Zachara J. M., 1996. Microbial Reduction of Crystalline Iron(III) Oxides: Influence of Oxide Surface Area and Potential for Cell Growth. *Environ. Sci. Technol.* **30**, 1618-1628.

Stumm W. and Sulzberger B., 1992. The cycling of iron in natural environments: Considerations based on laboratory studies of heterogeneous redox processes. *Geochim. Cosmochim. Acta* **56**, 3233-3257.

Thieme J., McNulty I., Vogt S., and Paterson D., 2007. X-ray Spectromicroscopy - A Tool for Environmental Sciences. *Environ. Sci. Technol.* **41**, 6885-6889.

van der Giessen A. A., 1966. The structure of iron (III) oxide-hydrate gels. *Journal of Inorganic and Nuclear Chemistry* **28**, 2155-2156.

Weber K. A., Achenbach L. A., and Coates J. D., 2006. Microorganisms pumping iron: anaerobic microbial iron oxidation and reduction. *Nat. Rev. Microbiol.* **4**, 752-764.

Williams A. G. B. and Scherer M. M., 2004. Spectroscopic Evidence for Fe(II)-Fe(III) Electron Transfer at the Iron Oxide-Water Interface. *Environ. Sci. Technol.* **38**, 4782-4790.

Zachara J. M., Kukkadapu R. K., Fredrickson J. K., Gorby Y. A., and Smith S. C., 2002. Biomineralization of Poorly Crystalline Fe(III) Oxides by Dissimilatory Metal Reducing Bacteria (DMRB). *Geomicrobiol. J.* **19**, 179-207.

Acknowledgements/ Danksagung

I exceptionally thank my supervisor Prof. Andreas Kappler for the possibility to work on a challenging and highly interesting topic, which matched perfectly my understanding of an interdisciplinary, applied research field. I want to thank for the opportunity to broaden my horizon not only on a scientific, but also on a personal level in numerous discussions, presentations, meetings with visiting scientists and at conferences or courses where I was able to participate and meet people from all over the world. Starting up the Geomicrobiology group at the University of Tübingen right from the beginning was an exciting experience, I would never want to miss.

I would also like to thank my second examiner Prof. Stefan Haderlein, for co-supervising my thesis throughout the four years, for asking critical questions at the right points and any support I obtained from him during my time at the University of Tübingen. I would also like to acknowledge my third examiner Prof. Kirsten Küsel.

Many thanks go to Dr. Kristina Straub for being a patient, perfectly organized, great teacher in the lab whose advice made it possible for me to learn the secrets of microbiology and sterile work in a relatively short time and thereby building the basis of my experimental work. Thank you for being open for tricky questions and for the invitation to lovely Vienna.

I am indebted to Prof. Thomas Borch from Colorado State University, who helped a lot writing the successful proposal for beam time at SSRL in Stanford, the measurements itself, the data analysis and interpretation. It was a pleasure discussing not only scientific topics and in general collaborating with you, from our first meeting until now. I extend my thanks to Prof. Michelle Scherer from the University of Iowa, for fruitful conversations and experimental advice throughout my thesis and a nice, hot summer shared together in one office and beyond that.

There were many people who helped me with their experience with methods and instruments I used to conduct my experiments. I am

Curriculum Vitae

KATJA AMSTÄTTER

Geburtstag	20. Juli 1979
Geburtsort	Kulmbach, Deutschland

AUSBILDUNG

1985 – 1989	Grundschule Untersteinach
1989 – 1998	Markgraf-Georg-Friedrich-Gymnasium Kulmbach *Allgemeine Hochschulreife* Abitur am 26.06.1998
1998 – 2000	Universität Bayreuth *Grundstudium Chemie Diplom* Vordiplom am 26.07.2000
2000 – 2003	Universität Leipzig *Hauptstudium Chemie Diplom mit Vertiefung Umweltchemie* - Diplomarbeit: „Versuche zur Immobilisierung von Arsen in einem Tailingmaterial durch Coating mit Eisenoxihydroxiden" am Helmholtz Zentrum für Umweltforschung Leipzig - Betreuer: Prof. Dr. U. Stottmeister, Dr. H. Seidel - Colloquium am 26.05.2003
2001	Bayerisches Landesamt für Umweltschutz Kulmbach *Praktikum im Labor für Radiotoxikologie* Strontiumisolierung und –analytik mit RFA
2003 – 2004	Universität Bayreuth, Atmosphärische Chemie *Wissenschaftliche Angestellte* Aufbau der Forschungsstelle
2005 – 2008	Universität Tübingen, Geomikrobiologie *Doktorandin* - Betreuer: Prof. Dr. A. Kappler - Colloquium: 12.12.2008

2005	Universität Berkeley
	▪ *MSA Short course* "Molecular Geomicrobiology"
2007	Ludwig Maximilians Universität München
	▪ *9th EMU Summer School* "Nanoscopic approaches in earth and planetary sciences"

VERÖFFENTLICHUNGEN

2005	Seidel H., Görsch K., Amstätter K., Mattusch J., Immobilization of arsenic in tailings material by ferrous iron treatment. *Water Research* **39**, 4073-4082
2005	Amstaetter K., Jiang J., Navarro L., Kappler A., Redox transformation of arsenic by microbial reduced ferric iron oxides and humic substances. *AGU*, San Francisco, Posterpräsentation
2007	Amstätter K., Kappler A., Microbial and Geochemical Interactions with iron minerals. *EMU Summer School*, München, Posterpräsentation
2008	Amstätter K., Kappler A, The Role of Humic Substances in Microbial Fe(III) Mineral Transformation. *DMG*, Berlin, Posterpräsentation
2009	Amstaetter K., Kappler A, Influence of humic substance concentration on electron shuttling and mineral transformation during microbial 2-line ferrihydrite reduction. *Geochimica Cosmochimica Acta*, eingereicht
2009	Amstaetter K., Borch T., Larese-Casanova P., Kappler A., Redox transformation of arsenic by Fe(II)-activated goethite (α-FeOOH). *Environmental Science & Technology*, eingereicht
2009	Bauer I., Amstaetter K., Kappler A., Influence of ionic strength on electron transfer by humic substances. *Geochimica Cosmochimica Acta*, in Vorbereitung